دور الاتصال والتواصل في مدن التوابع المعلوماتية

إشراف : هدى عبد الصاحب العلوان
أستاذ مساعد
كلية الهندسة- جامعة بغداد
قسم الهندسة المعمارية

بلسم علوان شلال
E-mail- [b.1architect@yahoo.com]
ماجستير هندسة معمارية
كلية الهندسة- جامعة بغداد
قسم الهندسة المعمارية

مستخلص البحث :-

يتقصى البحث أثر أهم تطور أحدثته الثورة المعلوماتية وهو تكنلوجيا الاتصال (Technology Communication) الذي عمل على تقريب المسافات وإلغاء الحدود الجغرافية وتحويل العالم الى قرية كونية (Global Village)، مما ادى الى بروز اشكال وهيئات جديدة لتلك التجمعات العمرانية، لعل أهمها هو تفتيت المدن الكبرى وظهور مدن توابع (Satellite Cities) ذات ارتباطات عالمية اكثر من كونها تُشكل ظهيراً لمراكز المدن العواصمية المحلية كما كان في السابق. ولكن وعلى الرغم من ذلك المد التكنلوجي للاتصال وتأثيراته الحتمية فإنه يبقى بكل إمكانياته عبارة عن فعل لا يحدث إلا باتجاه واحد وضمن حدود الإرسال والتلقي ليس أكثر، ومن هنا ظهرت **مشكلة بروز الفعل الاتصالي كـ(دوغماتية) بسبب تمحورالعالم بأسره حول شبكة الاتصالات**... التي أصبحت بدورها قلب منظومة هذا العصر. **وعلى ضوء تلك المشكلة فقد سعى البحث إلى إيجاد الفعل الموازي إن لم يكن البديل الذي يطوي الاتصال بين جناحيه، جاعلاً منه مرحلة من مراحل عملية الاستجابة والتفاعل متجاوزاً حدود الارسال والتلقي، بمعنى أخر الانتقال من طور استيراد التكنلوجيا الى طور المساهمة في الا نتاج،** وهذا لايتحقق إلا من خلال استثمار تكنلوجيا الاتصال لتحقيق ما هو أعلى وأسمى والذي يطرح هنا بفعل التواصل(Communicativeness) بين المجتمعات.

ولتحقيق هذا الهدف تم طرح الإطار النظري النظري الذي الذي في ضوئه طُرحت فرضية البحث ونصها**(إن الاتصال ببعده التكنلوجي والتواصل ببعده الاجتماعي لهما دور في صياغة مدن التوابع المعلوماتية من خلال تأثيرهما الجوهري في البنية المادية والإجتماعية والإقتصادية لتلك المدن)**. ومن ثم سعى البحث إلى اختبار صحة الفرضية والخروج بإستنتاجات وتوصيات خاصة بالبحث.

Abstract:-

This research attempts to trace the most significant development caused by the information revolution, namely "the Communication Technology" which reduced the distances between different urban communities, or within a single one, eliminated the geographical boundaries and the transformed the world into a global village. This led to the emergence of new forms and bodies to those urban communities; perhaps the most important is the fragmentation of the major cities and the emergence of (Satellite Cities) with global links, rather than hinterlands to the local capital cities as in the past. But in spite of the technological tide of communications and its inevitable impacts, it stays, with all its possibilities, a reaction that occurs only in one direction and within the limits of no more than sending and receiving nothing more. This is what Arab cities had seen in the recent stages of their change.

Here arises **the problem of the emergence of the communication act as a "Dogmatic" because the whole world revolved around the communications network ...** Which in turn became the heart of the system of this era. **In light of this problem, this research has sought to find the act parallel if not alternative that will fold the " Communication " between its wings, making it, the stage of the process of response and interaction surpassing the limits of sending and receiving. In other words the transition from importing technology to the process of contributing to its production.** This only takes place through the investment of the Communications Technology to achieve that which is the highest and noblest, posed in this research by the "Communicativeness" between communities. To achieve this goal it took the building of the theoretical framework, in the light of which we put forward the hypothesis of the research that reads **(Communication in its technological dimension and Communicativeness in its social dimension, both, play a role in the formulation of Satellite Cities of the twenty-first century through their essential impact on the physical, social and economic infrastructure development of those cities).** The research, then, sought to test the validity of this hypothesis and draw conclusions and recommendations.

كلمات رئيسية:- الاتصال، التواصل، عصر المعلوماتية، المدن التوابع المعلوماتية، سياسة التصغير، الانتشار الافقي، اللامركزية والتوازي، النسيج الشبكي،التواؤم، الخصوصية، التغذية الاسترجاعية.

1. المقدمة:-

" إن التكنلوجيا ليست مجرد الأداة أو الوسيلة التي يستخدمها الإنسان في حل الوسيلة وكذلك الجوانب المختلفة للسلوك الاجتماعي فيما يخص تطبيقها. في إطار هذا المفهوم تَصبح التكنلوجيا عنصراً ذا ثلاثة أبعاد: ألبعد الفني(التكنيكي)، وألبعد الثقافي-الأخلاقي، وألبعد التنظيمي " (Pacey, 1991, P6)

فمن خلال الاعتماد على تعريف (بيسي Pacey) للتكنلوجيا كان البدء بالدراسة والتحليل أثر الثورة المعلوماتية الاتصالية في صياغة مدن القرن الحادي والعشرين، وذلك لأجل الارتقاء بالمدينة إلى منظومة معلوماتية اتصالية متكاملة تسهم في حل المشكلات التي تواجهها، وتعمل في الوقت ذاته على تطوير وتحسين مستويات المعيشة فيها. فالبعد الأول لتلك الثورة وهو البعد(التكنيكي) المتمثل **بالاتصال(Communication)** ، نجده قد أخذ حيزاً مميزاً في العقود الأخيرة من القرن الماضي، إذ حقق الإنسان تطوراً مذهلاً في مجال التكنلوجيا الرقمية وعلى رأسها تكنلوجيا الاتصال(Communication Technology). وإن البحث في تناوله لمدن القرن الجديد إنما يحاول تسليط الضوء على دور الإتصال في إزالة الحواجز الجغرافية وتحقيق الانفتاح في العلاقات الاجتماعية على مستوى العالم، وطرحه لإسلوب عالمي جديد فيما يتعلق بالمدن.

ولكن وعلى الرغم من تأثر أغلب المفاصل الحضرية بالتقنيات الاتصالاتية الحديثة والناجمة بطبيعة الحال من تأثر الأنشطة الإنسانية التي تحتويها تلك المفاصل، تبقى تلك التقنيات بمثابة الوسيلة والأداة كما اشار(Pacey) التي تستغلها المجتمعات لتحقيق بعدها التنظيمي من خلال إمكانية إستثمار تلك الوسيلة الاتصالية لتحقيق **التواصل (Communicativeness)** والذي يطرحه البحث هنا باعتباره يشكل البعد الثاني للثورة المعلوماتية الاتصالية وهو البعد (الثقافي-الأخلاقي)، حيث يقوم التواصل على أساس حدوث عملية التغذية الاسترجاعية الرابطة بين المرسل والمتُلقي، وهنا يتم التركيز على قيم (الآخر) دون الارتكان الى قيم (الأنا) المهيمنه التي تحاول تكنلوجيا الاتصال تكريسها عبر استجلابها من خارج الحدود الجغرافية والتي باتت تُهمش الى حد الإزالة النهائية لها بفضل ثورة الاتصالات وسرعتها.

1.1. مشكلة البحث:-

لطالما كانت المدينة بنظر الكثيرين المهد الذي تترعرع فيه الحضارات وتُبنى فيه المجتمعات، وميداناً للتعبير عن عطاء سكانها و معتقداتهم الفكرية والاجتماعية. ولعل المدينة العربية التقليدية مثال صريح لهذا الانعكاس. إلا إن للتأثيرات الفكرية العالمية أيضا أثرها في تاريخ تغير المدن وتحول بنيتها، فقد فعلت الحداثة والعصرنه فعلهما في

المدينة، فتآكل نسيجها وتفكك بعد أن كان بنياناً مرصوصاً ويرجع السبب في ذلك الى تبني الفعل الاتصالي الذي يهتم بنقل التكنلوجيا من المرسِل إلى المرسل إليه(المتلقي) بآليات تُظهر سيطرة الرسالة وهيمنة المبلغ على المتلقي. إنها "دوغماتية الاتصال" التي تُلغي دور المتلقي. واليوم تعصف على مستقبل المدن رياح التقدم االتكنلوجي في مجالات عديدة أهمها تكنلوجيا الاتصالات حتى أصبح العالم بأسرهِ يتمحور حول شبكة الاتصالات... التي أصبحت بدورها قلب منظومة هذا العصر **مما يعني بروز الفعل الاتصالي بشكلٍ أكبر مما كان عليه في السابق**. وهذا التمحور حول شبكة الاتصال **قد** أفرز صياغة جديدة وإسلوب عالمي حتمي يفرض على المدن وهو تفتيت المدن المحلية الكبرى وخلق مدن توابع تُشكل ظهيراً للمدن العالمية اكثر منه للمدن المحلية. وهذا ما يضع المدن أمام تحديات جمة أهمها معرفة الآلية المثلى لاستثمار المد التكنلوجي في صياغة المدن التوابع للقرن الجديد بعيداً عن الإسلوب العالمي الذي تحمله تكنلوجيا الاتصال بنسيجها الشبكي. وبما يحقق **التواصل** الذي يعني حتمية التطور والتواؤم مع المستجدات العالمية، والتفاعل الحضاري مع الحذر والتمحيص بعيداً عن توليد تماثل حضاري مفرط أو إحداث تَصدع في المباديء والقيم التصميمية المتعارف عليها للمدن المحلية.

2.1. فرضية البحث ومنهجه:-

وبناءاً على ما تقدم فإن البحث يقدم فرضيته بالشكل الآتي**(إن الاتصال ببعده التكنلوجي والتواصل ببعده الاجتماعي لهما دور في مدن التوابع المعلوماتية من خلال تأثيرهما الجوهري في الكيان الاجتماعي والاقتصادي وبالتالي الكيان العمراني لتلك المدن).**

ولتحقيق أهداف البحث والتحقق من صحة الفرضية المطروحة، فإن البحث يتخذ منهجاً نظرياً استقرائياً، يعمل على الإستفادة من كل الأدوات النظرية المتوفرة، وتتبلور استنتاجاته تِباعاً مع تطور بنيته العامة

القرن الحادي والعشرين:- عصر المعلومات:-

إن عصر المعلومات ليس عصراً عادياً، وقراءة مفرداته وأُسسهِ ومترتباتهِ الاجتماعية والثقافية والاقتصادية هي مثار بحث وجدل ودراسة كل الدول لمواجهة استحقاقاته، والاستفادة من معطياته إيجابياً بدون اختراقات ثقافية أو اقتصادية أو علمية. فهو قائم على التحول والتغيير والديناميكية وسرعة التطور والانطلاق في طريق الإسراع الزمني والتوسع المكاني وإلغاء الحدود والحواجز.

يقول (وولتر ستون Walter Stone) في كتابه " أفول السيادة The Twilight of Sovereignty" إن المؤرخين والفلاسفة يطلقون على العصور والحقب التاريخية مسمياتها بعد إنقضائها، مثل العصور الوسطى

أو العصر الحجري أو عصر النهضة، ولكن الفلاسفة أو العلماء اليوم لم ينتظروا حتى يعلنوا بأن القرن الحادي والعشرين هو عصر المعلومات (الخوري، 1998، ص207). ولعل السبب في ذلك يعود إلى أن تاريخ البشرية وهو يطوي صفحات العقد الأول من القرن الحادي والعشرين يشهد نقلة نوعية كبيرة يعيشها المجتمع البشري إذ تنقله الى حضارة جديدة جوهرها المعلومة من حيث إيجادها، واستخدامها وانتقالها بسرعة تفوق سرعة الادراك البشري ولهذا وصف عصرنا بعصر المعلومات. إن الثورة المعلوماتية قد جعلت من المعلومات سلعة جديدة قيد التداول بين الجماعات والمجتمعات، إلى الحد الذي أمكن تصنيفها، بالنسبة إلى مستقبل الأولويات البشرية، جنباً إلى جنب مع الموارد الطبيعية. كما إنها أصبحت مورداً جديداً يكمل الموارد الطبيعية المعروفة كالغذاء والطاقة مع فارق مهم وهو إن المعلومات تختلف عنها في إنها مثل المادة لا تُفنى بالإستعمال(انطون بطرس، 1987، ص9).

1.2. تكنلوجيا المعلومات:-

إن لكل تكنلوجيا مادتها الخام التي تتعامل معها، وأداتها الأساسية التي تعالج بها هذه المادة، ومصدر طاقتها الرئيسي الذي تستخدمه هذه الأداة لتحويل تلك المادة الخام إلى منتجات يتم توصيلها إلى المستفيد من خلال وسائل التوزيع المختلفة والتي لابد أن تتلاءم مع طبيعة هذه المنتجات وظروف إستخدامها (Toffler,1980,P25) وإذا ما طبقنا هذا الأطار العام على تكنلوجيا المعلومات، فمادتها الخام هي البيانات والمعلومات والمعارف وأداتها الأساسية هي بلا منازع الكُمبيوتر وبرمجياته التي تستهلك طاقته الحسابية في تحويل هذه المادة الخام إلى سلع وخدمات معلوماتية، أما التوزيع فيتم من خلال التفاعل الفوري - Direct Interaction – بين الإنسان والآلة، أو من خلال أساليب البث المباشر وغير المباشر كما هو الحال في أجهزة الإعلام، أو من خلال شبكات الاتصال Communication Networks التي تصل بين كمبيوتر وآخر أو بينه وبين وحداته الطرفية Peripherals.

ومن هنا وضعت الموسوعة الدولية لعلم المعلومات تعريف تكنلوجيا المعلومات على إنها التكنلوجيا الألكترونية اللازمة لتجميع واختزان وتجهيز وتوصيل المعلومات، وهناك فئتان من تكنلوجيا المعلومات.. الأولى هي تلك الفئة التي تتصل بتجهيز المعلومات كالنظم المحوسبة. أما الفئة الثانية فهي الفئة المتصلة ببث المعلومات كنظم الاتصالات عن بعد، فالمصطلح يشمل النُظم التي تجمع بين الفئتين (طارق محمود، 2004، ص150).

وعليه فإن تكنلوجيا المعلومات هي منظومة متكاملة مادتها المعلومات وأداتها الكُمبيوتر وبرمجياته، أما انتقال المعلومات وتبادلها فيكون عن طريق شبكات الاتصال- التي تُمثل نقطة البحث-

2.1. تكنلوجيا الاتصال:-

إن تكنلوجيا الاتصال هي عصب عصر المعلومات، فبسبب تطورها وانتشارها تضاءلت المسافات مما أدى الى ضمور حجم الأرض، مما جعل البيئة الدولية تنكمش بجميع مظاهرها، وجعل أي تطور في مكان يؤثر في مكان آخر. كما ان شبكة الأنترنت، وطريق معلوماتها فائق السرعة، قد حولت تلك التكنلوجيا من مجرد وسيلة اتصال إلى وسيلة لنقل منتجات الثقافة، حيث إن شبكة الانترنت تُمثل اليوم عماد المجتمع المعلوماتي الجديد ومعجزته التي يبشر بها، إذ فتحت هذه الأداة الجديدة العالم على أبوابه. فـ الإنترنت بلا منازع ، هي شبكة الشبكات أو(الشبكة الام) التي طوت في جوفها مئات الآلاف من شبكات تبادل المعلومات، سواءاً كانت عالمية أو إقليمية أو محلية **(بهاء الدين شاهين، 1996، ص24).** اما الواقع الخائلي Virtual Reality* فهو مفهوم أخر من تلك المفاهيم التي أضافتها تكنلوجيا المعلومات إلى قاموس حياتنا المعاصرة، والذي جاء نتيجة دخول الذكاء الأصطناعي Artificial Intelligence والتحكم الأوتوماتيكي Automatic Control الى منظومة تكنلوجيا المعلومات. ويمكن النظر إليه على إنه بيئة اصطناعية لممارسة الخبرات بصورة أقرب ما تكون إلى تلك في دنيا الواقع. لقد أسقطت هذه البيئة الاصطناعية الحاجز الرابع (الزمن)، لينفذ مستخدمها إلى ما وراء شاشة الكمبيوتر، يجوب عوالم الوهم متحرراً من قيود الجسد وقيود قوانين الطبيعة وقيود قوانين المجتمع. فلا يوجد عائق يعوقه من أن يخترق الحوائط، ويجوب أركان المعمورة، وكما يمكن الواقع الخائلي الانسان من الإبحار في المكان، يمكنه أيضا من الإبحار إلى أزمنة الماضي الغابرة، واقتحام أزمنة المستقبل القادمة، أو الخلط بينها فيما يعرف بالخلط الزمني Time Scrambling **(نبيل علي ، 2001، ص109).** وفي هذا إشارة إلى إن عالم الآلفية الثالثة يتحرك نحو علاقات حضرية أساسها قائم على الاتصال من خلال استخدام الرسائل والإشارات والمعلومات الأِلكترونية

3. منظومة عصر المعلوماتية:-

يشخص البحث إشكالية ظهور مفاهيم وأبعاد معرفية جديدة أفرزها عصر المعلوماتية من خلال ثورته الاتصاليه التي تسعى الى تحقيق إسلوب عالمي جديد ونموذج كوني يفرض على العالم بأسره بواسطة طريق المعلومات السريع (Information

---

* تعددت المصطلحات العربية المقابلة للمصطلح الانكليزي Virtual Reality، من الواقع الافتراضي إلى العالم الوهمي والواقع الخيالي، وكلها لاتُعبر عن المفهوم المحوري، علاوة على كونها جميعاً مصطلحات مركبة يصعب الاشتقاق منها، ونظراً الى إن المفهوم يعد من المفاهيم الأساسية في تكنلوجيا المعلومات حالياً، ومن المتوقع استخدامه بسرعة، لذلك تم اختيار إسم الفاعل (خائل) كمقابل (Virtual) مما يسمح باشتقاق: خائلية، خائلي، يخيئل، مخيئل، خيئلة وخائليات، وذلك لأن الفعل خال هو متعدي(في مثل: خال السراب ماء) الى معنى التعدية بأداة (خال له الأمر كائناً) وهو المعنى الدقيق الذي يعبر عنه المصطلح الأنكليزي **(نبيل علي، 2001، ص118).**

Superhighway)، تلك المفاهيم التي يعتمد في تداولها على تكنلوجيا الاتصال دون التواصل مما ينعكس وبشكل جوهري على المنظومة المعرفية والقاعدة التصميمية المتبعة في عملية التطوير المكاني للتجمعات العمرانية الجديدة، والعلاقة فيما بينها وبالتالي شكل وهيئة المدينة الناتجة. فالاتصال الذي يسعى البحث الى تقديمه على إنه يمثل الشق التكنلوجي لمنظومة عصر المعلوماتية، وعصب هذا العصر في الوقت نفسه، وكان لتطبيقه أثر كبير في صياغة شكل وهيئة مدن الآلفية الثالثة، حيث أوجد إسلوباً عالمياً لشكل وهيئة هذه المدن يمثل الإسلوب العالمي الجديد والقائم على (الآنا) المهيمنه لذلك الشق التكنلوجي، وهذا الشكل هو(المدن التوابع ذات الخواص المعلوماتية)، المرتبطة بالنسيج العالمي أكثر من ارتباطها بكل ما هو واقع ضمن النطاق المحلي. إن تكنلوجيا الاتصال عصب عصر المعلوماتية باتت اليوم تُمثل حتمية تكنلوجية، فلن تكون هنالك أي نقطة في العالم بمنأى عن تأثيراتها بفعل نسيجها الشبكي الذي بات يلف الكرة الارضية بأجمعها، فلم تعد هنالك نقطة نائية أو بعيدة عن تأثيرها. ويتلخص ذلك التأثير في إحداث تلاقح حضاري يولّده انتقال المعلومة عبر شبكتها، هذا التلاقح الذي يعمل على ربما سيطرة قيم وثقافة البلد المصدر للمعلومة والتكنلوجية في آن واحد (المرسِل المهيمن)، وبالتالي يولد حالة ما يسمى بالصدمة الألكترونية، التي سرعان ما تتحول بالبلدان المستوردة (المستقبِل المستهلك) من الانبهار بالواقع الخائلي إلى الاصطدام بالواقع الحقيقي للبلد المصدر (انطوان بطرس، 1987، ص122).

وهذا ما يجعل المدن تدخل دوامة تكنلوجيا هذا العصر المتسارع حثيث الخُطى. ومن هنا جاء طرح التواصل والذي يسعى البحث الى تقديمه على إنه يمثل الشق الاجتماعي لمنظومة عصر المعلوماتية، في محاولةٍ لتحقيق توازن تلك المنظومة، من خلال إيجاد (الاخر) المختلف صاحب الخصوصية والهوية المميزة، القادر على إحداث التغذية الاسترجاعية لكل ما يتعلق بالإسلوب العالمي المطروح من قبل الشق التكنلوجي ذي الحتمية الاتصالي.

3.1. الاتصال والتواصل Communication and Communicativeness:-

إذا ما اردنا تعريف الاتصال بعيداً عن شقه التكنلوجي نجد إن الاتصال يعني وصل شيء بشيء أي رغبة أحد الطرفين إقامة علاقة مع الطرف الآخر مع استجابة هذا الطرف، واحتمال عدم استجابته. وهذا يختلف عن التواصل الذي يشترط حصول الاستجابة والتفاعل والمشاركة (الطاهر، 2000، ص 143).

أما الظاهرة الاتصالية فهي عملية إخبار وإعلام، تهتم بنقل الخبر من مرسِل إلى مرسل إليه، تهتم هذه العملية بتوضيح الخبر المنقول والإبداع في التبليغ، وأحياناً حتى في الإلزام المادي والمعنوي. هنا تظهر سيطرة الرسالة وهيمنة المبلغ على المتلقي. فلا سؤال إلا ما

كان في ضمير المتلقي، ولا حوار يفسح المجال للسؤال والاستفسار والتعليق وإبداء الرأي. ظاهرة يكون فيها المبلغ محمولاً علىالاسترسال، ويكون فيها المتلقي مكرهاً على الاستماع **(الملاخ، 2005، ص 1).**

إن عملية الاتصال تقوم على ستة عناصر هي:- **مرسِل** يقوم بنقل **رسالة** (معلومات) إلى **متلقي** بواسطة **قناة**، بحيث يستلزم ذلك النقل من جهة، وجود شفرة Code. ومن جهة ثانية تحقيق عمليتين اثنتين: **ترميز المعلومات او الهدف** Encoding، وفك الترميز Decoding الذي يعني أشكال **الاستجابة** للرسالة (المتضمنه فهم الرسالة وتفسيرها فقط) **(Muchielli, R,1980).** إننا نرى هنا إن الاتصال يعد تواصلاً سلبياً، فهو عملية تفتقر إلى التغذية الاسترجاعية Feedback بين المرسِل والمتلقي والتي تُشكل أساس التواصل الإيجابي. وهو بذلك يعمل طرح النموذج الكوني القائم على التوحدية وأُحادية الـ(أنا المهيمن)، كونه يتضمن توجيه رسالة من طرف لآخر دون تلقي رد أو استجابة عليها، وهو بهذا يكون ذا بنية خطية باتجاه واحد وعلاقة انفعالية بين المرسل (الأنا المهيمنه) والمستقبِل أو المتلقي(الآخر) الذي يكون منفعِل ومستهلك. أما التواصل فيعرفه عالم الاجتماع (**تشارلز كولي** Charles Cooley) التواصل قائلاً: " **هو الآلية التي بواسطتها تُوجد العلاقات الإنسانية وتتطور**". إنه يتضمن كل رموز الذهن مع وسائل تبليغها عبر المجال وتعزيزها في الزمان. ويتضمن أيضاً تعابير الوجه وهيئات الجسم والحركات ونبرة الصوت والكلمات والكتابات والمطبوعات والقطارات والتلغراف والتلفون وكل ما يشمله آخر ما تم في الاكتشافات (شبكة الإنترنت) في المكان والزمان (Charles,1969,P 42).

ويرى (لوزير Lussier) إن الهدف من التواصل هو: محاولة التأثير والإقناع وليس مجرد إرسال الرسائل المختلفة، فلا قيمة للتواصل دون تحقيق هدف، ولا نجاح للتواصل دون إحداث تأثير، فالفرد يتصل ليؤثر، ويتعرض للتواصل ليتأثر، ويتصل مع الآخرين لنشر المعلومات والتعبير عن المشاعر وقد يكون وسيلة لفظية أو غير لفظية. أما الهدف النهائي للتواصل: هو البقاء، فعندما نفقد التأثير على بيئتنا الخارجية (والتي تمثل البيئة المبنية جزء منها)، فإننا نعزل أنفسنا ويؤدي ذلك في النهاية إلى الموت **(انعام مجيد ،2002،ص 9).** وعليه فإن التواصل أساسه التفاهم وتبادل الأدوار بين المرسِل والمتلقي، فلا يمكن أن يوجد التواصل بغياب أحدهما، فالتواصل (كِلا الاثنين معاً)، ويتحقق ذلك من خلال وجود التغذية الاسترجاعية بينهما، وهذا ما يشكل نقطة اختلاف جوهرية بين فعل الاتصال وفعل التواصل.

إن التواصل الخاص بعصر الاتصالات لا يعني التمسك بما هو موروث والانعزال بالفكر التقليدي خوفاً من التغيير، ولا يعني الخلط التام والقبول المطلق لكل ماهو قادم من الأنا بمرجعيته الكونية ذات الطابع الحتمي، ولكن

التواصل المطروح هنا يتناول حتمية التغيير والتواؤم مع المستجدات العالمية القادمة بفعل تكنلوجيا الاتصال، مع الانتقاء الحذر الذي يقوم على التحليل البرهاني والفحص والتدقيق. فالتواصل هنا عبارة منظومة تتأسس من بنية مجالية قِوامها (التفاهم– التذاوت – الاجماع) وسياق مكون من (المجتمع- الثقافة- الشخصية)، وعلاقة تفاعلية تربط (الأنا والآخر)... حيث يكون فيها الآخر متفاعل ومنتج.

4. مدن عصر المعلوماتية:-

عرف كوهين (Cohen) المدينة المعلوماتية بأنها الحاضرة ذات الروابط الاتصالاتية والهندسة الشبكية التي تحكم من قبل قطاع تقنية المعلومات لتنفيذ عمليات تبادل المعلومات، وعرفت سوسيلين (Couclelis) المدينة المعلوماتية بأنها " محاكاة شاملة تعتمد على تقنية شبكة الاتصالات لتنفيذ الوظائـف الاعتيادية لقاطني المدن بطريقة إلكترونية الطابع وينفذها أشخاص عاديون في مدينة عادية". ومن هذا التعريف يبرز إن المدينة المعلوماتية هي مدينة مرتبطة بالجغرافيا (وليس الافتراض الجغرافي)، وإنها مدينة روادها هم الأشخاص الاعتياديون وليست مقصورة على متخصصي الحاسوب والشبكات (حيدر فرحات ، 2003، ص 3). ولكن وصف مدينة القرن الجديد بـ المدينة المعلوماتية، وإنها تلك المدينة التي تُؤدي وظائفها وإنشطتها من خلال أنظمة المعلومات والاتصالات لا يكفي أن يعطي تصوراً عن شكل تلك المدينة وهيئتها.

وعليه كيف يمكن وضع تصور لمدينة القرن الجديد تحت ظل تأثير تكنلوجيا الاتصال (تكنلوجيا العصر)؟؟؟ وللاجابة على هذا التساؤل يسعى البحث الى التعرف على الهيئة الجديدة التي أوجدتها تكنلوجيا الاتصال- التي تتعامل مع اللامحسوس واللاملموس- إلا إن أثرها في المدن بات أكثر من كونه محسوس وملموس بل هو تأثير حتمي في صياغة هيئة وشكل مدينة عصر المعلوماتية.

4.1. تأثير الاتصال في مدن عصر المعلوماتية:-

لقد فعلت الثورات التكنلوجية فعلها في المدن عبر العصور. حيث أدت إلى إحداث تغييرات حتمية في هيئة وشكل المدينة. فمن مركزية المبنى العقائدي في قلب مدن العصور الاولى إلى اللامركزية التي تُنادي بها شبكة عصر المعلوماتية. ومن هرمية وتوالي الارتباط ذو القمة التراتبية المتجهه صوب المركز المدني الى توازي وتساوي عقد ونَوى النسيج الشبكي لتكنلوجيا الاتصال. ومن حيز المكان المغلق الى القرية الكونية المتضائلة بفعل ذلك النسيج. ومن المدن المتروبولية الكبرى المحاطة بالأسوار إلى مدن التصغير والانتشار كعقد في تلك الشبكة العالمية. (محمود حسن،2001، ص2). وسوف يكون البدء بطرح الدور الذي تلعبة المنظومة التكنلوجية للاتصال في صياغة هيئة مدن القرن الجديد كونها تُمثل الحتمية التكنلوجية

صاحبة اليد العليا في التأثير المباشر والظاهر على المدينة.

4.1.1. تأثير سياسة التصغير في مدن عصر المعلوماتية:-

لقد نجحت تكنولوجيا الاتصال وربما لأول مرة في تحقيق المعادلة الصعبة في الأجهزة، في أن تجمع ما بين الأكفأ والأعلى قدرة وبين الأرخص والأكثر انتشاراً في الاستخدام . فقد أطلقت اليابان قمراً صناعياً في منتهى الصغر يقترب حجمه من حجم أجهزة الكمبيوتر اليدوية والتليفونات المحمولة، كما توجد ألعاب الفيديو الحديثة التي تستخدم الواقع الخائلي حيث يمكن برمجتها بحيث تؤدي جميع الألعاب الخطرة المتاحة في مدينة ملاهي كبيرة مثل والت ديزني وأن تُحقق جميع مظاهر الحياة هنا. وإذا ما حاولنا عكس هذه النظرية التكنلوجية في واقع المدن فإننا نجد إنه وعلى الرغم من أن المتوالية السكانية تزداد بمعدلات مرتفعة، وإن تضخم المدن وارتفاع معدلات التلوث بها من أهم المشاكل إلى تُعاني منها المدن في الوقت الراهن، ومن المنتظر أن تعاني منها بصوره أكبر في المستقبل، إلا إن الحجم الصغير للمدينة من المفترض إنه سوف يكون الأكثر شيوعاً في المستقبل وذلك بالرجوع إلى سياسة التصغير التي سوف تمتد إلى جميع الاختراعات الإنسانية، حيث إن مدينة صغيرة الحجم سوف يمكنها أن تقوم بجميع وظائف وخدمات المدينة الكبيرة، وهذه المدن المدمجة الصغرى سوف يطلق عليها(مدن الإكتفاء الذاتي)، هذا بالإضافة إلى التقدم السريع والمذهل في وسائل الاتصال التي من المفترض أن تعمل على تقريب المسافات الكبيرة بين المدن مما يلغي الحاجة إلى التجاور الشديد والتزاحم داخل المدينة الواحدة. وإذا كانت السيارة قد أدت إلى تضخم حجم المدينة، وإن كانت هناك مشاكل قد نتجت عن هذا التضخم، فإن الاعتماد على شبكات الاتصال سيؤدى الى العكس، حيث إن شبكات الاتصال ستقلل هناك من التنقل الكثيف داخل المدينة أو السفر، إنها ستجعل المدينة بل والعالم يأتى إلى الإنسان على شاشات الكمبيوتر كما في الشكل(1).

4.1.2. تأثير الانتشار الافقي في مدن عصر المعلوماتية:-

5. وإذا ما أردنا طرح جدلية العلاقة بين هيئة المدينة وشكلها في عصر المعلوماتية و سياسة الانتشار الأفقي نجد إن تكنلوجيا الاتصال تعمل على تحقيق الانتشار الأفقي للمدن من خلال قدرة شبكاتها من الوصول الى كافة أرجاء المعمورة، حيث إن قُدرة هذه الشبكة بحزمها الضوئية تركت تأثيرات مكانية تربط الفضاءات المتباعدة بفضاءات خائلية مجردة في نفس الوقت الذى تسعى فيه إلى تفتيت المدن الكبرى وإضعاف التقارب الفيزيائي. وفي الوقت نفسه فإن تكنلوجيا الاتصال تُوفر فرصاً للمدن والأقاليم الهامشية لفك عزلتها من خلال المنافع التي تملكها **(البحراني،2002، ص29)**. وفي هذا الصدد يؤكد(سايموند

Simmonds) إن شبكات الاتصال تُشجع على جعل الأنشطة الحضرية لا تسلك قُرب مصادر المواد الاولية أو الطاقة أو قُرب التقاطعات الرئيسية للطرق ولكنها تقع في أي مكان تستطيع الشبكة الاتصالية النفاذية فيه إلى جميع هذه العناصر(Simmonds 2000, p 277). كما إن تلك الشبكة قد أدت إلى إيجاد واقع جديد، حيث إن التعاملات تتم ولكن من خلال الفضاء الخائلي، حيث تحدث فيه المقابلات بشكل افتراضي، من خلال شاشة الكمبيوتر وليس من خلال التفاعل المكاني الحقيقي، وهذا ما يوفر فرص إمكانية الوصول إلى أبعد نقطة في العالم.

4.1.3. تأثير اللامركزية والتوازي في مدن عصر المعلوماتية:-

إن مفهوم اللامركزية هو ليس تجسيداً لرغبةٍ أو مطالبٍ إنما هو ظهور تلقائي اقترن بتغير طبيعة المحيط خصوصاً لما يتعلق بتكنولوجيا الاتصال التي أسهمت بشكلٍ فاعل في تحقيقه من خلال أنظمتها ووسائلها. حيث تؤكد(Shoshana Zubaff) إن تكنولوجيا الاتصال قد ولدت نظاماً مختلفاً تماماً، وذلك لأن المادة المتحركة هي المعلومات التي هي غير فيزيائية، حيث عمدت إلى تغيير مفاهيم السلطة وبنية القوة للتنظيم(Groak, 1993, p 116). فالتكنولوجيا اليوم تسمح للناس بالعمل بسهولة بينما هم يتنقلون أو في البيت إذ سوف تساهم بطريقة ما في تغيير أداء الأنشطة. حتى إننا لنجد هذا واضحاً من تغيير عنوان الشخص نفسه بعد أن كان محدداً بمكان فيزيائي واحد، وأصبح الأن ممتداً ليشمل أشكال مختلفة منه، في البيت في السيارة، وحتى وهو يمشي.

وكالعادة لم يقتصر تأثير تكنولوجيا الاتصال في تجاوز مركزية المدينة كـ وحدةٍ مفردة ومعزولةِ التأثير والتأثر، بل إنها تنظر إلى كل مدينة مهما كانت على إنها تُشكل عقدة في النسيج الشبكي العالمي للاتصال، وهذا ما يؤدي بالتالي إلى تكامل منظومة الشبكية العالمية، والتي تتجه نحو التشبه بمنظومة شبكة الاتصال العالمية والانترنت بالتالي فإن ما يخص المدن كـ مجموعة عقد يطرح إن النظر إلى نسيج التوابع الحضرية نهاية القرن العشرين بات يؤكد إنه لم يعد مناسباً النموذج الحضري الذي يصور المدينة المركزية كمحيط لمعظم الامكانات الإنتاجية في المناطق العواصمية، أي إن الإحتكار التقليدي لمركزية المدن كموقع لمعظم الانشطة والشركات هو في طور النهاية (البحراني،2002، ص 60).

4.1.4. تأثير النسيج الشبكي في مدن عصر المعلوماتية:-

إن هيمنة تكنولوجيا الاتصال على المنجزات التكنولوجية لهذا العصر جعلت نمط النسيج الشبكي يشكل الهيكل الأساسي لعصر المعلوماتية. حيث أشار (كاستلس Castells) في هذا الصدد - إن الشبكات ستكون مورفولوجية المجتمع-. كما أطلـق (باتين

Batten)على المدن المتداخلة مع شبكة الاتصال بـ المدن الشبكية Network City (Batten, 1994, p 2). وإن هذه التفاعلات المعقدة بين المدن كأماكن ثابتة وبين الشبكات كثيفة الانتقال(شبكات الاتصال) تُشكل الحياة الحضرية والتطور الحضري لعصر المعلوماتية (Graham & Marvin, 1996, p 71). وما زال الحديث عن النسيج الشبكي للاتصال ودوره في صياغة شكل وهيئة مدن القرن الحادي والعشرين، حيث أكد (كاستِلس Castells) إن ضم الشبكات الحزمية لتكنلوجيا الاتصال للمناطق ضمن وبين الفضاءات الحضرية يدعم مادياً ديناميكية وإنتاج لا مساواة هائلة للترابط العالمي الكثيف. كما دعا(كاستِلس) في الوقت نفسه إلى التجمع ألعلائقي Relational للمدن حيث تظهر كعقدٍ عالمية تربط بينها محاور الألياف الضوئية، مما يجعلها تُشكل مواقع استراتيجية تُمفصل الشبكات الحزمية العالمية (Castells ,1996, P 366-380). وفي الوقت نفسه نجد إن نمط النسيج الشبكي في واقع الأمر لا ينحصر تأثيره ضمن المجتمع الواحد وإنما يهيئ لنا محيطاً عالمياً واسعاً يتميز باللامادية واستبعاد احتكاك المسافة، وهذا المحيط يجمع في أساسياته صفتي التجمعية Convergence والترابطية Connectivity للعقد المكونه لهذا النسيج المحيطي، فهو يضم جميع العقد في هذه النظام العام (ويمكن اعتبار المدينة عقدة أو شبه نظام Sub-System) وتزيد ترابطها في شبكة متكاملة من قنوات الاتصال(المحاور) كما في الشكل(2). ويرى البعض إن هذه الشبكة ربما تخلق نوعاً من الهرمية العالمية للعقد الاتصالية، وهذا ما يجعل شبكة الاتصال ربما تسلك سلوكاً غير محايدٍ ومتحيز لعقد(أقاليم أو مدن) معينة ضد عقد أُخر بالاعتماد على مفهوم المنافسة التي تعطى الهيمنة للعقد ذات المستوى الاتصالي الأفضل والتي تَختار أساساً العقد الصفوة، وهذا ما يجعل من اللافت للنظر إن المدن المتطورة اتصالياً هي من تملك مؤشرات الهيمنة دون غيرها على الرغم مما تحمله شبكات الاتصال عبر فراغاتها التدفقية من دعوة لخلق مستويات متشابهة في أي جزء من أجزاء الكيان الفضائي الكبير اعتماداً على نمط عملها(البحراني،2002، ص 61).

4.2. هيئة مدن عصر المعلوماتية - مدن التوابع المعلوماتية -:-

ظهرت فكرة (المدن التابعة Satellite Towns) لأول مرة بمعرفة المخطط (رايموند Raymond) عام 1922، ووضح تأثره بنظرية المدينة الحدائقية التي جعلها تابعةً لمدينةٍ رئيسة، وكان السبب الرئيس لاعتماد هذا النموذج من المدن هو تجاوز المدن لحجم معين مما قد اضطر المدينة لأن تبحث عن وسائل تُخفف بها عن نفسها من الضغط المتزايد (الاشعب، 1983 ص، 87).كما في الشكل(2) ومن ملاحظة أُسس تكنلوجيا الاتصال ومفرداتها الفرعية نجد إن هذه النظرية تُعد أكثر نظريات التخطيط ملاءمةً لتطبيق النموذج الخاص بمدينة عصر المعلوماتية، هذا إن لم تكن ستصبح واقعاً ملموساً كون إن تأثيرات

تكنلوجيا الاتصال تُشكل فعلاً حتمياً لا يمكن تجاوز تأثيراته، ولكن إذا ما طُبقت هذه النظرية فإنه حتماً ستكون هنالك اختلافات بين مميزات المدن التوابع التي ظهرت مطلع القرن الماضي والمدن التوابع التي من المتوقع أن تظهر في مطلع القرن الحادي والعشرين، إذ تمتاز مدن توابع عصر المعلوماتية بكونها مدناً تُحقق سياسة تصغير التجمع العمراني وتعدد النوى –المستقلة والمكتفية ذاتياً- بفعل التداخل والانضغاط والاندماج لعناصر منظومة المدينة والذي تحقق نتيجة تغلغل أنظمة وشبكات تكنلوجيا الاتصال في وبين عناصر تلك المنظومة، هذا بالإضافة إلى ميزة الانتشار الأفقي التي يغلب على ترابطها النسيج الشبكي ولكن ستكون مدناً توابع لا تُشكل ظهيراً محلياً- أي غياب مفهوم - المدينة العواصمية- التي تجمع باقي المدن التوابع حولها ضمن الحدود الجغرافية المحلية- وفي ذلك فقدان لكثير من الخصائص المحلية التي تُعطي للمدينة تَميزها وشخصيتها، وتجعلها عرضة للذوبان في شبكة الاتصال العالمية. **وبناءاً على ما طُرح يخرج البحث بتعريف مبسط للمدن التوابع المعلوماتية استناداً إلى الخصائص التي أوجدتها أُسس تكنلوجيا الاتصال وهو (إن المدن التوابع المعلوماتية هي تجمعات عمرانية صغيرة الحجم تُحقق الإتحاد بين المادية والخائلية، وتمتاز بإنها ذات منظومات مدمجةً ومضغوطة بفعل بنيتها التحتية التكنلوجية ذات النسيج الاتصالي، فهي إذاً مدن مكتفية ذاتياً اقتصادياً واجتماعياً وعمرانياً، وتُشكل عقدةً من عقد النسيج الشبكي العالمي، حيث إنها وعلى الرغم من اكتفائها الذاتي إلا إنها تُعد مدناً تابعةً على أساس ترابطها العالمي- ذو الهيمنة الاتصالية- وليس على أساس كونها توابع وظهيراً محلياً للمراكز العواصمية ضمن الحدود الجغرافية). كما في الشكل(3).**

4.3. تأثير التواصل في مدن عصر المعلوماتية:-

لقد بينت الفقرات السابقة كيف إن أُسس تكنلوجيا الاتصال قد ساهمت بشكل كبير ومؤثر في صياغة شكل وهيئة مدن الآلفية الثالثة، من خلال إنتاجها لمدن التوابع المعلوماتية ذات التبعية العالمية والبعيدة الارتباط ضمن المدار المحلي ذو الحدود الجغرافية التي ألغاها النسيج الشبكي لتكنلوجيا عصر المعلوماتية. وإن هذه المدن التوابع باتت تسعى اليوم من خلال ارتباطها بشبكة النسيج العالمي الى أن تكون عقدة من عقد ذلك النسيج ذو الهيمنة التكنلوجية، لا ظهيراً محلياً للمدن العواصمية كما كان متعارف عليه في السابق. وهذا ما يعد مشكلةً أساسية تواجه الهيئة الجديدة لمدن القرن الحادي والعشرين، حيث إن هذا التفكك في الارتباط للمدن المحلية من شأنه أن يجعل منها كيانات معزولة محلياً وفي الوقت نفسه يجعل منها نُسخاً مكررة عن النماذج العالمية التي يسعى الإسلوب الجديد لتكنلوجيا الاتصال إلى

فرضِها. وعليه إذاً فلا بد للمدن من أن تواجه ذلك الإسلوب باستراتيجية تُحقق لها اللحاق بركب هذه الثورة التكنلوجية مع حفاظها في الوقت نفسه على كيانها ونموذجها المتميز. وهذا ما يحمل معنى التطور الذي تنشده المنظومة التواصلية ذات الأُسس الاجتماعية المتمثلة بـ**(نظرية التواؤم- الخصوصية- التغذية الاسترجاعية)** التي تُعطي للآخر شخصيتهِ وكيانهِ، هذه الأُسس التي تُقيم بها المجتمعات والأفراد وكياناتهم مدى الاستجابة ومقدار التكيف مع مستجدات المنظومة التكنلوجية للاتصال. وفي هذا تأكيد على إن التواصل من خلال هذه المرونة لا يقف بالضد من مفهوم الاتصال وتقنياته، وإنما يسعى من خلال منظومته أن يجعل الاتصال بكل امكانياته المتاحة في هذا القرن جزءاً من المنظومة التواصلية. حيث إن التواصل يرى إنه وعلى الرغم من التأثيرات الحتمية للاتصال ذات الإسلوب العالمي إلا إنه في الوقت نفسه يوفر فرصةً كبيرةً وجديدة للمنجزات المتحققة أن تقطع المجتمعات طولاً وعرضاً بسرعة لا متناهية حاملةً معها رجع الصدى الذي يعكس بدوره الواقع الحقيقي والتميز للمجتمعات والأفراد، مع بيان مقدار وحجم الازاحة التي بالإمكان أن تتحقق في مواكبة التطورات دون المساس بالثوابت والخصوصية.

4.3.1. <u>تأثير نظرية التواؤم في مدن عصر المعلوماتية:-</u>

إن النظريات المختلفة للإنسان لم تكن سوى استجابات فكرية لمتطلبات الواقع ومشكلاته وتساؤلاته التي كانت تعرض للإنسان ذاته وما تلك النظريات إلا التعبير النظري للإنسان عن تجاربه وتفاعله مع حقائق الواقع الموضوعي ونضاله من أجل إيجاد المخارج والحلول لمشكلات واقعة وكثيراً ما تأتي النظريات خيالية وغير قادرة على الاستجابة لمستلزمات الواقع فيبقيها الإنسان تراثاً فكرياً ودليل عمل لأنشطته من أجل الوصول إلى حالات نظرية أكثر واقعية وأكثر فاعلية في التطبيق ومن ثم أكثر قُدرة على حل المشكلات التي يواجهها. لقد طُرحت العديد من النظريات والبدائل التي تسعى لتكون الحل الأمثل في مواجهة تحديات تكنلوجيا الاتصال، وفيما يأتي عرض موجز لبعض تلك النظريات:-

- نظرية الانعزال Theory of Seclusion :- والتي تتلخص باللجوء إلى الموروث والانطواء والانعزال
- بالفكر التقليدي خوفاً من التغيير، نتيجة التعلق بمفاهيم تصور سلبية التحديث خوفاً من الذوبان والانصهار في النسيج الشبكي للإسلوب العالمي لتكنلوجيا الاتصال.
- نظرية الاندماج Theory of Merging :- وهي القبول المطلق لكل إفرازات الحضارة العولمية بإيجابياتها وسلبيتها، مع الخلط التام

لكل المناهج المستوردة، على اعتبار أن الآلات والتكنولوجيا هى منجزات علمية تعبر عن قمة الحضارة، وإن المتخلف عن ركبها يعبر عن الرجعية بعينها، وهى مرفوضة من وجهات النظر العقائدية والاجتماعية وغيرها.

- نظرية التحدى Theory of Challenging:- تحتاج هذه النظرية إلى قدرات ومهارات عالية، وأكثر من ذلك إنها تحتاج إلى عقول مفكرة وعزيمة فائقة وقدرات مادية وتنظيمية عالية، لدخول حلبة التنافس والتفوق على المد العالمى الغربى والشرقى.

- نظرية التواؤم Theory of Adaptability:- تتناول هذه النظرية حتمية التغيير والتواؤم مع المستجدات العالمية، والانتقاء الحذر الذى يقوم على الفحص والتدقيق، حيث إن هذه المستجدات قِوامها اليوم هو المعرفة. وهذا ما أكد عليه البحث في المحورالاول(عصر المعلوماتية)،
- وهذا بدوره ما يصنع اليقين بأن الرجوع إلى الوراء أمر مستحيل وإن دخول حلبة المنافسة لهذه الثورة التكنلوجية أمر واجب النفاذ، وبعيداً عن حمى ونعرة "التراث" وقضايا الدفاع عنه، والتباكى على أهداب الماضى ونبذ كل ما هو جديد. **وبناءاً على ما طُرح يرى البحث إن نظرية التواؤم هى أكثر النظريات قبولاً، إذ إن هذه النظرية تفرض حتمية التغيير مع شرط الانتقاء الحذر من كل ماهو مستجد وخارجي، حيث تُؤكد على مدى التأثر بأساليب حياة وحضارة (الأنا) ذو النفوذ التكنلوجي لا يرجع إلى قوته ومدى إختراقيته هو، وإنما يعود إلى مديات الطاقة الكامنة بداخل(الآخر) وقدرتة على مجابهة تحديات (الأنا) من خلال الأرضية المشتركة التي خلقتها تكنلوجيا الاتصال ومنجزاتها التكنلوجية متمثلةً بـ النسيج الشبكي والفضاء الخائلي.**

4.3.2. **<u>الخصوصية وهيئة مدن عصر المعلوماتية:-</u>**

إن الطاقة الكامنة بداخل(الآخر) وقدرتة على مجابهة تحديات (الأنا) وإسلوبه العالمي الجديد في ظل هذه الثورة الاتصالية إنما تتأتى من أحد أهم الأسس التي أوجدتها منظومة التواصل وهي الخصوصية... والتي تتشكل في سياق **العالم المعاش** "Living World المؤلف من(الشخصية والمجتمع والثقافة)، فهي كما رأينا تُشكل عوارض التحدي في مواجهة الإسلوب العالمي الجديد لتكنلوجيا الاتصال، ولكن في الوقت نفسه لا تقف بالضد من تلك التكنلوجية وإنما تُشكل القاعدة

الرصينة التي تُحقق فعل رجع الصدى لكل ماهو قادم من خارج الحدود وبالتالي يحصل التلاقح الحضاري القائم على التآخي الاختياري بعيداً عن الحتمية التكنلوجية للاتصال. ومن هذا المنطلق فإن التأكيد على الخصوصية يقوم على شقين رئيسيين هما:-

- التأكيد على خصوصية المدن ومفردات عالمها المعاش(الشخصية، المجتمع، الثقافة).
- التأكيد على مواكبة التكنلوجيا بما يضمن التطور والاستمرارية. **وبالاعتماد على مفردات الخصوصية سوف تُعاد صياغة شكل وهيئة المدن التوابع للقرن الحادي والعشرين بإسلوب يؤكد على الخصوصية ومفرداتها الفرعية، بالشكل الذي يقوي ارتباط تلك المدن التوابع ضمن النسيج المحلي ويجعل منها ظهيراً للمدن العواصمية المركزية مع إفساح المجال لها في الوقت نفسه إلى أن تُهيأ نفسها لتُشكل عقداً ضمن نسيج شبكة الاتصال العالمية.**

4.3.3. **التغذية الاسترجاعية وهيئة مدن عصر المعلوماتية:**

لقد بين البحث في طرحه لمبادئ التواصل إن التغذية الاسترجاعية تُمثل أهم العوامل التي يركز عليها البحث في طرحه لمفهوم التواصل كونها تُعد الوسيلة التي تُقيم بها المجتمعات مدى استجابتها للمستجدات والمؤثرات الخارجية وبالتالي تحديد ردود الافعال واستراتيجيات التَكيف مع تلك المستجدات والمؤثرات. إن التغذية الاسترجاعية أو رجع الصدى لكفيلة بأن تكسب المجتمع الحديث القدرة على تصويب أخطائه ذاتياً، والتكيف ديناميكياً مع كافة المتغيرات الاجتماعية والاقتصادية والتكنلوجية، وهي بذلك تُشكل الوسيط بين خصوصية الأفراد والمجتمعات وثقافاتهم وبالتالي خصوصية المدن والمستجدات التكنلوجية والمؤثرات الخارجية، كما هو موضح في الشكل (4). حيث إن حقيقة تطور الأُمم والمجتمعات تعتمد اساساً على مدى قدرتها على التواؤم مع المتغيرات اللازمة لتطوير حركتها التصاعدية وعلى نوعية استجابتها للتغيرات الخارجية والداخلية معاً. **وخلاصة القول إن منظومة التواصل من خلال أُسسها المتمثلة بـ(الخصوصية ورجع الصدى ونظرية التواؤم) إنما تُمكن المدن من امتلاك القدرة على خلق الحوار المتكافيء مع(الأنا) تحقيقاً لمبدأ التآخي الاختياري بعيداً عن حتمية الإسلوب العالمي، من خلال امتلاكها سمة الضبط الذاتي الناجم عن رجع الصدى والذي يعمل على الاستشعار لمدى الحيود والانحراف عن الثوابت والمعايير والأهداف المرسومة.**

وبعد دراسة دور الأُسس الخاصة بالمنظومة التواصلية في تشكيل هيئة مدن عصر المعلوماتية، فإن البحث يخرج بتعريف مبسط للمدن التوابع المعلوماتية استناداً إلى الخصائص التي أوجدتها تلك الأُسس وهو (تجمعات عمرانية صغيرة الحجم تُحقق الاتحاد

بين المادية والخائلية، وتمتاز بأنها ذات منظومات مدمجةً ومضغوطة بفعل بنيتها التحتية التكنلوجية ذات النسيج الاتصالي، فهي إذاً مدن مكتفية ذاتياً اقتصادياً واجتماعياً وعمرانياً، وتُشكل عقدةً من عقد النسيج الشبكي العالمي، ولكنها، وعلى الرغم من اكتفائها الذاتي وارتباطها بالنسيج العالمي إلا إنها تُعد بالدرجة الاولى مدناً تابعةً وظهيراً محلياً للمراكز العواصمية ضمن الحدود الجغرافية). والشكل (5) يوضح الهيئة التخطيطية لمدن عصر المعلوماتية(مدن التوابع المعلوماتية) بفعل تأثير أُسس منظومة التواصل.

4.4. أمثلة تطبيقية :-

إن كانت بعض دول العالم قد قدمت نماذج مميزة لهذه المدن التوابع المعلوماتية كما في مدينة كاواساكي في اليابان ومدينة بوتراجايا في ماليزيا ومدينة بونديونك في اندونيسيا، فإن الدول العربية قد خطت خطوات تُعد بدائية في هذا المضمار المتعلق بتظافر المنظومة الاتصالية والتواصلية مع منظومة المدن كما هو الحال في مدينة السادس من أُكتوبر في جمهورية مصر العربية.أما التجربة العراقية للعاصمة استهدف تغيير طبيعة التكتل الحضري لها مع باقي المدن اليابانية الأُخرى،

a- طبيعة الارتباط بينهما. وتُعد كاواساكي إحدى المدن المتنافسة لهذا الموقع، حيث تتميز بالوقوع على مقربة من العاصمة ومن شبكة المواصلات الرئيسية المتضمنة مطار طوكيو

في هذا المجال لم تدخل بعد حيز التخطيط أو التنفيذ، إذ اقتصر الأمر على تقديم العديد من البحوث والدراسات لوضع لِبنات استراتيجية قيام هكذا مدن جامعة لكل من الخصوصية المحلية وأحدث تقنيات الاتصال وتكنلوجيا تبادل المعلومات بما يحقق قيام مدن عراقية تتبنى نظرية التواؤم مع مستجدات عصر المعلوماتية وشبكة اتصالاته العالمية. وبناءاً على ذلك يقدم البحث مدينة كاواساكي نموذجاً تطبيقياً لهذه المدن.

مدينة كاواساكي Kawasaki – اليابان (2001) :-

موقع المدينة:- تقع مدينة كاواساكي إلى الجنوب من العاصمة طوكيو على ضفاف نهر تاما بالقرب من مدينة يوكوهاما، فهي مطلة على الجهة الشرقية على خليج طوكيو وتمتد 33 كم من الجنوب الشرقي إلى الشمال الغربي وبمساحة (142.63 كم^2) الشكل (6).

ولما كانت الفكرة المستقبلية لتخطيط منطقة العاصمة تتجه نحو اللامركزية في الفعاليات المتجمعة حالياً في طوكيو، فإن المخطط الجديد

من خلال محاولة إيجاد مدن نواة جديدة ذات استقلالية واكتفاء ذاتي بالشكل الذي يغير الدولي، خليج طوكيو بالإضافة إلى شبكة السكك الحديد وخطوط المرور السريعة التي تربطها بالمدن الداخلية كما في الشكل (7). وجميع هذه المواصلات تعتمد سياسة تكنلوجية

متقدمة في الاتصال. أما على الصعيد العالمي فإن مدينة كاوسـ ـاكي تُعد نموذجاً متميزاً لمدن التوابع المعلوماتية... فهي تقـ ـع ضمن منطقة أسيا – باسيفيك حيث مجال عملها ولها امتدادات إلى بقية انحاء العالم من خلال الألياف الضوئية، وهي بذلك تدخل ضمن سياق التجمع العلائقي لمدن النسيج الشبكي لتكناوجيا الاتصال من خلال سعيها لتُشكل عقدةً متقدمة من عقد ذلك النسيج العالمي.

b- **تخطيط المدينة:-**

تعد مدينة كاواساكي من المدن القائمة التي تتصف بمعالم تاريخية وطبيعة متعددة إذ تمتاز بصفة صناعية بالإضافة إلى المعالم التاريخية والمباني التراثية، كالمعالم التاريخية لمعبد كاواساكي وإيشي والمساكن اليابانية التراثية في منطقة إيكونا الخضراء، والمناطق السكنية ذات السمات التاريخية فضلاً عن المناطق الحديثة. وبذلك فإن مدينة كاواساكي متعددة الخصائص ترتبط بأنشطة حضارية متكاملة وهو ما يكسب المدينة خصوصية حضارية وتراثية مميزة لها ولباقي المدن اليابانية.ولهذا فإن التوجهات التخطيطية للمدينة التي بدء التنفيذ بها مطلع القرن الحالي تتميز بتوجهها نحو فضاءات حضرية تعتمد شبكة تكناوجيا الاتصالات وهذا الإتجاه جاء نتيجة التحول الحاصل في طبيعة الصناعات الموجودة في كاواساكي ضمن مدينة صناعات معتمدة على المادة إلى مدينة صناعات معتمدة على المعرفة المركزة، فظهرت المشاريع الجديدة منها مدينة مايكوم (Mycom City) ومدينة مايكرو كومبيوتر (Micro Computer City) ومنطقة محطة كاواساكي وجزيرة الميناء المدني ومركز ناشيكمادا التجاري ومشروع المترو الجديد الممتد على طول المحور العمودي للمدينة بالإضافة إلى متنزة العلوم. حيث إن المدينة تسعى لتحقيق التوازن بين خصوصيتها الحضارية والمستجدات التكناوجية.

c- **إستعمالات الاراضي:-**

نظراً لتوجهات المدينة التخطيطية الحديثة نحو المعلوماتية والاتصالات فقد أصبح من الضروري تحديد الهوية الجديدة لمدينة كاواساكي حيث إنها تُمثل مرحلةً جديدة وستبقى في الأذهان عبر الأجيال، ولهذا فإن مدينة كاواساكي بصدد الدخول في عصر جديد يمتاز بالإبداع والإبتكار ومفاهيم جديدة لتخطيط المدينة، والذي اعتمد على دمج منظومتي المعلومات والاتصالات مع البنية الحضرية ، وكانت القرارات نتيجة لوضع المدينة الحالي بعد أن اتخذ الأساس الحضري فيها موقعه وتم تحديد استعمالات الفضاءات وهذا ما جعل من الصعب توسيع الرقعة الحضرية شكل(8)، بالاضافة إلى تغير المستوى الثقافي والاجتماعي للمواطنين وظهور الحاجة إلى نوع جديد من الأنشطة والخدمات التي تفرض حتمية التغيير.

إن المنظومة الاتصالية التي يستند إليها مخطط كاواساكي الجديد ذات تقنية وتخصص

عالٍ، حيث يهدف المخطط إلى دمج النسيج الشبكي للاتصال مع البنية الحضرية بهدف خلق شبكة تعمل على خدمة المجتمع بصورة فعالة ولإنجاز ذلك يتطلب توفير منظومات رئيسة وهي :-

1. منظومة اتصالات ومعلومات لربط ساحات الذكاء متعددة الأنشطة(المدنية والثقافية والاقتصادية).
2. منظومة اتصالات ومعلومات لربط أجنحة ومواقع الأنشطة.

منظومة اتصالات ومعلومات لربط الفضاءات والمنشآت. إن سياسة التخطيط الجديدة في مدينة كاواساكي كانت من السياسات المهمة في كيفية التعامل مع البيئة الحضرية من خلال استعمال واستخدام التكنلوجيا المتطورة للاتصال وجعلها في خدمة النسيج الحضري للمدينة الذي يتميز بنسيج عمراني ذي هوية مميزة، وتم ذلك من خلال تبني خطة دمج منظومة الاتصال التكنلوجية في محاولة إضافة هوية جديدة تتميز بسياسة محاولة تحقيق التواؤم بين البنية الحضرية المادية ومنظومة الاتصالات وشبكتها النسيجية، جاعلةً من المدينة شبكةً واحدةً تتميز بساحات ذكية تربط جميع المجالات الاقتصادية والتجارية والاجتماعية و الثقافية، إذ كونت منظومة اتصالات متطورة تجعل من مستخدميها(سواءاً أكان المستخدم فرداً أم مؤسسة) يحصلون على جميع المعلومات بسهولة و سرعة. لقد سعى المخططون إلى تحقيق هدفهم من خلال محاولة الحفاظ على الهوية والخصوصية المحلية للنسيج الحضري مدعماً بشبكة معلوماتية واتصالاتية حديثة تخدم المجتمع وتحقق في الوقت نفسه الارتباط العالمي. ولكن لا يمكن قياس مدى نجاح هذه الساسية على المدى القريب، ويعود السبب في ذلك الى ارتباطها بالعوامل الاجتماعية التي تحتاج مدة زمنية أكبر لدراسة النتائج المترتبة عليها. وبناءاً على ما سبق نجد :- إن التصميم والتخطيط الحضري الجديد للعاصمة طوكيو(المدينة الام) قد اعتمد تطبيق مؤشرات المنظومة التكنلوجية للاتصال، ولكن بدرجات متفاوتة وهذا ما يشكل تدعيماً لسياسة المدن التوابع المعلوماتية والتي تُعد مدينة كاواساكي أحد هذه المدن المتنافسة على ذلك نظراً لمميزاتها سابقة الذكر. وإذا ما تفحصنا كل مؤشر على حِده فيتضح لنا ما يأتي:-

1. **سياسة التصغير:-** نجد إن مدينة كاواساكي طبقت هذه السياسة من خلال سعيها لِتكون نواة معلوماتية مكتفية ذاتياً من خلال اعتماد استراتيجية دمج الأنشطة والفعاليات الحضرية المتحققة عن طريق استخدام منظومة المعلومات والاتصالات لربط مواقع تلك الأنشطة والفضاءات وتداخلها مع بعضها البعض.

2. **سياسة الانتشار الأفقي :-** نجد إن ظهور هذا المؤشر يتحقق من خلال اعتماد تكنلوجيا الواقع الخائلي ذو البعد الاتصالي. فعلى الرغم من من علاقة المدينة مع شبكة

المواصلات الرئيسية إلا إن استخدام تكنلوجيا الاتصال وأليافها الضوئية قد أضعف الحاجة إلى البعد الفيزيائي الرابط بين المدينة مع المدن الأخرى ومن ضمنها العاصمة(طوكيو).

3. **اللامركزية والتوازي :-** إن هذا التوجه نراه يظهر من خلال الاعتماد على تصميم مدينة طوكيو(العاصمة ألام) الذي يتجه نحو اللامركزية في الفعاليات المتجمعة حالياً في طوكيو، وهذا ما انعكس بدوره على التوجهات التخطيطية لمدينة كاواساكي.

1. **4. النسيج الشبكي:-** إن ظهور هذا المؤشر قد وجد صداه في مدينة كاواساكي داخلياً وخارجياً، حيث إن المنظومة الاتصالية التي يستند اليها مخطط المدينة الجديد يهدف على المستوى الداخلي إلى دمج النسيج الشبكي للاتصال مع البنية الحضرية بهدف خلق شبكة تخدم المجتمع وتربط الفضاءات التي أصبح من الصعب توسيع رقعتها الحضرية. أما على الصعيد العالمي فنجد إن النسيج الشبكي للاتصال يوفر فرصة لدخول مدينة كاواساكي ضمن التجمع العلائقي للمحيط العالمي لكونها تقع ضمن منطقة أسيا – باسيفيك.

أما فيما يخص ربط تخطيط المدينة مع **مؤشرات منظومة التواصل** فإننا نجدها تتحقق من خلال التوجه الجديد للمدينة نحو المعلوماتية والاتصالات، والذي يعني حتمية التغيير لتحقيق التطور والاستمرار. وهذا ما دفع القائمين على تصميم وتخطيط المدينة الى وضع تحديد الهوية الجديدة للمدينة في أولويات ذلك التخطيط نظراً لكونها مدينة ذات نسيج اجتماعي متميز وتحوي خصائص متعددة ترتبط بأنشطة حضارية متكاملة. حيث إن الاعتماد على الخصائص الحضرية للمدينة قد دفع المصممين إلى تبني سياسة استخدام ذكية لتكنلوجيا الاتصال، عملت على جعل هذه التكنلوجيا في خدمة النسيج الحضري وليس العكس، وفي ذلك محاولة لتحقيق هدف منظومة التواصل وهي الحفاظ على الهوية والخصوصية المحلية للنسيج الحضري مدعماً بشبكة معلوماتية واتصالاتية حديثة تخدم المجتمع وتحقق الارتباط العالمي في الوقت نفسه وفي ذلك سعي لتحقيق مفهوم التغذية الاسترجاعية. ولكن وعلى الرغم من ذلك فإنه ليس من السهولة تحديد مدى درجة نجاح هذه السياسة في تسخير تكنلوجيا الاتصال لتحقيق خصوصية المدينة اعتماداً على المستجدات التكنلوجية والمؤثرات الخارجية

-5. الاستنتاجات والتوصيات :-

- إن القرن الحادي والعشرين هو عصر المعلوماتية، فهو عصر قائم على اقتصاد المعلومة وسرعة تداولها.
- إن لعصر المعلوماتية منظومة قائمة على تعاضد وتكامل كُلاً من(المنظومة التكنلوجية للاتصال- والمنظومة الاجتماعية للتواصل) فلا يمكن الارتكان لإحداهما دون الأخرى، كما لا يمكن نجاح إحداهما بمنأى عن الأخرى.

فمنظومة هذا العصر هي (كِلا المنظومتين معاً).

- إن (مدن التوابع المعلوماتية) تُمثل النموذج العالمي الذي تطرحه تكنلوجيا الاتصال، والقائم على الأُسس والمعطيات للإسلوب العالمي الذي جاءت به تلك التكنلوجيا، محاولةً فرضه كـ نموذج كوني وحتمي لمدن القرن
- وبين معطيات تكنلوجيا الاتصال، هذا التواؤم الذي لايقف بالضد من التكنلوجيا وإنما يجعلها وسيلة لتحقيق التطور في المدينة ومنظومتها .
- إن هذه الرؤية المستقبلية لهيئة مدن القرن الجديد إنما وضعت كافة مدن العالم وفي مقدمتها المدن العربية أمام تحديات هذا العصر ومنظومته التي طالت كافة جوانب الحياة الحضرية.
- ضرورة العمل على تفهم المكونات المختلفة لمنظومة عصر المعلوماتية، وكذلك التعرف على متطلبات كل مكون منها وتأثيره المباشر وغير المباشر على المدينة كونها تُشكل هي الأخرى منظومة تسعى للوصول لحالة التوازن والتكيف مع كافة المستجدات لتحقيق التطور والاستمرار.
- إن تأثيرات تكنلوجيا الاتصال هي تأثيرات حتمية لا مناص للمدن منها، لذلك يجب اعتماد وتجهيز الحادي والعشرين. والتي تدفع بخصوصية المدن وخصائصها المحلية – تلك الخصائص التي تُوجِد الاختلاف المولد للحضارات- إلى الانصهار في بوتقة العالمية والعمومية. وفي ذلك تآكُل للمدن وإنهياراً لحضاراتها.
- أما منظومة التواصل المطروحة هنا إنما تسير بالمدينة نحو تحقيق التواؤم بينها بنية أساسية لتلك التكنلوجيا في التصميم الهيكلي للمدينة.
- من الضروري أن تُصيغ مجتمعات مدن عصر الآلفية الثالثة القوانين والتشريعات الجديدة والتي يمكن من خلالها ضبط وإدارة الحياة في هذا العصر، بهدف تيسير واستيعاب وتوظيف تلك التكنلوجية بالشكل الأمثل.
- ضرورة الأخذ بالأبعاد الاجتماعية والثقافية عند النظر إلى هيئة وشكل مدن القرن الجديد، حيث يجب النظر إلى الموضوع على إنه تحدي اجتماعي ثقافي أكثر من كونه تحدي تكنلوجي أو تقني.

6- المصادر :-

1. **Batten, D.,** “Network Cities, Flexible Urban Configurations for the 21st Century” Mimeo, 1994.
2. **Castells. M.,** “The Rise of Network Society”, Oxford: Blackwell, 1996.
3. **Charles, C.,** “social organization”, J.lohisse, la communication anonyme. Ed. Universities 1969.

4. **Graham, S. and Marvin, S.,** "Telecommunications and The City Electronic Space, Urban Place", Routledge , London and New York, 1996.
5. **Graham, S. and Marvin, S.,** "Planning Cyber-Cities? Integrating Telecommunications in to Urban Planning",Town Planning Review 70 (1), 1999.
6. **Groak, Steven,** "The Idea of Building- Thought & Action in the Design & Production of Building", E & FN Spon, London, U.K, 1993
7. **Muchielli R.**, "Communications et Reseaux de Communication Ed", E.S.F Paris, 1980.
8. **Pacey, A.,** "The Culture of Technology", the MIT Press, Cambridge, Massachusetts, 1991.
9. **Simmonds, R. and Hack, G.,** "Global City Region", Their Emerging Form, 2000.
10. **Toffler, A.,** "The Third Wave", Bantam Books, 1980.
11. http://www.kian.or.jp/home/guidetok
12. http://directrooms.com/japan/maps/kawasaki-maps.htm
13. **أفاية، محمد نور الدين**،" الحداثة والتواصل في الفلسفة النقدية المعاصرة: نموذج هابيرماس"، أفريقيا الشرق، بيروت، لبنان، 1998.
14. **الأشعب، خالص حسني، صباح محمود محمد**، "مورفولوجية المدينة"، جامعة بغداد، 1983م.
15. **البحراني، صفاء صالح** ، " اثر نمط الشبكة المعلوماتية في التغيرات الفيزياوية و الوظيفية للمدينة "، رسالة ماجستير مقدمة إلى مركز التخطيط الحضري و الإقليمي /جامعة بغداد 2002 .
16. **الخوري، هاني**، " تكنلوجيا المعلومات على اعتاب القرن الواحد والعشرين"، مركز الرضا للكومبيوتر، دمشق، 1998 م.
17. **الصفار، مازن ظافر**، " رؤيا مستقبلية لاثر التكنلوجيا المعلوماتية على منطقة الكرادة في مدينة بغداد "، رسالة ماجستير مقدمة إلى مركز التخطيط الحضري والإقليمي /جامعة بغداد، 2006.
18. **الظاهر، نعيم**، " وسائل الاتصال السياحي"، دار اليازوردي، عمان الاردن، 2000 م.
19. **الملاخ، نور الدين**،" مفاهيم في التواصل " ،2005 م . http://www.aljamaa.net/ar/document/2053.shtml
20. **انطوان بطرس**، " المعلوماتية على مشارف القرن الحادي والعشرين"، مكتبة لبنان ، بيروت،1987م.
21. **انعام مجيد**، " جدلية التواصل في تخطيط المدينة العراقية " ، رسالة ماجستير، مركز التخطيط الحضري والإقليمي، 2002 م.
22. **بهاء الدين شاهين**، " شبكة الانترنت "، العربية لعلوم الحاسب ،القاهرة، 1996.
23. **حيدر فرحات** ، " تخطيط المدينة الالكترونية: دراسة تحليلة "، المعهد العربي لإنماء المدن بالتعاون ، مسقط، عمان، 2003 م . http://arabcin.net
24. **طارق محمود**، " مجتمع المعلومات الرقمي "، المركز الاصيل للطبع والنشر والتوزيع ،القاهرة، 2004.
25. **محمود حسن**، " إشكالية التخطيط بمدينة المستقبل العربية بين الثوابت والمتغيرات "، ندوة مدن المستقبل ، المعهد العربي لإنماء المدن،الرياض،2001 م.
26. **نبيل على**، " الثقافة العربية و عصر المعلومات "، سلسلة عالم المعرفة، العدد

265، المجلس الوطني للثقافة والفنون والآداب، الكويت، 2001 م.

27. **ذوبي محمد حسن،** " البعد المعلوماتى ودوره فى صياغة إستراتيجيات تنمية المدن فى القرن الواحد والعشرين "، قسم العمارة، كلية الهندسة، جامعة اسيوط، مصر ،2000.

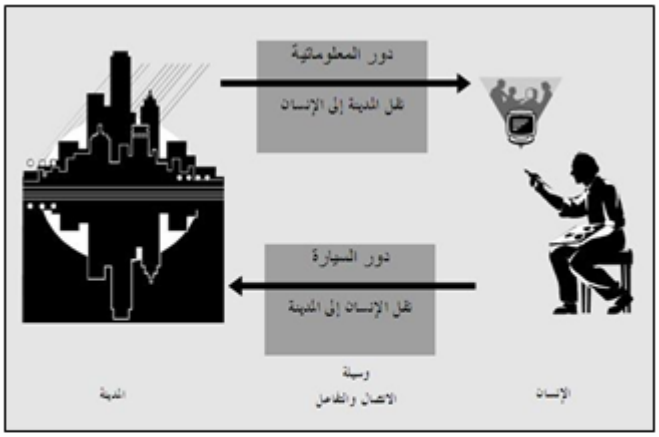

الشكل (1) الاختلاف بين دور السيارة ودور المعلوماتية في تحديد طريقة الاتصال (نوبي محمد، 2000، ص182).

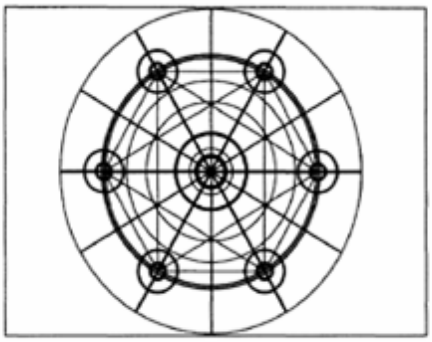

الشكل (2) يوضح نموذج المدن التوابع للمخطط رايموند (Hildebrand Frey , 2005, p 77)

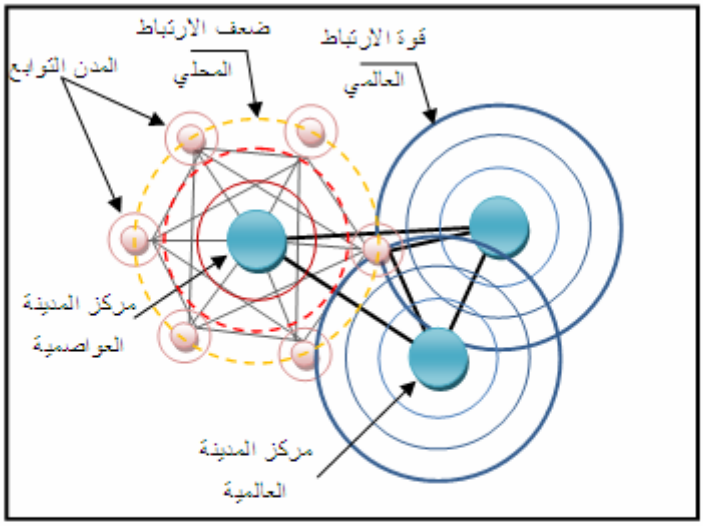

الشكل (3) يوضح الهيئة التخطيطية للمدن التوابع المعلوماتية
بفعل تأثير أُسس منظومة الاتصال (المصدر : الباحثة)

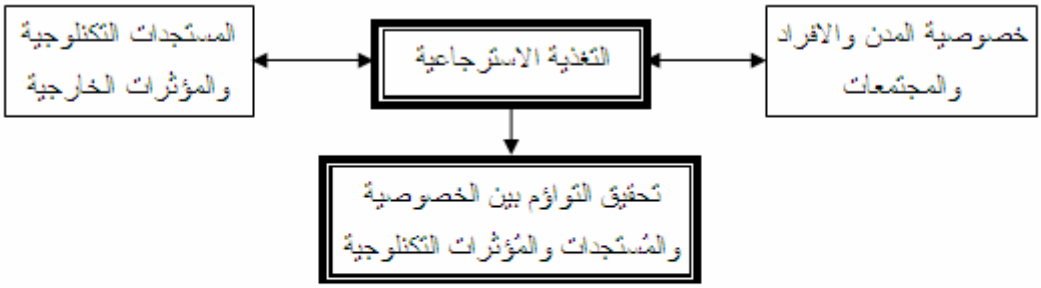

شكل رقم (4) دور التغذية الاسترجاعية في تحقيق التواؤم
بين الخصوصية والمستجدات والمؤثرات الخارجية
(المصدر : الباحثة)

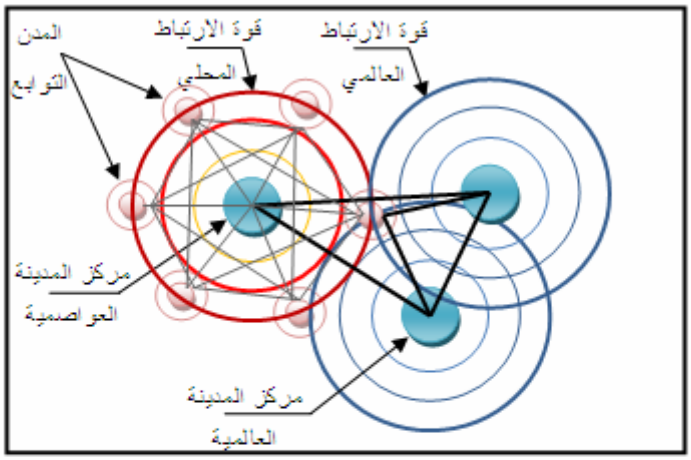

الشكل (5) يوضح الهيئة التخطيطية للمدن التوابع المعلوماتية بفعل تأثير أُسس منظومة التواصل (المصدر: الباحثة)

الشكل (6) يوضح الموقع الجغرافي لمدينة كاواساكي http://www.kian.or.jp/home/guidetok

شكل (7) علاقة مدينة كاواساكي بشبكة المواصلات الرئيسية

http://directrooms.com/japan/maps/kawasaki-maps.htm

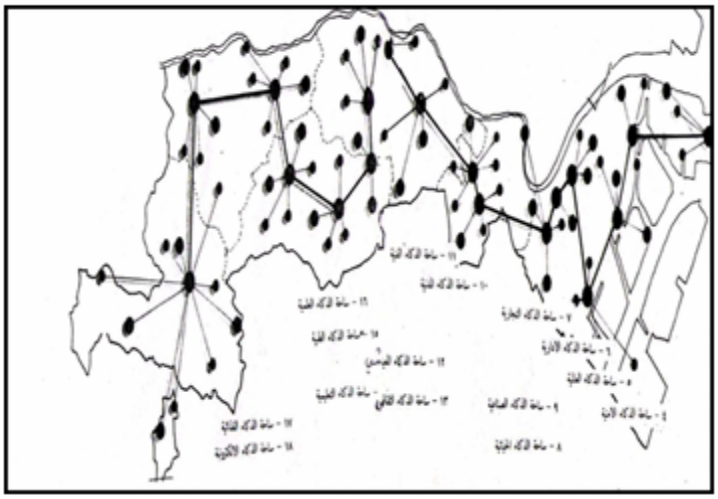

شكل (8) مخطط مدينة كاوساكي يبين مسارات الالياف الضوئية والساحات الذكية في المدينة (الصفار، 2006، ص 72)

CATHODIC PROTECTION OF CARBON STEEL IN 0.1N NaCl SOLUTION UNDER FLOW CONDITIONS USING ROTATING CYLINDER ELECTRODE

Basim O. Hasan and Marwa F. Abdul-Jabbar
Chemical Engineering Department-Al-Nahrain University-Iraq

ABSTRACT

The effect of applied current on protection of carbon steel in 0.1N NaCl solution (pH=7) was investigated under flow conditions (0-0.262 m/s) for a range of temperatures (35-55°C) using rotating cylinder electrode. Various values of currents were applied to protect steel from corrosion, these were $I_{app.}= I_{corr.}$, $I_{app.}=2I_{corr.}$ and $I_{app.}=2.4I_{corr.}$ under stationary and flow conditions. Corrosion current was measured by weight loss method. The variation of protection potential with time and rotation velocity at various applied currents was assessed. It is found that the corrosion rate of carbon steel increases with rotation velocity and has unstable trend with temperature. The protection current required varies with temperature and it increases considerably when the rotation velocity was increased. The protection potential decreases appreciably (shifts to more negative) with time and with increasing rotation velocity. Also it shifts to more positive with increasing temperature.

Keywords: cathodic protection, steel, impressed current flow, salt

الخلاصة

لقد تم دراسة تاثير تيارات مسلطة على الفولاذ الكاربوني في محلول تركيز الملح فيه ٠،١ مولاري وتحت ظروف جريان (٠ - ٢٦٢,. م/ثا) ودرجات حرارة (٣٥-٥٥م°) باستخدام قطب الاسطوانة الدوارة. سلطت قيم مختلفة لتيارات الحماية لحماية الفولاذ الكاربوني من التاكل ، تم تسليط تيار التاكل،ضعف تيار التاكل و٢،٤من تيار التاكل تحت سرع ودرجات حرارة مختلفة ، تم ملاحظة تغير فولتية الحماية مع الوقت ومع السرع في مختلف التيارات المسلطة. وجد ان معدل التاكل للفولاذ الكاربوني يزداد مع السرع ويكون تغيره مع درجات الحرارة غير ثابت وان تيارات الحماية المطلوبة تختلف مع درجات الحرارة وتزداد عند زيادة سرعة الدوران ، وفولتية الحماية تقل (تصبح اكثر سالب) مع زيادة الوقت ومع زيادة السرعة وتصبح أكثر موجب مع زيادة درجات الحرارة.

INTRODUCTION

Corrosion in aqueous solutions is an electrochemical reaction that involves charge transfer oxidation (loss of electrons) and reduction (gain of electrons). Corrosion is a metal dissolution process with the metal ions going into solution [**Fontana and Greene 1986**].

There are many methods for corrosion prevention, one mean of controlling is by the use of cathodic protection. Cathodic protection is an electrochemical technique in which a cathodic protective potential is applied to an engineering structure in order to prevent corrosion from taking place [**Perez 2004**]. Cathodic protection can be applied in practice to protect metals such as steel, copper, lead and brass against corrosion in all soils and in almost all aqueous media [**Uhlig 2008**].

The principle of cathodic protection is either in connecting an external anode to the material to be protected from corrosion or passing of an electrical DC current. So that all area of the metal surface becomes cathodic and therefore do not corrode. The external anode may be a galvanic (sacrifical) anode or it may be an impressed current anode where the current is impressed from external DC source. Cathodic protection requires a source of direct current and an auxiliary electrode (anode) of noble material (such as graphite) located some distance away from the protected structure. The direct current (DC) source is connected with its positive terminal to the auxiliary electrode and its negative terminal to the structure to be protected; in this way, current flows from the electrode through the electrolyte to the structure. The applied voltage is not critical, it need only be sufficient to supply an adequate current to all parts of the protected structure. In waters of high resistivity, the applied voltage must be higher than in environment of low resistivity [**Uhlig 2008**].

Cooling water used industrially removes heat from production processes. It is one of the major applications for water and is a major factor in sitting plants and processes. It often contains some salts that enhance the corrosion of metals. Cooling systems suffer many forms of corrosion and failure [**Roberge 2008**]. The open recirculating cooling water system is one of the most vital units of a petroleum refinery [**Barhai 2010**].

It is well known that the rate controlling step in most natural water corrosion process is the cathodic half reaction. The most important cathodic process in half reaction is generally limited by the speed at which oxygen can reach the surface of the metal. This oxygen is transported from the bulk water to the surface across the boundary layer by diffusion. The boundary layer is defined as the region over which the property of interest, (velocity or oxygen concentration), is affected by the interface. For example, the oxygen concentration will vary from a minimum at the surface to bulk concentration at the outside edge of the boundary layer. This results in the concentration gradient and promotes the transport of oxygen [**Smith 1989**]. If the corrosion process is under cathodic diffusion control then agitation increases the corrosion rate. This effect generally occurs when an oxidizer is present in small amounts, as is the case for dissolved oxygen in acids or water [**Fontana and Greene 1986**].

The mechanism of cathodic protection is simply understood by reference to the following reactions.

$$O_2 + 2H_2O + 4e \rightarrow 4OH^- \quad \text{(cathode)} \quad (1)$$

$$Fe \rightarrow Fe^{2+} + 2e \quad \text{(anode)} \quad (2)$$

Making the surface more negative and increase the concentration of electrons which accelerates the rate of cathodic reaction and decreases the rate of the anodic reaction. (i.e the rate of the anodic reaction becomes zero and the whole surface of the metal becomes cathodic [**Shreir 1976**].

Temperature of the medium governs the solubilities of the corrosive species in the fluid, such as oxygen (O_2), carbon dioxide (Co_2), chlorides, and hydroxides. Temperature increases the rate of almost all the chemical reactions. When the rate determining step is the activation process, the temperature changes have the greatest effect [**Scott 1999**]. In open systems, the effect of temperature is complex in that the diffusivity of oxygen increases, but solubility decreases with temperature increase [**Fotana 1986**, **Scott 1999**, **Uhlig 1976**].

The limiting current is defined as the maximum current that can be generated by a given electrochemical reaction, at a given reactant concentration , under well-established hydrodynamic conditions, in the steady state. This definition implies that the limiting rate is determined by the composition and transport properties of electrolytic solution and by the hydrodynamic conditions at the electrode surface.

aerated waters is oxygen reduction. The rate of this

Nesic et.al.[**1995**] using rotating cylinder electrode, studied the effect of velocity on the limiting current density. For temperature of 22°C and Re up to 26000, the cathodic polarization curves showed that the limiting current density increases with velocity increase.

Konsowa and El-Shazly [**2002**] studied the effect of flow and temperature on the rate of zinc consumption during cathodic protection of a copper pipeline carrying saline water by measured the loss in weight. They found that the rate of zinc consumption increases with increasing solution flow rate and temperature. Also the authors concluded that the cathodic protection in saline water is controlled by the rate of diffusion of dissolved oxygen towards the walls of the copper tube.

Scantlebury [**2006**] studied corrosion of mild steel in marine environments under cathodic protection. Electrochemical studies at the two protection potential namely -780and -1100 mV were examined by different techniques. DC polarization experiments was carried out for mild steel in natural sea water and 18.5g/L NaCl solution to evolve corrosion current density. He concluded that mild steel does not corrode under the protection potentials, viz., -780 and -1100 mV.

Sami and Ghalib [**2008**] studied cathodic protection system for low carbon steel pipe. They investigated the influence of temperature and distance between cathode and anode on the minimum cathodic protection current that would provide a full cathodic protection for steel tube immersed in sea water for temperature range 30-50°C and distance between pipe (cathode) and graphite electrode (anode) of (10-20cm). The experimental results indicated that cathodic protection current density increases with increasing temperature.

The aim of present work is to study the impressed current cathodic protection of steel specimen in 0.1N NaCl solution at various temperatures under flow conditions using weight loss and electrochemical technique (limiting current density) to determine the cathodic currents and potentials required to obtain high protective percents.

EXPERIMENTAL WORK

Figure. 1 shows the experimental apparatus that was used for performing the experimental work.

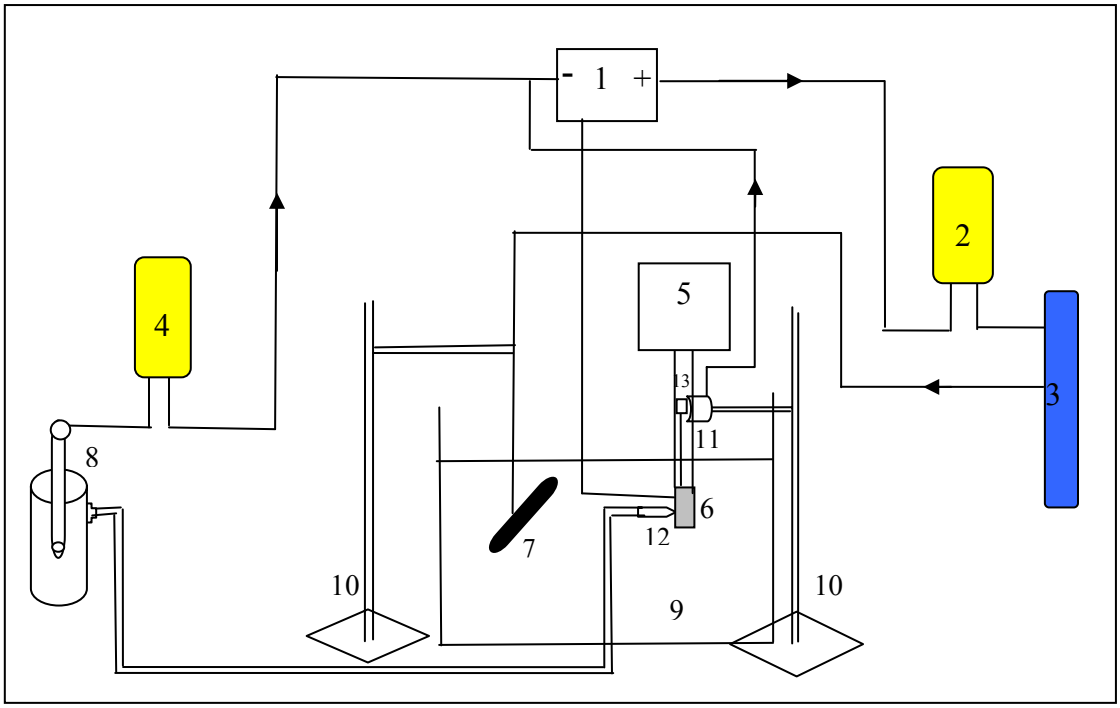

Fig. 1 Experimental apparatus 1) power supply, 2) ammeter, 3) resistance box, 4) voltmeter, 5) stirrer, 6) working electrode (specimen), 7) graphite electrode (anode), 8) calomel electrode (reference electrode), 9) water bath, 10) stand, 11) brush, 12) Luggin capillary, 13) metal for electrical connection with specimen

The experimental apparatus was composed of mechanical agitator to obtain different rotational velocities, water bath to obtain different solution temperatures, carbon steel specimen 3 cm long and 2.5 cm outside diameter (cathode) attached to the rode of agitator, power supply to apply the required protection potential, digital ammeter to measure the current, digital voltmeter to measure the potential, variable resistance (rheostate) to control the current flow, graphite electrode as auxiliary electrode (anode) and saturated calomel electrode (SCE) as reference electrode. Digital balance of high accuracy (4 decimal places of gram) to measure the weight loss. The electrical connection between cathode (specimen) and the cell was attained using brush.

In weight loss, before each experiment the specimen was washed by tap water followed by distilled water, dried with clean tissue, immersed in annular acetone for 5 minutes, rinsed with water and dried with clean tissue. The specimen then was stored in vacuum desiccator over high activity silica gel until use for 24 h before use. Then it was weighted to nearest 0.1 mg. The carbon steel specimen was immersed in corrosion rate (CR) was calculated by the solution (0.1 N NaCl) at a particular temperature to corrode freely before applying the impressed current (cathodic protection) to measure the corrosion rate at stationary condition at different temperature (35, 45 and 55 °C). The corrosion rate was measured at different speeds (25, 90, 120 and 200 rpm) at constant temperature of 45°C. After each test, the specimen was washed with tap water, immersed in acetone for 5 minute and washed with distilled water, then dried with paper tissue, dried and kept for 24 h in desiccator over high activity silica gel. Finally it was weighed using the digital balance. From the weight loss the corrosion rate (CR) was calculated by using:

$$CR(gmd) = \frac{weightloss(g)}{Area(m^2) \times Time(d)} \quad (3)$$

Where CR represents corrosion rate in $g/m^2.d$.

The protection percent (pp) was calculated as:

$$PP\% = \frac{CR_0 - CR}{CR_0} \times 100 \quad (4)$$

Here CR_0 and CR are the corrosion rate in absence and in presence of impressed current respectively.

A 12 liter of 0.1N NaCl solution was used in polarization experiments. The specimen was connected to –ve terminal of power supply to serve as cathode and graphite to +ve terminal to serve as anode. When the bath reached the required temperature, the specimen was immersed and the electrical circuit was switched on. The power supply was set at 5 V (applied voltage). The specimen (working electrode) was cathodically polarized from a particular potentials (-1.3 to -1.5 V) to the corrosion potential (where $i_{app.} = 0$) by changing the applied current using rheostat. The current was recorded for step changes in potential. Two minutes were allowed for steady state to be reached after each potential increment [**Pickett 1974**]. The capillary tube was placed at distance 1-2 mm from cathode (specimen) and connected to calomel electrode to measure the specimen potential. Thus polarization curve can be drawn and the limiting current can be obtained. In impressed current cathodic protection experiment the area of anode (graphite) immersed in water was 3 times the area of cathode (working electrode) to ensure the limiting current density occurs on cathode.

For the case of flow conditions experiments the specimen was attached to the agitator rod. A brush was used to ensure the electrical connection between cathode and the –ve terminal of power supply.

The limit current density (i_L) was also obtained from weight loss measurement as follows:

$$N_{Fe} = (\Delta w/M)/(A.t) \quad (5)$$

where Δw represents weight loss, M is the molecular weight of carbon steel (iron), A is the area in m^2 and t is the time in second, N_{Fe} is the moles of Fe lost per unit area per unit time ($gmole/m^2.s$)

$$i_{Fe} = z\,F\,N_{Fe} \quad (6)$$

where i_{Fe} is the corrosion current density in (A/m^2), F is Faradays constant (96487 columb/equivelant), z is the number of electron freed by corrosion reaction (for iron z=2).

$I_{Fe} = i_{Fe} \times A$

according to equ. (1) & (2)

$O_2 + 2H_2O + 4e \rightarrow 4OH^-$

$2Fe \rightarrow 2Fe^{2+} + 4e$

$O_2 + 2Fe + 2H_2O \rightarrow 4OH^- + 2Fe^{2+}$

2 mole of Fe requires 1 mole of O_2

Hence $N_{O2} = \frac{1}{2} N_{Fe}$

Since $N = \frac{i}{ZF}$

$$\frac{i_{O_2}}{z_{O2} \times F} = \frac{1}{2} \frac{i_{Fe}}{Z_{Fe} F}$$

$$\frac{i_{O2}}{4F} = \frac{1}{2} \frac{i_{Fe}}{2F}$$

$i_{O2} = i_{Fe}$

hence $I_{Fe} = I_{O2} = I_{corr.}$ at $E_{corr.}$

Since the system is neutral (PH=7) and hydrogen current is not present in the limiting current region [**Uhlig 2008**, **Shreir 1976**] hence

$i_{O2} = i_L$

Since the current plateau is not well defined, thus the method given by **[Gabe and Makanjoula 1986]** was adopted to obtain i_L as in Fig..2

$$i_L = \frac{i_1 + i_2}{2}$$

Where i_1 and i_2 are the currents associated with E_1 and E_2 respectively.

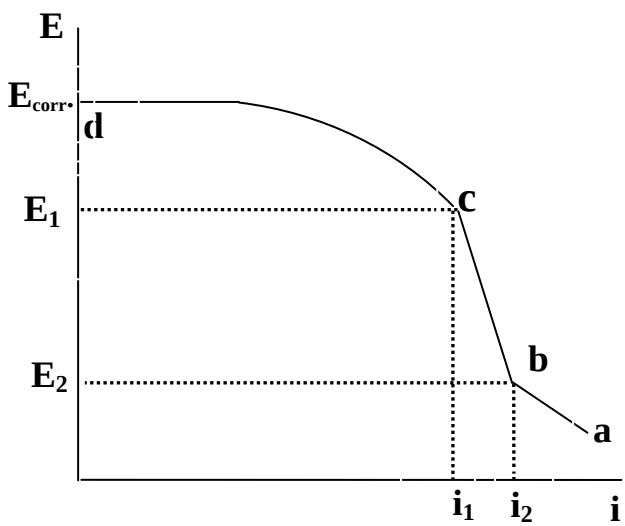

Fig.2 Typical polarization curve on carbon steel in 0.1N NaCl

After measuring $i_{corr.}$, different values of applied current were impressed to cathode at each temperature for 4 h to protect the metal and the potential was recorded at every 15 min to obtain the protection potential change with time. The values of applied current that were used to protect the metal at stationary and flow conditions at 45°C were $I_{app}=I_{corr.}$, $I_{app}=2I_{corr.}$ and $I_{app}= 2.4I_{corr.}$ to determine the protection percent for different values of rotation velocity at 45°C. The distance between anode and cathode was 30 cm.

was obtained from weight loss measurements for 4 h time of exposure. Since $I_{corr.}$ is lower than I_L where the later is for clean surface while $I_{corr.}$ for 4 h includes the corrosion product effect that reduces the corrosion rate [**Mahato et. al. 1968**, **Slaiman and Hasan 2010**], so applying $I_{corr.}$ is not expected to protect the clean surface and it is needed to apply higher values.

RESULTS AND DISCUSSION

Table 1 lists the experimental results for the stationary conditions.

Table 1 protection percent at various temperatures and applied currents ($A_{specimen}$ = 2355 mm^2).

Temp. (°C)	$I_{app.}$ (mA)	C.R (g/m^2.d)	PP%
35	0	22.549	-
	$I_{corr.}$=1.99	6.543	69.88
	$2I_{corr.}$=3.97	2.786	86.70
	$2.4I_{corr.}$=4.76	0.805	96.38
45	0	25.270	-
	$I_{corr.}$=2.41	5.636	78.22
	$2I_{corr.}$=4.83	3.413	87.1
	$2.4I_{corr.}$=5.79	0.249	99
55	0	24.49	-
	$I_{corr.}$=2.29	4.341	82.3
	$2I_{corr.}$=4.59	2.366	90.62
	$2.4I_{corr.}$=5.51	0	100

Table 2 lists the values of corrosion rate and protection percent for different rotational velocities at 45°C.

Table 2 Effect of rotation speed on the cathodic protection percent ($A_{specimen}$=2355mm^2).

Speed (m/s)	$I_{app.}$ (mA)	C.R (g/m^2.d)	PP%
0.033	0 $I_{corr.}$=3.04 2$I_{corr.}$=6.08	31.310 11.301 2.689	- 64.56 99.2
0.118	0 $I_{corr.}$=5.65 2$I_{corr.}$=11.3	59.418 23.499 3.255	- 60.59 94.498
0.157	0 $I_{corr.}$=8.88 2$I_{corr.}$=17.76	94.895 34.068 4.407	- 62.8 95.42
0.262	0 $I_{corr.}$=14.76 2$I_{corr.}$=29.52	154.440 59.931 15.348	- 62.39 90.27

Corrosion rate and corrosion potential

The best indication for cathodic protection is by weight loss. The corrosion rate from the experimental results of metal specimen at different temperatures without impressed current and cathodic current density are shown in Fig.3. The results show that increasing temperature leads to unstable trend of corrosion rate and corrosion current. Unstable trend was also noticed by previous workers [**Mahato et.al. 1968**, **Mahato et.al**. **1980**, **Hassan 2003**]. From this figure it can be seen that the corrosion rate at 45°C is higher than at 35°C and the corrosion rate at 55ºC is slightly lower than at 45ºC this can ascribed to the lower concentration of O_2 at 55ºC than 45°C. Increasing the temperature will increase the rate of oxygen diffusion to the metal surface and decrease the viscosity of water which will aid the oxygen diffusion. All these factors enhance the corrosion rate. On the other hand, increasing temperature decreases the oxygen solubility the factor that restrains the corrosion [**Henry and Scott 1999**] as shown in table 3.

Table 3 Values of oxygen Diffusivity and solubility at different temperatures (Audin 1972, Sense 2001)

T(°C)	D×10^9 (m^2/s)	Solubility (mg/l)
30	2.374	7.5
40	3.010	4.389
50	3.562	5.399
60	4.834	4.49

Figures 5 to 8 show the polarization curves at 45°C and different speeds. It can be seen as the

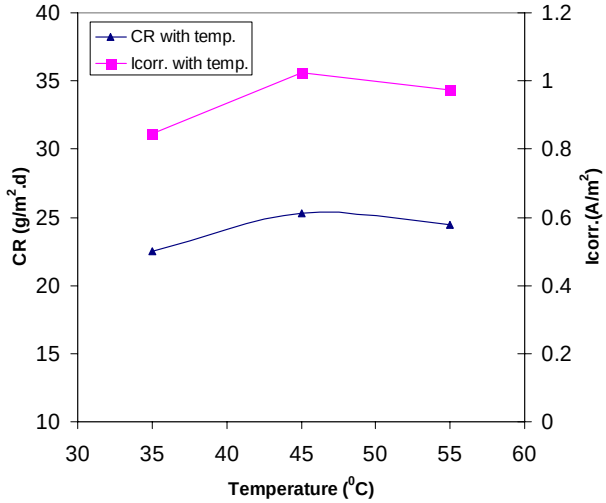

Fig. 3 Corrosion rate and Icorr. vs. temperature for free corrosion at stationary conditions

Polarization results

The typical polarization curves for carbon steel in 0.1N NaCl solution (pH=7) at temperatures of 35°C, 45°C and 55°C are shown in Fig.4. The most important characteristic of the cathodic polarization is the limiting current density of oxygen reduction(i_L). The corrosion potentials (Ec) were also determined from the polarization curves when the applied current becomes zero, i.e, open circuit potential (or free corrosion potential). It can be seen that I_L for 55°C (1.2 mA) is lower than that for 35°C (2.5 mA) and 45°C (1.7 mA). The I_L for 45°C is lower than for 35°C this is because of higher concentration of O_2 at 35°C.

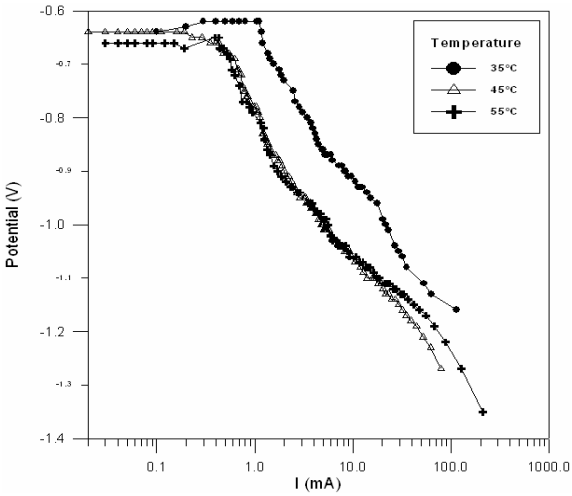

Fig.4 Polarization curve at stationary conditions at different temperatures

velocity increases I_L is increased, for example at speed of 0.033,. 0.118, 0.157 and 0.262 m/s, I_L is 5, 14.5, 19.5 and 22 mA respectively. This can be attributed to the increase in oxygen supply from the bulk of the solution to the metal surface leading to higher I_L [**Mahato et.al 1968, Mahato et.al 1980, Foroulis 1979, Hasan 2003**].

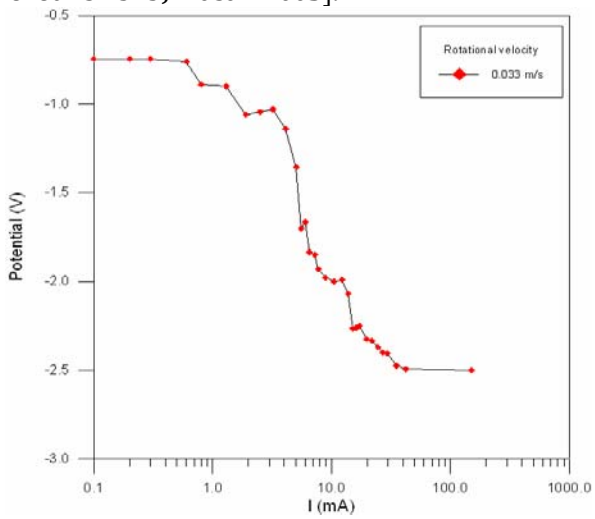

Fig.5 Polarization curve at velocity of 0.033 m/s at temperature=45°C

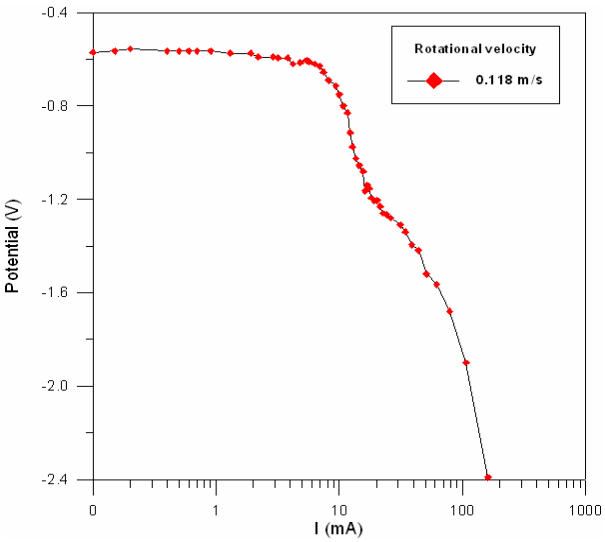

Fig. 6 Polarization curve at velocity of 0.118 m/s at temperature= 45°C

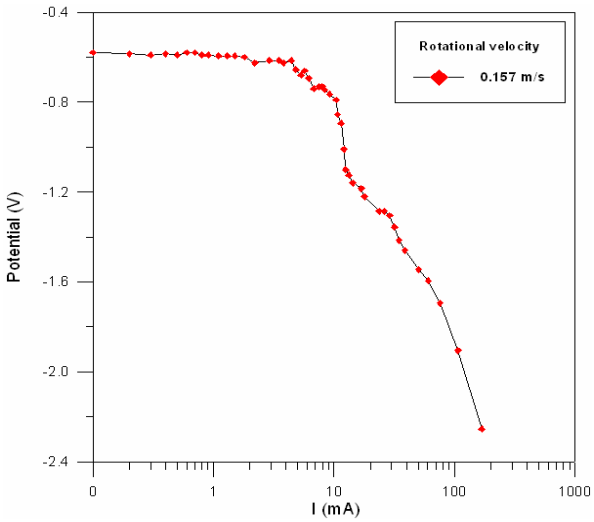

Fig.7 Polarization curve at velocity of 0.157m/s at temperature=45°C

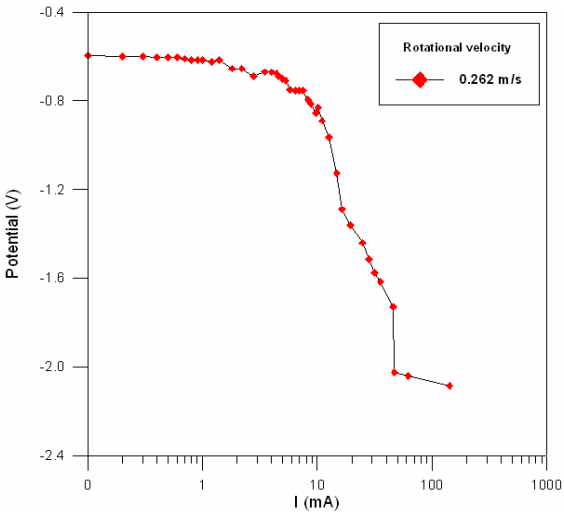

Fig. 8 Polarization curve at velocity of 0.262 m/s at temperature=45°C

Impressed current results

A metal in an aqueous environment, can be protected by impressing an electric current at its surface, delivered by a DC generator to polarize the potential to a value more negative than the equilibrium potential. Fig.9 shows the corrosion rate versus temperature at different applied currents values. The results in this figure indicate that as the applied current increases, the corrosion rate decreases this means the metal is protected by impressed current. For example the corrosion rate at 35ºC is 22.549 $g/m^2.d$ before applying protection current. When applying corrosion current (1.99 mA) is 6.543 $g/m^2.d$, at double corrosion current (3.97 mA) is 2.786 $g/m^2.d$ and at current greater is 0.805 $g/m^2.d$.

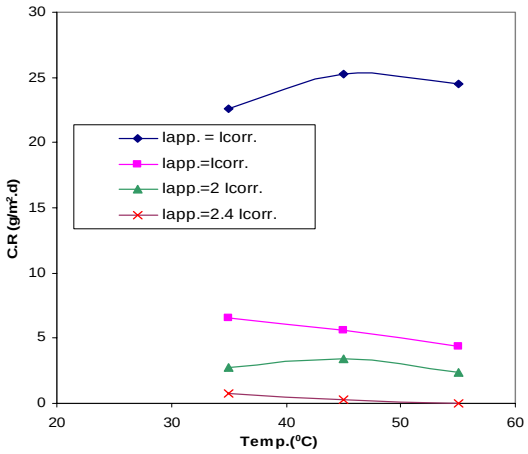

Fig. 9 Corrosion rate vs. temperature at stationary conditions

It is important to determine the amount of current or potential that needed to be applied to protect a structure and to make sure that the anode can provide that current uniformly across the structure at a reasonable DC output voltage [**Varmani and Clemena 1998**]. The relation between applied current and corrosion rate at different temperature is shown in Fig.10. It is clear that as the current for cathodic protection increases the corrosion rate decreases. The oxidizing of iron releasing electrons and ferrous ions, which dissolve in the solution surrounding the steel. The electrons are deposited on the steel surface, lowering the potential. In reduction current, electrons released by iron at the anode flow towards higher potential (cathodic) sites, where they combine with water and oxygen molecules to form hydroxyl ions. The corrosion reaction will only continue if there is cathodic reaction to accept released electrons, so these corrosion reactions can be stopped if oxygen and water are not available at the cathodic sites on the steel [**Bentur et.al 1997**].

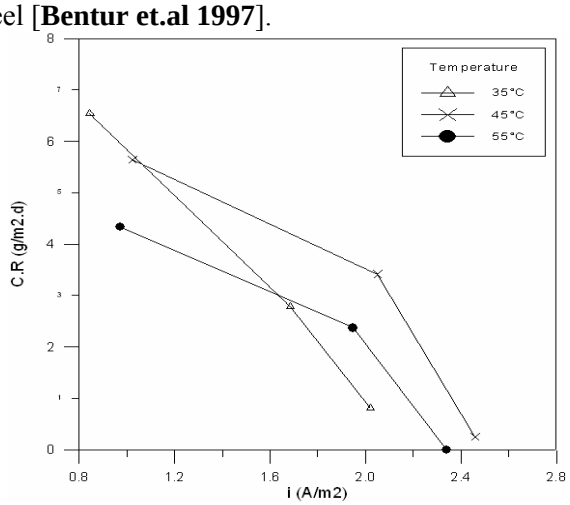

Fig.10 Corrosion rate vs. $I_{applied}$ at stationary conditions

oxygen concentration leads to shift Ec to more

The protection percent at three temperatures (35ºC, 45ºC and 55ºC) with applied current is shown in Fig. 11. From this figure it can be seen that the protection increases as the temperature increases , for example when applying corrosion current the protection percent are 69.88%, 78.22% and 82.3% for 35ºC, 45ºC and 55ºC respectively while when applying current density equal to $2I_{corr.}$. the protection percent are 86.70%, 87.1% and 90.62% for 35°C, 45°C and 55°C respectively, so for higher current ($I_{app.}$=2.4$I_{corr.}$) it is 96.38%, 99% and 100%. The protection percent increased with increasing impressed current ($I_{app.}$) due to the increased reduction of O_2 at the metal surface leading to decrease the corrosion of metal. Fig. 11 also reveals that the protection percent varies with temperature with unstable trend depending on O_2 solubility and diffusivity [**Shreir 2000, Mahato et.al.1980**].

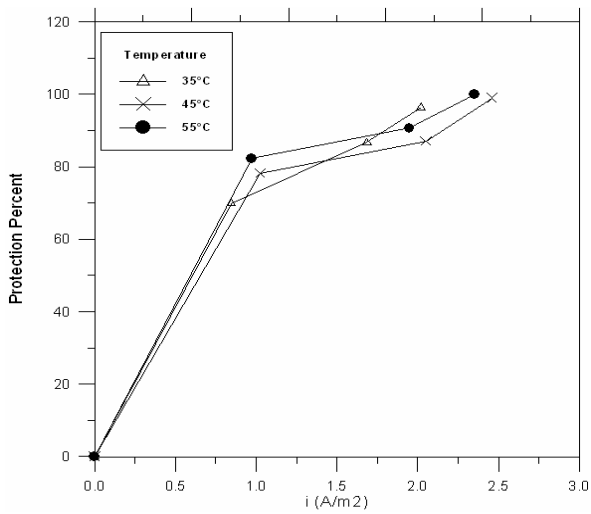

Fig. 11 Iapp. vs. protection percent at different temp. under stationary conditions

Protection Potential

Figure 12 shows effect of time on the protection potential of carbon steel pipe immersed in 0.1 N Nacl at different temperatures. The figure shows that the potential decreases with time, where the potential is recorded at each 15 min for an experiment time of four hour long. Precisely the potential becomes rapidly more negative in the first hour, and then the curve reaches asymptotic value at -990 mV, -990 mV and -1070 mV vs SCE which represent the protection potential for 55°C, 45°C and 35°C respectively. Numerous studies have demonstrated that Ec is generally influenced by the oxidizer concentration. Several investigators [**Foroulis 1979**, **Atia 1996**, **Al-mashta 1996**, **Kim 1998 and Ross 1966**] showed that decreasing

negative values. It is evident that Ec falls with increasing temperature this because Ec are affected by both anodic and cathodic process. The anodic (activation controlled) process is simulated by increasing bulk temperature to greater extent than that of cathodic (concentration controlled) process [**Shreir 1976 and Steigerwald 1968**]. The corrosion potential become more negative with time, because the oxygen level at the steel interface can be depleted over time when subject to constant current density [**Enos et.al 1997**]. This figure indicates that at applied current of $I_{app.}=I_{corr.}$ the higher the temperature is the more positive protection potential. The decrease in the potential with time can be ascribed to the fact that at low temperature the depletion of O_2 is higher due to its high reduction on the metal surface leading to more negative the protection potential.

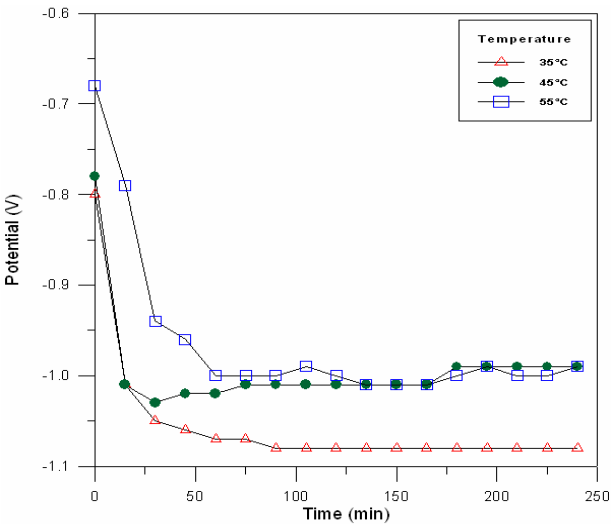

Fig. 12 Potential vs. time at Iapp. = Icorr. at stationary conditions

Figure 13 shows that the potential become more negative with increasing time at different applied current values at temperature of 35°C. The corrosion potential become more negative with time, because the oxygen level at the steel interface can be depleted over time when subjected to constant current density [**Enos et.al 1997**]. It can be seen that as the current increases, the potential becomes more negative because high $I_{app.}$ leads to high O_2 reduction, shifting the potential to more negative [**Foroulis 1979, Hasan 2003**]. The corrosion potentials for current applied and higher current is approximately similar while for lower current are less negative. The decrease in potential is rapid during the 90min for $I_{app.}$=1.99 mA while for $I_{app.}$=3.97 mA and $I_{app.}$=4.763 mA the decrease in potential is rapid during 30 min.

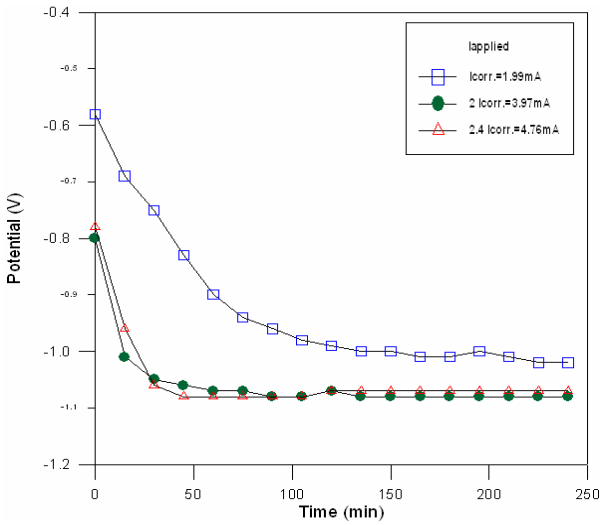

Fig.13 Potential vs. time at 35°C

Figure 14 shows the effect of rotational velocity on the corrosion rate of carbon steel specimen for different applied currents. It is clear that the corrosion rate decreases with increasing applied current and increases with increasing velocity. The increase in the rate of carbon steel dissolution with increasing solution velocity can be attributed to the decrease in the thickness of the hydrodynamic boundary layer and diffusion layer across which dissolved O_2 diffuses to the metal wall [**Fahien 1983, Brodkey and Harshy 1989**] with a consequent increase in the rate of O_2 transfer from bulk solution to the surface, since:

$$N_{O2}=KC_{O2}=(D/\delta)\ C_{O2} \qquad (7)$$

Where K is the mass transfer coefficient (m/s), D is the diffusivity of dissolved O_2 (m^2/s) and Co_2 is the concentration of O_2 in the solution bulk, δ is the diffusion layer thickness. In other word increasing velocity will increase the amount of oxygen arriving to the surface leading to higher corrosion rate. Increasing velocity leads to decrease the thickness of diffusion layer that represents the main resistance to oxygen transport [**Welty 2001, Brodkey and Harshy 1989**]. It is to be noticed from Fig. 14 that at high applied current values the effect of velocity on the corrosion rate is lower, however, the corrosion rate increases considerably with velocity when $I_{app.}$=0 while it increases little at $I_{app.}=I_{corr}$

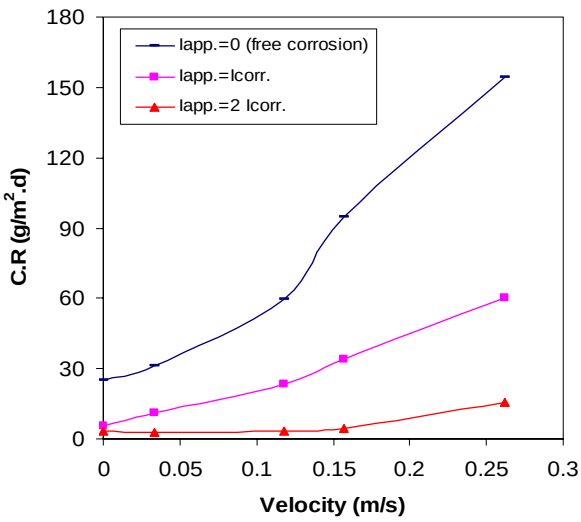

Fig.14 Effect of applied current by weight loss on the corrosion rate at 45°C

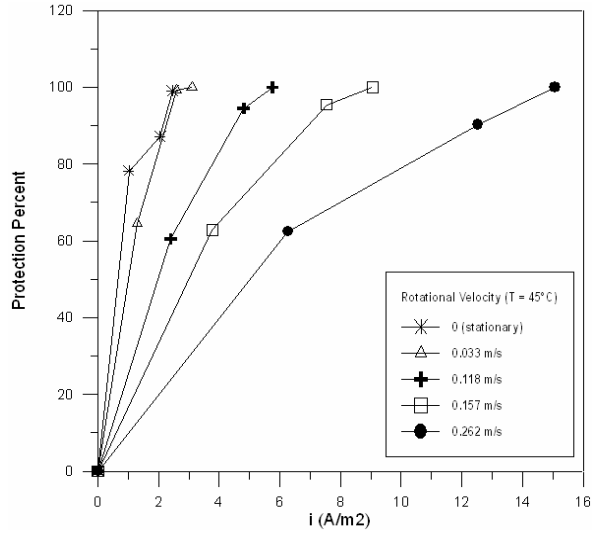

Fig.15 Iapp. vs. PP% at different speed and constant temp. 45°C

Figure 15 shows the protection percent versus applied current at stationary and flow conditions at 45°C. It is evident that as the applied current increases the percent of cathodic protection increases. In neutral solutions the cathodic corrosion process is usually the reduction of oxygen. The kinetics of this cathodic process are controlled by the rate at which oxygen can diffuse to the surface of metal, which is slower than the rate of consumption of oxygen by the cathodic reaction. Thus, the rate of this reaction remains constant unless the rate of supply of oxygen to the surface of metal is increased by increasing fluid flow rate. However, if the flow rate is increased the limiting current for the reduction of oxygen is increased and the current required to maintain the metal at the protection potential is increased. At stationary conditions the highest protection percent attained is 99% when Iapp.=5.79 mA. For a velocity of 0.033 m/s the highest protection percent is 99.2% when Iapp.=6.08 mA, for 0.118 m/s the highest protection percent is 94% when Iapp.=11.3 mA, for 0.157 m/s the highest protection percent is 95% for Iapp.=17.8 mA, and for 0.262 m/s the highest protection percent is 90.3% for Iapp.=29.52 mA. Hence the higher the velocity is the higher the required current for protection.

Figure 16 shows the variation of corrosion potential with time for different values of velocity at 45°C. This figure indicates that the corrosion potential more negative with time. Also the higher the velocity is the lower the protection potential due to high applied current required for protection.

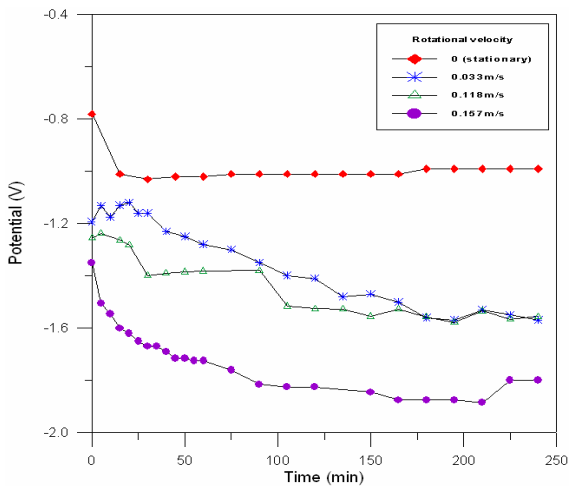

Fig.16 Corrosion Potential vs. time at Iapp.= $2I_{corr.}$ at temperature=45°C

Conclusions

1- The corrosion rate of carbon steel specimen exhibits unstable trend with temperature.
2- Increasing velocity (0-0.262 m/s) leads to increase the corrosion rate from 25.27 gmd to 154.44 gmd at Iapp.=0 and $i_{corr.}$ increases from 2.41 mA to 14.76 mA at 45°C.
3- The impressed current required for cathodic protection depends on temperature and rotational velocity. Applying $I=2I_{corrr.}$ gives protection percent between 90 to 99% depending on temperature and velocity.
4- The higher the rotational speed is the higher the cathodic currents required for protection.
5- The higher the impressed cathodic protection current is the lower the effect of velocity on the rotational speed will be.
6- The protection potential shifts to more negative values with time where it decreases by 40-68% depending on temperature. Also it shifts to more –ve with increasing velocity.
7- The lower the temperature is the more negative protection potential will be.

References

Al-Mashta S.E., M.Sc Thesis, Chem. Eng. Dept., Al-Nahrain University, Baghdad, 1996.

Atia M. A., Ph. D. Thesis, Dept. Chem. Eng., Al-Nahrain University, Baghdad, 1996.

Audin A., and L.John, J. Chem. Eng. Data, Vol. 17, No.3, p.789, 1972.

Barhai B & P.K.Gogoi, "Corrosion Inhibition of Carbon Steel in Open Recirculation Cooling Water System of Petroleum Refinery by A multi-component Blend Containing Zinc (II) Diethyldithiocarbmate", Indian Journal of Chemical Technology, Vol. 17, PP. 291-295, July 2010.

Bentur, Arnon, Diamond, Sidney and Berke, Neal S., " Steel Corrosion in Concrete", E and FN Spon, New York, NY. PP.201, 1997.

Brodkey R. S. and H. C. Hershey, Transport Phenonmena, 2nd Printing, Mc Graw Hill, New York, 1989.

Enos, D.G., Williams, A.J.Jr. and Scully, J.R., "Long-Term Effects of Cathodic Protection on Prestressed Concrete Structures: Hydrogen

Fahien R. W., Fundamentals of Transport Phenomena, McGraw Hill, NY, 1983.

Fontana M.G. and N. D. Greene, " Corrosion Engineering", 3rd edition McGraw- Hall, 1986.

Foroulis Z. A., Corrosion, Vol. 35. P.340, 1979.

Gabe D.R. and P.A. Makanjoula, EFCF Publication Series No. 15, Electrochemical Eng., AICHE Symposium Series, No. 98, P.309, 1986.

Hasan, B.O., "Heat, Mass and Momentum Analogies to Estimate Corrosion Rates under Turbulent Flow Conditions", Ph. D. Thesis. Chem. Eng. Dep., Al-Nahrain University, Baghdad, 2003.

Henry S.D and W.M. Scott " Corrosion in the Petrochemical Industry", 1st edition , ASM International, USA, 1999.

Kim Y.J., GE Research and Development Centre, Technical Formation Series, 97CRD 202, Feb.1998.

Konsowa A.H.and A.H El-Shazly, " Rate of Zinc Consumption During Sacrifical Cathodic Protection of Pipelines Carrying Saline Water", Desalination Vol. 153, pp. 223-226, 2002.

Mahato, B. K., F. R. Steward, and L. W. Shemlit, Corrs. Sci. Vol. 8, P. 737, 1968.

Mahato, B. K., C. Y. Cha, and W. Shemilt. Corros. Sci., Vol. 20, P. 42, 1980.

Nesic N., B. F. M. Pots, J. Postelthwaaite, and N. Trevenot, J.Corrosion Science and Eng., Ph.D. Study, Vol. 1, Paper 3, 1995.

Perez Nestor "Electrochemistry and Corrosion Science", 2004.

Pickett D.J. and K.L. Ong, Electrochmical Acta, Vol. 19, p. 875, 1974.

Roberge Pierre R., "Corrosion Engineering Principles and Practice", McGraw-Hall, 2008.

Ross T.K., G.C. Wood and I.J. Mahmud, Electro chem. Soc., Vol.113, P.334, 1996.

Sami, A.A. and A. A. Ghalib, "Variable Conditions Effects on Polarization Parameters of Impreesed Current Cathodic Protection of Low Carbon Steel Pipes', Eng. Technol. J. Vol. 26, PP. 1-12, 2008.

Embrittlement of Prestressing Steel", Corrosion, Vol 53, No. 11, PP. 891-908, Nov. 1997.

Scantlebury J.D. Dae Kyeong Kim, Srinivasan Muralidharan, Tae Hyun Ha, Jeong Hyo Bae, Yoon Cheol Ha and Hyun Geo Lee, " Electochemical Studies on the Alternating Current Corrosion of Mild Steel Uner Cathodic Protection Condition in Marine Environments", Electrochimica Acta, Vol 51. PP. 5259-5267, 2006.

Sense F., Oxygen Solubility, North California State, 2001.

Shreir L.L., Corrosion Handbook, 2nd edition, part 1, Newnes Butter, London, 1976.

Shreir L.L., Corrosion Handbook, 2nd edition, part 1, Newnes Butter, London, 2000.

Slaiman and Hasan, "Study on Corrosion Rate of Carbon Steel Pipe under Turbulent Flow Conditions", The Candian J. of Chem. Eng., Vol. 88, December, 2010.

Smith S. W., K.M. McCabe, and D. W. Black 'Effect of Flow Parameters on the Cathodic Protection of A steel Plate in Natural Seawater", Corrosion, October 1989.

Steigerwald R.F., Corrosion-NACE, P. 1, 1968.

Uhlig H.H., "The Corrosion Hand book", John Wiley & Sons, New York, 1976.

Uhlig, R., Herbert H. Winston Revie "Corrosion and Corrosion Control, An Introduction to Corrosion Science and Engineering", 4rd edition John Wiley &Sons, 2008.

Virmani, Yash Paul and Clemena, Gerardo G., "Corrosion Protection-Cocrete Bridges", Report No. FHWA-RD-98.088,Fedral Highway Administration, Washington, D.C., 1998.

Welty J. R., C. E. Wicks, and G. Rorrer, "Fundamental of Momentum, Heat and Mass Transfer, 4th edition, John Wiley and Sons, United State of America, 2001.

NOMENCLATURE

A: Area (m^2)
D: Diffusivity (m^2/s)
Ec: corrosion Potential (V)
F: Faradays constant (96487 columb/equivalent)
i: Current density (A/m^2)
$I_{app.}$: Applied current (mA)
I_{corr}: Corrosion current (mA)
I_L: Limiting current (mA)
K: Mass transfer coefficient (m/s)
M: Molecular weight (g/mole)
mA: mil ampere
t: time of exposure (hours)
V: Volts
Δw: weight loss (g)

Subscript

C: Corrosion
Corr: Corrosion
L: Limiting

Abbreviations

C.R: Corrosion rate ($g/m^2.d$)
PP: Protection percent
SCE: Standard Calomel Electrode

Greek Letters

δ: diffusion layer thickness (m)

EXPERIMENTAL AND NUMERICAL STRESS ANALYSIS OF INVOLUTE

SPLINED SHAFT

Dr. Majid H. Faidh-Allah **Zainab Amjed Abdul Khalik**
Mechanical Engineering

University of Baghdad

ABSTRACT

In this study, the induced splined shaft teeth contact and bending stresses have been investigated numerically using finite element method(Ansys package version 11.0) with changing the most effecting design parameter, (pressure angle, teeth number, fillet radius and normal module), for internal and external splined shaft. Experimental work has been achieved using two dimensional photoelastic techniques to get the contact and bending stresses; the used material is Bakelite sheet type “PSM-4”.

The results of numerical stress analysis indicate that, the increasing of the pressure angle and fillet radius decrease the bending stress and increase the contact stress for both internal and external spline shaft teeth while the increasing of the normal module and teeth number decrease the contact and bending stresses.

Keywords: Spline shaft, Finite Element Analysis, photoelastic

الخلاصة:

في هذا البحث تم دراسة اجهادات التماس والحناية المتولدة في اسنان عمود الدوران المخدد عدديا باستخدام طريقة العناصر المحددة وباستخدام برنامج ANSYS الاصدار (11) مع تغيير العوامل التصميمية المؤثرة، (زاوية الضغط، عدد الأسنان، نصف قطر الجذر ومعامل التضمين العمودي)، للأعمدة ذات التخدد الداخلي والخارجي. تم تحقيق الجانب العملي بأستخدام تقنية تحليل الاجهاد الضوئي ثنائيه البعد للحصول على قيم اجهادات التلامس والحنايه المتولدة في الاسنان، حيث ان المادة المستخدمة في التحليل التجريبي هي قطعه من البكالايت نوع (PSM.4).

بينت نتائج التحليل العددي بأن زيادة زاوية الضغط ونصف قطر الجذر تقلل من اجهادات الحناية وتزيد من اجهادات التماس للأسنان الداخلية والخارجية بينما الزيادة في التضمين العمودي وعدد الأسنان تقلل من اجهادات الحناية والتماس.

1. INTRODUCTION

A Spline is a geometric feature used to join one shaft to another. It transmits torsion, but permits axial sliding. splined connections are widely used as a coupling mechanism in rotating machinery.

Splined shafts transmit torque from one rotating member to another at the same value and direction.

Splines are essentially stubby gear teeth formed on the outside of the shaft and on the inside of the hub of the load-transmitting component. Splines are generally much more expensive to manufacture than keys and are usually not necessary for simple torque transmission. They are typically used to transfer high torques [Shigley, 2008].[D. A. Baker, 1999] calculated the maximum Von Mises stress for solid finite element models of splined shafts with straight-sided teeth for two types of spline shaft, stepped and partially spline shaft. Finite element analyses are performed for the cases of a stepped shaft of three different step size ratios (d/D). The second set of models consists of a solid cylindrical shaft with incomplete spline teeth. The incomplete regions of the spline teeth are

modeled in three radii (R). Bending, torsion, and combined loads are applied to each model, including several combinations of bending and torsion between pure bending and pure torsion. The stresses in the stepped splined shafts are up to 50% greater than nominal stresses in the non-splined section and up to 88% greater than nominal stresses splined section. Stresses in the partially splined shaft are up to 42% greater than the well developed nominal stress in the non-splined section of the shaft, and up to 7% greater than the nominal stresses in the splined section. [H. Yoshitake, 1962] presented an experimental investigation about the spline shaft by the three - dimensional photoelastic method and it is found that: The stress distribution of the spline shaft was measured, and the stress concentration factor was obtained. The results were coincident fairly well with those of other methods. The accuracy of the wedge method was checked and its value was about 5%.The stress distribution of the meshing spline shaft was investigated, and it was found that the maximum bending stress of the tooth was comparable with the maximum torsional stress. [A. Tjernberg, 2001] presented finite element model of a spline coupling between a shaft and a sleeve. The stress concentration factor is calculated and compared to analytical calculations .The pitch error caused by the irregular spacing between the spline teeth has been measured. The measurement of pitch error has been made of splines manufactured using two different milling methods. A simplified model has been created to calculate the approximate load on each tooth and the relative life. Induction hardened shafts with splines manufactured with one type of milling method have been fatigue tested. The calculations have showed that the life of a spline with pitch error is only 1/3-1/2 of the life of a spline with ideal pitching. [D. C. H. Yang and SH. H. Tong, 2007] studied the profile design of splines and keys components. The influence of spline profiles on the performance of power transmission is investigated. They presented the optimal design of spline profiles for three different design criteria. The method of calculus of variation is used to determine profile functions for maximum value. Analytical results are successfully obtained. They show that the splines with involute profiles lead to uniform deformation on the hub; in addition they can carry the maximum transmission load capacity. On the other hand, radial straight profiles result in optimum transmission efficiency

2.Numerical Stress Analysis of Spline Shaft Teeth:

Finite element analysis is a numerical method in which a particular body is subdivided into discrete partitions (called elements) that are bound by nodes. Each element is connected to adjacent elements by the nodes. The finite element method requires that the fundamental differential equations governing the overall problem be reduced to a system of algebraic equations from which a general solution is obtained. Boundary conditions and environmental factors are applied to the subdivided model. The equations governing the individual elements are then combined and solved to obtain the solution for the overall problem.

2.1 Convergence Test:

To ensure the accurate results of stress calculations, the element type must be chosen carefully, which is used to mesh the splined teeth models, so that the convergence test must be done at first and as follow:

1. Building up the internal and external spline models according to mathematical model.
2. Specifying the material properties as a structural, linear, elastic, isotropic with ν = 0.3, E= 200,000 N/mm^2 .
3. Specifying the applied load and boundary conditions (they are the same through the convergence test).

Specifying the element type as solid and using the following element type successively (anasio 64, Tetrahedrol 10 node 187, 8 node 185, 20 solid 186, 20 solid 95, Brick 8 node 45 and 10 node 92) with changing the coarser to each element in order to investigate the right element number as well the element type. The result of the convergence test show that the best element type that can be employed to mesh the model is 8 nodes 185 with 19964 elements with 29081 nodes as in Fig.1, Fig. 2 represents one external tooth meshed with these elements.

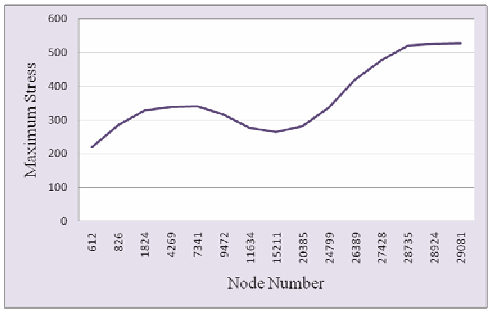

Fig. 1 Convergence test

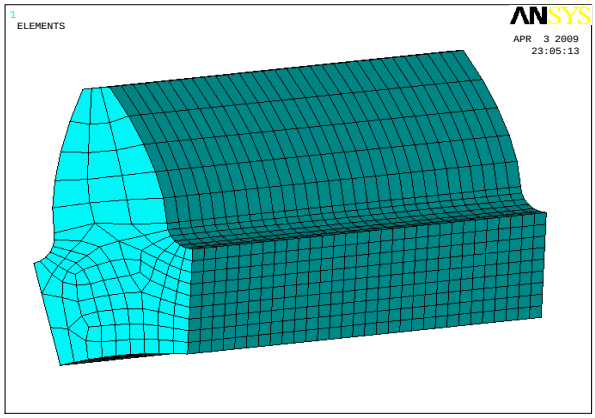

Fig. 2 One external tooth meshed with solid element 8 nodes

2.2 Development of Finite Element Models:

The development for finite element models is accomplished as follows [Jill Tombasco, 2004], [H. Tea Cong, 1996] and [Vera Nikolic, 2003].

1. Tooth surface equations of external and internal splines and portions of corresponding rim are considered for determination of the volumes of the designed bodies.
2. The proposed approach does not require an assumption on the load distribution in the contact area.
3. F. E. models of one tooth are applied.
4. Setting of boundary conditions is accomplished automatically.

The following ideas are considered:

- Node on the two sides and bottom part of the portion of the external rim are considered as fixed.
- Nodes on the two sides and bottom of the portion of the internal rim are considered as a rigid body.
- Input torque can be expressed as the sum of the applied nodal forces at radius of shaft (r_i), thus

$$T = \sum_{i=1}^{n} F_i \, r_i \qquad (1)$$

Where (T) is the input torque load, (n) is the total number of constrained nodes and (F_i) is the tangential nodal force (usually F_i=F, is a constant value).

The boundary conditions can be seen in **Fig.3**

5. The contact algorithm of (FEA) computer program requires definition of contacting surfaces [Jamesn F. Doyle, 2004]. To define a contact pair completely, contact and target elements, have to be referred to the same characteristic parameters.
6. The selected contact algorithm was Penalty method. The penalty method uses a contact "Spring" to establish a relationship between the two contact surfaces.

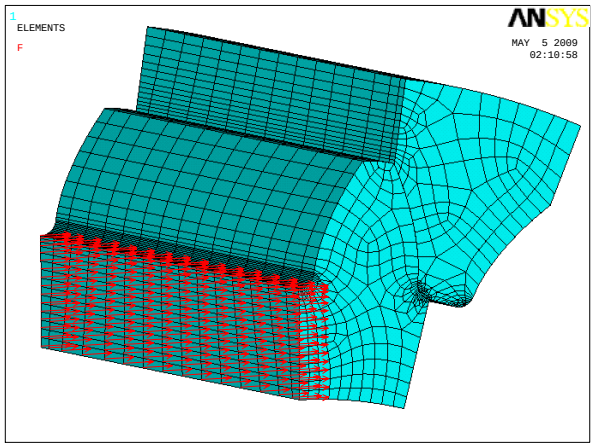

Fig. 3 Boundary conditions for external and internal involute splines

3. Experimental Stress Analysis of Spline Shaft Teeth

Photoelastic stress analysis (photoelasticity) is a well known technique to perform stress analysis experimentally with many economic benefits to engineering design. Photoelastic, which provides both quantitative and qualitative analysis, allows a loaded model to be analyzed while still in the design stages, which means a design can be adjusted before production. A non- destructive technique, photoelasticity allows the same model to reuse during analysis. The universality of this method provides for its application to all areas of engineering design **[U. Burgtorf, P. Dietz and M. Garzke, 1998].**

In present photoelastic study the three-dimensional problem was reduced to a series of two- dimensional problem by calculation the stresses at a number of thin cross sections along the tooth length **[R. Errichello,1978]**, it is sufficient to analyze only one slice of two-dimensional to determine the contact and bending stresses.

3.1 Photoelastic Method of Stress Analysis:

The birefringent material has been used to construct the transparent spline shaft models, internal and external splines. The basic equation that calculates experimentally the induced stresses is:

$$(\sigma_1 - \sigma_2) = n\, f / h \qquad (2)$$

Where (n) represent the number of fringes, (ν) is the material fringe constant and $(\sigma_1 - \sigma_2)$ is

the difference in the principle stresses, (*h*) represent the tooth width, Eq. (2) can be arranged as:

$$f = \frac{(\sigma_1 - \sigma_2)}{n}\, h \qquad (3)$$

Thus in a simple loading procedure for which a known principal stress difference can be easily expressed in terms of the applied load we can determine the fringe constant **[D. L. Hitt, 2003].**

3.2 Photoelastic Material and Photoelastic Model:

Used a transparent flat model made of a plastic material that is doubly refracting under stress such as Bakelite sheet type "PSM-4" with (6mm) thickness. This photoelastic material can be employed for two and three-dimensional studies. **Table1** shows the material properties determined from calibration test of specimen which has been cut from same material of sheet used to fabricate the tooth model. The segment model of one tooth profile has been made carefully to matching the output of the theoretical design. The spline teeth model was made 5 times the actual size, See **Fig.4**.The dimension of spline shaft geometry of the chosen profile are given in **Table 2.**

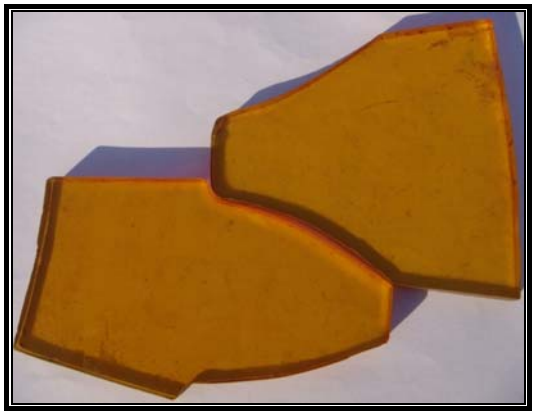

Fig. 4 Splined Shaft Photoelastic Models

Table 1 Mechanical Properties of Photoelastic Material

Modulus of elasticity N/mm^2	Elastic limit N/mm^2	Poisson's ratio
2.335714 e+003	1.692 e+003	0.4

Table 2 Dimensions of Splined Shaft Mode

Normal module (mm)	Normal pressure angle (Deg)	No. of teeth	Face Width (mm)
6	30	20	6

3.3 Experimental Apparatus and Experimental Procedure:

In the present photoelastic analysis, the splined teeth model was positioned in the loading fixture such that the area of contact on the external tooth profile matched the area of contact on the internal tooth profile. The external tooth model was firmly clamped to prevent rotation during applying load, and connected to the load sensor which was connected to the load cell to read the applied load. While the internal tooth model was connected to an arm connects to the crank handle to apply load by turning the load crank on the loading fixture.

Both a light and dark field was employed to increase the accuracy of the account of the fringes. Once load was established, the light and dark field photographs were taken of the fringe pattern in the spline model.

Before conducting any test on the model, the calibration of load cell must be checked. The model is then aligned in the field of the polariscope and the load is gradually applied to the models. **Fig. 5** shows the details of apparatus used in experimental analysis

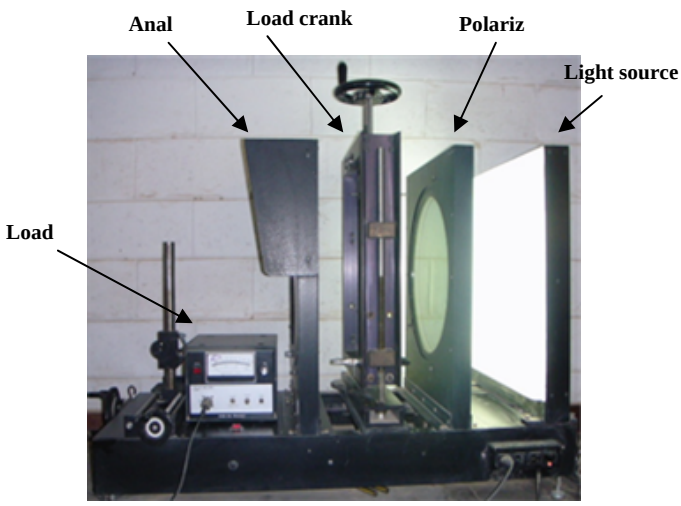

Fig.5 Experimental Apparatus

4. Transition from Model to Prototype:

For many practical two dimensional elastic problems with forces applied to external boundaries, the stress depends upon geometry and external forces only [F. James Doyle and James W .Phillips, 1982].

The profile of the model is made geometrically similar to that of the prototype to be studied but not of the same size, and the applied load must be similarly distributed, but they may differ in magnitude by a factor of proportionality. Any stress (σ_p) in the prototype can be determined from the corresponding stress (σ_m) at the corresponding point in the model. The bending stress for the mating teeth can be calculated as follow **[E. J. Hearn, 1977].**

$$\sigma_b = (M\,y)/I \qquad (4)$$

Where (σ_b) is the bending stress, (M) is the moment, (y) is the half of width of the tooth and (I) is the moment of inertia. The relation between the model and the prototype for bending stresses is:

$$\sigma_{bp}/\sigma_{bm} = ((M\,y)\,/\,I)_p/((M\,y)\,/\,I)_m \qquad (5)$$

Where all dimensions of model are five times the prototype dimensions and that leads to:

$$\sigma_{bp} = 25\left(\frac{F_p}{F_m}\right)\sigma_{bm} \qquad (6)$$

Table 1 shows the values of (E and) for models. The prototype properties are E=200,000 MN/m^2 and ν = 0.3.

5. Results and Discussions:

The results of teeth stress analysis obtained experimentally by using photoelastic analysis and numerically by using Finite Element Analysis, (Ansys package), Version 11.0, are investigated.

In the numerical F.E.A several models have been analyzed with different cases of design of splined shaft such as pressure angle, normal modules, fillet radius and number of teeth and their effects on contact and bending stresses have been stated. Photoelastic study was performed to check the numerical analysis by determined values of contact and bending stress.

Form finite element (ANSYS) results, the variation of maximum contact and bending stresses with pressure angle, normal modules, fillet radius and number of teeth are plotted in **Fig.** (6) -- (13). The results showed that the increasing of the normal pressure angle decreases the bending stress and increase the contact stress due to decrease the horizontal teeth load component, increasing the teeth number and normal module decrease the shared load (the applied load on each meshed tooth) and cause decreasing in both contact and bending stress and the increasing of the fillet radius decrease the bending stress due to the decreasing of stress concentration factor while that cause an increasing in the contact stress. At last it is important to notice that the internal spline shaft are in general have more resistance to the bending stresses than the external spline shaft and the cause of that is they have larger cross section area at the root region than the mating spline.

Fig.14 shows the photographs of photoelastic analysis that gives the maximum contact and bending stresses which were calculated from the analysis of photographs of the fringes. The comparison between experimental and numerical stress analyses for contact and bending stresses at load case (1) and load case (2) are given in Tables 3, 4, 5 and 6.

In case (1), the percentage errors of the maximum contact stress between two results are 14.742% and 16.666% in external and internal spline teeth , respectively and the percentage errors of the maximum bending stress between two results are 6.166% and 4.388% in external and internal spline teeth, respectively.

In case (2), the percentage errors of the maximum contact stress between two results are 12.116% and 17.006% in external and internal spline teeth, respectively and the percentage errors of the maximum bending stress between two results are 4.509% and 5.685% in external and internal spline teeth, respectively.

There was a difference in results between experimental and finite element analyses because of the errors in profile during cutting process. That's all because:

1. In the cutting process, the errors in the profile will be produced and this produce problems in practical application which effect on the localized of bearing contact.
2. The fringe order at contact point is very high because of the localized contact load and, therefore, the fringe order exactly at the contact point can never be measured accurately.
3. There may be some error in the calculation of the material fringe constant.

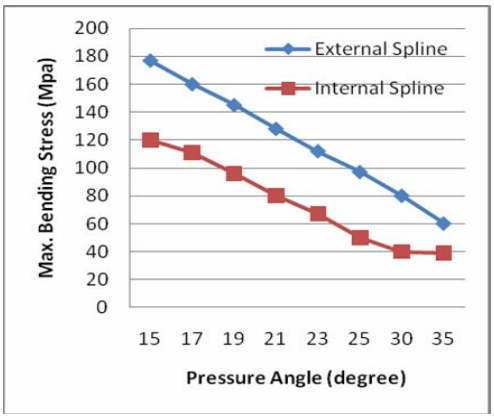

Fig. (6) Variation of bending stress for external and internal spline with pressure angle

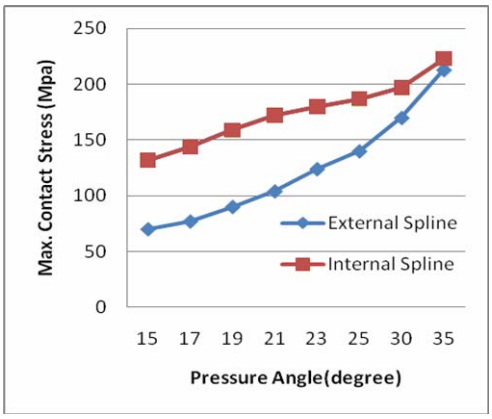

Fig. (7) Variation of bending stress for external and internal spline with pressure angle

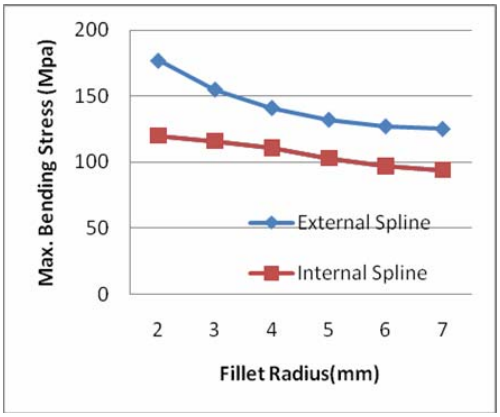

Fig. (8) Variation of bending stress for external and internal spline with pressure angle

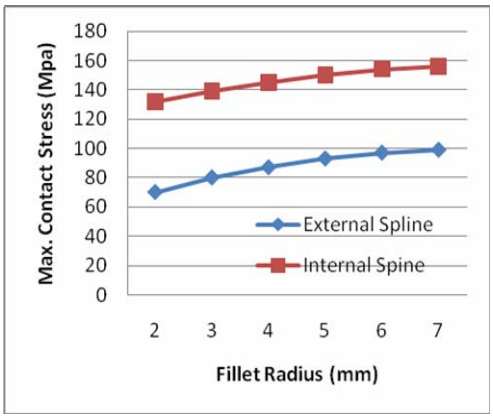

Fig. (9) Variation of bending stress for external and internal spline with pressure angle

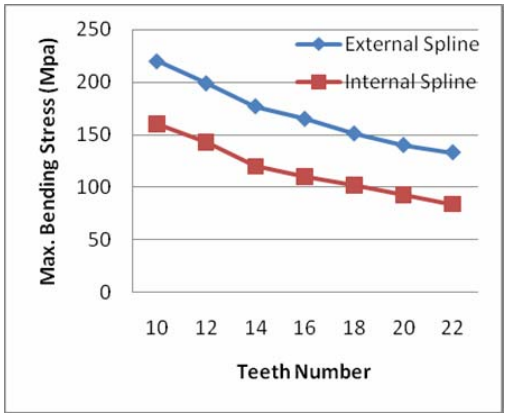

Fig. (10) Variation of bending stress for external and internal spline with pressure angle

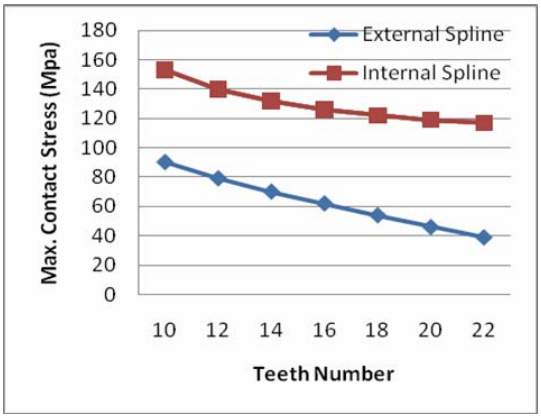

Fig. (11) Variation of bending stress for external and internal spline with pressure angle

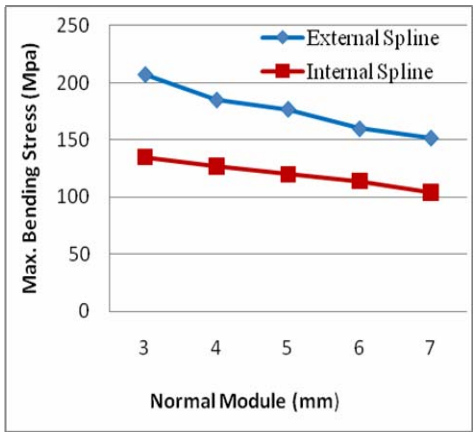

Fig. (12) Variation of bending stress for external and internal spline with pressure angle

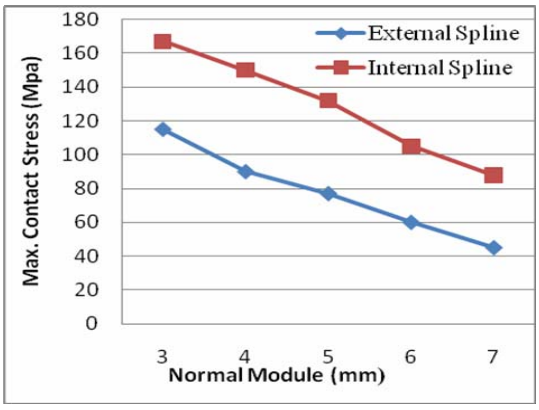

Fig. (13) Variation of bending stress for external and internal spline with pressure angle

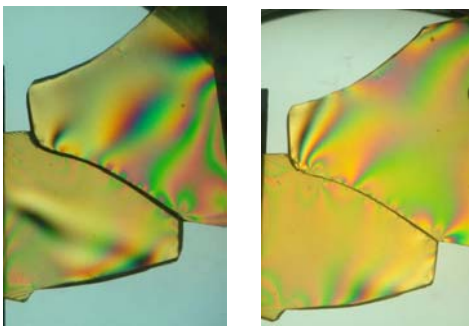

Fig. 14 Results of photoelastic fringes show the contact and bending stresses for two load cases of spline teeth .

Table 3 Comparison between experimental and numerical contact stress at load case (1)

Maximum Contact Stress(Mpa)			Percentage Error (%)
	Experimental	Numerical	
External	83.639	98.102	14.742
Internal	135.6	162.719	16.666

Table 4 Comparison between experimental and numerical bending stress at load case (1)

Maximum Bending Stress(Mpa)			Percentage Error (%)
	Experimental	Numerical	
External	237.814	224	-6.166
Internal	171.301	164.1	-4.388

Table 5 Comparison between experimental annumerical contact stress at load case (2)

Maximum Contact Stress(Mpa)			Percentage Error (%)
	Experimental	Numerical	
External	111.02	126.327	12.116
Internal	204.831	182.06	-17.006

Table 6 Comparison between experimental and numerical bending stress at load case (2)

Maximum Bending Stress(Mpa)			Percentage Error (%)
	Experimental	Numerical	
External	188.163	275.73	-4.509
Internal	205.03	194	-5.685

6. Conclusions:

The main conclusions obtained from the present work can be summarized as follow

1. In general the internal spline teeth offers a high resistance to the bending stress than the external spline teeth while they have a higher contact stresses than the external one so that the failure of the internal spline teeth occur at the flank region and at the fillet in the external spline teeth.
2. The increasing of the pressure angle and fillet radius reduce the induced fillet bending stress and increases the flank contact stress for both external and internal spline teeth.
3. Teeth number and normal module have a positive role one the performance of the spline shaft because of their substantial effect in the decreasing of the contact and bending stresses.
4. The bending stresses on the external teeth have the highest value comparable with bending stresses on internal teeth and contact stresses in internal and external teeth.

REFERENCES

A.Tjernberg, “Load Distribution and Pitch Errors in a Spline Coupling”. Journal of materials and design, No. 22, Pages 259-266, 2001.

D. A. Baker, “A Finite Element Study of Stresses in Stepped Splined Shafts, and Partially Splined Shaft under Bending, Torsion, and Combined Loadings”. A thesis submitted in partial fulfillment of the requirements for the degree of Master of Science in Mechanical Engineering/ Virginia Polytechnic Institute and State University 1999.

D. C. H. Yang and SH. H. Tong, “On the Profile Design of Transmission Splines and Keys”, Journal of Mechanism and Machine Theory, No.42, Pages 82-87, 2007.

D. L. Hitt, “Notes on Quantitative Photoelastic Analysis”. ME124, 2003.

E. J. Hearn, “Mechanics of Materials”. International series on material science and technology, VOL. 19, 1977.

F. James Doyle and James W. Phillips, “Manual on Experimental Stress Analysis”. Fifth Edition, Society for Experimental Mechanics, 1982.

H. Tea Cong, “A Design Support System Gear Drive”. Dep. Mech. Hanyang Univ., Korea, 1996.

H.Yoshitake,”Photoelastic Stress Analysis of the Spline Shaft”. Japan society of Mechanical Engineers, Vol.5, No17, Pages195-201, 1962.

J. F. Doyle, “Modern Experimental Stress Analysis”. Purdue University, Lafayette, USA, 2004.

J.Tombasco, “Photoelastic Dynamic Stress Analysis using Synchronized Strobe Techniques”. Internet / Keywords: Photoelastic stress analysis, 2004.

R. Errichello, “Bending Stress in Gear Teeth Having Circular Arc Profiles- Part 2: Experimental Investigation”. Transaction of the ASME, Journal of Mechanics Design, Vol.100, pages 395- 404, 1978.

Shigley, “Shigley’s Mechanical Engineering Design”. Eighth Edition, McGraw -Hill Companies, 2008.

U. Burgtorf, P. Dietz and M. Garzke, “Calculation of Involute Splines under Elastic Material Behaviour”. International design conference, Germany, 1998.

V. Nikolic, “The Analysis of Contact Stress on Meshed Teeth’s Flank Along the Path of Contact for a Tooth Pair”. Series: Mechanics, Automotive, control and robotic, Vol. 15, pages 1055-1066, 2003

NOMENCLATURES

English symbols

Symbol	Description	Unit
E	Modulus of elasticity	MN/m^2
f	Material fringe constant	N /mm
F_i	Nodal Force	N
h	Thickness of the specimen	mm
I	Moment of inertia	mm^4
M	Moment	N.m
n	Number of fringes	----
n	Node number subjected to force	----
r_i	Radius of Nodes Subjected to Force	Mm
T	Applied torque	N.m

Greek symbols

mbol	Description	Unit
ν	Poisons ratio	----
σ_1 and σ_2	Principal stresses	Mpa
σ_b	Bending stress	Mpa
ϕ	Pressure Angle	degree

Laboratory Investigation on Roller Compaction Technique in Concrete Construction

Prof. Saad I. Sarsam Dr. Abeer A. Al-Rawi Ahmed S. Abdul Rahim

ABSTRACT

Roller compacted concrete (RCC) is a concrete compacted by roller compaction. The concrete mixture in its unhardened state must support a roller while being compacted. The aim of this research work was to investigate the behavior and properties of roller compacted concrete when constructed in the laboratory using roller compactor manufactured in local market to simulate the field conditions. The roller compaction was conducts in three stages; each stage has different loading and number of passes of the roller. For the first stage, a load of (24) kg and (5) passes in each direction had been employed. For the second stage, a load of (104) kg and (10) passes in each direction were conducted. Finally, at the third stage, a load of (183) kg and (15) passes were adopted. Such procedure was in accordance to previous work conducted by the author. The effects of the type of coarse aggregate (crushed and rounded), fine aggregate (river and natural) and cement type (OPC and SRPC) on the mechanical properties of RCC were investigated. The effect of compaction method on compressive strength and indirect tensile strength was also discussed. A total of (26) roller compacted concrete slab samples of (380×380×100 mm) were prepared in the laboratory, Then, the slab specimens are taken out of the molds and immersed in the curing tank for (28) days. Core and Beam specimens were obtained from the slab samples for the determination of mechanical properties. Such properties include compressive, indirect tensile, flexural strengths using one point loading. It was concluded that the compressive strength of RCC using crushed aggregate is higher than that when using rounded aggregate in a range of (15-66) % for core specimens, while the compressive strength of RCC when using river sand is higher than that when using natural sand in a range of (9-26)% for core specimens. When river sand is implemented, RCC samples show higher indirect tensile strength than those with natural sand, such variation is within (7-8) %.

Keywords: roller compacted concrete, dense gradation, compressive strength, splitting tensile strength, flexural strength.

المستخلص

الخرسانة المرصوصة بالحدل تتمثل بكونها خرسانة ترص بالحادلات المدولبة حيث الخلطة الخرسانية في حالتها غيرالمتصلبة يجب ان تكون قادرة على تحمل حمل اسطوانة الحدل اثناء الرص. ان الغرض من هذا البحث هو التحري عن سلوك وخواص الخرسانة المرصوصة بالحدل تم تصنيعها مختبريا بأستخدام جهاز حدل صنع في الاسواق المحلية يشابه في هيكليته هيكلية الحادلة في الموقع من اجل ايجاد ظروف مشابه للظروف الطبيعية الموقعية. عملية الحدل تمثلت بثلاثة مراحل رئيسية كل مرحلة لها وزنها وعدد مرات مرور الحادله الخاصه بها حيث المرحلة الأولى كانت بوزن (٢٤) كغم وبعدد مرات مرور (٥) والمرحلة الثانية بوزن (١٠٤) كغم وبعدد مرات مرور (١٠) واما المرحله الأخيرة فكانت بوزن (١٨٣) كغم وبعدد مرات مرور (١٥). وقد كانت اتجاه الحدل بأتجاهين من اجل التخلص من المناطق الغير مرصوصة ولكل اتجاه ثلاثة مراحل رئيسية .تم اعتماد هذه الطريقة في الحدل استنادا لدراسة سابقة من قبل الباحث. تم دراسة تأثير نوع الركام الخشن (المكسر - المدور), نوع الركام الناعم (النهري- الطبيعي) ونوع السمنت المستخدم (العادي – المقاوم للكبريتات) على خواص الخرسانة المرصوصه بالحدل كما وتم اجراء مقارنة بين نتائج الخواص الميكانيكية (مقاومة الانضغاط ومقاومة الشد غيرالمباشر) لكل من النماذج التي تم رصها بواسطة المطرقه القياسيه وبين نماذج تم رصها بواسطة جهاز الحدل. تضمن الجزء العملي تهيئة (٢٦) بلاطة خرسانيه مرصوصه بالحدل بأبعاد (٣٨٠×٣٨٠×١٠٠ ملم) وتم استحصال النماذج والتي تتمثل (اللباب والاعتاب) من اجل اجراء الفحوص الخاصة بالخواص الميكانيكية. ان الخواص الفيزيائية للخرسانة المرصوصه بالحادلة المطلوبة في البحث هي مقاومة الانضغاط، مقاومة الشد غير مباشر (الأنشطار)، مقاومة الأنثناء (بنقطة تحميل واحدة). تم الاستنتاج بان مقاومة الانضغاط للخرسانة المحدولة تون اعلى عند استخدام الركام المكسر عند مقارنتها بالركام المدور وبما يتراوح مابين (15-66)% لعينات اللباب، بينما ادى استخدام الرمل التهري الى ارتفاع مقاومة الانضغاط بمعدل (9-26)% للخرسانة المحدولة عن تلك التي استخدم فيها الرمل الطبيعي. عند استخدام الرمل النهري لوحظ ارتفاع في مقاومة الشد غير المباشر بمقدار (7-8)% للخرسانة المحدولة عن تلك المقاومة عند استخدام الرمل الطبيعي.

INTRODUCTION

Roller-compacted concrete (RCC) is a lean no-slump, minimal shrinkage, almost dry concrete that is compacted in place by vibratory roller. RCC is a mixture of aggregates, cement and water. Supplementary cementing materials such as fly ash can also be used. Cement contents range from 60 to 360 kg per cubic meter. Mixing is done with conventional batch mixers, continuous mixers, or in some instances tilting-drum truck mixers, **(Kosmatka and Kerkhoff, 2002)**.

Roller compacted concrete is placed in layers thin enough to allow complete compaction, the optimum layers thickness ranges from 20 to 30 cm to ensure adequate bonding between the new and old layer or at construction joint, segregation must be prevented and high plasticity bedding mix must be used at the start of the placement, **(Shetty, 2009).** For effective consolidation, roller compacted concrete must be dry enough to support the mass of the vibrating equipment, but wet enough to allow the cement paste to be evenly distributed throughout the mass during mixing and consolidation process **(PCA, 2006)**.

In Japan, **Mamlouk and Zaniewski, (1999)** use RCC in construction. They find several advantages. These were:

1- The mix is economical because of the low cement content.

2- Formwork is minimal because of the layer construction method.

3- The low cement factor limits the heat of hydration, reducing the need for external cooling of the structure.

4- The placement costs are lower than conventional concrete methods due to the use of high-capacity equipment and rapid placement rates.

5- The construction period shorter than conventional concrete

MATERIAL CHARACTERISTICS

1. Cement

Both ordinary Portland cement (OPC) and sulfate resisting cement (SRPC) manufactured in Iraq with a commercial name of (Tasluga, Al-jesser) are used for RCC mixes throughout the present work. This cement complied with the Iraqi specification **(IOS, No.5:1984).** Testing of cement is conducted in the National Center for Construction Laboratories and research. The physical properties and chemical analysis of the cement used are given in the **Tables (1)** and **(2)**.

2. Aggregate

2.1 Coarse Aggregate

Two types of coarse aggregate (crushed and rounded) are used from Al-Nibaii in Iraq with a nominal size of (19 mm). The gravel is sieved through sieve size of (25 mm). The properties of two types of aggregate are shown in **Tables (3)**.

2.2 Fine Aggregate

Two types of fine aggregates, (passing sieve No.4 BS.) natural sand (N.S) from Al-Akhaider in Iraq and river sand (R.S) from Toz-khirmato are used for RCC mixes. The fine aggregate is sieved through sieve size (9.5 mm) to separate the aggregate particles of diameter greater than (9.5mm). The physical properties and chemical properties of the sand for two types are listed in **Table (4).**

The desired weight of each size of aggregate is taken and combined to obtain the required gradation. The design over all gradation of aggregate is selected by using (**SCRB, 2004**) dense gradation usually used for asphalt concrete pavement in Iraq. **Table (5)** illustrates the combined gradation used throughout the investigation.

DETIALS of EXPERIMENTAL WORK

1. Casting Molds preparation

All the slab test specimens used in this investigation are cast in steel molds to obtain a slab specimen having size of (380×380 mm) and a total depth of (100 mm) as shown in **Figure (1).**

2. Apparatus Description

The apparatus consists of steel skeleton as shown in **Figure (2).** It is designed to simulate steel roller which is usually used in the site for compaction. A solid cylinder 150 mm diameter, 360 mm in length and 15 kg in weight is fixed to the chase by two ball bearings to allow movement of the roller during compaction. The total weight of this apparatus is 24 Kg. It is supplied with a container capable of supporting standard steel weights up to (183 Kg).

Mix Design and Proportions

The concrete mix is designed according to **(ASTM D-1557)** standard. This proportioning method involves establishing a relationship between the density and moisture content of the mix by compaction of the mix in steel molds of (101.6 diameter × 116.4 high mm). A moisture-density test is used to determine the optimum

moisture content and maximum density of RCC mixtures for each mix as shown in **Figures (3-a), (3-b).** Five different percentages of cement content are used (10, 12, 14, 16, 18) by weight of oven dried aggregate and six different percentages of moisture content of a range of (4-8%) with 1% increment are used to determine the dry density-moisture content relationships. The types of mixes are shown in **Table (6)** After mixing thoroughly, the materials are placed by filling these cylinders in five layers and compacting each layer with (25) blows of a modified Proctor hammer (4.5 kg) falling from (450 mm) height according to (**ASTM D-1557)** (modified proctor) test method. A total of 48 cylinder samples of size (100 diameter × 115 high mm) were prepared by using hammer compaction.

COMPACTION

Compaction is achieved by placing the slab mold on vibrating table. The slab mold is subjected to three cycles of (8 seconds) vibration for each. The influence of this compaction is to create some initial compactive effort to the freshly laid surface, which is usually the case when using paving machine; then, the concrete mix is compacted using a roller device as shown in **Figure (4).**The design of rolling process is conducted in three stages after many trials on slab samples to obtain the designed dry density. The rolling sequence was in accordance to that adopted by **Sarsam (2002).** At the first stage, a total load of (0.66 kg/cm width) is implemented with five passes of the roller. The concrete is settled in a level position and completely fill the slab mold and gives a level surface. This can represent the initial compaction in the field. At the second stage, the load is increased to (2.9 kg/cm width) with ten passes, in each direction. This may simulate the intermediate field compaction. At the final stage, the load is further increased to (5 kg/cm width) with 15 passes of the roller, each horizontal direction was subjected to (15) passes. This represents the finishing compaction in the field. At this stage, the slab surface is smooth and level. For other parameters the number of passing of the roller are changed to determine the variations of the mechanical properties of RCC with number of passing.

Obtaining Drilled Cores, Sawed Beams and Cubes

A total of (26) samples were constructed using the roller device. **Figure (5)** shows part of the slabs obtained. The coring process (Hilti Diamond Coring System DD-250EE) is carried out according to **(ASTM C42-03),** set perpendicular to the laid surface of the RCC. The cylinders are cored from the slabs using a 72 mm diameter diamond core bit. Wet concrete diamond sawing process is used to cut the slabs to obtain beams and cubes. A total of 96 core specimens of (60 diameter × 100 high mm) are obtained from slabs specimens, 80 cubes of (100×100×100 mm) are also obtained from slab specimens, and 80 beams of (70×100×380 mm) are also obtained from slabs specimens, using mechanical diamond saw. **Figures (6), (7)** Shows part of the samples obtained.

Testing Hardened Concrete

1. Compressive Strength

Compressive strength test is carried out according to **(ASTM C-39 -01),** using a digital testing machine with a capacity of (2000 kN). Two core specimens of (60 diameter × 100 high mm) are tested from each mix. The compressive strength is then calculated by using **equation (1)** as follows:

$$\sigma = P/A \qquad (1)$$

Where;
σ: Compressive strength, MPa
p: Maximum applied load,(N)
A: Surface area, (mm^2).

2. Splitting Tensile Strength

Splitting tensile strength test is carried out according to **(ASTM C496-96),** using a digital testing machine with a capacity of (2000 kN). Two core specimens of (60 mm diameter ×100 mm height) are obtained from each mix, for the determination of splitting strength. The average of two test specimens is taken. The splitting tensile strength is then calculated by using **equation (2)** as follows:

$$f_{sp} = 2p/\pi DL \qquad (2)$$

Where;
f_{sp}: Splitting tensile strength, (MPa)
p : Maximum applied load,(N)
D: Diameter of concrete cylinder, (mm)
L: Length of concrete cylinder, (mm)

3. Flexural Strength

The flexural strength test is carried out according to (**ASTM C78- 02).** The flexural strength of (380×100×70 mm) beam specimens is determined by applying point loads at one-third span over a

length of (380 mm).The flexural strength is then calculated by using **equation (3)** as follows:

$F_r = PL/bd^2$ (3)

Where;
Fr = modulus of rupture, (MPa)
P= maximum applied load, (N)
L= span length, (mm)
d= depth of the specimens, (mm)
b= width of the specimens, (mm).

Result and Discussions

1. Compressive Strength

Figure (8) show the relationship between compressive strength and cement content of crushed and rounded aggregates for core specimens. When crushed aggregates are implemented higher compressive strength is obtained for all range of cement content. When core specimens are tested, 16% cement shows compressive strength higher than that of rounded aggregate by a range of (18-51) %. **Figure (8)** show the relationship between compressive strength and cement content of ordinary and Sulphate resisting Portland cement for core specimens. These results show that the compressive strength when used Sulphate resisting Portland cement work better in RCC mixes rather than when use ordinary Portland cement, when Sulphate resisting Portland cement are implement high compressive strength could be obtained for all of the cement percentage used, when core specimen were tested, 16% cement shows of compressive strength higher than that of ordinary Portland cement by a range of (24-29) %. **Figure (9)** show the relationship between compressive strength and cement content of river and natural fine aggregate for core specimens. These results show that the compressive strength when used river sand typically work better in RCC mixes rather than when use natural sand, when river sand is implement high compressive strength was obtained for all of the cement percentage used, when core specimen are tested, 16% cement shows of compressive strength higher than that of natural sand by a range of (8-18) %. Such result agrees well with Sarsam (2002) findings.

2. Splitting Tensile Strength

Figure (10) shows the relationship between the splitting tensile strength and cement content of crushed and rounded aggregates for core specimens. It is clear from the test results that the splitting tensile strength for crushed aggregate show superior tensile strength when compared with rounded aggregate. **Figure (11)** shows the relationship between the splitting tensile strength and cement content of ordinary and Sulphate resisting Portland cement for core specimens.
It is clear from the test results that the splitting tensile strength for Sulphate resisting Portland cement show superior tensile strength when compared with ordinary Portland cement. **Figure (12)** shows the relationship between the splitting tensile strength and cement content of river and natural fine aggregates for core specimens. It is clear that the splitting tensile strength for river sand show superior tensile strength when compared with natural sand.

3. Flexural Strength

Figure (13) present the relationship between flexural strength and cement content for center point loading of crushed and rounded coarse aggregates. Flexural strength of crushed aggregate shows higher values than rounded aggregate. When testing beam specimens under center point loading with 16% cement, the flexural strength was higher than of rounded aggregate by a range of (30-50) %. **Figure (14)** show the relationship between Flexural strength and cement content for center point loading of ordinary and Sulphate resisting Portland cement. Flexural strength of Sulphate resisting Portland cement shows higher values than ordinary Portland cement. When Sulphate resisting Portland cement is implementing, high flexural strength could be obtained for all range of cement content. When testing beam specimens by center point loading with 16% cement, shows of flexural strength higher than of ordinary Portland cement by a range of (26-34) %. **Figure (15)** shows the relationship between Flexural strength and cement content for center point loading of river and natural fine aggregates respectively. Flexural strength of river sand show higher values than natural sand. When river sand are implement, high flexural strength could be obtained for all of the cement percentage used, when beam specimens were tested by center point loading with 16% cement, shows of flexural strength higher than of natural sand by a range of (6-16) %. Such result agrees well with Sarsam (2002) findings.

CONCLUSIONS

The following conclusions can be drawn out of the experimental work of the present study.

1- The percentage of 16% for cement content is the ratio for the best rates to another 10%, 12% that was used in the various mixtures that were used which gave better results in terms of compressive, splitting tensile and flexural strength.

2- The compressive strength of RCC using crushed aggregate is higher than of using rounded aggregate in a range of (15-66) % for core specimens.

3- The compressive strength of RCC when using river sand is higher than when using natural sand in a range of (9-26)% for core specimens.

4- Sulphate resisting cement shows higher compressive strength than ordinary Portland cement. Such variations are within (40-50) % for core specimens.

5- The indirect tensile strength for RCC when crushed aggregates are implemented is higher than that when using rounded aggregates, such variations are within (10-32) %.

6- When river sand is implemented, RCC samples show higher indirect tensile strength than those with natural sand, such variation is within (7-8)%.

7- When Sulphate resisting cement is implemented, RCC samples show higher indirect tensile strength than those with ordinary Portland cement, such variation is within (51-56) %.

8- The flexural strength of RCC using crushed aggregate is higher than that with using rounded aggregate in a range of (30-50) % for center point loading.

10- The flexural strength of RCC using river sand is higher than that when using natural sand in a range of (0-4) % for center point loading.

11- The flexural strength of RCC when using Sulphate resisting cement is higher than that with using ordinary Portland cement in a range of (26-34) % for center point loading.

REFERENCES

• **ASTM D-1557, (1978**), "*Standard Test Method for Moisture-Density Relations of Soils and Soil-Aggregate Mixtures Using 10Ib (4.54 kg) Hammer and 18-in. (457-mm) Drop*", Annual Book of ASTM Standards American Society for Testing and Materials, vol.04.08, pp.206-210.

• **ASTM C-42, (2003),** "*Standard Test Method for Obtaining and Testing Drilled Cores and Sawed Beams of Concrete*", Annual Book of ASTM Standards American Society for Testing and Materials, vol.04.02.

• **ASTM C-39, (2001),** "*Compressive Strength of Concrete Cubes*", Annual Book of ASTM Standards American Society for Testing and Materials, vol.04.02.

• **ASTM C-78, (2002),** "*Standard Test Method for Flexural Strength of Concrete (Using Simple Beam with Third-Point Loading"*, Annual Book of ASTM Standards American Society for Testing and Materials, vol.04.02.

• **ASTM C-805, (2002),** "*Standard Test Method for Rebound Number of Hardened Concrete*", Annual Book of ASTM Standards American Society for Testing and Materials, vol.04.02.

• **ASTM C-597, (2002),** "*Standard Test Method for Pulse Velocity through Concrete*", Annual Book of ASTM Standards American Society for Testing and Materials, vol.04.02.

• **ASTM C-642, (1997),** "*Standard Test Method for Density, Absorption, and Voids in Hardened Concrete*", Annual Book of ASTM Standards American Society for Testing and Materials, vol.04.02.

• **Iraqi Organization of Standards, IOS 5: 1984,** for Portland cement.

• **Kosmatka and Kerkhoff, (2002)**, "*Design and Control of Concrete Mixtures*", 14th Edition, pp.326.

• **Mamlouk,.M. S. and Zaniewski, j. P., (1999)**, "*Materials for Civil and Construction Engineers*", 6th Edition, PP. (202).

•**Portland cement Association, (2006),** "*Production of Roller Compacted Concrete*" IS 332, Skokie I1.

• **Shetty, M. S., (2009)**, "*Concrete Technology*".

• **SORB, (2004)**, "*Standard Specification for Roads and Bridge*" Ministry of Housing and Construction, Iraq.

•**Sarsam S.I., (2002)** *"Evaluation of Roller Compacted Concrete Pavement Properties"*, Engineering and Development, Scientific Journal of Al-Mustansyreiah University, Vol. (6), No. (1).

Table (1) Physical properties of cement

Physical Properties	Test Result		IQS (No.5:1984) limits	
	O.P.C	S.R.P.C	O.P.C	S.R.PC
Specific Surface area, Blaine method, m^2/Kg	258	357	≥230	≥ 250
Setting time, Vicat Method Initial setting , hr : min	2:35	1:30	≥ 45 minutes	
Final setting , hr : min	4:45	4:10	≤ 10 hours	
Compressive strength MPa 3-days	15.8	18.3	≥15	
7-days	20.3	23.8	≥23	

Table (2) Chemical composition of cement

Oxide	Percentage (%)		IQS (No.5:1984) limits	
	O.P.C	S.R.P.C	O.P.C	S.R.P.C
Cao	55	60.63	-----	-----
SiO_2	18.33	21.63	-----	-----
Fe_2O_3	3.28	4.76	-----	-----
Al_2O_3	5.88	4.19	-----	-----
MgO	1.93	2.72	≤ 5	≤ 5
SO_3	1.87	2.04	≤ 2.8	≤ 2.5
L.O.I	2.36	1.94	-----	-----
I.R	0.15	0.92	≤ 1.5	≤ 1.5
L.S.F	0.89	0.86	0.66-1.02	0.66-1.022
Compound Composition	Percentage (%)		IQS (No.5:1984) limits	
C_3S	35	42.6	-----	-----
C_2S	26.21	29.95	-----	-----
C_3A	10.03	3.06	-----	3.5
C_4AF	9.97	14.47	-----	-----
C_3S/C_2S	1.35	1.42	-----	-----

Table (3) Properties of coarse aggregate

properties	Test results		IQS (No.5:1984) limits
	crushed	rounded	
Sulphate content SO_3 (%)	0.08	0.08	≤ 0.1
Specific gravity	2.68	2.63	-----
Absorption (%)	1	1.5	-----

Table (4) Properties of fine aggregate

Properties	Test results		IQS (No.5:1984) limits
	Natural sand	River sand	
Sulphate content SO_3 (%)	0.45	0.1	≤ 0.5
Specific gravity	2.42	2.6	-----
Absorption (%)	3.31	2.25	-----

Table (5) Combined gradation used for RCC, Sarsam(2002)

Sieve Size (mm)	% Finer by weight
25.4 (1 inch)	100
19.0 (3/4 inch)	100
12.5 (1/2 inch)	85
9.5 (3/8 inch)	76.5
4.75 (No. 4)	62.5
0.3 (No.50)	26.5
0.075 (No. 200)	9

Figure (1) Molds details of slab specimens

Figure (2) General view of apparatus

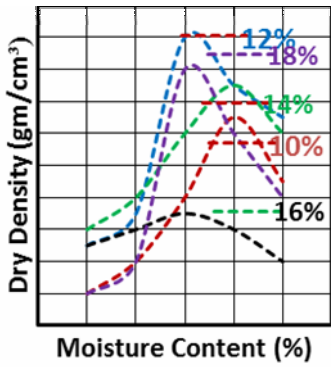

Figure (3-a) Dry density-moisture content relationship, natural sand and OPC for different cement content

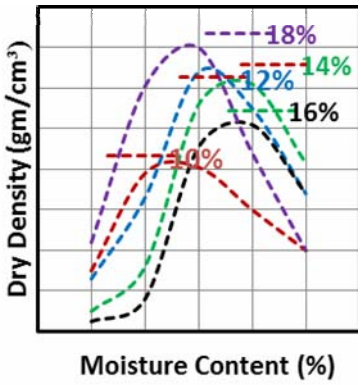

Figure (3-b) Dry density-moisture content relationship, natural sand and OPC for different cement content

Table (6) Design mixes implemented

Mix Symbol	Type of Mixes
Crushed-1	Crushed Aggregate + River Sand + Ordinary Portland cement
Crushed-2	Crushed Aggregate + Natural Sand + Ordinary Portland cement
Rounded-1	Rounded Aggregate + River Sand + Ordinary Portland cement
Rounded-2	Rounded Aggregate + Natural Sand + Ordinary Portland cement
River-1	Rounded Aggregate + River Sand + Ordinary Portland cement
River-2	Rounded Aggregate + River Sand + Sulphate Resisting Portland cement
Natural-1	Rounded Aggregate + Natural Sand + Ordinary Portland cement
Natural-2	Rounded Aggregate + Natural Sand + Sulphate Resisting Portland cement
Ordinary-1	Crushed Aggregate + River Sand + Ordinary Portland cement
Ordinary-2	Crushed Aggregate + Natural sand + Ordinary Portland cement
Sulphate-1	Crushed Aggregate + River sand + Sulphate Resisting Portland cement
Sulphate-2	Crushed Aggregate + Natural sand + Sulphate Resisting Portland cement

Figure (4) Casting and compaction in process

Figure (5) Slab samples constructed

Figure (6) Core specimens obtained

Figure (7) Beam specimens obtained

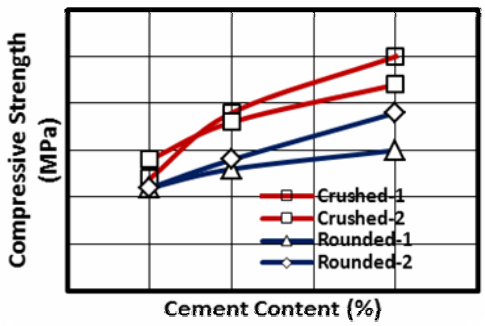

Figure (8) Variation in compressive strength

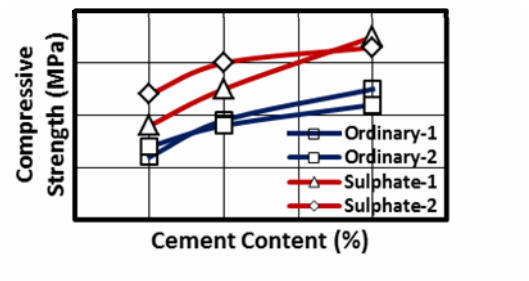

Figure (9) Variation in compressive strength with cement content using (O.P.C) and(S.R.P.C) for core specimens

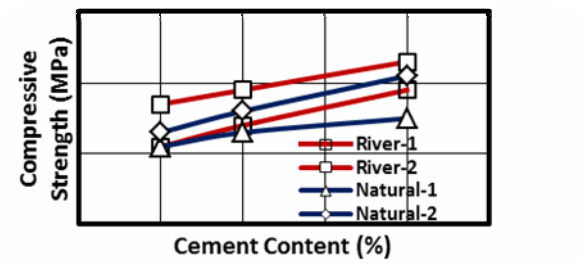

Figure (10) Variation in compressive strength with cement content using river and natural sand for core specimens

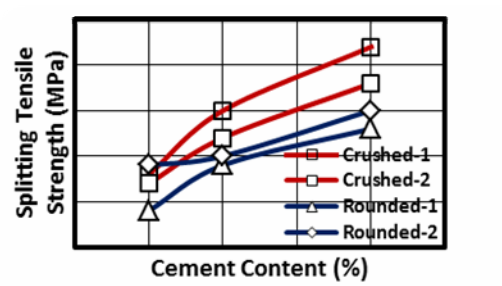

Figure (11) Variation in splitting tensile strength with cement content using crushed and rounded aggregates for core specimens

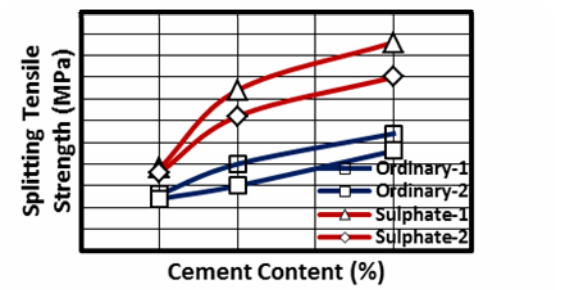

Figure (12) Variation in splitting tensile strength with cement content using (O.P.C) and (S.R.P.C) for core specimen

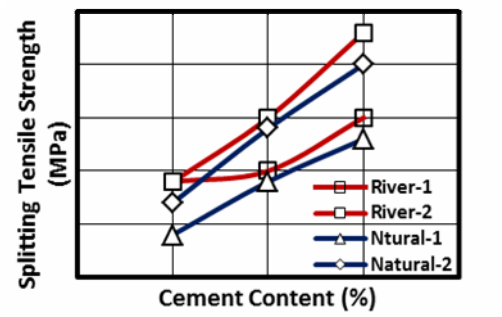

Figure (13) Variation in splitting tensile strength with cement content using river and natural sand for core specimens

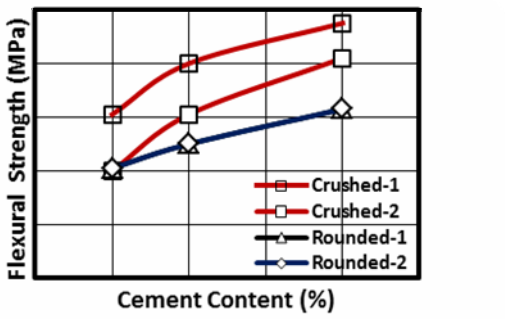

Figure (14) Variation in flexural strength with cement content using crushed and rounded aggregates for center point loading

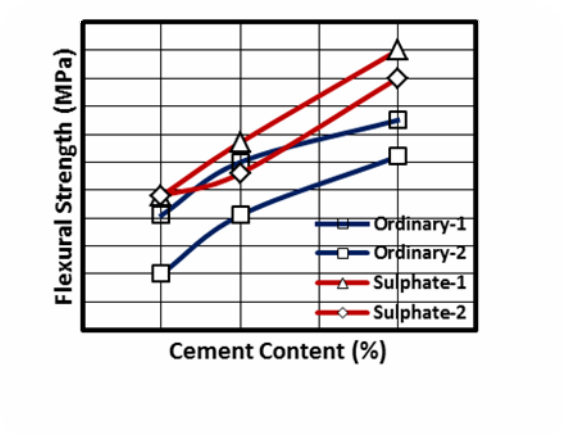

Figure (15) Variation in flexural strength with cement content using (O.P.C) and (S.R.P.C) for center point loading

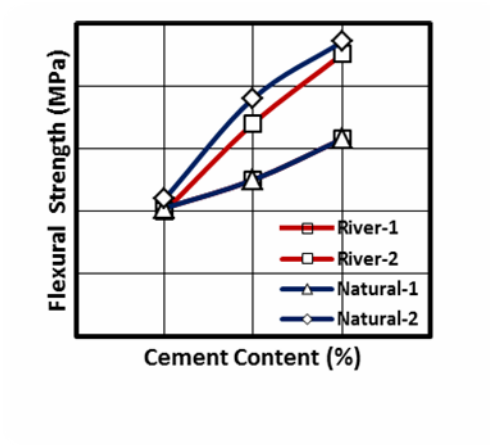

Figure (16) Variation in flexural strength with cement content using river and natural sand for center point loading

Performance Evaluation and Comparison Between LDPC and Turbo Coded MC-CDMA

Aqiel N. Almaamory **Husam Abduldaem. Mohammed**
aqiel.almamori@gmail.com **info@hs-engineer.com**
Assistant Lecturer \ Baghdad University\ College of Engineering

Electronic and Communications Engineering Department

ABSTRACT

This work presents a comparison between the Convolutional Encoding CE, Parallel Turbo code and Low density Parity Check (LDPC) coding schemes with a MultiUser Single Output MUSO Multi-Carrier Code Division Multiple Access (MC-CDMA) system over multipath fading channels. The decoding technique used in the simulation was iterative decoding since it gives maximum efficiency at higher iterations. Modulation schemes used is Quadrature Amplitude Modulation QAM. An 8 pilot carrier were used to compensate channel effect with Least Square Estimation method. The channel model used is Long Term Evolution (LTE) channel with Technical Specification TS 25.101v2.10 and 5 MHz bandwidth bandwidth including the channels of indoor to outdoor/ pedestrian channel and Vehicular channel. The results showed that the performance of the proposed system was better when the LDPC was used as a coding technique.

تقييم و مقارنة كفاءة LDPC and Turbo **Coded MC-CDMA**

***عقيل نعمه المعموري** ***حسام عبد الدائم محمد**
***مدرس مساعد\جامعة بغداد\كليه الهندسة\قسم الهندسة الالكترونية والاتصالات**

الخلاصة

يقدم هذا العمل مقارنة ل Convolutional Encoding CE, Parallel Turbo code and Low density Parity Check (LDPC) coding schemes مع نظام (MC-CDMA) متعدد المستخدمين ذو الخرج المفرد خلال قناة الخفوت متعدد المسارات. تقنية فتح الشفرات المستخدمة في البحث هي فك الشفرات التكراري لأنه يعطي الكفاءة القصوى مع عشرة تكرارات . نوعيات التضمين المتبعة هي Quadrature Amplitude Modulation QAM. تم استخدام 8 pilot carriers لمعادلة تأثيرالقناة مع Least Square Estimation method. القناة المستخدمة في النموذج هي قناة الجيل الثالث (LTE) ذات المواصفات التقنية TS 25.101v2.10 مع عرض قناة مقداره 5MHz وتشمل القنوات داخل وخارج ألابنيه والقنوات المتحركة. بينت النتائج ان كفاءة النظام المقترح افضل مع تقنية تشفير الLDPC.

KEY WORDS

MC-CDMA, PARALLEL TURBO CODE, LDPC, SUM-PRODUCT DECODING ALGORITHM, CONVOLUTIONAL CODING

Introduction

The enormous growth of interest for multicarrier (MC) systems can be ascribed to its high bandwidth efficiency and its immunity to channel dispersion. Recently, different combinations of orthogonal frequency division multiplexing (OFDM) and code division multiple access (CDMA) have been investigated in the context of high data rate communication over dispersive channels [Rodriguez 2003, Mottier 2002, Phan2003]. One of these systems is multicarrier CDMA (MC-CDMA), which has been proposed for downlink communication in mobile radio. In MC-CDMA the data symbols are multiplied with a higher rate chip sequence and then modulated on orthogonal carriers.
The MC-CDMA proved to be a suitable technique for the downlink transmission. Uplink transmission, due to the more complex propagation conditions, introduces additional problems which result in harder applicability of MC-CDMA in uplink [Ivan 2002]. MC-CDMA is very suitable for the downlink. The time and frequency synchronism between the users in the downlink allows a simple realisation of efficient channel estimation at the mobile station required for coherent detection [Ivan 2002].

It was in 1993, an epoch of CDMA application, that three types of new multiple access schemes based on a combination of code division and OFDM techniques were proposed, such as "multicarrier (MC) CDMA, multicarrier DS-CDMA, and multitone (MT) CDMA. These schemes were developed by different researchers, namely. MC-CDMA by N. Yee. J. P. Linnartz and G. Fettweis For more details about MC-CDMA refer to [Husam 2010, Aqiel2011 and Shinsuke 1997].

Wireless mobile communication systems present several design challenges resulting from the mobility of users throughout the system and the time-varying channel (Multipath fading). There has been an increasing demand for efficient and reliable digital communication systems. To tackle these problems effectively, an efficient design of forward error coding (FEC) scheme is required for providing high coding gain. To obtain high coding gains with moderate decoding complexity, concatenation of codes with iterative decoding algorithms has proved to be an attractive scheme [Husam 2010]. From these codes are the TURBO CODE and the Low Density Parity Check LDPC codes.

In the next sections a brief review of both the Parallel Concatenated Convolutional (TURBO CODE) codes and Low-Density Parity-Check (LDPC) codes are given. The system proposed and the simulation results were introduced then. Finally, conclusions of the work were given.

Parallel Concatenated Convolutional (TURBO CODE) Encoding

The convolutional turbo coder consists of a parallel concatenation of recursive systematic convolutional RSC encoders separated by a pseudo-random interleaver [Ramasmay 2006, Husam 2010]. The main aim of RSC is to produce more high weight codes even though input contains more number of zeros [Shanmugam 2005]. A natural rate for such a code is 1/3 (one systematic bit and two parity bits for one data bit). The rate can be relatively easily increased by puncturing the parity bits but reducing the rate below 1/3 is more difficult and may involve repetition of some bits [Ramasmay 2006]. The structure of such a Turbo coder is shown in Figure (3a).

One important feature of turbo codes is the iterative decoding which uses a soft-in/soft-out (SISO) like the Max-Log- Maximum A Posteriori (MLMAP) algorithm is a good compromise between performance and complexity [Vogt 1999]. It is very simple and, with the correction operation, also very effective [Robertson 1995]. Compared to the Maximum A Posteriori (MAP)/Log-MAP algorithm no SNR-information is necessary and the critical path within the add-compare-select (ACS) unit is shorter because of the maximum operation without the correction term [Robertson 1997].

Like other methods max-log-APP algorithm calculates approximate log-likelihood ratios LLR's for each input sample as an estimate of which possible information bit was transmitted at each sample time[Robertson 1995].They are calculated according to [Robertson 1995, Robertson 1997, Husam 2010]

$$L_i = \max_m [A_i^m + D_i^{0,m} + B_{i+1}^{f(0,m)}] - \max_m [A_i^m + D_i^{1,m} + B_{i+1}^{f(1,m)}] \quad [1]$$

where i is the sample time index, m $\in\{0, \dots, N_s\text{-}1\}$ is the present state, N_s is the number of encoder states, f(d, m) is the next state given present state m and input bit d $\in \{0,1\}$, A_i^m is the forward state metric for state m at time i, B_i^m is the reverse or backward state metric for state m at time i, and $D_i^{d,m}$ is the branch metric at time i given present state m and input bit d$\in\{0,1\}$. More formally, the state and branch metrics are given by [Robertson 1995, Robertson 1997, Husam 2010]

$$A_i^m = \max[A_{i-1}^{b(0,m)} + D_{i-1}^{0,b(0,m)}, A_{i-1}^{b(1,m)} + D_{i-1}^{1.b(1,m)}] \quad [2]$$

$$B_i^m = \max[D_i^{0,m} + B_{i+1}^{f(0,m)}, D_i^{1.m} + B_{i+1}^{f(1,m)}] \quad [3]$$

$$D_i^{d,m} = \frac{1}{2}(x_i d^t + y_i c^{td,m}) \quad [4]$$

where b(d,m) is the previous state given present state m and previous input bit d$\in\{0,1\}$, x_i is the ith systematic sample, y_i is the ith parity sample, d is a systematic bit, $c^{d,m}$ is the corresponding coded bit given state m and bit d, $d^{td,m}$ =1-2d , and $c^{td,m} = 1 - 2c^{d,m}$. The state metrics provide a measure of the probability that state m is the correct one at time i, while the branch metrics are a measure of the probability that each possible combination of encoder outputs is the correct one given the channel outputs x_i and y_i.

The Max-Log-APP algorithm is sub-optimum due to the approximations involved. However, most of the performance loss associated with this sub optimality can be recovered by applying a simple scale factor correction to the output of the constituent decoder. The so-called extrinsic information may be approximated as [Robertson 1995, Robertson 1997, Husam 2010]

$$L_{ex}^n = sf \cdot \left(L_{out}^n - L_{in}^n\right) \quad [5]$$

where $n \in \{1,2\}$ denotes one of the constituent decoders, L_{out}^n represents the set of LLRs produced by the max-log-MAP decoder, L_{in}^n represents the set of input LLRs, and *sf* is an appropriate scale factor. The turbo concatenated decoder architecture is shown in Figure (3b).

LDPC CODING

LDPC codes are linear block codes specified by a very sparse (containing mostly 0's and only a small number of 1's) random parity-check matrix, but are not systematic. The parity-check matrix of an LDPC is an $M \times N$ matrix **A** , where M is the number of parity bits, and N is the transmitted block length ($N = K + M$, with K as the source block length). The matrix **A** is specified by a fixed column weight j and a fixed row weight $k = j\ N\ /M$ (in the MacKay's and Neal's codes k is as uniform as possible (MacKay 1999, Aqiel 2011), and code rate $R = K\ /N$. LDPC codes can be decoded using probability propagation algorithm known as the

sum-product or belief propagation algorithm [Kschischang 2001], which is represented by a factor graph [Tanner Graph] that contains two types of nodes: the "bit nodes" corresponding to a column of the parity-check matrix, which also corresponds to a bit in codeword and the "check nodes" corresponding to a row of the parity-check matrix, which represents a parity-check equation.

SUM-PRODUCT DECODING ALGORITHM

The decoding problem is to find the most probable vector x such that **A**x mod 2 = 0 , with the likelihood of x given by $x_n \Pi_n f_n$, where $f_n^0 = 1 - f_n^1$ and $f^1_n = 1/(1 + \exp(-2y_n / \sigma^2))$ for AWGN channel or $f^1_n = (y_n / \sigma^2) \exp[-y^2_n / 2\sigma^2]$ for Rayleigh channel, and y_n , σ^2 represent the received bit and noise variance, respectively. We denote the set of bits, n , that participate in check m as $N(m) \equiv \{n : A_{mn} = 1\}$, where A_{mn} represents the element of the mth row and nth column in the parity-check matrix. Similarly, we define the set of checks m in which bit n participates as $M(n) \equiv \{m : A_{mn} = 1\}$. We denote a set N (m) with bit n excluded as N (m) \ n. The algorithm has two alternating parts, in which quantities q_{mn} and r_{mn} associated with each non-zero element in the matrix A are iteratively update. The quantity x q_{mn} is meant to be the probability that bit n of x is x, given the information obtained via checks other than check m. The quantity r_{mn} is meant to be the probability of check m being satisfied if bit n of is *x* considered fixed at x and the other bits have a separable distribution given by the probabilities $\{q_{mn'} : n' \in N(m) \setminus n\}$. The aposteriori probabilities for a bit are calculated by gathering all the extrinsic information from the check nodes that connect to it, which can be obtained by the following iterative sum-product procedure [Luis 2006, Aqiel 2011].

Step 1: Initialization The variables q^0_{mn} and q^1_{mn} , which are the probabilities sent from the nth bit node to the $_m th$ check node along a connecting edge of a factor graph, are initialized to the values f^0_n and f^1_n ,respectively.

Step 2: Horizontal Step (bit node to check node) We define $\Delta q_{mn} \equiv q^0_{mn} - q^1_{mn}$ and compute eq.(6) and eq. (7) for each m, n and x = 0,1:

$$q^0_{mn} = \prod_{n' \in N(m) \setminus n} q^0_{mn'} \qquad (6)$$

$$r^0_{mn} = \{1 + (-1)^0 \Delta_{mn}\}/2$$

$$r^0_{mn} = \{1 + \Delta_{mn}\}/2 \qquad (7)$$

$$r^1_{mn} = \{1 - \Delta_{mn}\}/2$$

Where, r_{mn} represents the probability information sent from the m_{th} check node to the nth bit node.

Step 3: Vertical Step (check node to bit node)

For each n , m and x = 0,1 we update eq.(8):

$$q^0_{mn} = \alpha_{mn} f^0_n \prod_{m' \in M(n) \setminus m} r^0_{m'n}$$

$$q^0_{mn} = \alpha_{mn} f^o_n \prod_{m' \in M(n) \setminus m} r^0_{m'n} \qquad (8)$$

Where, α_{mn} is a normalization factor chosen such that $q^0_{mn} + q^1_{mn} = 1$. We can also update the aposteriori probabilities q^0_n q^0_n and q^1_n q^0_n, given by eq. (9):

$$q^0_{mn} = \alpha_{mn} f^o_n \prod_{m' \in M(n) \setminus m} r^0_{mn} \qquad (9)$$

Where, α_n is a normalization factor chosen such that $q_n^o + q_n^1 = 1$.

Step 4: Check stop criterion soft decision is made on the q_n^1 q_n^1 . The resulting decoded vector x^ is checked against the parity-check matrix A. If Ax^ = 0,the decoder stops and outputs ^x. Otherwise, it repeats the procedure from the Step 2. The sum-product algorithm sets a maximum number of iterations: if the number of iterations reaches that maximum, the decoder stops and outputs ^x as the results of the decoding.

The Proposed System and Results

The proposed system is a MUSO MC-CDMA system. A complete block diagram of the proposed system is shown in Figure (4). The simulation was done using MATLAB R2010a package. A 20 Mbps was transmitted using the system. The channel is ITU LTE Vehicular channel. First the incoming data encoded using the Convolution code CE or TURBO CODE code or LDPC code as illustrated in the mentioned figure. The main parameters of the system are listed in table (1).

The parallel Turbo coder with both the upper and lower coder of a generator polynomial of [1 0 1 1; 1 1 0 1]) polynomial generators and a constraint length of (4). With the Max-Log-MAP decoding algorithm which is an iterative decoding algorithm. The random interleaver length was 1024 in both cases

The LDPC specifications used are irregular [16384] parity check matrix of rate ½ .The decoding algorithm is Sum-Product Decoding Algorithm, which is the soft decision type of message passing.

The performance of both Turbo code and LDPC code systems depend upon the number of iteration of the decoder. Since variations of the multipath fading channel affect the performance of the system, knowledge of the channel is crucial for accurate signal demodulation. Pilot-symbol aided-modulation (PSAM) is one of the well known techniques to estimate the channel state at pilot symbol positions. The method of estimation was the least square LS method.

Table 1 Simulation parameters for the indoor to outdoor/pedestrian environment

No. of active users	4
Total Number of users	48
Spreading code	Walsh Hadmard
Bandwidth	5 MHz
Spreading factor	48
FFT size	256
Effective symbol Duration	5.5556e-005
Guard time duration	¼FFTlength, 1.1111e-005
No of paths	8
Pilot carriers	8
Channel estimation	LS
Doppler velocity	60Km/h
Modulation technique	QAM with M = 4,16and 64
Convolution code generator polynomial	[53, 75] octal
CC decoding algorithm	Viterbi

Figures (5, 6 and 7) show the performance of the system (BER versus SNR) over LTE channel for uncoded data, convolution, TURBO CODE and LDPC coded data data with QAM with M= 4, 16 and 64 respectively with AWGN channel. It can be seen that the LDPC coded MC-CDMA system behaves better than any one of the others uses the TURBO CODE or CE or uncoded data.

Conclusions:

One can observes from the results that the LDPC gives a better BER for the Rayleigh channel for low SNR and the difference in dBs increases for higher values of SNR.

References:

J Rodriguez, D. T. Phan Huy et al. , "Radio Link Layer Design for IST MATRICE project", *IST Mobile and Wirless Communication Summit 2003*, vol II pp847.

D. Mottier et al. "Physical Layer Simulation Chain Description", *IST-2001-32620 MATRICE, D3.1*, Nov. 2002.

D. T. Phan Huy et al.,"Specification of the performance evaluation methodology and the target performance*",*IST-2001-32620 MATRICE, D1.3, Jan. 2003.

Ivan Cosovic, Michael Schnell, "Time Division Duplex MC-CDMA for Next Generation Mobile Radio Systems", 10th Telecommunications forum TELFOR'2002, Belgrade, Yugoslavia, Nov. 26-28, 2002.
Shinsuke Hara and Ramjee Prasad, " Overview of multicarrier CDMA" IEEE Communications Magazine, December 1997.

Husam A. Mohammed, "TURBO CODE MC-CDMA Combination Performance Over Multipath Rayleigh Fading Channel, Journal of Engineering, V.15, No.3, 2010.

Aqiel N. Almaamory,"LDPC Coded Multiuser MC-CDMA Performance Over Multipath Rayleigh Fading", to be published

Ramasmay K., Mohammed U. S., mohammed Y. A. and A. Arunagiri, " Performance comparison of convolutional and block codes",IEICE Electronic Express, V. 3, N. 13, pp, 322-327, 2006.

Shanmugam A., A. R. Abdul Rajak, "Optimal design of forward error correcting codes for wireless communication", Academic open Internet journal, V. 14, 2005, http://www.acadjournal.com/.

Vogt J., K. KOORA, A. FINGER and G. FETTWEIS: "Comparison of Different Turbo Decoder Realizations for IMT-2000", in Proc. of the IEEE GLOBECOM '99, Rio de Janeiro, Dec. 1999, pp. 2704-2708.

Robertson P., E. Villebrun, and P. Hoeher, "A Comparison of Optimal and Sub-Optimal MAP Decoding Algorithms Operating in the Log Domain", Proceedings of the 1995 International Conference on Communications (ICC'95), Seattle, WA, USA, pp. 1009-1013, June 1995.

Robertson, P. Hoeher, and E. Villebrun, "Optimal and Sub-Optimal Maximum a Posteriori Algorithms Suitable for Turbo Decoding", *IEEE Communications Theory*, Vol. 8, No. 2, pp. 119-125, March-April 1997.

G. D. Forney Jr., Concatenated Codes, MIT Press, Cambridge, Mass,1966.

Sergio, Dariush Divsalar, Guido Montorsi and Fabrizio Pollara, "Serial concatenation of Interleaved Codes: Performance Analysis, Design, and Iterative Decoding", IEEE Transactions on information theory, V. 44, No. 3, May 1998.

D. J. C. MacKay, R. M. Neal, "Good Error-Correcting Codes based on Very Sparse Matrices", *IEEE Trans. Inform. Theory*, vol. 45, pp. 399-431, Mar. 1999.

T. Richardson, A. Shokrollahi, R. Urbanke, "Design of Provably Good Low Density Parity-Check Codes", *IEEE Trans. Inform. Theory*, pp. 199, 25-30 June 2000.

F. R. Kschischang, B. J. Frey, H. A. Loeliger, "Factor Graphs and the Sum-Product algorithm", *IEEE Transactions on Information*

Theory, vol. 47, Issue 2, pp. 498-519, Feb. 2001.

Luis Alberto Paredes Hernández and Mariano García Otero" A New LDPC-STB Coded MC-CDMA Systemswith SOVA-Based Decoding and SOFT- NterferenceCancellation", 14th European Signal Processing Conference (EUSIPCO 2006), Florence, Italy, September 4-8, 2006, copyright by EURASIP

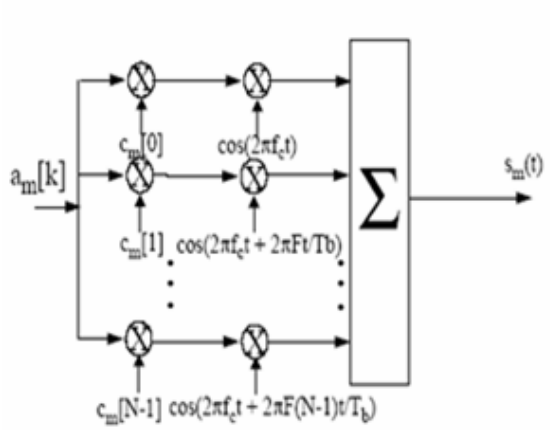

Fig.(1): MC-CDMA transmitter.

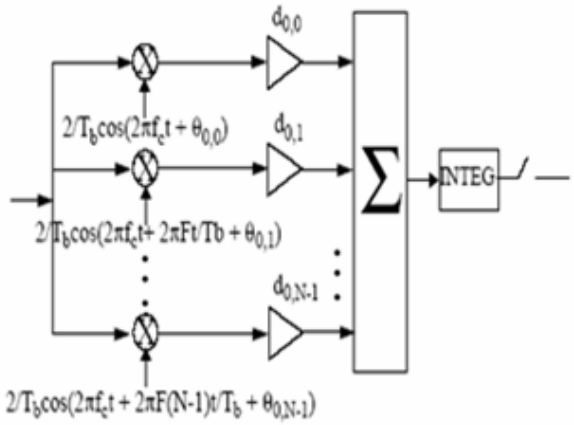

Fig.(2): MC-CDMA receiver.

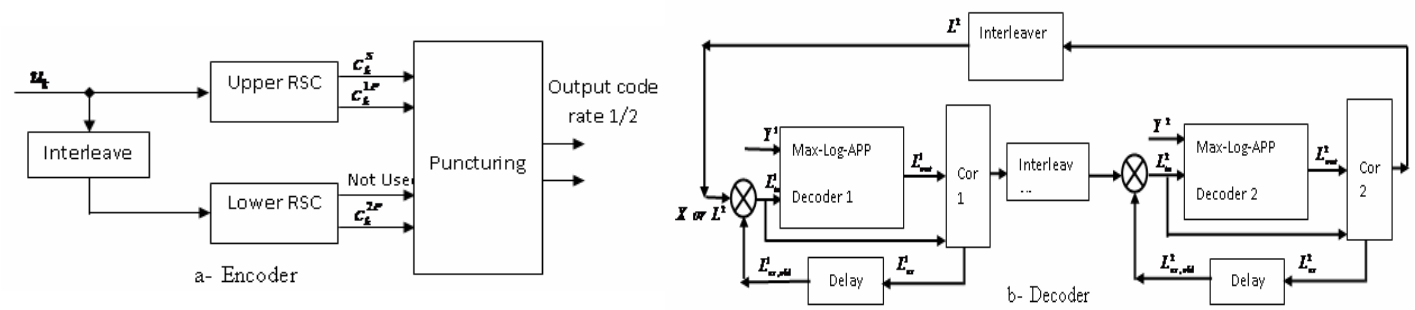

Fig. (3) Parallel concatenation convolutional code (TURBO CODE) a- Encoder b- Decoder

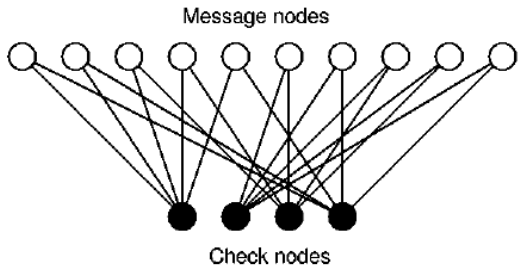

Fig. (4): Tanner Graph

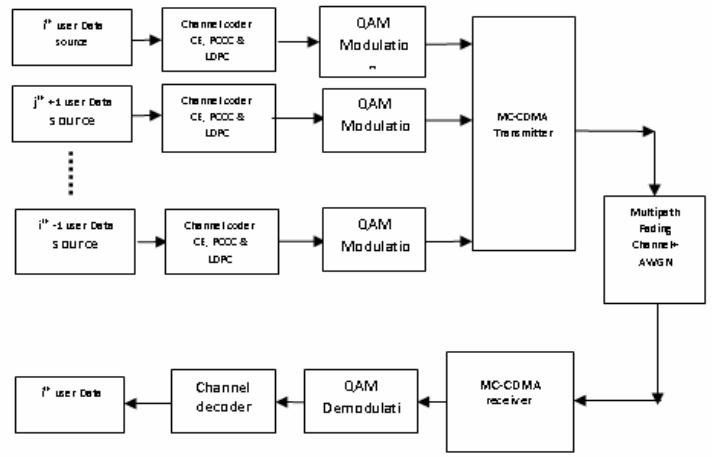

Fig. (4) Block Diagram of the Proposed MUSO Coded MC-CDMA System

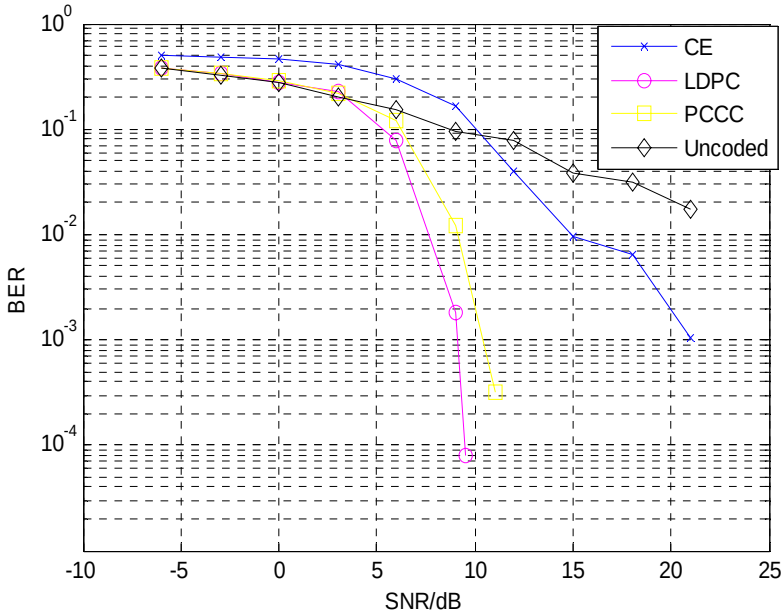

Fig. (5): Coded MC-CDMA performance for Rayleigh Fading channel with 4QAM modulation.

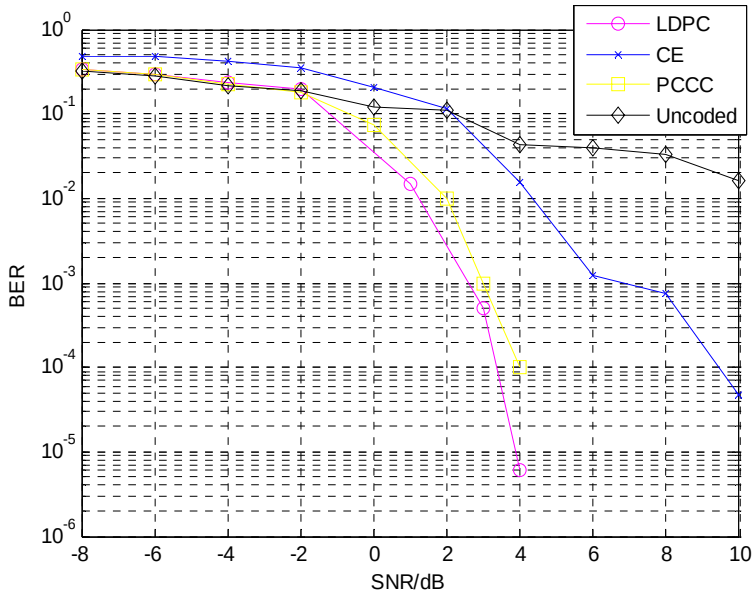

Fig. (6): Coded MC-CDMA performance for Rayleigh Fading channel with 16QAM modulation.

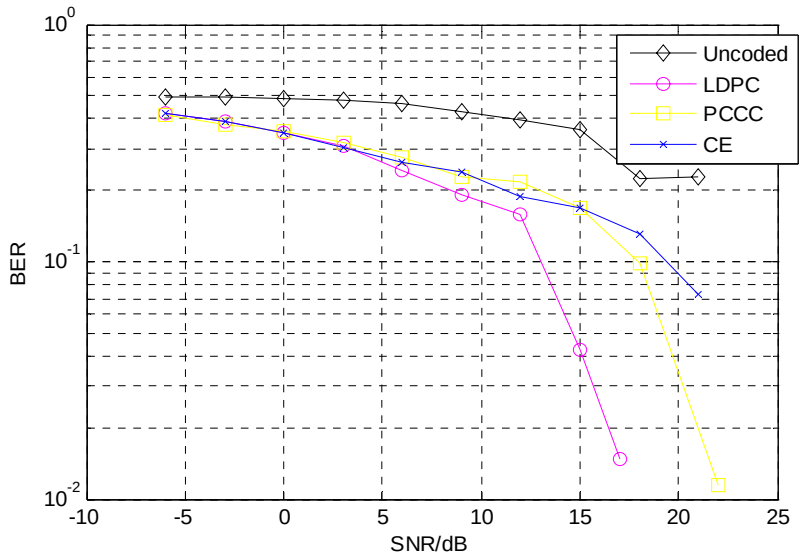

Fig. (7): Coded MC-CDMA performance for Rayleigh Fading channel with 64 QAM modulation.

FINITE ELEMENT ANALYSIS OF HUMAN AND ARTIFICIAL ARTICULAR CARTILAGE

Dr. Sadiq Jafer Abbass
College of Engineering
Nahrain University

Eng. Farah Mohammed Reda Abdulateef
College of Engineering
Nahrain University

Joint diseases, such as osteoarthritis, induce pain and loss of mobility to millions of people around the world. Current clinical methods for the diagnosis of osteoarthritis include X-ray, magnetic resonance imaging, and arthroscopy. These methods may be insensitive to the earliest signs of osteoarthritis. This study investigates a new procedure that was developed and validated numerically for use in the evaluation of cartilage quality. This finite element model of the human articular cartilage could be helpful in providing insight into mechanisms of injury, effects of treatment, and the role of mechanical factors in degenerative conditions, this three-dimensional finite element model is a useful tool for understanding of the stress distributions within articular cartilage in response to external loads and investigating both the prevention of injury and the pathological degeneration of the joints.

In this study, 21 models were analysed by using ANSYS workbench v12.1: four normal articular cartilage models (distal femur, patella, medial and lateral tibia). A redesign to the distal femur model was done to get osteoarthritis articular cartilage (simple and deep) seven models by making partial cut without affecting the subchondral bone, and full cut with part of the subchondral bone in different diameters. Finally a treatment done by replacing the defective parts with artificial articular cartilages with different types of treatment. The finite element analysis studied depending on a Von Mises criteria and total deformation in different activities. The results shows that Autologous Chondrocyte Implementation is the best treatment way and it is close by 87.50% to normal cartilage. This procedure can be used as a diagnostic procedure for osteoarthritic patients and to choose the best treatment options.

الخلاصـــــــة

أمراض المفاصل، كـ (إلتهاب المفاصل الضموري)، تسبب الالم وعدم القدرة على الحركة لملايين الناس في العالم. طرق التشخيص الحالية للمرضى تستخدم الاشعة السينية، و جهاز الرنين المغناطيسي، و الناظور المفصلي، هذه الطرق لا تكون حساسة لإكتشاف العلامات الاولى لحدوث هذا المرض. لذلك هذه الدراسة بحثت طريقة جديدة طُورت حسابياً لتستخدم في تقييم كفاءة الغضروف عن طريق تصميم نموذج للغضروف المفصلي في الانسان بإستخدام العناصر المحددة لإلقاء الضوء على ميكانيكية الجرح و تأثيرات المعالجة و دور العوامل الميكانيكية في حدوث الأضرار و يعتبر نموذج العناصر المحددة ثلاثي الابعاد للغضروف المفصلي هذا طريقة مفيدة في فهم توزيع الاجهاد ضمن الغضروف المفصلي ضد الاجهادات الخارجية و بحث كل من منع حدوث الاضرار والامراض التي تحدث في المفاصل. في هذه الدراسة تم تحليل واحد وعشرون نموذجاً بإستخدام برنامج (ANSYS workbench v12.1) يتضمن أربع نماذج للغضروف المفصلي الطبيعي (غضروف عظم الفخذ السفلي، و غضروف الرضفة، و غضروفي عظم القصبة الداخلي والخارجي)، وبعدها تم إزالة جزء من الغضروف المفصلي لعظم الفخذ ليصبح كأنه مصاب بمرض (إلتهاب المفاصل الضموري) البسيط والعميق وذلك عن طريق عمل قطع جزئي بدون التأثير على العظم الذي تحت الغضروف، ومن ثم عمل قطع كامل لجزء من الغضروف مع جزء من العظم الذي تحته، وبأبعاد مختلفة بكلتا الحالتين، ثم معالجة الجزء المقطوع بإستبداله بغضروف مفصلي صناعي بإستخدام عدة طرق للعلاج ثم دراسة التحليل بإستخدام العناصر المحددة بالاعتماد على معايير (Von Misses) و التشوه الكلي في نشاطات مختلفة.

Key Words:
Finite element analysis, Articular Cartilagr, Artificial AC, Osteoarthritis, Arthritis, ANSYS.

Introduction

Articular cartilage is a complex tissue, which covers the ends of long bones in synovial joints. It protects the subjacent bone from high friction, increases contact area, and consequently improves the local joint congruence [C. Bratianu 2004][J. Yao 2003]. Articular cartilage is a biphasic material that consists of a solid and a fluid phase. As a result of this biphasic structure articular cartilage is viscoelastic [G. Li 1998]. Cartilage plays an extremely important role within the bod
y's joints [W. Bogatay 2009]. In combination with the synovial fluid, articular cartilage enables furthermore a nearly frictionless movement of the joint over the whole lifespan of a person. As articular cartilage has only a limited capacity for self-repair, this process, once started, can hardly be reversed [S. Knecht 2006]. It has been well established that articular cartilage is compositionally and mechanically inhomogeneous through its depth [R. Krishnan 2003]. This unique structure generates a complex mechanical response under physiological or extreme loads related to sports activities. Therefore, an accurate understanding of the joint biomechanics considerably improves the prevention and treatment of the joint disorders and injuries [C. Bratianu 2004]. Calculating cartilage stress is technically challenging, as many factors can influence stress, including the joint contact force, material properties of the tissue, the geometry of the articulating surfaces, and the cartilage thickness [T. Besier 2005].

Articular Cartilage Structure

In normal human joints, the thickness of the articular cartilage layer varies from 0.5 to 1.5 mm in upper extremity joints and from 1 to 6 mm in lower extremity joints [8, 9]. Structure and components of synovial joint are shown in **Figure** (1). Furthermore, articular cartilage distributes the loads over a larger contact area, thereby minimizing the contact stress, and absorbing part of the energy transferred through the joints during normal activities [D. Schneck 2003].

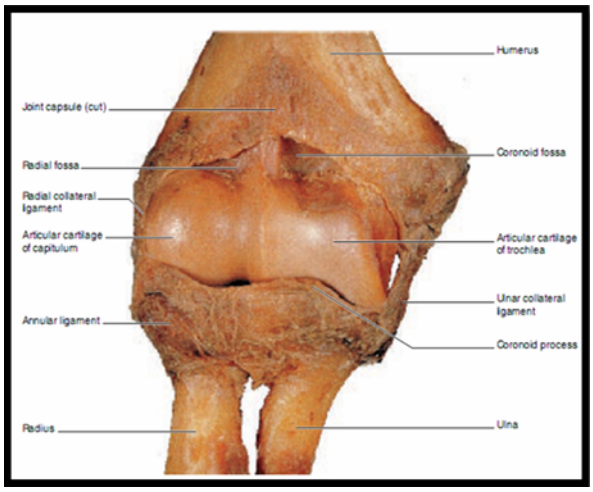

Figure (1) Structure and components of synovial joint (elbow joint) [V. Graaff 2001].

Articular cartilage plays a vital role in the function of the musculoskeletal system by allowing almost frictionless motion to occur between the articular surfaces of a diarthrodial joint for smooth joint movement [A. Iftekhar 2004], The coefficient of friction between articulating surfaces is remarkably low during dynamic loading (in human joints 0.001 - 0.08).

The low coefficient of friction results from the biphasic nature of cartilage and the lubrication induced by the synovial fluid [T. Besier 2005][W. Wilson 2005].

Articular or hyaline cartilage forms the bearing surfaces of the movable joints of the body. The importance of articular cartilage as a bearing surface has led to extensive mechanical and tribologic studies of this tissue [J. Black 1998]. **Figure** (2) shows the structure of the synovial joint.

Due to the avascular nature of articular cartilage, the provision of metabolites to the cells is assumed to occur via diffusion from the synovial fluid or, to a lesser extent, the underlying bone. However, the lack of blood supply severely diminishes the ability of cartilage to heal once it has been damaged [S. Knecht 2006][A. Iftekhar 2004].

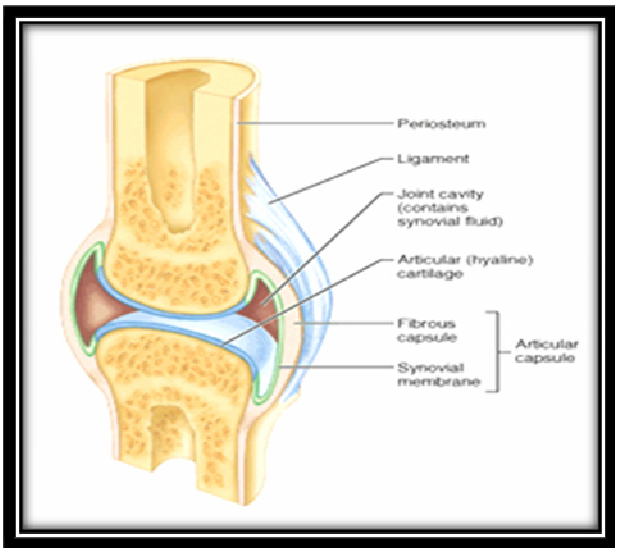

Figure (2) Structure of the synovial joint [T. Gill 2006].

The cartilage does not possess a uniform thickness. It is influenced by different factors, e.g., size of bone, pressure, stress, and age [M. Mlejnek 2006]. The interactions between collagen, proteoglycans, and fluid play an important role in the mechanical response of cartilage [T. Besier 2005].

Organization of the articular cartilage

The structural arrangement of the biochemical components in articular cartilage is highly anisotropic and inhomogeneous. Based on its composition and orientation of the components with depth of the tissue, articular cartilage is divided into a superficial zone, a middle zone, a deep zone, and a calcified cartilage zone [A. Bhosale 2008]. The four zones of the articular cartilage are shown in **Figure** (3).

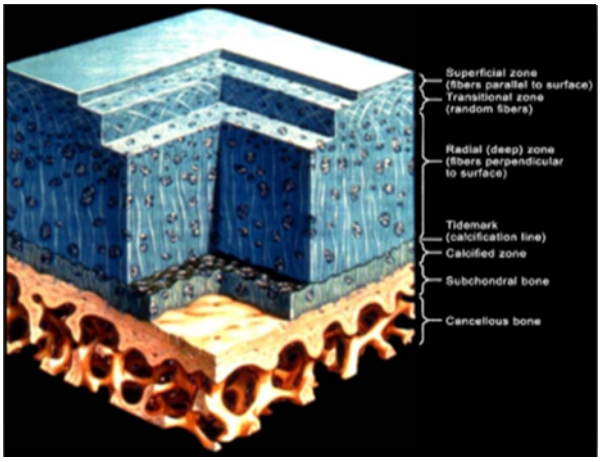

Figure (3) The four zones of the articular cartilage [W. Wilson 2005].

Articular cartilage damage and repair

Degenerative arthritis is an enormous problem, which affects millions of people around the world [W. Holmes 2004]. The overall prevalence for moderate to severe osteoarthritis is approximately 20%. By the age 55-65, up to 85% of all people will have some degree of osteoarthritis in one or more joints [F. DT 1997].Example of osteoarthritic articular cartilage is shown in **Figure** (4).

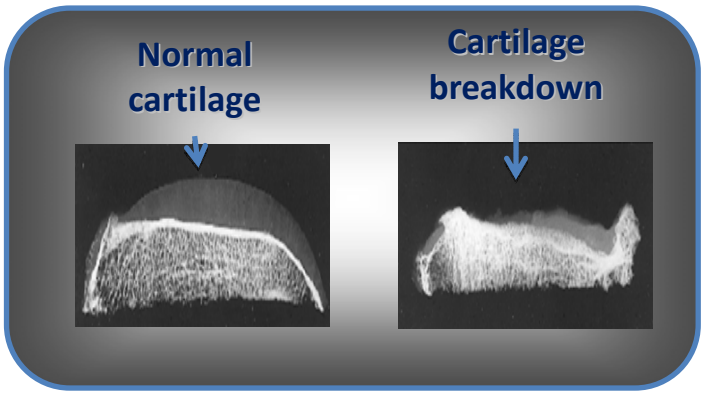

Figure (4) Normal and osteoarthritic articular cartilage (patella) [Janssen 2004].

Articular cartilage damages

Surgeons classify defects in the knee cartilage using a grading scale from I to IV. In grade I tear, the cartilage has a soft spot. Grade II lesions show minor tears in the surface of the cartilage. Grade III lesions have deep crevices. In grade IV lesions, the tear goes all the way to the underlying bone, as shown in **Figure** (5).

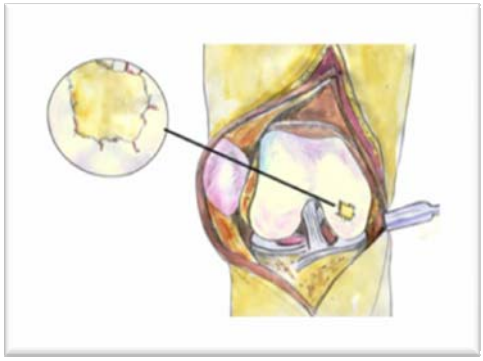

Figure (5) Knee cartilage lesions [T. Besier 2005].

A grade IV lesion goes completely through all layers of the cartilage. It is diagnosed as a full-thickness lesion. Sometimes part of the torn cartilage will break off inside the joint. Since it

is no longer attached to the bone, it can begin to move around within the joint, causing even more damage to the surface of the cartilage. Some doctors refer to this unattached piece as a loose body [Orthopod 2003].

Cartilage lacks a supply of blood or lymph vessels, which normally nourish other parts of the body. Without a direct supply of nourishment, cartilage is not able to heal itself if it gets injured [Orthopod 2003].

Treatment of articular cartilage injuries

The treatment of articular cartilage injuries is made in two ways, operative and non-operative treatments.

Nonsurgical Treatment

Nonsurgical management includes oral medications, physical modalities (physical therapy, weight loss), bracing (knee sleeve and unloaded brace), and injections (corticosteroids and hyaluronic acid derivatives). Traditionally, treatment of articular cartilage lesions has included a combination of nonsteroidal anti-inflammatory drugs, activity modification, and oral chondroprotective agents such as glucosamine or chondroitin sulfate. Such management is often ineffective in highly active and symptomatic patients and may only prove beneficial in low-demand patients [T. Pylawka 2004].

Surgical Treatment

The spectrum of different cartilage repair approaches has considerably been increased in the recent years [Gelse K. 2010]. The treatment options to restore the articular cartilage surface involve consideration of many factors: defect size, depth, location, response to previous treatment, patient age and expectations [T. Pylawka 2004].

1. Arthroscopic debridement and lavage

Arthroscopic lavage entails inserting arthroscopic instruments into the knee and irrigating the joint with sterile fluid, as shown in **Figure** (6).

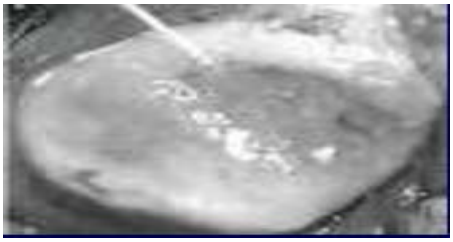

Figure (6) Arthroscopic debridement and lavage [R. Baxter 2008].

2. Repair stimulation techniques

Repair stimulation techniques try to take advantage of the normal tissue repair processes to create a new joint surface. [W. Holmes 2004].

a. Drilling

The subchondral plate is penetrated using a drill, the subchondral bone is drilled with a 0.185-cm drill to stimulate a fibrocartilagenous repair of a full-thickness chondral defect [T. Gill 2006].

b. Microfracture

This surgery, which aims to stimulate blood flow and promote regeneration, is a popular procedure for young patients but it is not performed on patients in their forties or fifties. A surgical procedure that can help such a patient is osteochondral autograft replacement [W. Bogatay 2009].

c. Abrasion arthroplasty

When osteoarthritis affects a joint, the articular cartilage can wear away, leaving bone rubbing on bone. This causes the bone to become hard and polished. During arthroscopy the surgeon can use a special instrument known as a burr to perform an abrasion arthroplasty, as shown in **Figure** (7).

In this procedure, the surgeon carefully scrapes off the hard, polished bone tissue from the surface of the joint. The scraping action causes a healing response in the bone. In time, new blood vessels enter the area and fill it with fibrocartilage [Orthopod 2003].

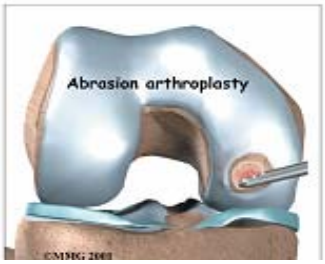

Figure (7) Abrasion arthroplasty [Orthopod 2003].

3. Cell and tissue transplantation

These techniques show promise in recreating a new articular surface with similar properties to native articular cartilage.

a. Osteochondral autografting

An autograft is a procedure for grafting tissue autograft from the patient's own body [Orthopod 2003].

b. Osteochondral allografting

An allograft is a lot like the osteochondral autograft, but instead of taking tissue from the patient's donor site, surgeons rely on tissue from another person, much like using donor hearts, kidneys, and other organs [Orthopod 2003].

c. Autologous chondrocyte implantation

Autologous chondrocyte implantation is a two-stage procedure involving a biopsy of normal articular cartilage, usually obtained through an arthroscopic procedure, in which the cartilage is harvested from a minor load-bearing area (upper medial femoral condyle or intercondylar notch). These chondrocytes are then cultured in vitro and implanted into the chondral defect beneath a periosteal patch during a second-stage procedure that requires an arthrotomy [T. Pylawka 2004]. Surgeons may recommend this procedure for active, younger patients (20 to 50 years old) when the bone under the lesion hasn't been badly damaged [Orthopod 2003].

4. Soft tissue replacement (polymers for cartilage replacement)

Replacement or augmentation of orthopedic soft tissues can be used to treat injury or disease-based degradation to the original tissue. Osteoarthritis characterized by degradation of the articular cartilage that progresses to the bony surfaces themselves is one of the most common pathologies experienced by the aging population. The density of polyethylene has been increased and joint bearings are now typically constructed from ultra-high-molecular-weight polyethylene (UHMWPE). The material has proven to provide good articulation, with the main concern being long-term wear. The problem with wear is not only the mechanical impingement that can occur as a result of a change in the articulating surface geometry but, more importantly, the effect of wear debris on the surrounding tissue [M. Grimm 2004].

Articular Cartilage Biomechanics

The histologic structure of articular cartilage is influenced by the local mechanical loading of chondrocyte in the different zones [U. Meyer 2006]. Because the fluid primarily is exuded from the surface layer, the distribution of strains through the cartilage thickness is highly nonuniform (**Figure** 8). Tissue results in compressive strains of over 50% in the superficial cartilage zone, but these strains reduce to near zero in the middle and deep regions of cartilage [D. Carter 2004].

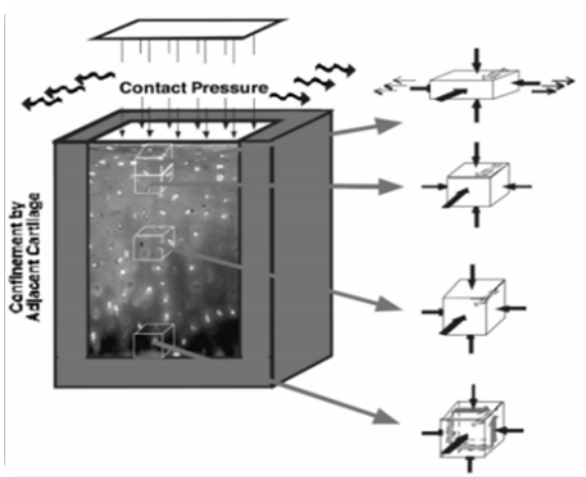

Figure (8) Schematic representation of the mechanical environment of articular cartilage under intermittent joint loading and motion [D. Carter 2004].

Chondrocytes are directly attached to the extracellular matrix and can be considered part of the fluid continuum of cartilage tissue. The zonal structure of articular cartilage is essential to its ability to support physiologic joint forces. Patterns of stress, strain, and fluid flow created in the joint result in spatial and temporal alteration in chondrocyte function. The external forces are transmitted through the joint and the adjacent tissues resulting in the generation of pressure over contact area of the two opposing cartilage surfaces [U. Meyer 2006], Nonlinear stress–strain curve for pure collagen employed for articular cartilage fibrils showen in (**Figure** 9).

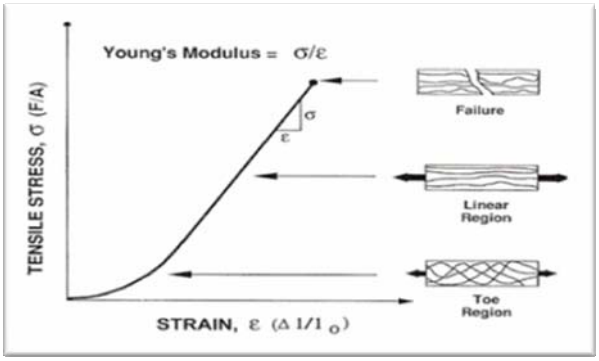

Figure (9) Nonlinear stress–strain curve for pure collagen employed for articular cartilage fibrils. The slope of the curve monotonically increases at smaller strains and becomes constant at larger strains [B. Nigg 1999].

Loads tend to deform the cartilage tissue but these compressive loads and subsequent tissue deformations are resisted by the stress in the solid phase, and the generation of the fluid pressure,and the restriction of tissue deformation by impermeable subchondral bone and the surrounding adjacent cartilage surfaces (**Figures** 10-14) [U. Meyer 2006].

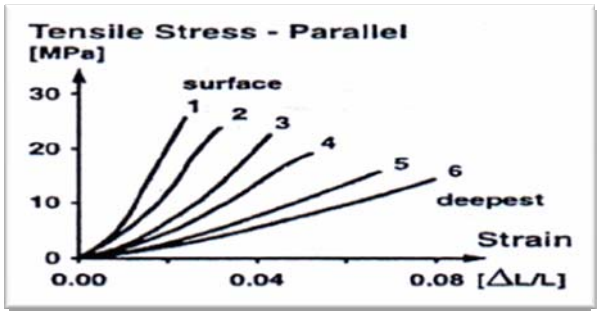

Figure(10) Variation in tension stress behaviour with depth in articular cartilage parallel to the predominant fiber direction [B. Nigg 1999].

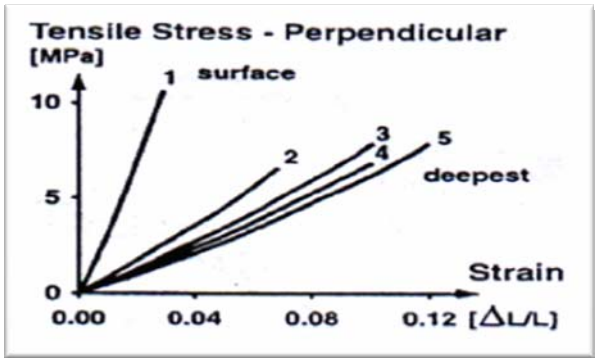

Figure (11) Variation in tension stress behaviour with depth in articular cartilage perpendicular to the predominant fiber direction [B. Nigg 1999].

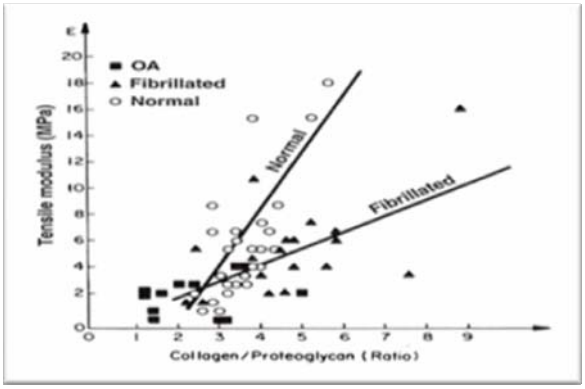

Figure (13) The variation of the human knee joint cartilage tensile stiffness for normal, fibrillated, and osteoarthritic articular cartilage [B. Nigg 1999].

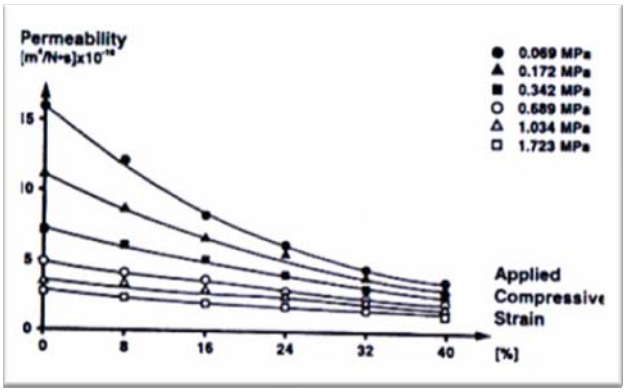

Figure(14) Expermental curves for articular cartilage permeability show a strong dependance on compressive strain and applied pressure [B. Nigg 1999].

Biomaterial Properties of Articular Cartilage

Cartilage behaves as a fiber-reinforced, porous, and permeable composite material. The greatest indicator of the mechanical properties of cartilage is the water content. The modulus of the material decreases with increased water content in a linear relationship. Articular cartilage exhibits both a viscoelastic and a biphasic response under tension, compression, and shear. In this model, the solid phase of articular cartilage is modeled as a hyperelastic anisotropic material. Cartilage exhibits its viscoelastic behavior because of the fluid flow of the liquid phase through the solid phase of the tissue [S. Fening 2005]. Material testing to determine the coefficients in a proposed constitutive law of cartilage is usually through confined compression, unconfined compression and indentation tests (**Figure**15) [S. Knecht 2006].

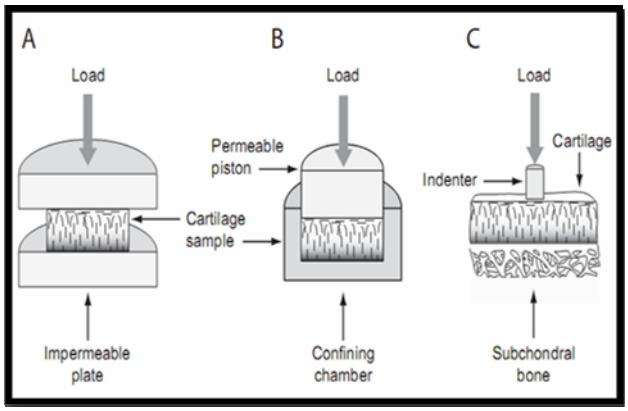

Figure (15) Sketch of common experiments applied to articular cartilage: unconfined compression (A), confined compression (B), and indentation (C) [S. Knecht 2006].

Articular Cartilage Finite Element Analysis

To study the finite element analysis for human articular cartilage, the
articular cartilages of the knee was chosen (the intermediate joint of the lower limb) because it is the largest and most complex joint in the body and containing four articular cartilages (distil femur, medial and lateral proximal tibia, and patella) [A. Iftekhar 2004]. Because the articular cartilages have no exact dimensions and their thickness is changing from place to other and in the cartilage itself so the only way to draw the articular cartilage is by using MRI images. MRI images for articular cartilage were taken from healthy volunteer person with (70 kg) weight and (169 cm) height, and by using a (Syngo FastView software) the images that have the best resolution were taken to be used, then imported as DICOM format in the (SimpleWare software), by using this software the three-dimensional model of the articular cartilages was drawn, then the result was imported in the (AutoCAD 2008) to rearrange the model and finally the last model was imported in the (ANSYS Workbench v 12.1) in order to build three dimensional finite element model which the load will be applied to.

In this work, there are (21) models including: (4) models for normal articular cartilage, (7) models for osteoarthritic articular cartilage, and (10) models for artificial articular cartilage. Each model was studied in two activities (walking and squatting).

Materials properties

Depending on the physical properties it can be seen that the articular cartilage is anisotropic material, the material properties are changing with thickness so the Young's modulus and Poisson's ratio are considered depth-dependent change when moving from lowermost layer at the subchondral bone to the articular surface depending on the organization of the articular cartilage. The superficial articular cartilage layer material characteristics are transversely isotropic poroelastic material (representing 20% of the total articular cartilage thickness), The middle and deep zone articular cartilage layers are isotropic poroelastic material (representing 75% of the total articular cartilage thickness), the calcified cartilage (representing 5% of the total articular cartilage thickness) and bone are elastic material, and finally the fibrocartilage is transversely isotropic elastic material [J. Yao 2003][A. Iftekhar 2004][A. Bhosale 2008]. The material properties for articular cartilage layers, bone, and fibrocartilage are shown in **Table (1),** and the material properties for UHMWPE that was used for total articular cartilage replacement are shown in **Table (2)**.

Table (1) Material properties [J. Yao 2003][A. Iftekhar 2004][A. Bhosale 2008]

	Elastic or Young's Modulus (MPa)	Poisson's Ratio	Permeability (m^4/Ns)	Shear modulus (MPa)
Cartilage (Superficial layer)	$E_x=E_y=5.8$, $E_z=0.46$	$\nu_{xy}=0.0002$ $\nu_{yz}=0$	$k=5.1*10^{-15}$	$G_{xz}=0.20$
Cartilage (Middle and deep zone layers)	E=0.69	$\nu=0.018$	$k=3*10^{-15}$	-
Calcified Cartilage	E=10	$\nu=0.499$	-	-
Bone	E = 220	$\nu=0.3$	-	-
Fibrocartilage	$E_x=100$, $E_y=E_z=0.075$	$\nu_{xy}=0.001$ $5\nu_{yz}=0.5$	-	-
Normal synovial fluid	Elasticity (Pa)	77		
	Viscosity	45		
Osteoarthritic synovial fluid	Elasticity (Pa)	9		
	Viscosity	5		

Table (2) UHMWPE Material Properties [S. Kurtz 2004].

UHMWPE Material Properties	
Young's Modulus (GPa)	0.8
Poisson's Ratio	0.46
Tensile Yield Strength (MPa)	21
Tensile Ultimate Strength (MPa)	21

Creating Mesh

The mesh for the model was done with three dimensional 10-Node Tetrahedral Structural Solid element type (SOLID 187), the shape of the element is shown in **Figure**(16).

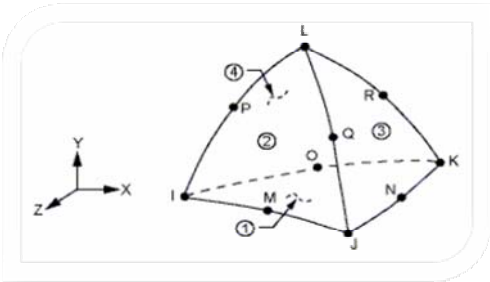

Figure(16) SOLID 187 element shape [S. Leffler 2009].

The reason for choosing (SOLID 187) that it has a quadratic displacement behavior and is well suited to modeling irregular meshes (such as those produced from various CAD systems).
The element is defined by 10 nodes having three degrees of freedom at each node: translations in the nodal x, y, and z directions.
The element has plasticity, hyperelasticity, creep, stress stiffening, large deflection, and large strain capabilities. It also has mixed formulation capability for simulating deformations of nearly incompressible elastoplastic materials, and fully incompressible hyperelastic materials. In addition to the nodes, the element input data includes the orthotropic or anisotropic material properties. Orthotropic and anisotropic material directions correspond to the element coordinate directions [S. Leffler 2009]. The finite element model mesh for distal femur articular cartilage, patella articular cartilage, medial tibia articular cartilage, and lateral tibia articular cartilage are shown in **Figures** (18-21).

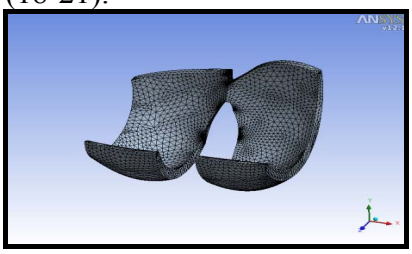

Figure (18) Distal femur articular cartilage mesh.

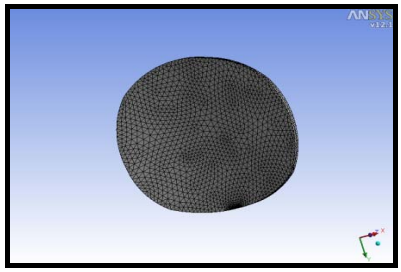

Figure (19) Patella articular cartilages mesh.

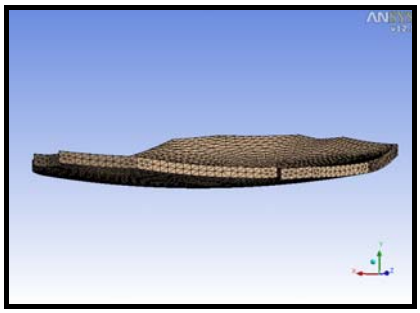

Figure (20) Medial tibia articular cartilage mesh.

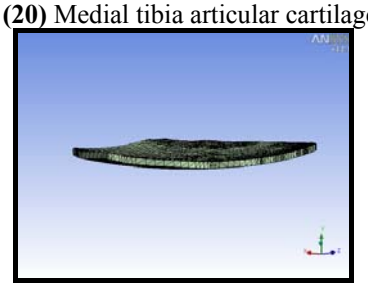

Figure(21) Lateral tibia articular cartilage mesh.

The finite element model meshes for 1, 5, 7.5, and 10 mm are shown in **Figures** (22-27) for different cases.

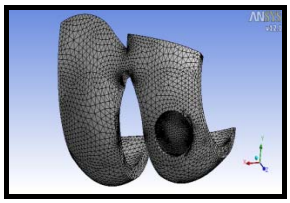

Figure (22) Partial cut without affecting the subchondral bone articular cartilages mesh 10 mm.

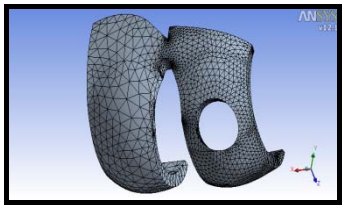

Figure (23) Full cut with part of the subchondral bone articular cartilages models 10 mm.

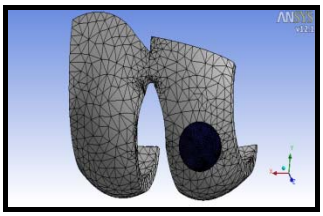

Figure (24) Partial cut without affecting the subchondral bone replaced by using ACI mesh 10 mm.

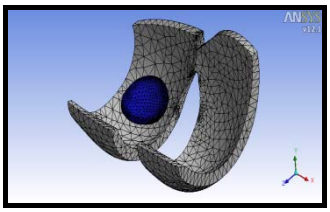

Figure (25) Full cut with part of the subchondral bone replaced by Osteochondral autograft or allograft mesh 10mm

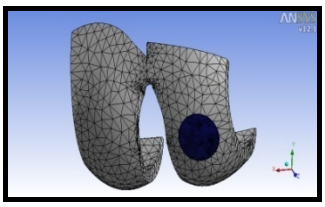

Figure (26) Full cut with part of the subchondral bone replaced by microfracture repair stimulation technique mesh 10 mm.

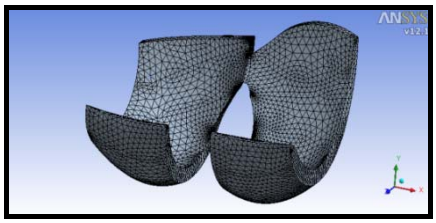

Figure (27) Total replacement of cartilage with (UHMWPE) mesh.

Insert structural loads

Early models to predict the forces across the knee joint are statically indeterminate because the number of independent soft tissue structures acting across the knee joint is greater than what can be solved for using the equations of static equilibrium. However, by making simplifying assumptions in the number of active muscle groups across the joint during a particular activity, it turns out that reasonable estimates of joint reaction forces may be obtained for activities such as walking, stair climbing/descent, squatting, and rising from a chair as shown in Table (3) [S. Kurtz 2004].

Table (3) Summary of average knee joint loading for activities of daily living [S. Kurtz 2004].

Activity	Patello-femoral Joint Force (x BW)	Tibio-femoral Joint Force (x BW)
Walking	0.5	0.4
Squatting	6.0-7.6	2.9-3.5
Rising from a chair	3.1	2.3
Stair climbing /descent	3.3	0.6
Force is expressed in units of body weight (BW).		

The human articular cartilage will be studied in two activities (walking and squatting): In walking the tibiofemoral joint angle is 5° so the force applied is equal to 0.4 of the body weight. While for patellofemoral joint, the angle is 10° during walking so the applied force is 0.5 of the body weight. While in squatting , the tibiofemoral joint angle is 122° so the force applied is equal to 3.5 of the body weight. While for patellofemoral, the joint angle is also 122° during squatting so the applied force is 7.6 of the body weight [S. Kurtz 2004]. Depending on Table (3), the loads were inserted as a distributed pressure (force over area).

Boundary conditions

The fixed support was applied to the faces of articular cartilage that are connected to bone. In addition, the fluid solid interface was applied to the articular cartilage parts that faced the synovial fluid, this assumption is due to the fact that the fluid flows in and out of the healthy articular cartilages, and a connection between a fluid analysis and structural analysis is done to insert the material properties of the synovial fluid and the porosity and permeability of articular cartilage.

RESULTS

To study the finite element analysis of the articular cartilage, the Von Misses stress, and the total deformation were chosen to be solved. The Stress-Strain Relationship is represented by [B. Nigg 1999]:

$$\{\sigma\} = [D]\ \{\varepsilon\} \qquad (1)$$

where:

$\{\sigma\}$ = stress vector = $[\ \sigma_x\ \sigma_y\ \sigma_z\ \sigma_{xy}\ \sigma_{yz}\ \sigma_{xz}\ ]^T$

[D] = elasticity or elastic stiffness matrix or stress-strain matrix

$\{\varepsilon\}$ = total strain vector = $[\ \varepsilon_x\ \varepsilon_y\ \varepsilon_z\ \varepsilon_{xy}\ \varepsilon_{yz}\ \varepsilon_{xz}\ ]^T$

$$[D]^{-1} = \begin{bmatrix} 1/E_x & -\nu_{xy}/E_x & -\nu_{xz}/E_x & 0 & 0 & 0 \\ -\nu_{yx}/E_y & 1/E_y & -\nu_{yz}/E_y & 0 & 0 & 0 \\ -\nu_{zx}/E_z & -\nu_{zy}/E_z & 1/E_z & 0 & 0 & 0 \\ 0 & 0 & 0 & 1/G_{xy} & 0 & 0 \\ 0 & 0 & 0 & 0 & 1/G_{yz} & 0 \\ 0 & 0 & 0 & 0 & 0 & 1/G_{xz} \end{bmatrix}$$

Also equation (4.1) may be inverted to:

$$\{\varepsilon\} = [D]^{-1}\ \{\sigma\} \qquad (2)$$

The flexibility or compliance matrix, $[D]^{-1}$ is:

(3)

where typical terms are: E_x = Young's modulus in the x direction , ν_{xy} = major Poisson's ratio, ν_{yx} = minor Poisson's ratio, G_{xy} = shear modulus in the xy plane. For orthotropic material transformation for axisymmetric models the input for x-y-z coordinates gives the following stress-strain matrix for the non-shear terms:

$$[D_{x-y-z}]^{-1} = \begin{bmatrix} 1/E_x & -\nu_{xy}/E_x & -\nu_{xz}/E_x \\ -\nu_{yx}/E_y & 1/E_y & -\nu_{yz}/E_y \\ -\nu_{zx}/E_z & -\nu_{zy}/E_z & 1/E_z \end{bmatrix} \quad (4)$$

The principal stresses (σ_1, σ_2, σ_3) are calculated from the stress componsents by the cubic equation:

$$\begin{vmatrix} \sigma_x - \sigma_0 & \sigma_{xy} & \sigma_{xz} \\ \sigma_{xy} & \sigma_y - \sigma_0 & \sigma_{yz} \\ \sigma_{xz} & \sigma_{yz} & \sigma_z - \sigma_0 \end{vmatrix} = 0 \quad (5)$$

where: σ_o = principal stress (3 values)
The three principal stresses are labeled σ_1, σ_2, and σ_3. The principal stresses are normal stresses, acting on principal planes on which the shearing stresses are zero, and are calculated by using the existing six normal and shearing stress components σ_x, σ_y, σ_z, τ_{xy}, τ_{xz}, and τ_{yz}.

The principal stresses are ordered so that σ_1 is the most positive (tensile) and σ_3 is the most negative (compressive).The stress intensity σ_I is the largest of the absolute values of σ_1- σ_2, σ_2-σ_3, or σ_3 - σ_1.
That is:

$$\sigma = \mathrm{MAX}\,(|\sigma_1 - \sigma_2|\,|\sigma_2 - \sigma_3|\,|\sigma_3 - \sigma_1|) \quad (6)$$

The von Mises or equivalent stress σ_e is computed as:

$$\sigma_e = \left(\frac{1}{2}[(\sigma_1 - \sigma_2)^2 + (\sigma_2 - \sigma_3)^2 + (\sigma_3 - \sigma_1)^2]\right)^{\frac{1}{2}} \quad (7)$$

Or

$$\sigma_e = \left(\frac{1}{2}\left[(\sigma_x - \sigma_y)^2 + (\sigma_y - \sigma_z)^2 + (\sigma_z - \sigma_x)^2 + 6(\sigma^2{}_{xy} + \sigma^2{}_{yz} + \sigma^2{}_{xz})\right]\right)^{\frac{1}{2}} \quad (8)$$

Normal Models Results

For normal articular cartilage, the results were taken for each model in two activities (walking and squatting) represented as a contour in the **Figures** (29-39).

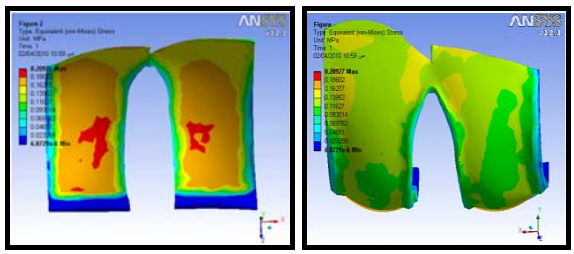

(a) Top view (b) Front view
Figure (29) Von Mises stress for normal distal femur articular cartilage during walking.

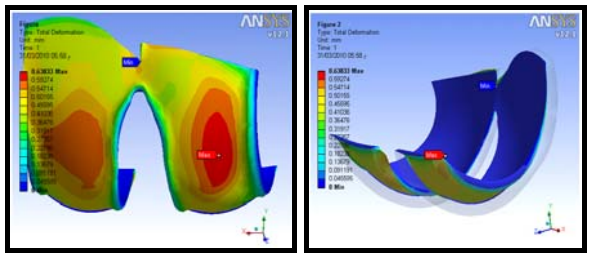

(a) Front view (b) Isometric view
Figure (30) Total deformation for normal distal femur articular cartilage during walking.

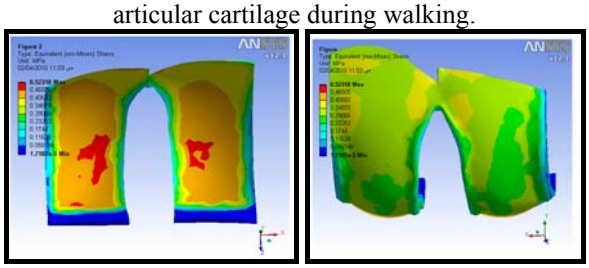

(a) Top view (b) Front view
Figure (31) Von Mises stress for normal distal femur articular cartilage during squatting.

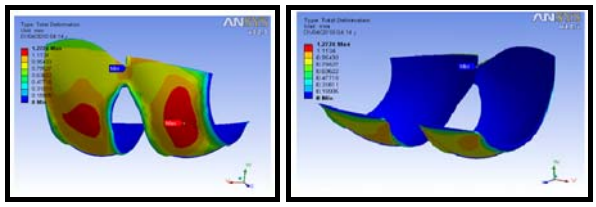

(a) Front view (b) Isometric view
Figure (32) Total deformation for normal distal femur articular cartilage during squatting.

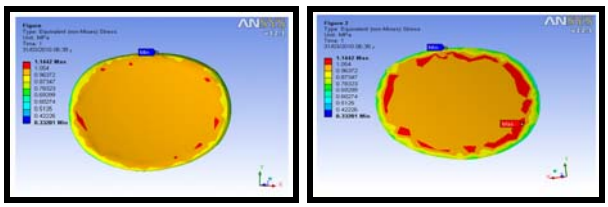

(a) front view (b) back view
Figure (33) Von Mises stress for normal patella articular cartilage during walking.

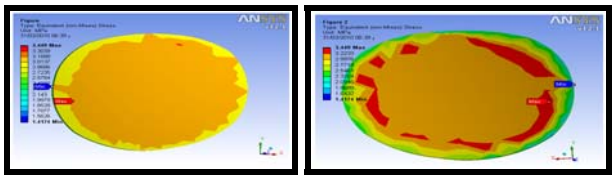

(a) Front view (b) Back view

Figure (34) Von Mises stress for normal patella articular cartilage during squatting.

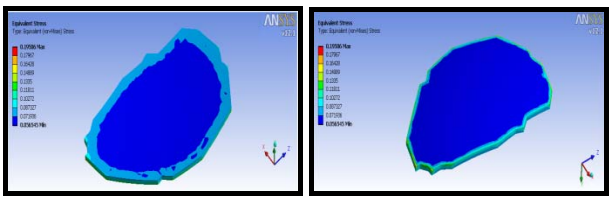

(a) Top view (b) Bottom view

Figure (35) Von Mises stress for normal medial tibia articular cartilage during walking.

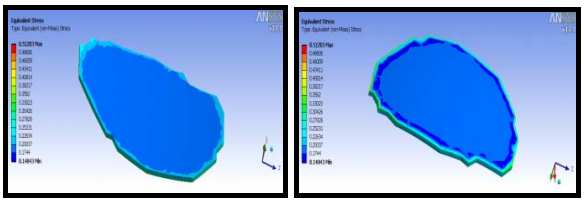

(a) Top view (b) Bottom view

Figure (36) Von Mises stress for normal medial tibia articular cartilage during squatting.

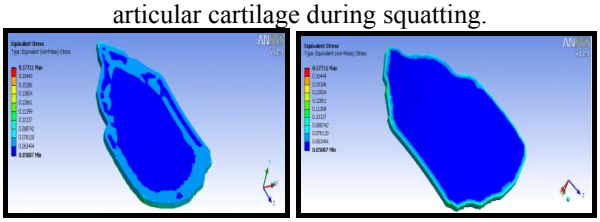

(a) Top view (b) Bottom view

Figure (37) Von Mises stress for normal lateral tibia articular cartilage during walking.

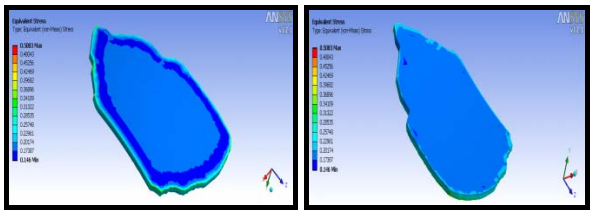

(a) Top view (b) Bottom view

Figure (38) Von Mises stress for normal lateral tibia articular cartilage during squatting.

Table (4) Maximum Von Mises stress for normal articular cartilage models during walking and squatting.

No.	Model	Maximum Von Mises stress (MPa)	
		Walking	Squatting
1	Distal femur	0.20927	0.52318
2	Patella	1.1442	3.449
3	Medial tibia	0.19506	0.51203
4	Lateral tibia	0.17711	0.5083

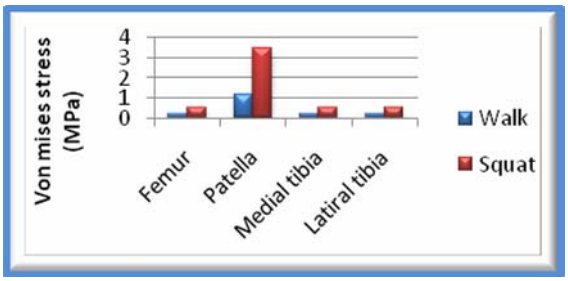

Figure (39) Maximum Von Mises stress for normal articular cartilage models during walking and squatting.

Osteoarthritic articular cartilage

For Partial cut without affecting the subchondral bone it can be see that there is a big difference between normal and osteoarthritic articular cartilage stresses even when the defect is just 1 mm, and this is be so obvious in the squatting. In the four models, the maximum stress is on the sides of the cut parts and increases with increasing the cut diameter. For total deformation result, it can be seen that there is no or small deformation in the cut parts but it is the maximum in the peripheral parts as shown in **Figures** (40-43).

While for Full cut with part of the subchondral bone it's obvious the big differences are between the normal and full cut defective articular cartilages stresses, especially in squatting. In the three models, the maximum stress is on the sides of the cut parts and its increases with increasing the cut diameter. For total deformation results, the maximum deformation is in the peripheral parts of the cuts and there is no deformation in the cartilage - bone interface. The percentage for two types of Osteoarthritic articular cartilage close to normal are 19% for walking and 16% for squatting, as shown in **Figures** (44-46).

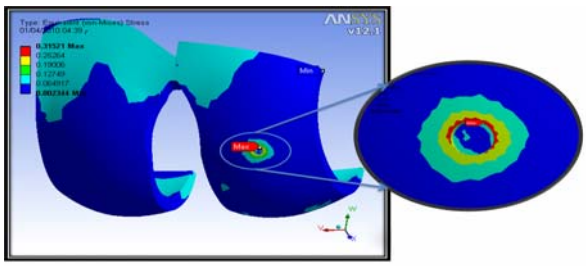

Figure (40) Von Mises stress for 1mm partial cut articular cartilage during walking.

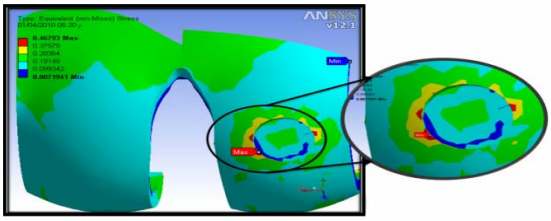

Figure (41) Von Mises stress for 7.5 mm partial cut articular cartilage during walking.

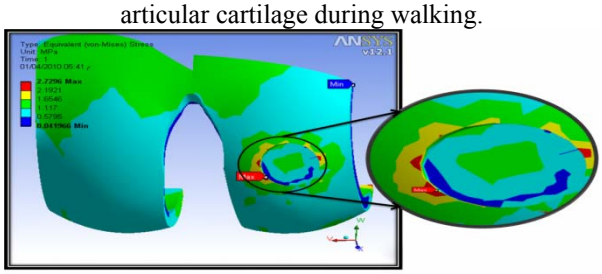

Figure (42) Von Mises stress for 7.5 mm partial cut articular cartilage during squatting.

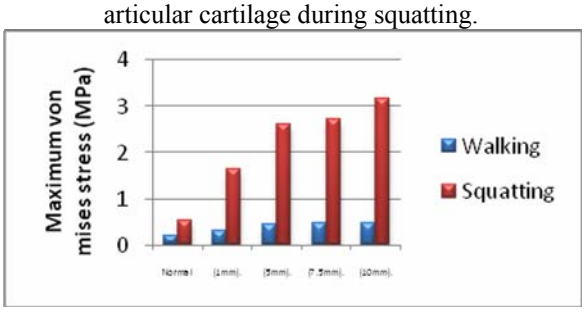

Figure (43) Maximum Von Mises stress for osteoarthritic articular cartilage with Partial cut without affecting the subchondral bone models during walking and squatting.

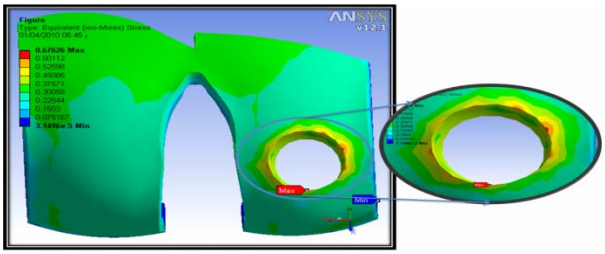

Figure (44) Von Mises stress for 7.5 mm full cut articular cartilage during walking.

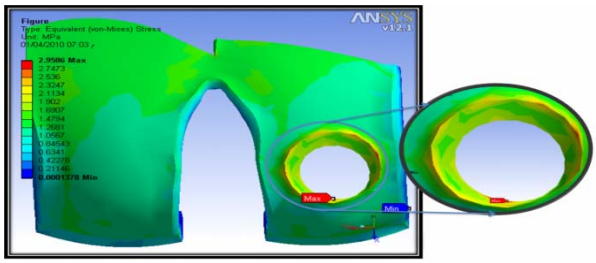

Figure (45) Von Mises stress for 7.5 mm full cut articular cartilage during squatting.

Table (5) Maximum Von Mises stress for osteoarthritic articular cartilage models during walking and squatting.

No.	Model	Maximum Von Mises stress (MPa)	
		Walking	Squatting
1	Partial cut without affecting the subchondral bone (1mm).	0.31521	1.6549
2	Partial cut without affecting the subchondral bone (5mm).	0.44807	2.6138
3	Partial cut without affecting the subchondral bone (7.5mm).	0.46793	2.7296
4	Partial cut without affecting the subchondral bone (10mm).	0.48082	3.1554
5	Full cut with part of the subchondral bone (5 mm).	0.6554	2.8483
6	Full cut with part of the subchondral bone(7.5 mm).	0.67626	2.9586
7	Full cut with part of the sub chondral bone(10 mm).	0.71384	3.2387

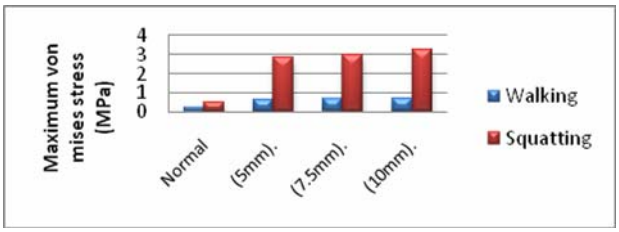

Figure (46) Maximum Von Mises stress for osteoarthritic articular cartilage with full cut with part of the subchondral bone models during walking and squatting.

Artificial articular cartilages models

For Partial cut without affecting the subchondral bone replaced by using autologous chondrocyte implantation (ACI), It can be seen that the maximum stresses for the artificial articular cartilage is very close to the normal articular cartilage but it is concentrated in the artificial part. The advantages and disadvantages of this technique are shown in **Figures** (47-49). The percentage for how ACI close to normal is 87.50% for walking and 90% for squating.

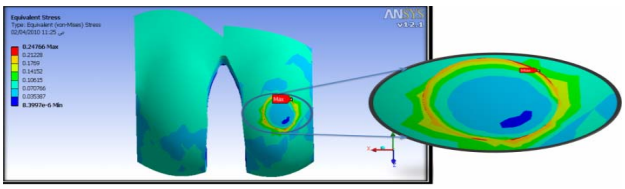

Figure (47) Von Mises stress for 7.5 mm artificial articular cartilage replaced by using (ACI) during walking.

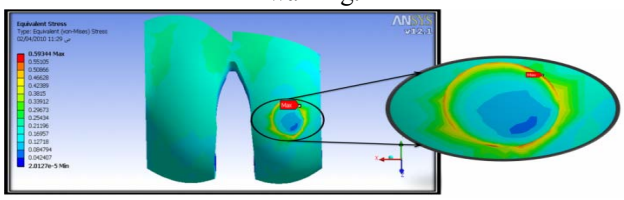

Figure (48) Von Mises stress for 7.5 mm artificial articular cartilage replaced by using (ACI) during squating.

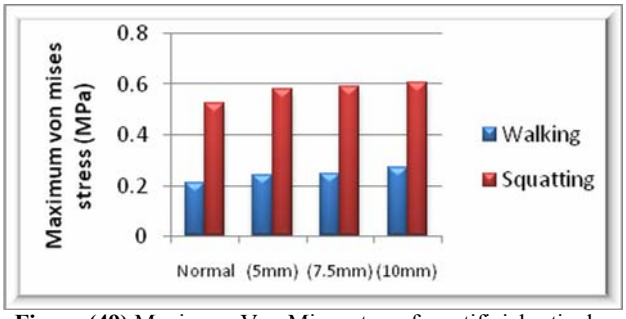

Figure (49) Maximum Von Mises stress for artificial articular cartilage replaced by using autologous chondrocyte implantation (ACI) during walking and squatting.

For Full cut with part of the subchondral bone replaced by Osteochondral autograft or allograft. The maximum stresses concentrated in the artificial part. The advantages and disadvantages of this technique are shown in **Figure**(50-52). The percentage for how osteochondral autograft or allograft close to normal is 61% for walking and 17% for squating.

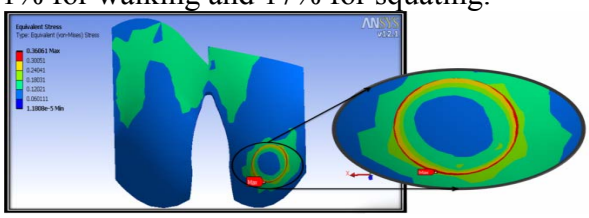

Figure (50) Von Mises stress for 7.5 mm artificial articular cartilage replaced by graft during walking.

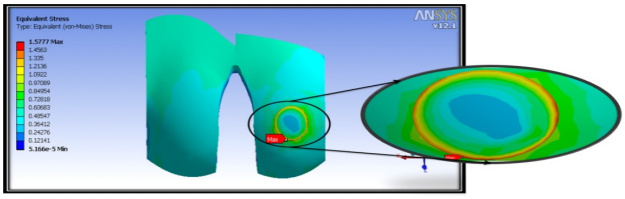

Figure (51) Von Mises stress for 7.5 mm artificial articular cartilage replaced by graft during squating.

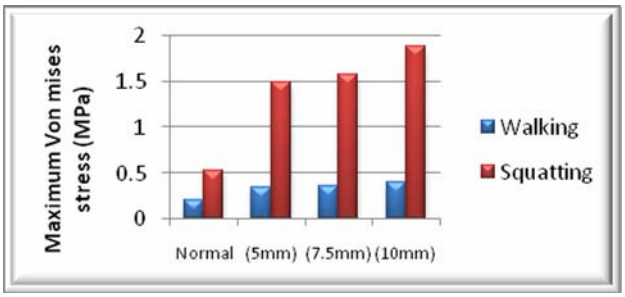

Figure (52) Maximum Von Mises stress for artificial articular cartilage replaced by osteochondral autograft or allograft during walking and squatting.

For Full cut with part of the subchondral bone replaced by using Microfracture Repair stimulation technique, The maximum stress for the artificial articular cartilage is greater than that of the normal articular cartilage especially in squatting but it is still lower than when it defected. The maximum stresses are concentrated in the artificial part. The advantages and disadvantages of this technique are shown in **Figures** (53-55). The percentage for how Microfracture technique close to normal is 51% for walking and 26.5% for squating.

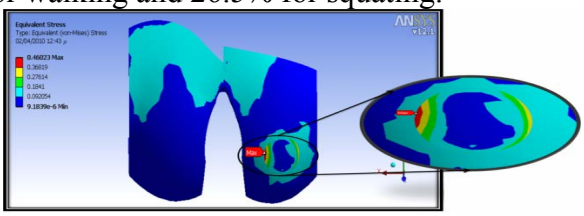

Figure (53) Von Mises stress for 7.5mm artificial articular cartilage replaced by using microfracture repair stimulation technique during walking.

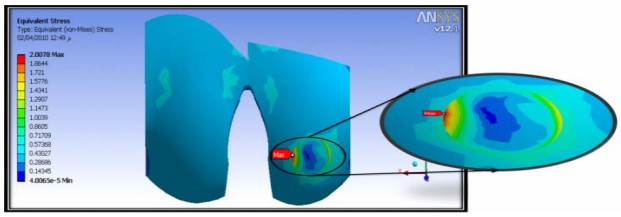

Figure (54) Von Mises stress for 7.5 mm artificial articular cartilage replaced by using microfracture repair stimulation technique during squatting.

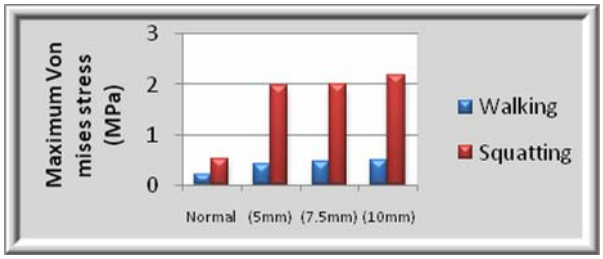

Figure (55) Maximum Von Mises stress for artificial articular cartilage replaced by using microfracture repair stimulation technique during walking and squatting.

Total replacement of cartilage with ultra high molecular weight polyethylene (UHMWPE), It can be seen that the maximum stress for the artificial articular cartilage is not very close to the normal articular cartilage but it is much better than the osteoarthritic articular cartilage. The maximum stress is on the sides of artificial articular cartilage and this is due to the thickness differences between the sides and the middle as shown in **Figures** (56-58).

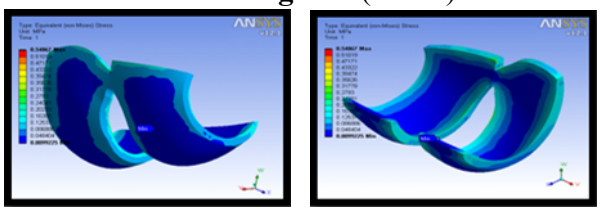

(a) front view (b) back view

Figure (56) Von Mises stress for total replacement of cartilage with ultra high molecular weight polyethylene (UHMWPE) during walking.

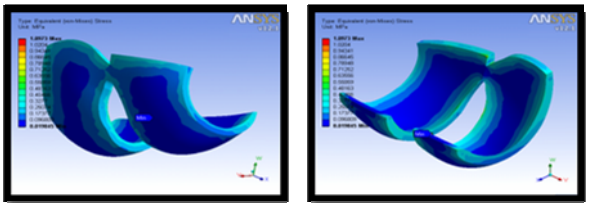

(a) front view (b) back view

Figure (57) Von Mises stress for total replacement of cartilage with ultra high molecular weight polyethylene (UHMWPE) during squatting.

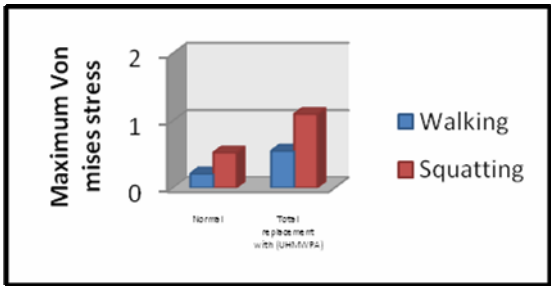

Figure (58) Maximum Von Mises stress for total replacement of cartilage with ultra high molecular weight polyethylene (UHMWPE) during walking and squatting.

Table (6) Maximum Von Mises stress for artificial articular cartilage models during walking and squatting.

No.	Model	Maximum Von Mises stress (MPa)	
		Walking	Squatting
1	Partial cut without affecting the subchondral bone replaced by using ACI (5 mm)	0.23909	0.58064
2	Partial cut without affecting the subchondral bone replaced by using ACI (7.5 mm)	0.24766	0.59344
3	Partial cut without affecting the subchondral bone replaced by using ACI (10 mm)	0.27011	0.60775
4	Full cut with part of the subchondral bone replaced with Osteochondral autograft or allograft (5mm)	0.34272	1.4994
5	Full cut with part of the subchondral bone replaced with Osteochondral autograft or allograft (7.5mm)	0.36061	1.5777
6	Full cut with part of the subchondral bone replaced with Osteochondral autograft or allograft (10mm)	0.39666	1.8932
7	Full cut with part of the subchondral bone replaced by using Microfracture Repair stimulation technique (5mm)	0.41223	1.9744
8	Full cut with part of the subchondral bone replaced by using Microfracture Repair stimulation technique (7.5mm)	0.46023	2.0078
9	Full cut with part of the subchondral bone replaced by using Microfracture Repair stimulation technique (10mm)	0.49869	2.1866
10	Total replacement of cartilage with ultra high molecular weight polyethylene (UHMWPE)	0.54867	1.0973

Conclusions

1. The maximum stress of normal articular cartilage is in cartilage-bone interface during walking and squatting, but the stress is reach the double during squatting, which means the stress is increasing with knee flexion angle increasing. Also, the maximum stress in the patellar articular cartilage is greater than that in the other knee joint articular cartilages specially in squatting because the load reaches 7.6 of

the total body weight on the patella articular cartilage.

2. For the autologous chondrocyte implantation, the maximum stress for the artificial articular cartilage is very close to the normal articular cartilage. It represents the best results for replacement but it needs two operations and cannot be useful for older patients or for patients with deep osteoarthritis.

3. For osteochondral autograft, allograft, or microfracture repair stimulation technique for replacement, the maximum stress of the artificial articular cartilage is greater than that of the normal articular cartilage but it is still lower than when it is defected.

4. For total replacement of cartilage with UHMWPE, the maximum stress for the artificial articular cartilage is not very close to the normal articular cartilage but it is much better than the osteoarthritic articular cartilage. The maximum stress is on the sides of artificial articular cartilage, this is due to the thickness differences between the sides and the middle.

REFERENCES

Abhijit M. Bhosale, and James B. Richardson, "Articular Cartilage: Structure, Injuries And Review Of Management", Institute of Orthopaedics and Arthritis Research Centre, UK, British Medical Bulletin; 87: 77–95, 2008.

Arif Iftekhar, "Standard Handbook Of Biomedical Engineering And Design", University of Minnesota, Minneapolis, The McGraw-Hill Companies, chapter 12, 2004.

Ateshian G A, and Hung C T, "The Natural Synovial Joint: Properties Of Cartilage", Proc. IMechE Vol. 120 Part J: J. Engineering Tribology, 2006.

Benno M. Nigg, and Walter Herzog, "Biomechanics of the Musculo-Skeletal System", University of Calgary, Calgary, Alberta, Canada, second edition, p. 86-105, 1999.

Constantin Bratianu, Paul Rinderu, and Lucian Gruionu," A 3D Finite Element Model of a Knee for Joint Contact Stress Analysis during Sport Activities", Key Engineering Materials Trans Tech Publications, Switzerland, Vols. 261-263, pp 513-518, 2004.

Daniel J. Schneck, Joseph D. Bronzino, "Biomechanics Principles And Applications", Boca Raton London New York Washington, D.C., 2003.

Dennis R. Carter, Gary S. Beaupré, Marcy Wong, R. Lane Smith, Tom P. Andriacchi, and David J. Schurman, "The Mechanobiology of Articular Cartilage Development and Degeneration", pp. S69–S77, Lippincott Williams & Wilkins, 2004.

Felson DT, Zhang Y, Hannan MT, Naimark A. Weissman B, and Aliabadi P., "Risk factors for incident radiographic knee osteoarthritis in the elderly", Arthr Rheum, 22:716-733, 1997.

Gelse K., Olk A., Eichhorn S., Swoboda B., Schoene M., and Raum K., "Quantitative Ultrasound Biomicroscopy For The Analysis Of Healthy And Repair Cartilage Tissues", Germany, Vol. 11, p. (58-71) , 2010.

Guoan Li, Orlando Lopez, "Reliability Of A 3D Finite Element Model Constructed Using Magnetic Resonance Images Of A Knee For Joint Contact Stress Analysis", Harvard Medical School, Boston, 1998.

Janssen P.J.F.M., "Influence of Excessive Loading on The Mechanical Properties of Articular Cartilage", Technical University Eindhoven, 2004.

Jiang Yao, Art D. Salo, Monica Barbu-McInnis, and Amy L. Lerner, "Finite Element Modeling Of Knee Joint Contact Pressures And Comparison To Magnetic Resonance Imaging Of The Loaded Knee", Washington, D.C., November 16-21, 2003.

Jonathan Black, and Garth Hastings, "Handbook of Biomaterial Properties", First edition, Chapman & Hall, London, 1998.

Matej Mlejnek, "Medical Visualization for Orthopedic Applications", Ph.D., Institute of Computer Graphics and Algorithms, Vienna University of Technology, Austria, 2006.

Michele J. Grimm, "Standard Handbook Of Biomedical Engineering And Design", Detroit, Michigan, The McGraw-Hill, chapter 15,2004.

Orthopod, "A Patient's Guide to Articular Cartilage Problems of the Knee", 116 West Main St., Suite D, Missoula, MT 59802-2295, , Medical Multimedia Group, LLC, 2003.

Ramaswamy Krishnan, Seonghun Park, Felix Eckstein, Gerard A. Ateshian, "Inhomogeneous Cartilage Properties Enhance Superficial Interstitial Fluid Support and Frictional Properties", Journal of Biomechanical Engineering, Vol. 115, 2003.

Richard Baxter, "Articular Cartilage Injuries and Management", 2008.

Sam Leffler, Glenn Randers, Andreas Dilger, Guy Eric Schalnat, Jean-loup Gailly, Mark Adler, David E. Steward, and Zbigniew Leyk, "ANSYS 12.1 Inc. Theory Reference", ANSYS Inc., Southpointe, 2009.

Seeley−Stephens−Tate, "Anatomy and Physiology", Sixth Edition, McGraw−Hill Companies, p. 114-126, 146, 2004.

Stephen D. Fening, "The Effects Of Meniscal Sizing On The Knee Using Finite Element Methods", Ph. D. thesis, Ohio University, 2005.

Steven M. Kurtz, "The UHMWPE Handbook", Principal Engineer, Elsevier Academic Press, 2004.

Sven Knecht, "Biomechanical Assessment of Native and Tissue Engineered Articular Cartilage", Ph.D., Dipl. Ing., University Stuttgart, Citizen of Germany, 2006.

Tamara K. Pylawka, Richard W. Kang, Brian J. Cole, "Articular Cartilage Injuries", chapter 30, 2004.

Thomas J. Gill, Peter D. Asnis, Eric M. Berkson, "The Treatment of Articular Cartilage Defects Using the Microfracture Technique", Journal of Orthopaedic, 18(10):716-738, 2006.

Thor F. Besier, Garry E. Gold, Gary S. Beaupré, And Scott L. Delp, "A Modeling Framework to Estimate Patellofemoral Joint Cartilage Stress In Vivo", Medicine and Science In Sports and Exercise, American College of Sports Medicine, 2005.

Ulrich Meyer, and Hans Peter Wiesmann, "Bone and Cartialge Engineering", Springer, 2006.

Van De Graaff, "Human Anatomy", Sixth Edition, McGraw−Hill Companies, p.117-130, 2001.

Wendell S. Holmes Jr, "Articular Cartilage Injuries in the Athlete's Knee: Current Concepts in Diagnosis and Treatment", Columbia, 2004.

William Bogatay, "Finite Element Analysis of Knee Cartilage with an Osteochondral Graft", Mechanical Engineering, The Ohio State University, 2009.

Wouter Wilson, "An Explanation for the Onset of Mechanically Induced Cartilage Damage", Ph.D., Technische Universiteit Eindhoven, 2005.

SECURED SMART CARD SIMULATION

Zahraa Ali Jwad, Sarkout N. Abdulaah, and Oday A.L.A Ridha

ABSTRACT:

Different methods of encryption that are widely used in smart card have been presented. Because of the usefulness and widespread application of Food Ration Card throughout our country, three models of designing and simulations are developed. A comparison between the different models is done. The first model is the Food Ration Card without using any security method. The second model is the Food Ration Card with using an AES algorithm as a security method. The third model is the Food Ration Card with using RSA method. All models are implemented and simulated using
BasicCard Development kit Environment. For the first model, a Compact BasicCard version ZC1.1 is used. While for the second and third models, a Professional BasicCard version ZC4.5 is used. From obtained results, we noticed that AES-method is faster than RSA and takes less memory size, but RSA is more secure than AES, since it uses two different keys instead of one as in AES.

الخلاصة:

دراسة البطاقة الذكية واهم طرق التشفير المستخدمة فيها. في هذه المقالة تم تقديم ثلاث نماذج للبطاقة التموينية باستخدام البطاقة الذكية لما تمتلكه الاولى من اهمية كبيرة في قطرنا. حيث انها تعتمد كوثيقة رسمية في الكثير من الدوائر الحكومية. النموذج الاول هو تنفيذ البطاقة التموينية بدون استخدام اي طريقة من الطرق الامينة. اما النموذج الثاني فهو تنفيذ البطاقة التموينية باستخدام طريقة معيار التشفير المتقدم كطريقة امينة. اما ما يخص النموذج الثالث فتم استخدام طريقة RSA كطريقة امينة لتنفيذ البطاقة التمونية. في النموذج الاول تم استخدام بطاقة BasicCard المضغوطة باصدار1.1، بينما النموذج الثاني والثالث تم استخدام بطاقة BasicCard المتخصصة باصدار4.5. بعد تنفيذ النماذج الثلاث تم عمل مقارنة بينها. من خلال النتائج التي حصلنا عليها من تنفيذ البرامج لاحظنا بان طريقة معيار التشفير المتقدم اسرع من RSA وتاخذ حجم ذاكرة اقل. في حين استخدام RSA يعطي البطاقة اكثر امنية من طريقة معيار التشفير المتقدم كونها تعتمد على مفتاحين مختلفين بدل المفتاح الواحد.

Keywords: Smart card, AES, RSA, Encryption, Foot Ration Card.

INTRODUCTION

The smart cards are the youngest and cleverest member of the family of identification cards in the ID-1 format. Its characteristic feature is an integrated circuit embedded in the card, which has components for transmitting, storing and processing data. The data can be transmitted using either contacts on the surface of the card or electromagnetic fields, without any contacts.

Smartcards offer several advantages compared with magnetic-stripe cards. For instance, the maximum storage capacity of a smart card is many times greater than that of a magnetic-stripe card. However, one of the most important advantages of smart cards is that their stored data can be protected against unauthorized access and manipulation [Wenzhou L., 2010]. Since the data can only be accessed via a serial interface that is controlled by an operating system and security logic, confidential data can be written to the card and stored in a manner that prevents them from ever being read from outside the card. Such confidential data can be processed only internally by the chip's processing unit. In principle, both hardware and software mechanisms can be used to restrict the use of the storage functions of writing, erasing and reading data and tie them to specific conditions. This makes it possible to construct a variety of security mechanisms, which can also be tailored to the specific requirements of a particular application[Stefan M., 2010]. In combination with the ability to compute cryptographic algorithms, this allows smart cards to be used to implement convenient security modules that can be carried by users at all times, for example in a purse or wallet. Some additional advantages of smartcards are their high level of reliability and long life compared with magnetic-stripe cards, whose useful life is generally limited to one or two years [Rankl W. and Effing W., 2003].

SECURITY OF SMART CARD

The encryption algorithm (also called a cipher) is used to transform plaintext (the original information to be hidden) into ciphertext (the hidden information) or ciphertext into plaintext (decryption).

An encryption algorithm has known as an "asymmetric algorithm" if the encryption and decryption keys that it uses are different, includes RSA and elliptic curve; otherwise, it is a "symmetric algorithm", examples include the Data Encryption Standard (DES), the International Encryption Standard (IDEA) and Advanced Encryption Standard (AES) [Schneier B., 1996]. In general, security provides the following objectives or services:

● Confidentiality is a service used to keep the content of information accessible to only those authorized to have it.

● Integrity is a service that requires that computer system assets and transmitted information be capable of modification only by authorized users. Modification includes writing, changing, changing the status, deleting, creating, and the delaying or replaying of transmitted messages.

● Authentication is a service that is concerned with assuring that the origin of a message has correctly identified. That is, information delivered over a channel should be authenticated as to the origin, date of origin, data content, time sent, etc.

● Non-repudiation is a service, which prevents both the sender and the receiver of a transmission from denying previous commitments or actions [Everett D., 1993].

The advantage of asymmetric algorithm is increased security. Since the receiver decrypts the message by using his/her private key, there is no need to expose the secret key to the insecure transmission medium [Schneier B., 1996].

Among the standard methods that have been used in the smart card are DES, AES, RSA and elliptic curve cryptography (ECC) [Everett D., 1993].

Data Encryption standard (DES)

DES is block cipher; it encrypts data in 64-bit block. The key length is 56-bits (the key is usually expressed as 64-bit number, but every 8th bit is used for parity checking and is ignored). DES is fast but is relatively insecure. Generally, it is avoided when possible [Schneier B., 1996].

Advanced encryption standard (AES)

NIST (National Institute of Standards and Technology) had selected Rijndael algorithm to be the proposed AES due to its high security strength, computational and memory efficiency, high configurability and simplicity. It can be implemented in wide ranges of devices from low memory devices like smart card to high-end workstations. It is a stronger symmetric encryption algorithm that was approved by NIST to replace the Data Encryption Standard (DES) and Triple DES encryption algorithm. For the AES algorithm, the length of the input block, the output block and the State is 128 bits**.** For the AES algorithm**,** the length of the Cipher Key, K, is 128, 192, or 256 bits [Daemen J. and Rijmen V., 199].

RSA (Rivest Shamir Adelman) public-key encryption

The RSA algorithm belongs to the public-key systems, namely architectures where the key is published to all parties**.**

The keys used in RSA are quadruples of (p, q, e, d), The mathematical definition of this scheme is $EK(P) = P^e \bmod pq$, $DK(C) = C^d \bmod pq$, with EK being the encrypting function, and DK being the decrypting function. P is the plaintext and C is the cipher text. The security of the RSA depends on the problem of factoring large numbers. That is meaning the difficulty of recovering p and q if only their product n has known, so cannot calculate the private exponent [Schneier B., 1996].

Elliptic Curve Cryptography

Elliptic curve cryptography (ECC) is public key cryptography. In public key cryptography each user or the device taking part in the communication generally have a pair of keys, public key and a private key, and set of operations associated with the keys to do the cryptographic operations [Schneier B., 1996].

The mathematics of cryptographic systems based on elliptic curves is relatively difficult. One factor limiting the use of elliptic curves for asymmetric cryptographic algorithms is that they are regarded as a relatively new discovery in the cryptographic world, even though they have been known for a long time. It will no doubt take some time until the use of ECC systems becomes commonplace in the cautious world of cryptographers and smart card application designers [Rankl W. and Effing W., 2003].

BASICCARD

Since 1996, a smart card operating system with an interpreter for the Basic programming language has been available from the German company Zeitcontrol. This operating system has called Basic Card, and it is available in various versions with different features and for hardware platforms with various memory sizes.

The procedure for generating downloadable programs for Basic Card has based on traditional Basic interpreters. A compiler translates the source code into P-code, which is transferred to a memory region of the smart card microcontroller reserved for this purpose. The transformation is done using a special loader program. After that, the program code stored in this region can be processed by the interpreter as necessary [Rankl W. and Effing W., 2003].

The ZeitControl's BasicCard family includes Compact BasicCard, the Enhanced BasicCard, Professional BasicCard, and the MultiApplication BasicCard. A BasicCard contains 256-1768 bytes of RAM, and 1-31 kilobytes of user-programmable EEPROM.

BasicCard has the following features:

- Inexpensive, where the development software is free of charge and most versions of the BasicCard cost less than half as much as other currently available programmable processor cards.
- Easy to program, where it uses a very Basic like programming language.
- Secure, where state-of-the-art cryptographic algorithms are available for all BasicCard types [Guilfoyle T., 2005].

FOOD RATION CARD APPLICATION WITHOUT SECURITY

The application of Food Ration Card is chosen as an example of the smart card applications, because it is useful and widespread application throughout our country. It is an official and important document.

The card issuer for the Food Ration Card will be Ministry of Trade. The following information will be written on the card: name of family head, the card serial number, the address, number of family members, number of infants, last date updated and the PIN (personal identification number) code (which will be known only by the owner), so as to prevent other people from making use of the card in case of theft or loss.

The name of process in which the information is written on the card is "personalization". After that, the cards will be distributed to the citizens by agents. Therefore, when a citizen wants to receives his/her share of rational food, he/she has to use his/her card. The last date updated refers to the date of issuing the card by Ministry of Trade.

At the beginning, the program is written without adding any security algorithms to check the size of the program, the speed of its implementation, and the required memory to implement the program.

The BasicCard Development Kit is selected as the development environment for this project, due its widespread, low cost and technical support available via internet. The application is written in ZC-Basic language, which is supported by the development kit.

The program includes three basic parts:

1. Terminal-Write program: this program is used to issue the Food Ration Card.
2. Terminal-Read program: this program is used to read the information written on the Food Ration Card.
3. Food Ration Card program: this represents the program of the smart card which saves the following information: name of family head, the card serial number, the address, number of family members, number of infants, last date updated and the PIN code.

We will conduct a simulation to the three programs mentioned above using a software development package, so that we can check the physical requirement of the BasicCard.

Terminal- Write program of Food Ration Card without security

This program is used to issue the Food Ration Card to users. The first step of the program is to check the status of the card whether it is inserted in to card reader or not, see fig.1. If not, the program will remain in the pool state, waiting for the card to be inserted. After the card is inserted, the communication between terminal and BasicCard will begin by sending Reset card command from the terminal to card. The card will respond by an Answer to Reset to the terminal program. The process will happen according to communication protocol, which is defined in ISO/IEC 7816-3.

Now, the program allows the issuer to enter the required information, which is as follow: name of family head, the card serial number, the address, number of family members, number of infants, last date updated and the PIN code. The PIN code aims at verifying the bearer of the card. The PIN code is four-character string.

The program will check the length of the entered PIN code, which has to be four-characters. If the length is not four-character, then the issuer will be allowed to enter another PIN. Then the COMD1 is called by terminal-write, to transfer information from terminal-write temporary buffer to EEPROM of BasicCard. Afterwards, SW1SW2 will be checked for each command.

The SW1SW2=9000 is defined in ISO/IEC 7816-4 (Interindustry commands for interchange) as a status word for successful command. The value that will back from the command has to be checked always so as to remove the card form the reader in case there are no error conditions. Finally, a message will appear on the screen, which says: "personalization successful".

Terminal-Read program of Food Ration Card without security

The second program in this application is the terminal read, fig.2. This program is used to read the information from BasicCard. The first step of the program is to check the status of the card whether it is inserted in to card reader or not. If not, the program will remain in the pool state, waiting for the card to be inserted.

After the card is inserted, the communication between terminal and BasicCard will begin by sending Reset card command from the terminal to card. The card will respond by an answer to Reset to the terminal program. Then the user is asked to enter the name of the application, which is saved in the smart card. If the name is wrong, then the user will be out of the program. But if the name is right, then a message will be displayed on the screen which says: "Right application name".

Then, the program will call "COMD2" to get the saved information on the card. The information will appear on the screen. Then the program asks the user whether he/she needs an update. This phase will be used when the citizen wants to receive his share from the agent. So if the citizen enters any number that means he/she does not want to receive his/her share. And he/she used the card in another place. If this happened, the user will go out of the program. But if the user entered "1", that means he/she wants to receive his/her share. If this happened, the program will ask the citizen to enter PIN code. Then the program will call the COMD3 command by which we can make sure whether the PIN is right or wrong.

Then the citizen has asked to enter a new date. That is the date in which he/she received his/her share. The reason we use this date is to make sure whether the citizen has received his/her share or not.

Food Ration Card program without security

The program of the Food Ration Card that stored in smart card contains series of commands that will be called from the terminal write/Read programs. All the details of the commands are explained below:

COMD1 command

This command is called by terminal-write program. This command makes the personalization process. The command reads entered information from the keyboard then stores them on internal EEPROM of the BasicCard.

COMD2 command

This command is called by terminal-Read program. It checks whether the card is personalized or not. If not, the command will terminate terminal-Read program; but if yes, the command reads the information (name of family head, number of serial card, the address, number of family members, number of infants, last date updated and the PIN code) from EEPROM of the card and send them to terminal-Read program.

COMD3 command

This command is called by terminal-Read program. It first checks whether the card personalized or not. If not, the command will terminate Read program; but if yes, it reads entered PIN code and compares it with actual PIN code. If they equal, the program will continue to update date. Otherwise the command permits the user to re-enter PIN code. The re-entering is permitted for 4 tries as maximum.

FOOD RATION CARD APPLICATION WITH SECURITY

In this section, the program is implemented with a security to verify whether terminal is a genuine one or not. Two methods of encryption will be used to implement the security. These methods are AES and RSA with a key length of 128 bits. To make a comparison between the two methods, the size, speed, and required memory are considered.

The programs that are changed are the terminal-Read program and Food Ration Card, where there is no need to alter the terminal-write program because it only issues the card and the issuer of the Food Ration Card is the ministry of Trade.

Terminal-Read program of Food Ration Card with security

The security level is added to manage the genuineness of the terminal. This security level is described as terminal generates a message. This message is sent to BasicCard to encrypt it and

returns an encrypted value to the terminal. The terminal decrypts the encrypted value received from BasicCard. The value obtained from terminal decryption process must equal to the original message, which generates before. If the value obtained from terminal decryption process is not equal to the original message the communication between the terminal and BasicCard stops (this mean that Terminal-Read program cannot read the information stored on the card), so the information stored on the card is protected from counterfeit terminal.
While if the two values are equal the communication between the terminal and BasicCard continues because the card ensures that, its communication partner is genuine terminal.

Terminal-Read program of Food Ration Card using AES-method

The first step of the program is to check the status of the card whether it is inserted in to card reader or not. If not, the program will remain in the pool state, waiting for the card to be inserted.
After the card is inserted, the communication between terminal and BasicCard will begin by sending Reset card command from the terminal to card. The card will respond by an answer to Reset to the terminal program.
AES method is applied to the terminal-Read program as a secretive method. Then, the program will generate message and sends it to Food Ration Card program to encrypt it by calling Encrypt command. See fig.3.
This command will encrypt the generated message. Then, by calling the COMD4 the terminal-Read program will get the encrypted value, after that the program decrypts the encrypted value by AES-function, by using the key stored in the program which the same the key stored in BasicCard program. The terminal-Read program compare between the decrypted value and the original message generated from this program, if not equal, the program will exit and print on the screen “The Terminal is counterfeit”. While, if the two values are equal the program will print on the screen “The Terminal is genuine” and complete the other steps that are declared in the “Terminal-Read program of Food Ration Card without security”.

Terminal-Read program of Food Ration Card using RSA-method

The first step of the program is to check the status of the card whether it has inserted in to card reader or not as described in previous program.
RSA-method is applied at the beginning of the terminal-Read program. First, the program will call COMD5 command to calculate the public key modulus (n), and then this program generate message and sends it to Food Ration Card program to encrypt it by calling Encrypt command. This command will encrypt the generated message. Then, the program decrypts the encrypted message by using RSA-function with key length 128-bits. The terminal-Read program compares between the decrypted value and the original message generated from this program, if the two values are different, the program will exit and print on the screen “The Terminal is counterfeit". While, if the two values are equal the program will print on the screen “The Terminal is genuine" and complete the other steps that are declared in the “Terminal-Read program of Food Ration Card without security”.

Food Ration Card program with Security

This program uses the same the commands that are used in the previous section but with adding some new commands. These new commands are:

Encrypt command

First, the command will check if the card is personalized or not. If not, then the command will exit. Else, the command will encrypt the received data (by using AES-function in the Food Ration Card project with AES-128 and RSA-function in the Food Ration Card project with RSA-128).

COMD4 command

The function of this command is to send the encrypted data N1 (that is obtained from Encrypt command) to terminal-Read program to decrypt it.

COMD5 command

First, the command will check the key length if less than 128-bit, if yes the command will exit from the program, while if more than 128-bits this command calculates the public key modulus (n) from p, q.

THE OPTION WINDOWS

To simulate this project, we must compile it and before we compile it must make setting to simulation options for both terminal program (write/Read) and BasicCard program.

The option windows of Food Ration Card application without security

In terminal program (Write/Read) option window the output file type must select one of 5 files (.DEG, .EXE, .IMG, .LST&.MAP). In our case .DBG files extension has chosen for debugging the software. **Fig. 4** shows the project option windows for terminal programs.

The initial value of communication port (COM port) must be selected. For simulation purposes, virtual card reader was chose in port 201. **Fig. 5** shows the setting virtual port for terminal program.

In BasicCard, option window COM 201 has been selected as virtual COM port and the Compact BasicCard version ZC1.1 has been selected as card type (EEPROM size 1K , RAM 256 bytes, Protocol Support: T=1). The option window for card program has shown in **fig. 6**.

The option windows of Food Ration Card with security

In BasicCard, professional BasicCard version ZC4.5 has been selected as card type (EEPROM size 30K, RAM 1K, Protocol Support: T=0, T=1) because it used AES & RSA encryption methods and its memory is enough for the application requirements.

The options of this project chosen just like what has done in the Food Ration Card without security; but setting of the card type to professional BasicCard ZC4.5 and virtual port to 201.

THE SIMULATION RESULTS

In order to discuss the results from each simulation of three models, we will discuss each one individually.

Simulation Results of the Food Ration Card without security

After writing (Terminal-Write, Terminal-Read &BasicCard) programs, the first step of the simulation was to compile the project files from source code form to p-code debugging form. The compilation results have shown in the **table 1**.

After, the compilation the Terminal-Write program will be opened in parallel with Food Ration Card to issue the initial information to card as shown in **fig. 7.** The follow of the Command-Response is done manually by press “step to card” and” step to terminal” bottoms in debugger window. After this all the information is written in the Food Ration Card and read from the card when Terminal-Read program opened in parallel with the Food Ration Card program.

Because, this project in simulation phase, each time the Food Ration Card program is closed, it must be reinitialized when we opened again, because no EEPROM is valid in the virtual card.

Simulation Results of the Food Ration Card with security

The compilation results of Food Ration Card with AES-128, RSA-128 have shown in table 2, 3 respectively.

After that, the simulation of the Terminal-Read program and BasicCard has done to read all the information has written in the Food Ration Card. The **fig. 8** shows the simulation process of Food Ration Card with AES-128.

The execution time of three models, (Food Ration Card without security and Food Ration Card with security by using AES-128 &RSA-128) has shown in **table 4**.

CONCLUSIONS

The following conclusions have been drawn from the simulation results of three models of the Food Ration Card (the first is Food Ration Card without using any security technique, the second simulates the same application but with security technique by using AES-method and the third by using RSA-method.).

- When we added the security to Terminal-Read program, we found that the code size and the data size of it is increased because of adding the code of security as well as the function of it.

Where, the difference in code size is (159 bytes) in AES-128 and (157 bytes) in RSA-128. While difference in data size is (84bytes) in AES-128 and (199 bytes) in RSA-128.

- When we added the security to Food Ration Card program, we found that difference in EEPROM of BasicCard is (387 bytes) in AES-128 and (675 bytes) in RSA-128.
- Another important point in this comparison is the execution time, where the execution time of Food Ration Card without security is (25 seconds), while the execution time of Food Ration Card with AES-128 is (29 seconds) & RSA-128 is (30 seconds).

REFRENCES

Wenzhou L., ChangQing C., and Zhuo Z., 2010, "Fingerprint ID Cards and the Recognition System", The 5th International Conference on Computer Science & Education.

Stefan M., Markus D., and Christoph G., 2010,"A Smartcard based approach for a secure energy
management node architecture", IEEE.

Daemen J. and Rijmen V., 1999, "AES Proposal:Rijndeal-Second Edition "

Everett D., 1993, "Smart Card Tutorial "

Guilfoyle T., March 2005, "The ZeitControl BasicCard Family", ZeitControl CardSystem GmbH, Germany

Rankl W. and Effing W., 2003, "Smart Card Handbook-Third Edition", Jhon Wiley& Sons, Ltd., Germany

Schneier B., 1996,"Applied Cryptography Algorithms and protocols- Second Edition", Jhon Wiley& Sons

LIST OF ABBREVIATIONS

AES**:** Advanced Encryption Standard
DES**:** Data encryption standard
ECC**:** Elliptic Curve Cryptography
EEPROM**:** Electrical Erasable Programmable
ISO**:** International Standard Organization
NIST: National Institute of Standards and Technology
PIN**:** Personal Identification Number
RAM**:** Random Access Memory
RSA**:** Rivest-Shamir-Adelman
SW1SW2**:** Status Signal.

Table 1: The compilation results of Food Ration Card

Program name	Size (bytes)	Description	Usage percent age
Termina 1-Write	3020	Code size	5%
	2623	Data size	4%
Termina 1-Read	3495	Code size	5%
	2847	Data size	4%
Food Ration Card	406	EEPROM size	41%

Table 2: The compilation results of Food Ration Card with AES-128

Program name	Size (bytes)	Description	Usage percentage
Terminal-Write	3020	Code size	5%
	2623	Data size	4%
Terminal-Read	3654	Code size	6%
	2931	Data size	4%
Food Ration Card	793	EEPROM size	3%

Table 3: The compilation results of Food Ration Card with RSA-128

Program name	Size (bytes)	Description	Usage percentage
Terminal-Write	3020	Code size	5%
	2623	Data size	4%
Terminal-Read	3652	Code size	6%
	3046	Data size	5%
Food Ration Card	1081	EEPROM size	4%

Table 4: The execution time of Food Ration Card

Program name	The execution time (sec)
Food Ration Card without security	25
Food Ration Card with AES-128	29
Food Ration Card with RSA-128	30

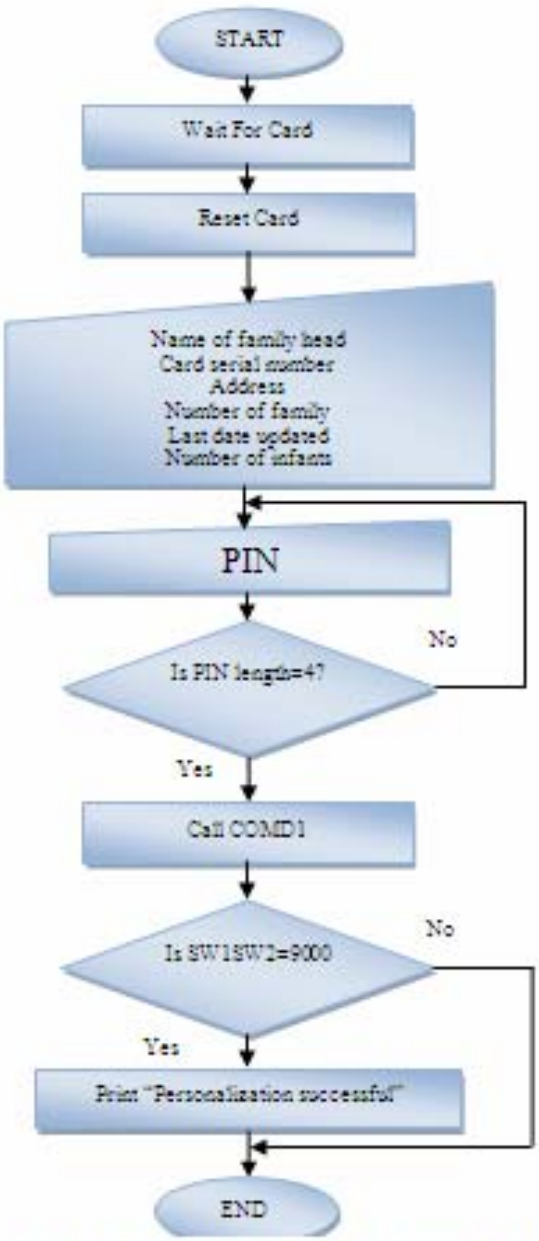

Fig. 1: Terminal- Write program flowchart

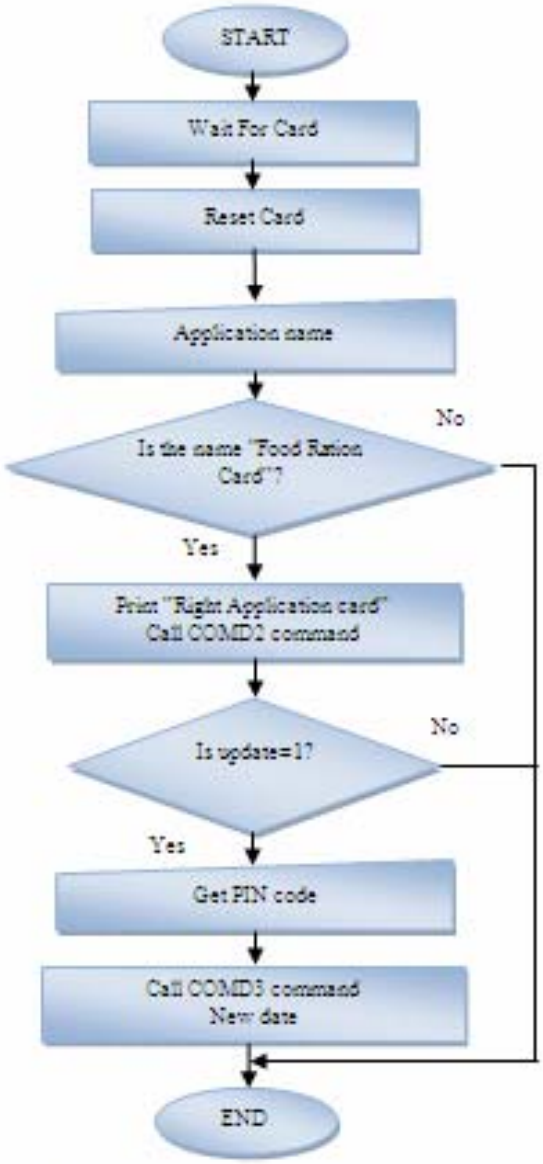

Fig. 2: Terminal- Read program flowchart

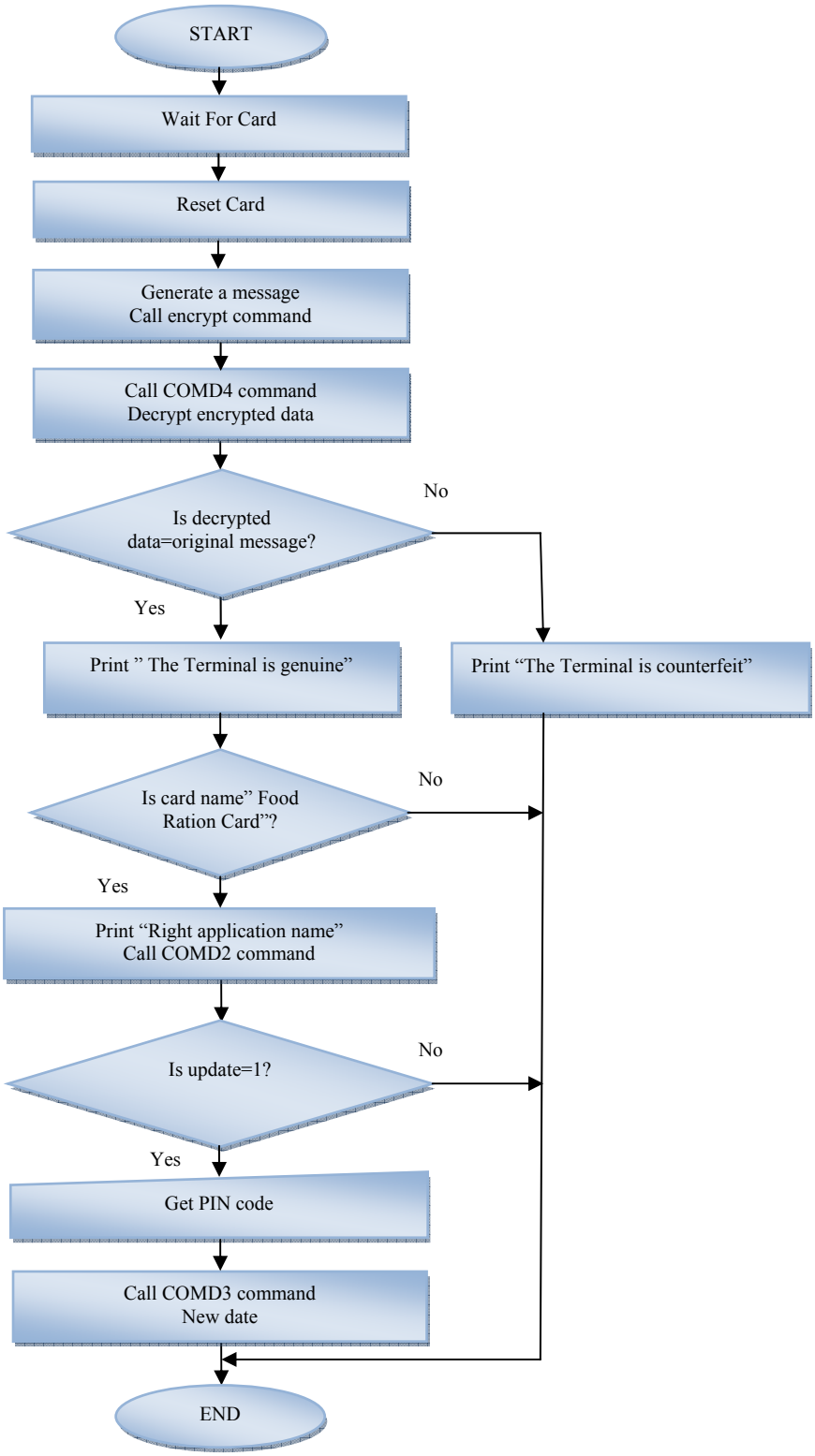

Fig. 3: The flowchart of the terminal-Read program with security

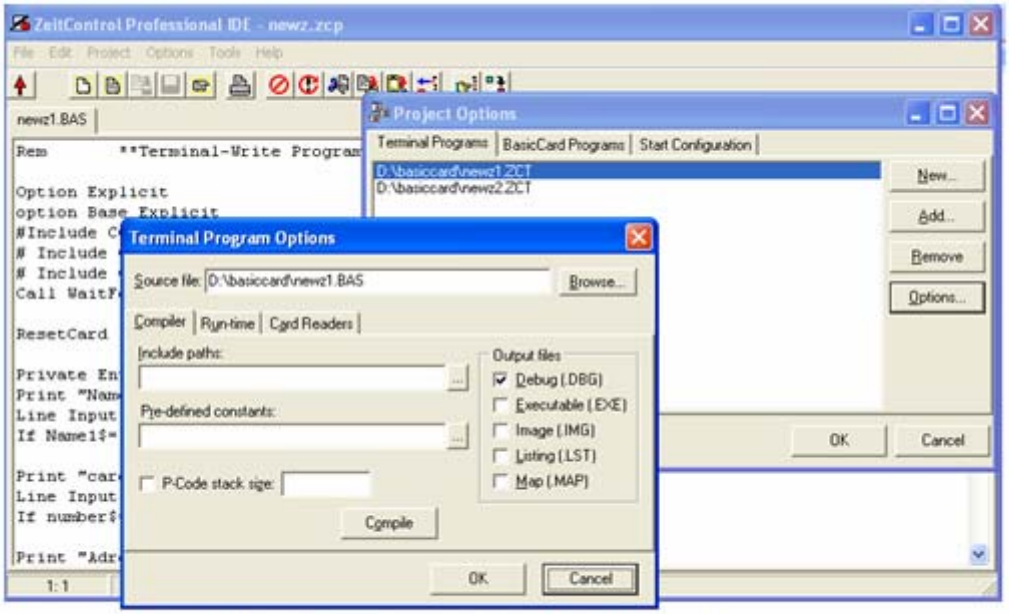

Fig. 4: Project option window for Terminal program

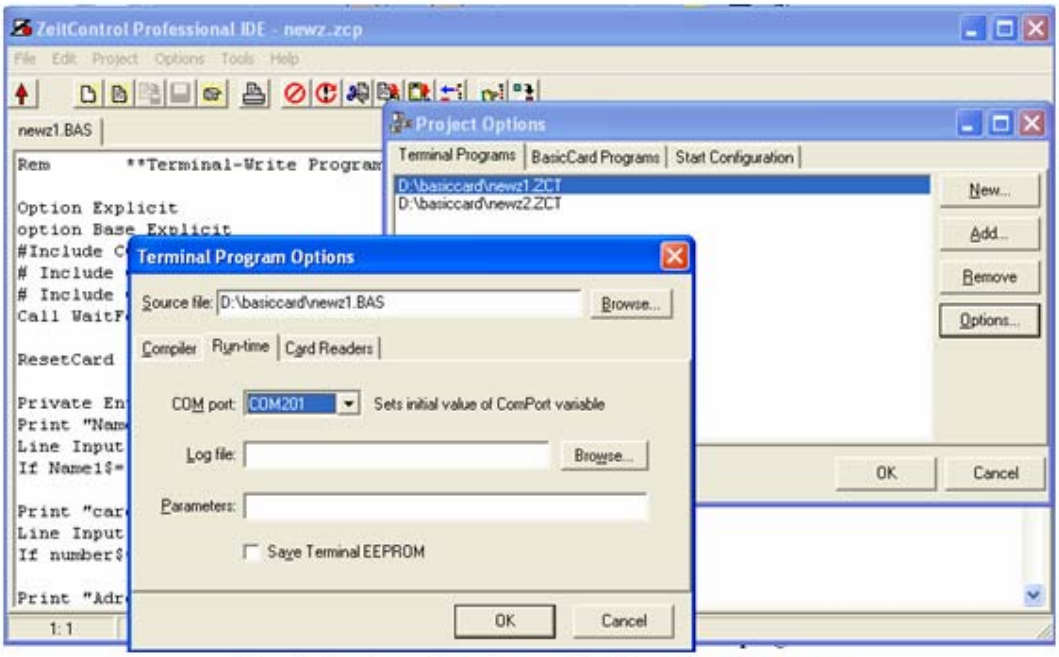

Fig. 5: Setting virtual port for Terminal program

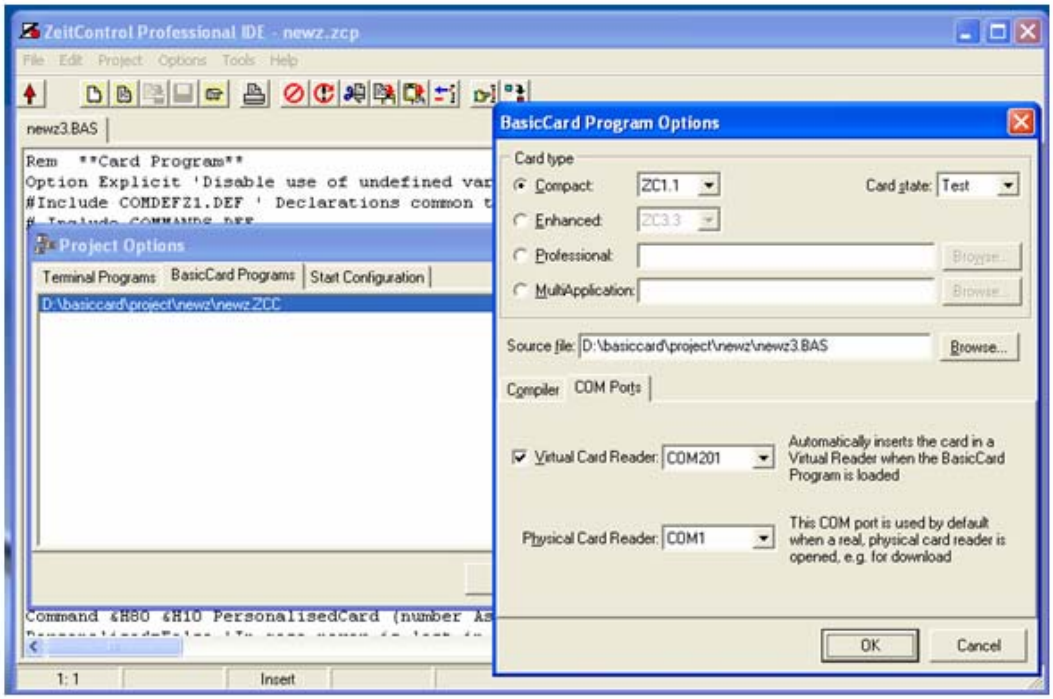

Fig. 6: Option windows for setting Card program

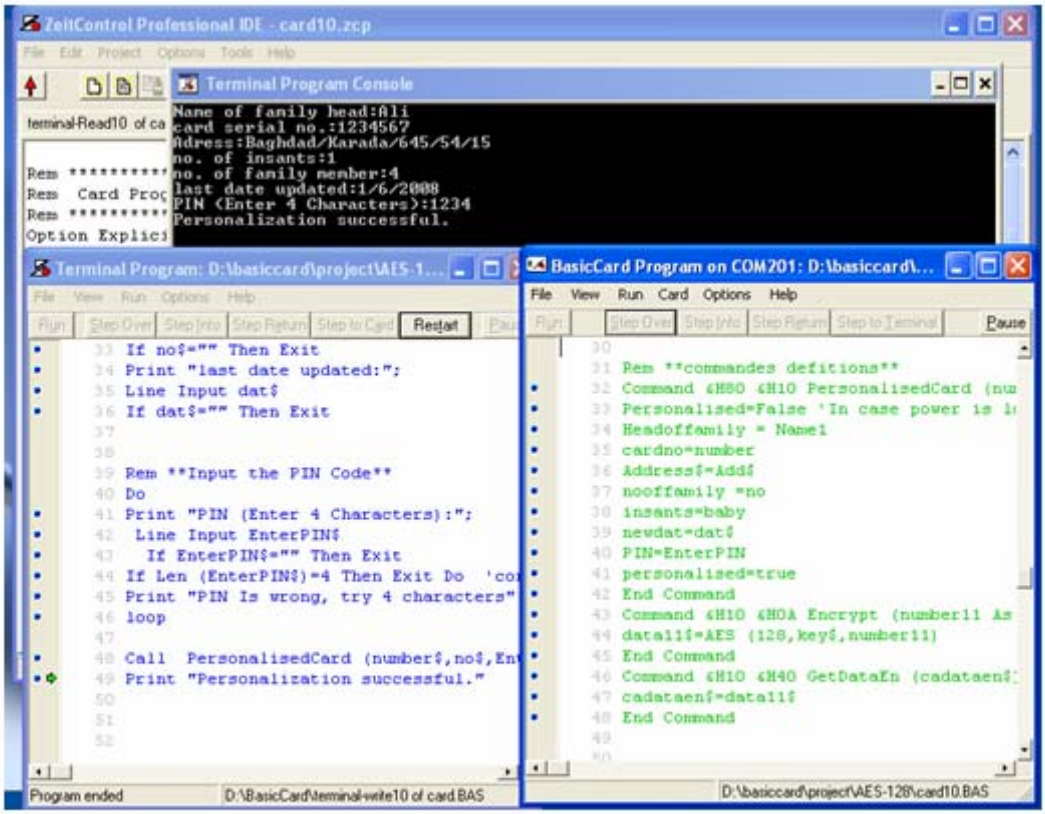

Fig. 7: The debugger windows for Terminal-write and Food Ration Card programs

Corrosion-Resistance Characteristics of Concrete Containing Furfural

Dr. Suhair kadhem Al-Hubboubi ,Prof. Dr.Zain Al-Abideen Raouf & Dr.Ra' id Hasan Abbood

Abstract

Corrosion inhibiting admixtures are unique among other methods to protect reinforced concrete from corrosion damage. In this study, the effect of furfural on the fresh and hardened properties of concrete mixes of 35 and 45 MPa compressive strengths as well as the corrosion inhibition of furfural was evaluated. Furfural was added at different dosages (1, 2 and 3% by weight of cement) with and without superplasticizer (HRWR). Different electrochemical measurements were performed (Half-cell potential, Tafel plot and linear polarization resistance). Electrochemical measurements confirmed that furfural dramatically reduces the rate of corrosion; the inhibition efficiencies were 62.7 and 63.8 % due to 3% furfural addition to 35 and 45MPa-concretes respectively. Results also showed that the combined presence of furfural and HRWR was found to provide an excellent corrosion protection to steel.

الخلاصة

تعد مثبطات التآكل من الطرائق المهمة لحماية حديد التسليح من خطر التآكل.في هذه الدراسة تم تقييم تأثير الفورفورال على الخواص الطرية والمتصلبة لخلطات خرسانية ذات مقاومة انضغاط 35 و45 ميكاباسكال بالاضافة الى تقييم الفورفورال كمثبط لتآكل حديد التسليح .اضيف الفورفورال بعدة وزمات (2,1 و3%من وزن السمنت) مع وبدون الملدن المتفوق .اجريت عدة فحوص كهروكيميائية تضمنت (جهد نصف الخلية،بيانات تافل ومقاومة الاستقطاب الخطي).بينت القياسات الكهروكيميائية ان استخدام الفورفورال ادى الى تقليل كبير للتآكل وان كفاءة التثبيط كانت 62.7 و63.8% نتيجة اضافة 3% للخرسانة ذات المقاومة 35 و45 ميكاباسكال على التوالي وبينت النتائج ايضا ان الاستخدام المشترك للفورفورال والمضاف الملدن المتفوق وفرت حماية ممتازة لحديد التسليح.

Keywords: Corrosion inhibitor, Furfural, Superplasticizer, Linear polarization resistance.

1.Introduction

Concrete construction in Arabian Gulf seaboard countries shows an alarming degree of deterioration within the short span of 10 to 15 years. The deterioration is accentuated by the geomorphic and climatic environmental conditions which are characterized by reactive and marginal aggregates, high temperature –humidity regimes, and severe ground and ambient salinity **(Rasheeduzzafar, 1990)**. Several solutions to this problem have been proposed and tested, though to date no ideal solution has been found. The high costs or lack of effectiveness for some of the other solutions reveal several advantages for the utilization of corrosion inhibiting admixtures. Some of the admixtures, however, may retard time of setting of the cement or be detrimental at later ages. Many would be subject to leaching and hence less effective in concrete that has lost soluble material by leaching **(ACI 222R-96)**. Studies on the effect of organic monomer/polymer additions on the properties of cement products have attracted the interest of researchers **(Singh ,2003)**. Cracks in concrete permit easier access of chloride ions, moisture, and oxygen to the reinforcing steel. Therefore, an effective corrosion- inhibiting admixture would need to remain effective when concrete is cracked **(Civjan ,2003)**.The corrosion behaviour of reinforcing steel embedded in concrete containing commercial corrosion inhibitor has received considerable attention in recent years**(kzair, 2001, Al–Hubboubi , 2001 , Amin ,2001 , Al-Ta'ie,2005,Brown,1999)**. However, very limited amount of work, have been carried out to investigate organic monomer as a corrosion inhibitor for reinforced steel in concrete **(Al-Hubboubi, 2002)**. This work, reports the effect of furfural on the fresh and hardened properties of concrete as well as its corrosion inhibition characteristics.

2. Experimental

2.1. Materials and proportion

Ordinary Portland cement Type (I) (Turabet-AL-Sabe'a) produced by Lebanon cement factory was used for concrete mixtures.Its chemical composition and physical properties are given in Tables 1 and 2 respectively.Natural sand of zone 3 and Crushed river gravel of 19mm maximum size conforming to Iraqi specification No.45/1980(IQS was used.A high range water reducing admixture (HRWR) known commercially as Eucobet super vz was used .Two reference mixes having characteristic compressive strengths of 35 and 45 MPa (A and B) have been prepared . Slump was kept within the range 60±15 mm.Commercial furfural was added to A and B mixes at different dosages (1, 2 and 3%) with and without HRWR.The details of mix proportions are given in Table3 .The pH of furfural

was found acidic (less than 5). It was neutralized by addition of 2.5% Na_2CO_3 to achieve a pH of around 7.

All specimens were wet-cured by covering the finished surface and molds with wet burlap. After one day, the specimens were de-molded and covered with wet burlap for two weeks and then left for air-curing under laboratory conditions for about two weeks, then the specimens were partially submerged in 3.5% NaCl solution for 350 days.

3. Experimental tests

Cubes with dimensions of 100*100*100 mm were prepared for the determination of compressive strength according to BS 1881 part 116 and initial surface absorption according to B.S 1881.part 5:1970. In order to identify the change in mineralogical composition upon furfural addition, x-ray diffraction analysis (XRD) was used. Two specimens, a reference of neat hydrated cement, and another with 3% added furfural were tested at 90-days age. The test was performed using a Chemadzu X-ray diffractometer-6000- Japan. Several electrochemical techniques were used for monitoring corrosion of steel in concrete such as half-cell potential, linear polarization techniques and the Tafel plot technique. The half-cell potential of the reinforcing steel was measured relative to copper-copper sulfate electrode (CSE) in accordance with the ASTM C876-99 standard. The corrosion rate measurements were conducted on specimens using a computerized potentiostat type Mlab200 of Bank Eleketronic, Germany. The test was conducted at 180 days of exposure to 3.5% NaCl saline solution. The reference electrode was saturated calomel (SCE); the auxiliary electrode was platinum electrode while the working electrode was the bar embedded in the concrete specimen. A good contact between the reference electrode and the concrete must be ensured in order to minimize the ohmic drops and avoid errors.The device was programmed to polarize the specimen potential to about 200 mV vs open circuit potential (OCP) in both the directions, i.e., cathodic and anodic. The time chosen scan was 10 mV /6.5 sec. The exposure area, (A) of steel embedded in concrete was calculated (1.25cm*3.14*18cm =70.65 cm^2), the corrosion current was divided on this area to obtain the corrosion current density. The Tafel curve and corrosion current were plotted and determined by the device. Polarization resistance was determined in the range± 30mV from the OPC.Current was linearly plotted against the potential. The polarization resistance Rp ($\Delta E/\Delta I$) is obtained from the slope of the polarization current curve near Ecorr in the cathodic and anodic direction. Tafel constants (anodic Tafel constant Ba and cathodic Tafel constant Bc) could be determined from the slopes of the straight line portions of a polarization curve. The polarization resistance Rp is related to the corrosion current Icorr through Stern-Geary relationship eq.(1).

$$\mathbf{Icorr} = \frac{\mathbf{B}}{\mathbf{Rp}} \quad \text{.....} \quad \mathbf{(1)}$$

Where, B is the Stern–Geary constant.

$$\mathbf{B} = \frac{\mathbf{Ba * Bc}}{\mathbf{2.3\ (Ba + Bc)}} \quad \text{.....} \quad \mathbf{(2)}$$

The corrosion current density, icorr is determined by dividing Icorr on the surface area, A. The corrosion rate in µm per year (µm/yr) is determined by multiplying icorr by 11.59 using Faraday's Law **(Trejo,2009)**.

4. Results and discussion

4.1 X-ray diffraction

The results of x-ray diffraction analysis (XRD) are shown in Fig.2.It is obvious that there exists some change in relative intensities of crystalline phases upon furfural addition. Moreover, a new crystalline (peak) phase has been detected. The change in peak intensity would be attributed either to a change in degree of crystallization of the specified phase and/or a change in its quantity. The relative intensity of $Ca(OH)_2$ at 2θ =34.11° (d=2.628 A) was reduced from 138 to 105 counts upon 3% furfural addition, while that of tobermorite phase ($C_5S_6H_5$) at 2θ =29.39° (d=3.03A) was increased from 124 to 160 counts.

2.3 Method of exposure

4.2 Water reduction due to furfural addition

The effect of furfural dosage on water reduction for concrete mixes with and without HRWR are shown in Fig.3 Results indicated that there would be a progressive water reduction as the dosage of furfural is increased. According to **(Singh ,2003)** the addition of water-soluble polymers permits the formation of highly workable paste with very little water. It seems that the additive acts as a lubricant. The water reduction was increased more by combined effect of furfural and HRWR than the effect of each admixture alone. The binary

admixture containing superplasticizer and polymer may result in certain beneficial effects to concrete that cannot be derived by using them individually **(Beaudoin,1989).**

4.3 Compressive strength

Compressive strength results for concrete mixes of 28 and 90 days are illustrated in Fig 4. These results indicate an increase in compressive strength upon furfural dosage increase. More improvement was observed due to the combined presence of furfural and HRWR .For 90 days results ,the compressive strength of concrete containing 1%HRWR and furfural was improved by a rate higher than HRWR -concrete compared to their mixes at 28 days.

4.4 Initial surface absorption (ISA)

The rate of water absorption by the surface zone of concrete under a fixed hydrostatic head is determined during a prescribed period between 10 minutes and two hours . The results indicated a decrease in ISA upon furfural dosage increase, Figs.(5 and 6).The percentage reduction in the ISA of 2 and 3% furfural-concrete (A2F and A3F) and for 2 hours duration of the test was 46.4 and 72.5% relative to its reference concrete (2A).This behavior is mainly attributed to the build-up of better microstructure, formation of additional C-S-H gel system and the filling of pores .The results had also shown that the percentage reduction in the ISA of HRWR-concrete (A1S) for 2 hours duration of the test , relative to its reference concrete was 49.3 % Further reduction in ISA was observed for A1S1F concrete compared to their reference concrete as well as to HRWR-concrete .The percentage reduction in 2 hours ISA of 2A1S1F was 70% compared to their reference . It is clear from these data that the synergistic effect of furfural and HRWR has a significant influence on the value of ISA of concrete.

4.5 Electrochemical measurements

4.5.1 Half-cell potential

The results of half-cell potentials of steel as referenced to a copper- copper sulphate electrode (CSE) are shown in Figs7 through 10. It is clear that the potentials of steel embedded in most of concretes were shifted towards negative potential at the beginning of exposure period. However, after ~30 days of exposure, the CSE potentials began to shift to more passive state. As per ASTM C876, -350 mV vs.CSE has been recognized as a threshold potential to reach an active condition of rebar .This level has been marked in the figures. It has been found that the addition of furfural improved the corrosion resistance of concretes, especially those with lower cement contents and weaker strengths. For example , in 35 MPa concrete (mix A) Fig7, the rebar embedded in concrete containing 2 and 3% furfural and reference concrete showed an initial potential values of -167,-197and -170 mV respectively. Specimens incorporating furfural, showed lower steel potential compared to reference concrete. However, rebar in reference concrete would tend to shift to more negative potential after about 150 days of exposure indicating a change in electrochemical status and the onset of the breakdown of passivity. At the end of 350 days of exposure the average potential of rebars in reference concrete (with cement content of 350 kg/m^3 and w/c of 0.563) reached -352.2 mV, while the average potentials of rebars embedded in 2 and 3% furfural –concrete reached -45 and -77 mV ,respectively. In 45 MPa concrete, Fig.8 , the higher cement content of reference concrete (with 450Kg/m^3 and w/c of 0.438) would initially provide a good protection to steel embedded in it, due to high alkalinity and denser structure that minimized chloride penetration towards the bars . However, the addition of 3% furfural (mix B3F) provided better protection and the best results were achieved by using 0.5% HRWR and 2% furfural (BS2F). The average potentials of bars in B, B3F, and BS2F at the end of 350 days were -72.5,-44 and +4 mV respectively. According to **(Babaei ,1986)**, positive half-cell potentials of small magnitude (generally less than +100mV) may result from large resistance in circuit (dry concrete or the absence of electrical continuity) or the absence of corrosion activity. It is suggested that such high reactivity contributes to the build-up of a protective passive layer. Hence, the trend of potentials of furfural-containing concrete shows some healing upon longer exposure duration. However, for furfural-free concrete, this layer does not exist, and the natural layer present due to high alkalinity of cement would be destroyed upon longer exposure duration. Accordingly, the potentials drop down to the level of high probability of corrosion. Reinforcing steel in HRWR- concrete exhibited lower potentials than those of steel embedded in reference concretes (mixes A and B).This behavior could be related to the reduction in water content and the formation of the denser gel. However , bars in HRWR- concrete of 35MPa were shifted to a more negative potential after about 280 days of exposure, refer to Fig.9.According to (Neville,2005) superplasticizer per se does not

affect the pore structure and, therefore, does not alter the process of corrosion. The results also demonstrated that the combined action of furfural and HRWR provide excellent protection to steel. The average potentials of bars in A1S , A1S1F, A1S2F and A1S3F at the end of 350 days were -222.5 , -55.5, -62 and - 62.5 mV, respectively .However, the efficiency of combined effect of furfural and HRWR in concrete containing higher cement content (450 kg/m^3) was affected by furfural dosages .The B1S3F mix provided little protection to rebar at the beginning of exposure as an evidence of concrete weakness but with time it became stronger and exhibited an excellent protection to the rebar, Fig.10 .This behavior may be attributed to the extent of polymerization of furfural with time.

4.5.2 Polarization measurement

4.5.2-1 Tafel Plots

The Tafel plots for reinforced concrete specimens were tested at age 180days of partial submergence in to 3.5%NaCl solution. Tafel plots for specimens represent the relation between the current (μA) and the potential (-mV) in a semi-logarithm scale. They are shown in Figs11through14. These figures were used to obtain the Tafel plots parameters: Ba, Bc, B and i_{corr} which represent respectively the anodic Tafel slope, cathodic Tafel slope, the B constant and the corrosion current. These parameters are listed in Table 4 as well as the current density (μA/cm^2) which can be obtained by dividing i_{corr} in (μA) by exposed surface area of the embedded reinforcing steel in concrete (cm^2).The results confirm that the corrosion process of the steel reinforcement for all specimens were anodically controlled depending on the Tafel slopes with the conclusion that the anodic process is the slower process (the one with the large polarization), whereas the rate of oxygen diffusion through the concrete determines the rate of corrosion. The constant B is dependent on the magnitudes of the Tafel slopes of the anodic and cathodic reactions characterizing the particular corroding system.

4.5.2.2. Linearpolarization resistance measurement

The linear polarization resistance represents the electrical resistivity of the passive film at the surface of the re-bars, and is determined graphically from the slope of the potential (mV)-current density (μA/cm^2) curves. According to **(Mancio,2005)** the greater the slope, the more difficult for the charge to transfer across the metal/electrolyte interface, and therefore the corrosion current density is smaller and, consequently, the corrosion reaction rate is slower. The potential –current (E-I) relationships for 35 MPa concrete and 45MPa concretes with and without furfural ,HRWR are given in Table 4 and shown in Figs.15 and 16 . Results showed that polarization resistance for 45 MPa - concrete (2.069 KΩ) was higher than 35MPa- concrete (1.685 KΩ).This improvement is due to higher cement content and lower w/c ratio. Polarization resistance measurements showed that furfural-treated concrete specimens had higher Rp values compared with the reference concrete. An additional improvement was achieved by combined effect of furfural and HRWR over HRWR-concrete. The calculated corrosion density determined by using Stern-Geary equation for reinforcement steel of 35 and 45 MPa-concretes showed that with an increase in cement content and a decrease in w/c ratio ,a decrease in corrosion current density was achieved,Fig.17. This improvement results from the development of passivity due to high alkalinity and dense structure. The use of 2 and 3% furfural resulted in 36.4 and 63% reduction in corrosion current density of steel in A2F and A3F mixes respectively compared to A(35 MPa) concrete. Similarly, the addition of 3% furfural to 45 MPa concrete led to a reduction in corrosion current density of about 64%.Less effectiveness was observed by the combined effect of furfural and HRWR .However a significant reduction in corrosion current density was achieved by 2%furfural and HRWR in B1S2F over HRWR-concrete B1S.

5. Conclusions

1- A progressive water reduction would take place as the dosage of furfural is increased. The water reduction was increased more by combined effect of furfural and HRWR than the effect of each admixture alone.

2- A decrease in ISA upon furfural dosage increase was observed .The percentage reduction in the ISA of 2 and 3% furfural-concrete (A2F and A3F) and for 2 hours duration of the test was 46.4 and 72.5% relative to its reference concrete (A).This behavior is mainly attributed to the build-up of better microstructure, formation of additional C-S-H gel system and the filling of pores .The results had also shown that the percentage reduction in the ISA of HRWR-concrete (A1S) for 2 hours duration of the test , relative to its reference concrete was 49.3 % Further reduction in ISA was observed for A1S1F concrete compared to

their reference concrete as well as to HRWR-concrete .The percentage reduction in 2 hours ISA of 2A1S1F was 70% compared to their reference . It is clear from these data that the synergistic effect of furfural and HRWR has a significant influence on the value of ISA of concrete.

3 Reinforcing steel in HRWR- concrete exhibited lower potentials than those embedded in reference concretes (35 and 45 MPa). However, rebars in HRWR- concrete of 35MPa were shifted to a more negative potential after about 280 days of continuous exposure to 3.5% NaCl solution.

4-The combined presence of furfural and HRWR was found to provide an excellent corrosion protection to steel. The potentials of rebar in A1S, A1S1F, A1S2F and A1S3F-concretes at the end of 350 days were -222.5,-55.5,-62 and -62.5 mV, respectively.

5-After six-month period of continuous exposure to 3.5% NaCl solution, electrochemical measurements confirmed that the utilization of furfural in concrete would result in a significant reduction in corrosion tendency. The effective dosage was 3% by weight of cement. Furfural dramatically reduces the rate of corrosion; the inhibition efficiencies were 62.7 and 63.8 % due to 3% furfural addition to 35- and 45-MPa-concretes respectively.

References

ACI Committee 222, "Corrosion of Metals in Concrete," ACI 222R-96, Manual of Concrete Practice,1996,30 pp.

Babaei ,K., "Evaluation of half-cell corrosion detection test for concrete bridge decks", Washington state department of transportation in cooperation with the United States department of transportation federal highway administration, Final report November 1986, 86 pp.

Beaudoin J.J. and Ramachandran V.S.,"Effect of Water Dispersible Polymers on the Properties of Superplasticized Cement Paste, Mortar, and Concrete", Reprinted from CANMET/ACI "Superplasticizers and other chemical admixtures in concrete , " Proceedings of Third International Conference 1989,Ottawa, Canada, ACI SP119-12, pp. 221-242.

Mancio, M., Carlos,C. J., Zhang.J., Harvey,J.T., Monteiro,P. J. M., and Ali,A," Laboratory Evaluation of Corrosion Resistance of Steel Dowels in Concrete Pavement Prepared for the California Department of Transportation," Pavement Research Center Institute of Transportation Studies University of California Berkeley and University of California Davis March, 2005 Revised May 2005,161 pp.

Neville, A.M., "Properties of Concrete," Pearson Education Limited, Fourth and final edition, 2005, 843 pp.

Rasheeduzzafar,Dakhil,F.H.,AL-Gahtani,A.S.,AL-Saadoun,S.S.and Bader,M.A., "Influence of Cement Composition on the Corrosion of Reinforcement and Sulfate Resistance of Concrete," ACI Journal ,Mar-Apr.1990,pp.114-122.

Singh,V.K., Singh, R.K. and Khatri ,S.D, " Effect of furfuryl alcohol on the properties of hydrated cement mortar", J. Mater. Res., Vol. 18, No. 5, May 2003, 10 pp.

Civjan, S.A., Lafave, J.M., Lovett, D., Sund, D.J.andTrybulski,J.," Performance Evaluation and Economic Analysis of Combinations of Durability Enhancing Admixtures (Mineral and Chemical) in Structural Concrete for the Northeast U.S.A., " Prepared for the New England Transportation Consortium, project No.97-2,2003, 165 pp.

كزير، بهاء جورج ، يوسف ،هناء عبد ، عيفان ،محمود ،والحبوبي ،سهير كاظم ،"ديمومة خرسانة قبعة الركائز نتيجة تأثير الماء والاملاح الخارجية عليها"، بحث غيرمنشور، مركز بحوث البناء ، العراق، بغداد 2001، 43صفحة.

Al-Hubboubi,S.K.,"Corrosion of Steel Reinforcement in High Performance Concrete Containing Local Slag and Corrosion Inhibitor," M.Sc. thesis, University of Technology,Iraq, 2001, 113 pp.

Amin,Z.H., "Corrosion of Steel Reinforcement in High Performance Concrete Containing RHA and Corrosion Inhibitor ", M.Sc thesis ,University of Technology,Iraq, ,2001, 126 pp.

Al – Ta'ie, S. A.," Durability of Concrete Incorporating Corrosion Inhibitor and Air-Entraining Agent Exposed to Cl - + $SO4^{--}$ Solution", M.Sc thesis ,University of Technology,Iraq, 2005, 108 pp.

Brown,M.C. , "Assessment of Commercial Corrosion Inhibiting Admixtures for Reinforced Concrete ",M.Sc. thesis ,Virginia Polytechnic Institute and State University, Civil and Environment Engineering , Blacksburg ,Virginia , Nov. 1999, 92 pp.

سهير كاظم الحبوبي،رواء علي، وعادل مصطفى كامل ،"تصنيع مثبطات تآكل حديد تسليح الخرسانة"، مركز بحوث البناء، العراق ،2002،بحث غير منشور، 37صفحة.

Trejo,D, Halmen,C and Reinschmidt,K., " Corrosion Performance Tests for Reinforcing Steel in Concrete:Technical Report," Performed in cooperation with the Texas Department of Transportation and the Federal Highway Administration October 2008 Published: October 2009,209 pp.

Table 1: Chemical composition and main compounds of cement.

Oxides composition ,%	Turabet Al-Sabe'a OPC	Limits of (IQS) No.5/1984
CaO	63.31	-
SiO_2	19.44	-
Al_2O_3	5.12	-
Fe_2O_3	3.57	-
MgO	1.07	≤5.00
SO_3	2.8	≤2.80
L.O.I.	3.87	≤4.00
Lime Saturation Factor,L.S.F.	0.975	0.66-1.02
C_3S	62.44	-
C_2S	8.97	-
C_3A	7.53	-
C_4AF	10.85	-

Table 2: Physical properties of cement

Physical Properties	Turabet Al-Sabe'a OPC	Limits of (IQS) No.5/1984
Specific surface area (Blaine method), cm^2/gm	3203	≥2300
Setting time(Vicate apparatus), Initial setting, hour: minute Final setting, hour: minute	2:05 3:50	≥00:45 ≤10:00
Compressive strength ,MPa 3 days 7 days	 28.6 30	 ≥15 ≥23

Table3: Concrete mixes

Symbol	Mix components						w/c	Slump (mm)
	Cement kg/m³	Sand kg/m³	Gravel kg/m³	Water kg/m³	Furfural % of cement Wt.	HRWR % of cement Wt.		
A	350	845	1033	197	-	-	.563	50
A2F	=	=	=	189.6	2	-	.542	65
A3F	=	=	=	182.3	3	-	.521	60
A1S	=	=	=	171.3	-	1	.49	80
A1S1F	=	=	=	162.6	1	1	.465	60
A1S2F	=	=	=	157.5	2	1	.45	55
A1S3F	=	=	=	156.1	3	1	.446	50
B	450	741.5	1033	197	-	-	.438	55
B3F	=	=	=	189.5	3	-	.421	55
BS2F	=	=	=	177.3	2	.5	.394	60
B1S	=	=	=	171	-	1	.38	50
B1S1F	=	=	=	197	1	1	.36	50
B1S2F	=	=	=	189.5	2		.35	75
B1S3F	=	=	=	177.3	3	1	.37	60

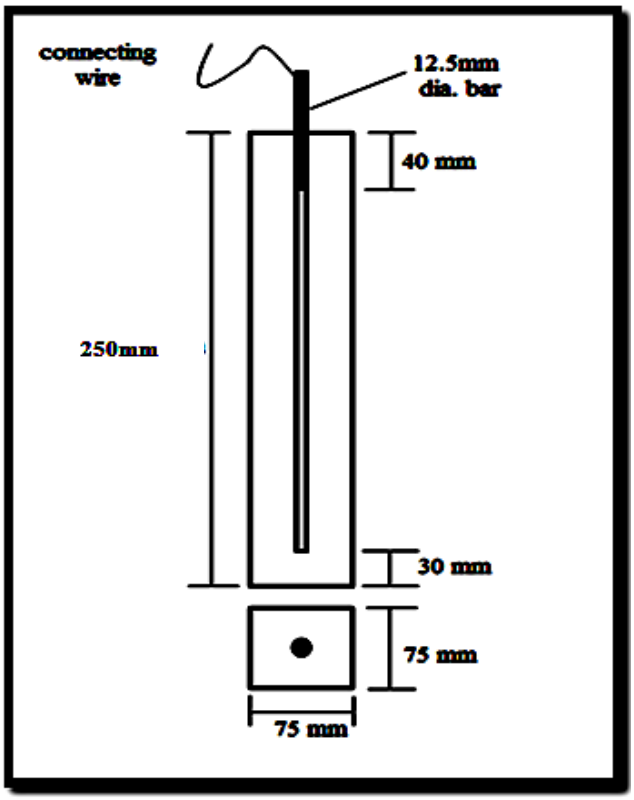

Fig.1: Sketch of reinforced concrete prism

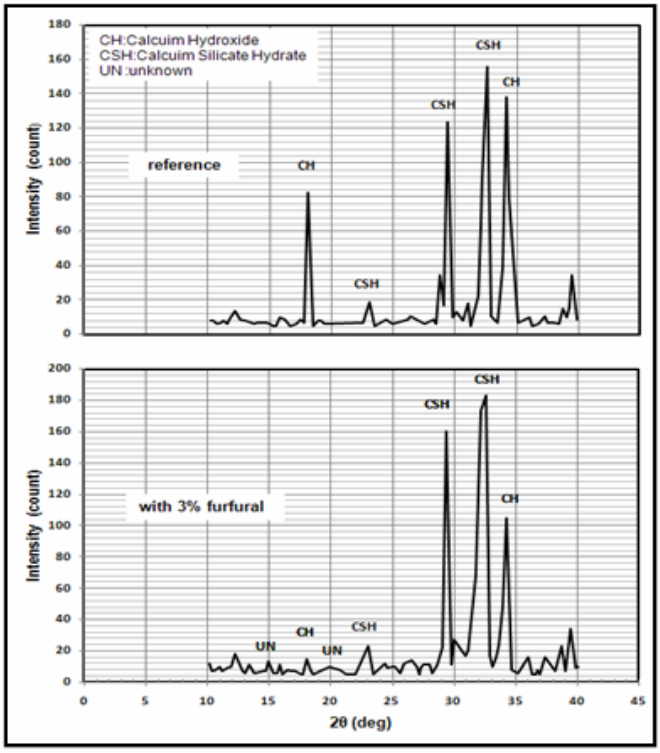

Fig.2: X-ray diffraction of neat hydrated cement with and without furfural.

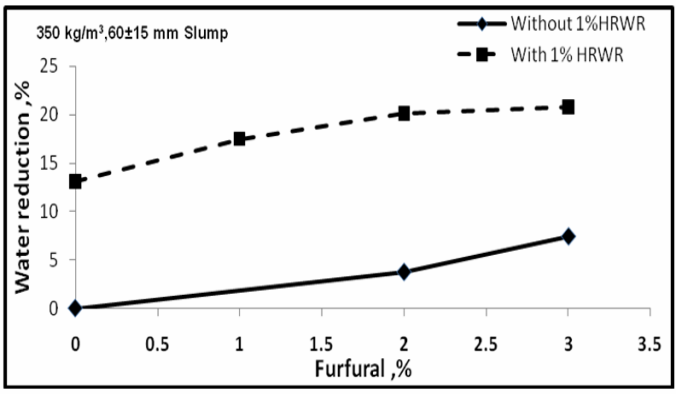

Fig.3: Effect of furfural dosage and combined effect of furfural and 1% HRWR on water reduction

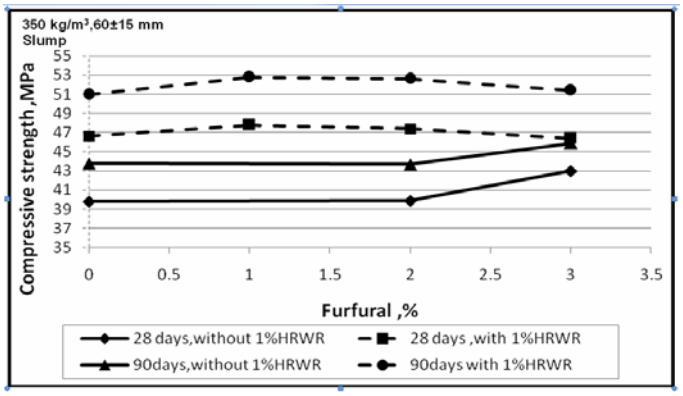

Fig. 4: Effect of furfural dosage on compressive strength of 1% HRWR –containing concretes.

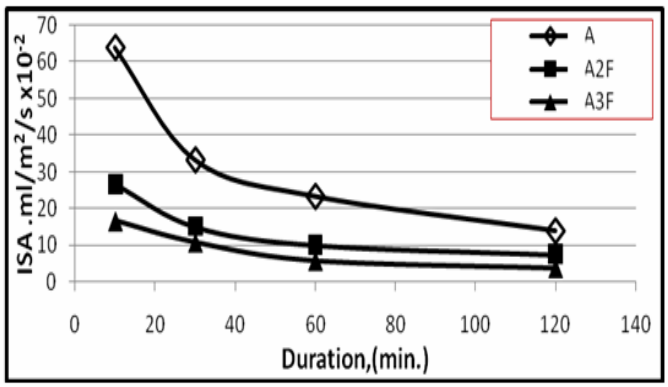

Fig.5 : Effect of furfural on initial surface absorption values at age of 28days

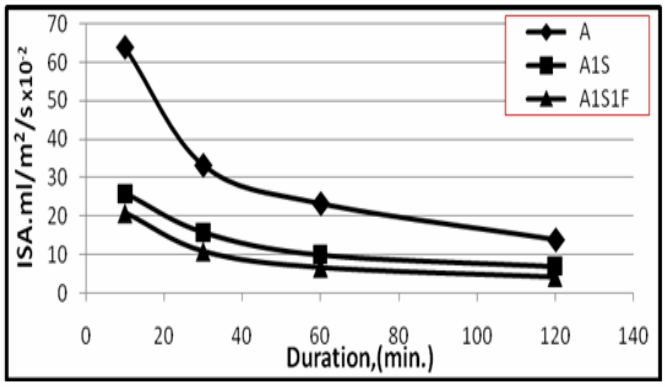

Fig.6: Combined effect of furfural and HRWR on initial surface absorption at age of 28days

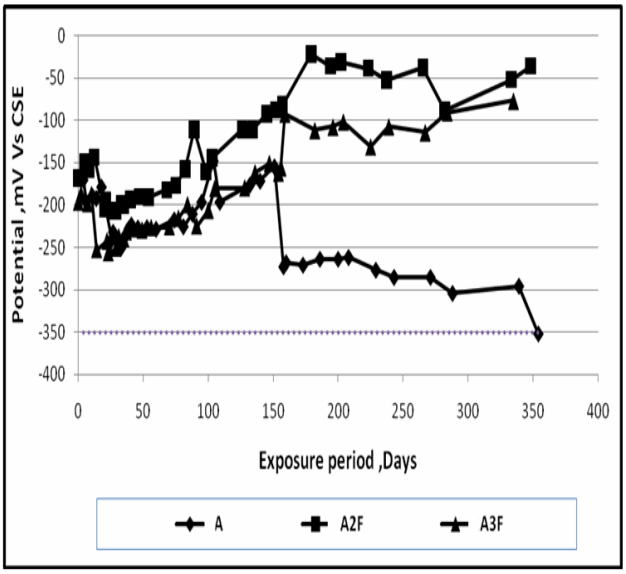

Fig.7: Potential versus time behavior of rebar embedded in furfural-concrete of 35MPa

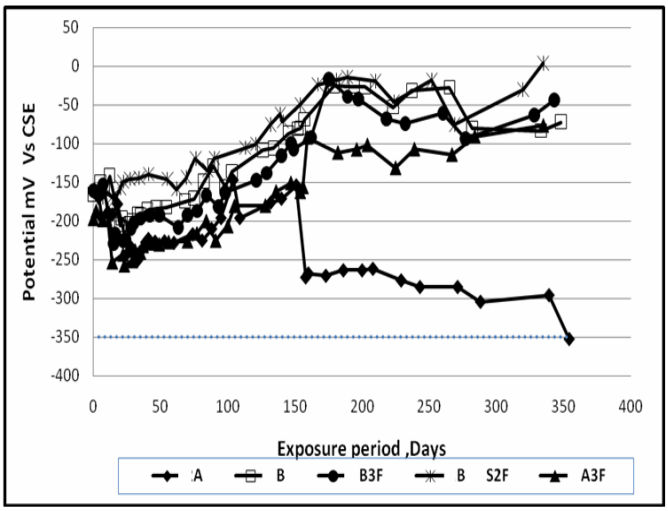

Fig.8: Potential versus time behavior of rebar embedded in furfural-concretes of 35MPa and 45 MPa.

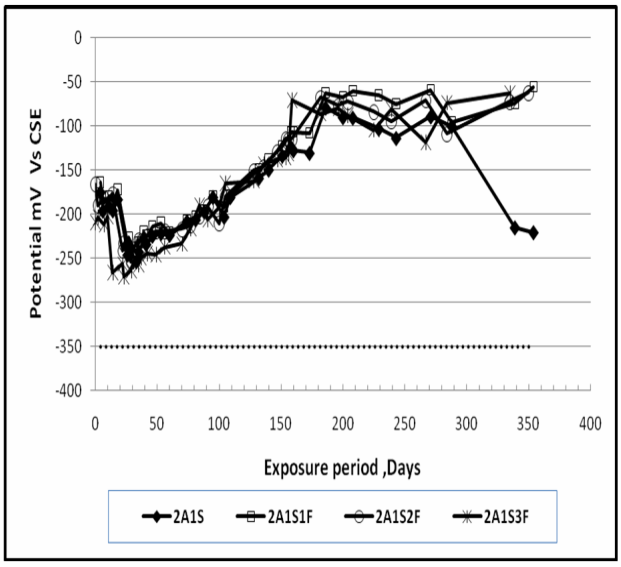

Fig.9: Potential versus time behavior of rebar embedded in HRWR and furfural-concrete of 35M

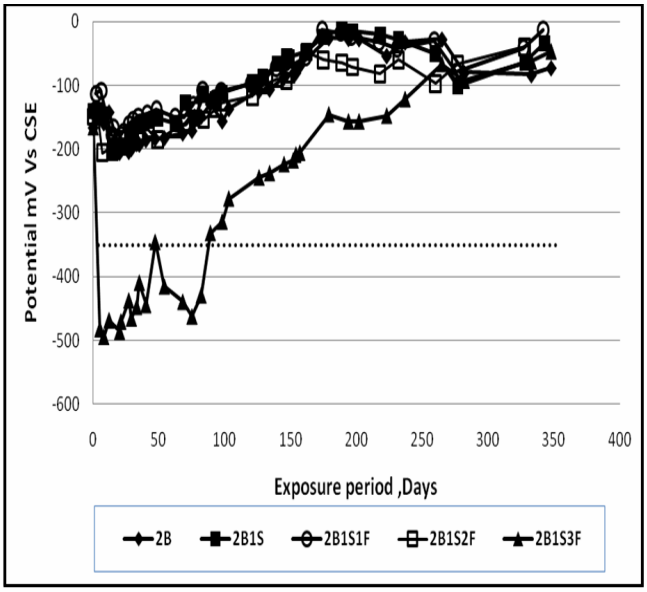

Fig.10: Potential versus time behavior of rebar embedded in HRWR and furfural-concrete of

Table 4:Tafel constant and linear polarization resistance results

Symbol	Tafel plot						Linear polarization resistance			
	E_{corr} SCE -mV	Tafel constant mV/decade			Corrosion current I_{corr} µA	Corrosion current density µA/cm²	Polarization resistance Rp-KΩ	Corrosion Current I_{corr} µA	Corrosion current density i_{corr} µA/cm²	Corrosion rate µm/yr
		Ba	Bc	B				B/Rp		
A	360	300	130	39.4	19	.27	1.685	23.4	.33	3.83
A2F	270	275	90	29.5	10	.14	2.183	14.8	.21	2.44
A3F	300	400	70	25.9	8	.11	2.970	8.7	.123	1.43
A1S	300	370	85	30.1	9	.13	2.609	11.5	.163	1.9
A1S2F	250	450	100	35.6	9	.13	3.158	11.3	.16	1.86
A1S3F	260	450	110	38.4	9	.13	3.158	12.2	.173	2
B	295	330	90	30.7	10.2	.144	2.069	14.8	.21	2.44
B3F	300	190	90	26.6	4	.057	4.918	5.4	.076	.88
B1S	240	250	115	34.2	7.5	.106	3.186	10.8	.153	1.77
B1S1F	200	255	115	34.5	6.5	.092	3.297	10.4	.147	1.7
B1S2F	300	230	110	32.3	4	.057	5.000	6.46	.09	1.044

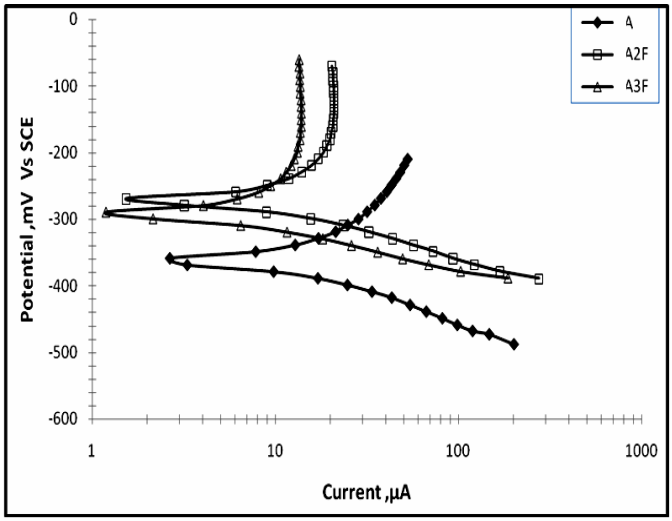

Fig.11: Tafel plot for steel in furfural – concrete (350 kg/m3) at 180 days of partially submergence in 3.5%NaCl solution.

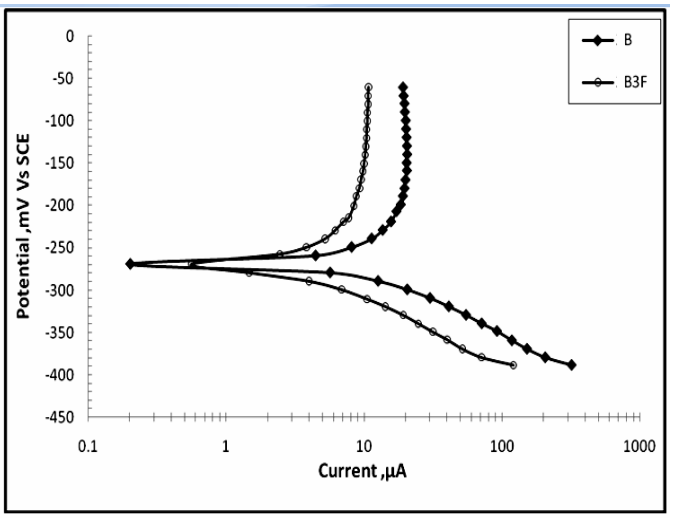

Fig.12:Tafel plot for steel in furfural –concrete(450 kg/m3) at 180 days of partially submergence in 3.5%NaCl solution.

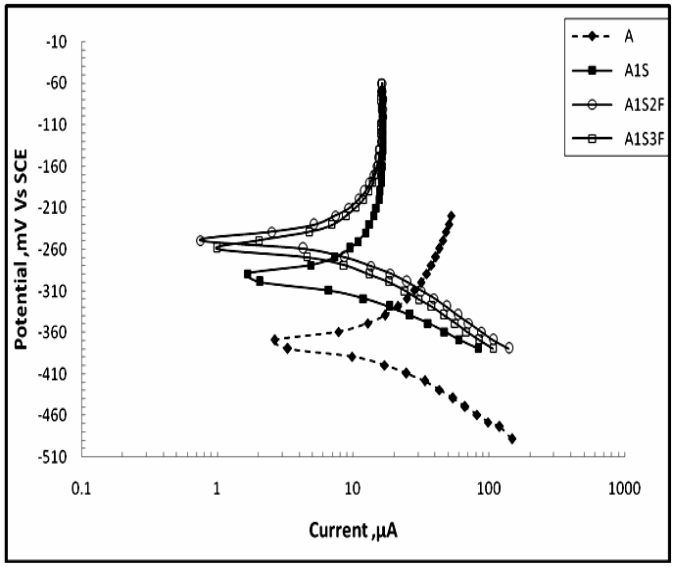

Fig.13: Tafel plot for steel in furfural – concrete (350 Kg/m3) with and without HRWR at 180 days of partially submergence in 3.5%NaCl solution.

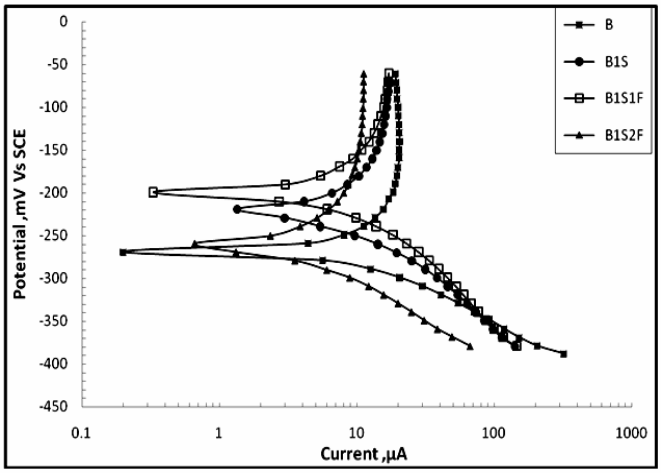

Fig.14:Tafel plot for steel in furfural-concrete (450 Kg/m3)with and without HRWR at 180 days of partially submergence in 3.5%NaCl solution.

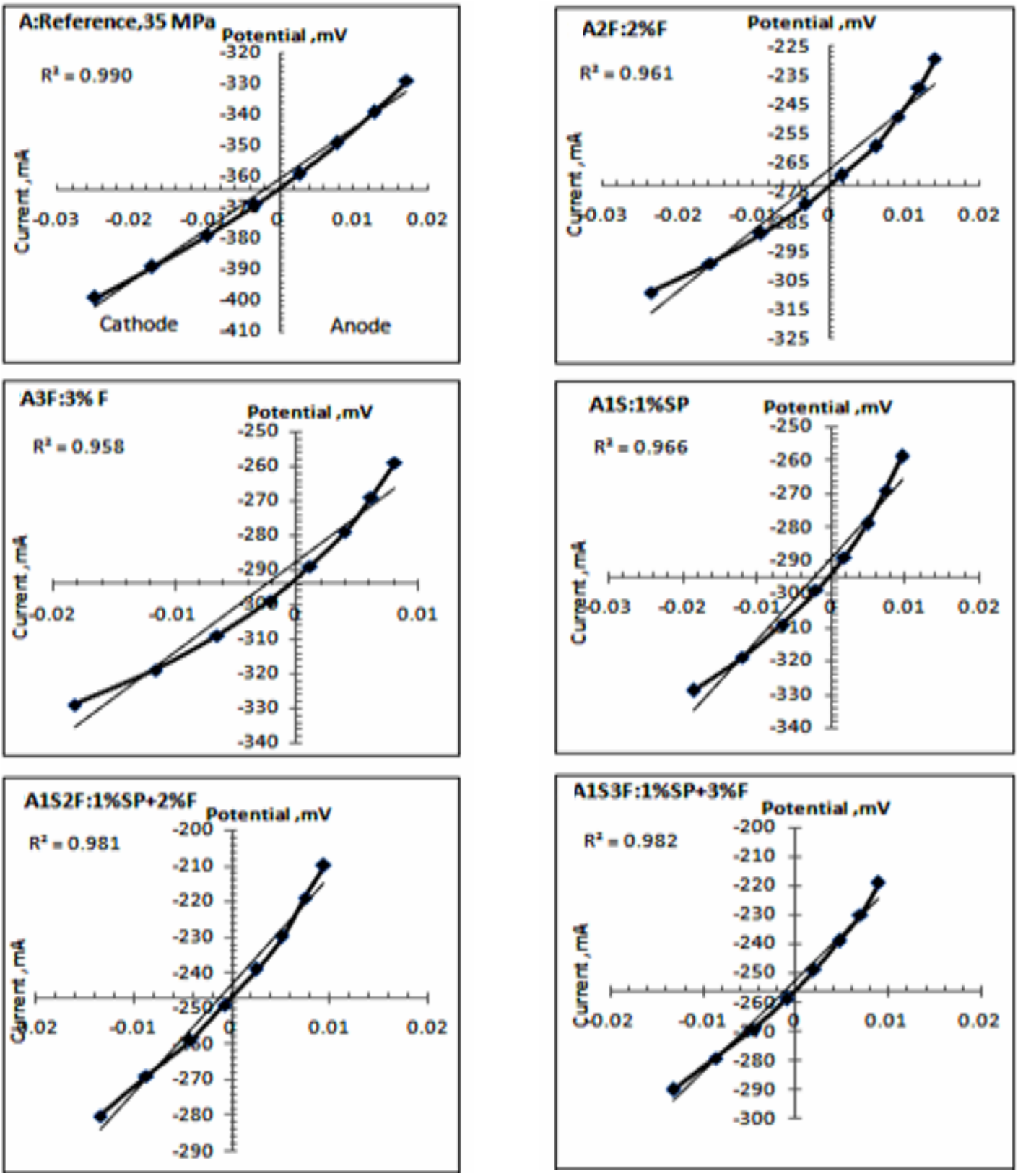

Fig.15: Polarization resistance of steel bars in 35 Mpa reference concrete and concretes with different admixtures.

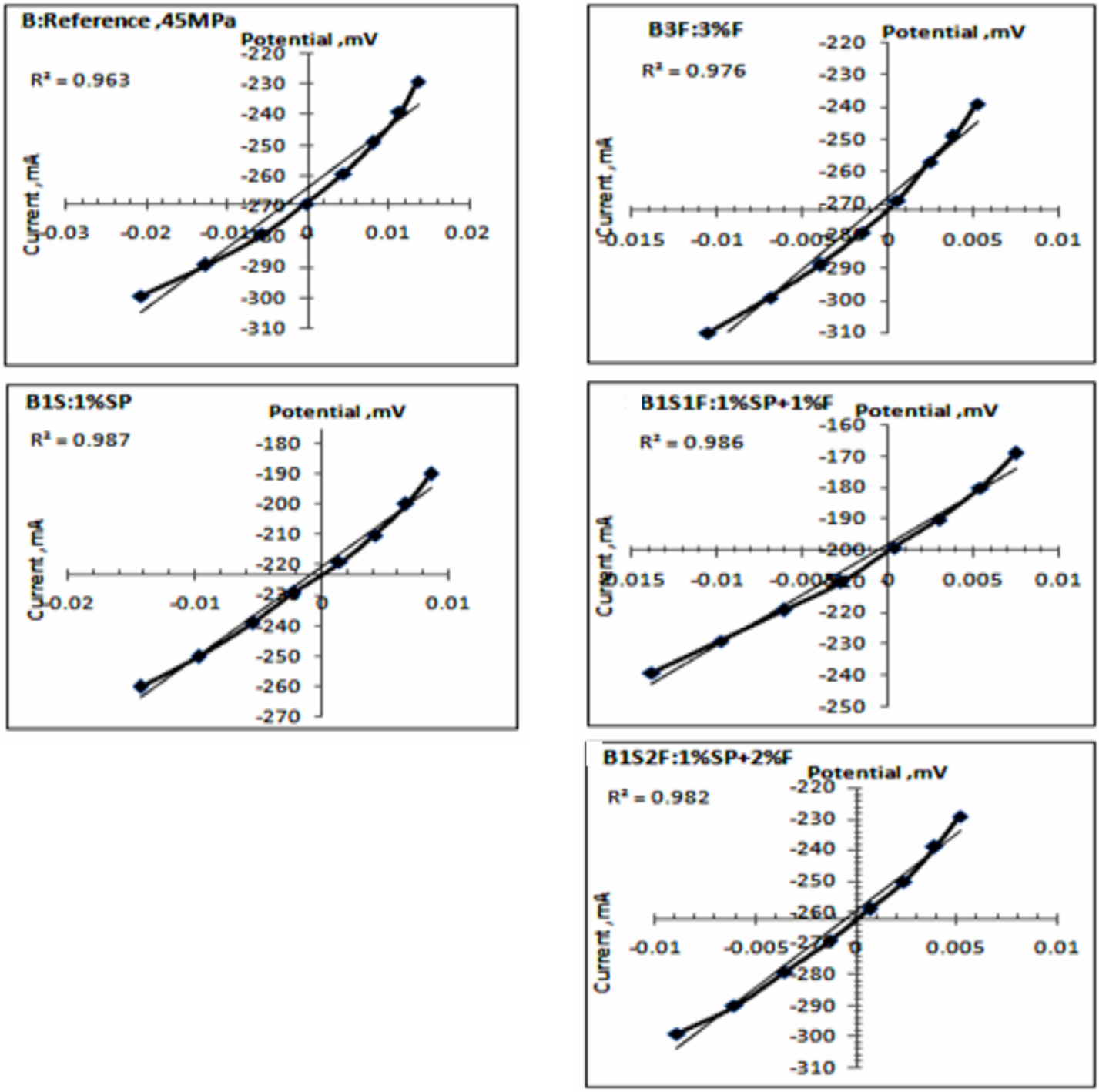

Fig. 16.Polarization resistance of steel bars in 45 MPa reference concrete and concretes with different admixtures...

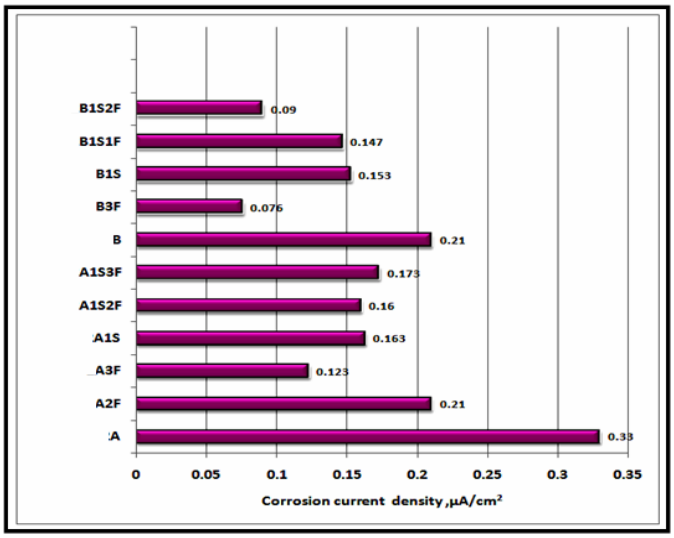

Fig.17: Corrosion current density as determined by using Stern-Geary equation (i_{corr}=B/Rp.A) for bars in tested concretes.

ESTIMATION OF THE OPTIMUM BED THICKNESS OF A FLOW-THROUGH POROUS ELECTRODE (FTPE) WORKING UNDER MASS TRANSFER CONTROL

Qasim J. M. Slaiman*, Sarmad Talib Najim*, Aws Abdulmahdi Sadeq**

*** Collage of Engineering/Chemical Eng. Dep. /Nahrain University**

**** Ministry of Oil/ Iraqi Drilling Company**

ABSTRACT:
In this paper, a theoretical analysis of optimum bed thickness operates under mass transfer control for realizing a high efficiency and reaction conversion of an electrochemical reactor has been made based on flow-through porous electrode (FTPE) configuration. Many models have been used to represent the optimum bed thickness by taking a look into previous works concerned and collecting all related information, data, and models. The parameters that affect the optimum bed thickness have been visualized and reviewed, and almost all of them have been examined by experimental data from different sources and based on the various models. It has been found that the increase in electrolyte flow rate, concentration, limiting current density, and specific surface area reduce the optimum bed thickness, and the increase in electrolyte conductivity, void fraction, and overpotential range increases optimum bed thickness. The most important design parameter that has a great effect on optimum bed thickness is found to be the electrolyte flow rate for any certain operation. It has been concluded that the most appropriate two models to represent the optimum bed thickness of FTPE electrochemical reactor operating under mass transfer control based on the results are those predicted theoretically and stated by Kreysa in (1978) and Doherty et al. in (1996).

الخلاصة:
أجري في هذاالبحث تحليل نظري لاقصى سمك حشوة لمفاعل كهروكيمياوي يعمل تحت ظروف سيطرة انتقال الكتلة لتحقيق نسبة تفاعل و كفاءة عالية قد تمت على مفاعل كهروكيمياوي نوع (FTPE). نماذج عدة قد تم استخدامها لتمثيل سمك الحشوق القصوي من خلال البحث في دراسات سابقة ذات علاقة وجمع المعلومات، البيانات و النماذج. العوامل الموثرة على سمك الحشوة القصوي قد تم تجسيدها وعرضها و قد تم اختبار معظمها باستخدام بيانات عملية من مصادر عدة وتصب في نماذج مختلفة. لقد وجد ان الزيادة في جريان المحلول الالكتروليتي، تركيز المتفاعلات،limiting current density و specific surface area تقلل من سمك الحشوة القصوي، كما وان الزيادة في توصيلية المحلول، المساميه و فرق الجهد الكهربائي يزيد من سمك الحشوه الأفضل. لقد وجد ان المتغير الأكثر اهميه و ذا تأثير كبير على سمك الحشوه الأفضل هو معدل جريان المحلول لأي عمليه معينه .تأثير موقع مدخل المحلول) او موقع مكان القطب (على سمك الحشوه الأفضل تم عرضه و النتائج لم تسجل اي تاثير هام .لقد وجد ان افضل النماذج موائمة (Flow-through) تمثيل سمك الحشوه الأفضل لمفاعل كهروكيمياوي نوع يعمل تحت بتحكم انتقال الكتلة من خلال النتائج كان نموذج Kreysa(1978) و Doherty et al. (1996).

Keywords: Optimum bed thickness; Packed bed; Porous electrode; Flow-through; Mass transfer

1- INTRODUCTION

Packed bed electrodes can be used for electrochemical recovery of heavy metals from a variety of industrial and laboratory model solutions (Bennion and Newman, 1972; Doherty et al., 1996; El-Deab et al., 1999; Gaunand et al., 1977; Lanza and Bertazzoli, 2000; Matloz and Newman, 1986 ;Podlaha and Fenton, 1995; Ponce de León and Pletcher, 1996;Saleh, 2004; Soltan et al., 2003; Trainham and Newman, 1977.The packed bed electrode forms a porous flow-through configuration providing large surface area usually depleting the concentration of metal ions below 0.1 ppm.

Some studies have reported that flow-through configurations suffer from non-uniform potential and current distribution (Bennion and Newman, 1972; Doherty et al., 1996; El-Deab et al., 1999; Gaunand et al., 1977; Matloz and Newman, 1986; Saleh, 2004; Sioda, 1971; Trainham and Newman, 1977). Newman et al. in 1962 demonstrated this problem when Tafel kinetic was coupled with significant solid phase (electrode material) and electrolyte resistivity. In another paper related to the potential and current distribution, Bennion and Newman (1972) used the deposition of copper ions on carbon flakes to study the design principles of flow-through porous electrodes.

The authors concluded that electrolyte flow rate and bed thickness determine the ohmic potential drop within the porous electrode. Another conclusion was that the potential difference between the carbon matrix and the solution at all points within the porous electrode should be sufficient, but not too large to ensure deposition without hydrogen evolution. Sabacky and Evans (1979) used a fluidised copper particles cathode for copper recovery and reported that the efficiency and power consumption depended on copper and acid concentration, particle size, resistivity of the electrolyte and superficial current density. Kreysa in (1978) studied the kinetic behavior of packed and fluidized bed electrodes. A macro-kinetic model of three-dimensional electrodes was established by introducing overpotential distribution within the electrode into the micro-kinetic rate equation. The developed model was used to derive analytical expression from limiting diffusion current for calculating the optimum bed depth for both packed and fluidized bed electrodes in terms of geometric, hydrodynamics, and kinetic parameters. Kreysa and Jüttner in (1993) in a study for flow-by three-dimensional electrode of cylindrical geometry operating under limiting current conditions re-introduced the arrangement of electrodes with respect to the direction of the current flow, electrolyte flow, and electrode position. Comparisons have been made among various types of electrode arrangements. Optimum bed thickness also had been investigated for both cylindrical and rectangular arrangements for various electrolyte conductivities. The model used for calculation was similar to that predicted by Kreysa (1978) with a little difference due to ignoring effects of void fraction.

Doherty et al. in (1996) presented a numerical model of flow-through porous electrodes simulates the distribution of potential and current density within a porous electrode. The model includes consideration of the electron transfer control regime of the electrode reaction, mass transport limitations and the finite conductivity of the electrode material. They re-introduced the expression predicted by Kreysa (1978) for calculation of the optimum bed depth in terms of specific surface area instead of particle size diameter. They concluded that at high electrode conductivities the optimum length is much less sensitive to electrode depth, whereas, at low conductivities the contrary is true. Therefore, greater accuracy is required when designing porous electrodes with very high porosities and, thus, low electrode conductivities, in order to achieve the optimum electrode depth.

Masiley and Pouddubny in (1997) presented mathematical simulation of the FTPE operation on the basis of one dimensional model with uniform conducting matrix and the cathode process involving the main and side reaction. They introduced the optimum bed thickness as a part of its total thickness L proportional to the integral mean value of the ratio of local current of the target reaction to its limiting diffusion value. They also studied the effect of solid and liquid phase conductivity on the effective electrode layer operating under limiting diffusion current. The expression that they obtained in case of solid phase conductivity is much higher than that for electrolyte and was quite similar to that used by Kreysa and Jüttner (1993).

In a more recent paper, Saleh in (2004) re-introduced the concept of effectiveness factor as the ratio between the total obtainable limiting current and the maximum limiting current in absence of ohmic drop. The study was based on the deposition of zinc in alkaline solution where the hydrogen evolution reaction and the deposition of zinc take place at similar potential. Saleh concluded that hydrogen evolution accentuates the ohmic effect. Similarly, Like and Langer in

(1991) discussed the internal ohmic limits in a flow-through porous electrode using Tafel kinetics. They showed that during the electrolysis, thinner electrodes help to maximize the current density.

Nava et al. in (2008) discussed the use of potential distribution analysis during the deposition of metal ions, at limiting current conditions and determine the optimum electrode thickness at which no hydrogen evolution occurs. The potential distribution studies were carried out on stainless-steel fibres of three different surface areas. The fibres were used as cathodic porous electrodes during the deposition of Ag(I) ions contained in 0.1 mol dm^{-3} KNO_3 and 0.6 mol dm^{-3} NH_4OH electrolyte. The comparison of both, experimental and theoretical potential distributions showed that flow rate and specific surface area of the electrode determine the potential drop within the packed bed cathode and therefore the effective thickness of the porous bed electrode at which hydrogen evolution can be avoided.

The aim of this study based on theoretical analysis to find out the optimum bed thickness (OBT) of flow-through porous electrode (FTPE) of an electrochemical reactor works under mass transfer regime and for porous bed conductivity higher than electrolyte ($k_m \gg k_s$) as shown in fig.1.

That is going through reviewing and examining several models accomplished by many authors via experimental data in order to ensure the maximum accuracy and objectivity for such theoretical study.

2- MODELS

2.1. Kreysa [15] in 1978 gave expression for optimum bed depth of packed bed electrode derived from diffusion limiting current density as follows:

$$i_L(x) = aK_m zF \int_x^{L_{op}} [C(x)]dx \tag{1}$$

$$i_L(x) = aK_m zFC(L_{op} - x) \tag{2}$$

For the electrolyte potential ϕ_s, one obtains the expression

$$\phi_s(x) = \int_0^x \frac{i_L(x)}{k_s \varepsilon} dx \tag{3}$$

Substitute eq. 2 into eq. 3 and integrate with boundary condition $\phi_s(0) = 0$ one obtains

$$\phi_s(x) = \frac{aK_m zFC}{k_s \varepsilon}(L_{op}x - \frac{x^2}{2}) \tag{4}$$

An electrode should be considered as an optimum in the sense explained above if at each point of it ≥ 99% of limiting current density are realized. Then for packed bed electrode the condition

$$\phi_s(L_{op}) = \eta_{B-F} - \eta_{0.99} \tag{5}$$

Substitute for spherical particles $a = \frac{6(1-\varepsilon)}{d_p}$ into eq.4 and rearranging to L_{op} gives the expression:

$$L_{op} = \left[\frac{\varepsilon k_s d_p (\eta_{B-F} - \eta_{0.99})}{3(1-\varepsilon)K_m zFC} \right]^{0.5} \tag{6}$$

Where L_{op}: the optimum bed depth for which limiting current conditions prevail.

$\eta_{0.99}$: the overvoltage holding the condition when $i(\eta_{0.99})=0.99i_L$

η_{B-F}: potential difference between solution potential at the electrode boundary plane nearest the counter electrode and feeder metal potential relative to the equilibrium potential of the electrode reaction.

2.2 Doherty et al. [2] showed similar expression as above (eq. 3.39) for penetration depth, p of the limiting current density for metal deposition (assuming that the electrode is fully conducting) is given by:

$$p = \sqrt{\frac{2\varepsilon k_s \Delta\eta}{aK_m zFC_o}} \tag{7}$$

Where $\Delta\eta$ is the range of overpotential where the metal deposition proceeds under limiting current conditions.

2.3 Kreysa et al. (1993) in more recent study than (1978) showed the optimum bed depth, L_{op} is given by the following expression:

$$L_{op} = \left(\frac{2k_s \Delta\eta}{a.i_L} \right)^{0.5} \tag{8}$$

2.4 Masliy and Poddubny (1997) presented the optimum bed thickness in studied the effect of solid and liquid phase conductivity on the effective electrode layer operating under limiting diffusion current.

$$L_d = \sqrt{\frac{2k_s \Delta\eta}{azFK_m C_\circ}} \tag{9}$$

The four models given above are all the same if some rearrangements are made, except a little difference in eq. 8 where the void fraction is not taken into account. Furthermore, these models based on electrode conductivity much higher than electrolyte ($k_m >> k_s$).

2.5 Newman et al. (1975, 1984 and 1986) introduced the penetration depth, p as a function of velocity, specific area, and mass transfer coefficient;

$$p = \frac{u}{aK_m} \tag{10}$$

2.6 Masliy et al. (1997 & 2007) understood the effectively operating thickness L_{eff} of porous electrode as a part of its total thickness, L proportional to the integral mean value of the ratio of local current of the target reaction $i(x)$, to its limiting diffusion value $i_L(x)$.

$$L_{eff} = \int_0^L \frac{i(x)}{i_L(x)} dx \tag{11}$$

2.7 Nava et al. (2008) in a more recent study concerned about determination of the effective thickness of porous electrode in a flow-through porous electrode shows the usefulness type of analysis to estimate the optimum bed thickness from potential distribution which allows efficient recovery of metals by avoiding hydrogen evolution.

$$\phi_s(x) - \phi_s(x=0) = -\frac{zFuC(x=0)}{\upsilon k_s}\left[\upsilon x + \exp^{-\upsilon x} - 1\right] \tag{12}$$

Where

$$\upsilon = \frac{K_m a(1-\varepsilon)}{u} \tag{13}$$

The effective bed thickness obtained can be achieved by plotting the potential distribution (eq. 12) vs. electrode thickness L before hydrogen evolution starts.

Since the main goal of this study is to find out a mathematical model to represent more suitably the optimum bed thickness for a FTPE, there are several parameters affecting the optimum bed thickness can be observed from above models. These parameters are 1) electrolyte flow rate; 2) mass transfer coefficient or limiting current density; 3) electrolyte concentration; 4) electrolyte conductivity (and electrode in case ($k_s = k_m$)); 5) specific surface area or particle size diameter; 6) electrode void fraction; 7) temperature; and 8) overpotential.

3- RESULTS AND DISCUSSION

All the results in this paper represented by several figures have been made as a result of calculations are carried out with aid of experimental data available in order to achieve reasonable and accurate results as possible to examine the models. More information and calculation procedure can be found in Sadeq et al (2009). The discussion takes two prospective sides. The first one discusses the effect of each parameter on the OBT and the second one discusses the efficiency of each model.

3.1 The effect of parameters on the OBT

3.1.1 Electrolyte Flow Rate & Mass Transfer Coefficient

Electrolyte flow rate shows a significant effect on the optimum bed thickness through the considered models and results. In spite of the fact that this parameter is not included in some models (1 – 4; i.e. 2.1 – 2.4 and so on), but its presence strongly affects the results represented by mass transfer coefficient. In addition to the importance of flow rate for such study on optimum bed thickness; many studies take it into account as a main parameter in the analysis which enhances its importance. Figs. (2 and 3) represent the effect of this parameter for many different studies [Bennion & Newman; 1972, Doherty et al.; 1996, El-Deab et al.; 1999, Gaunand et al.; 1977, Lanza & Bertazzoli; 2000] with large range of velocities (0.01 – 7.3 cm/s) based on models (2.1, 2.2, and 2.7). These figs. show that as the flow rate of electrolyte increases the optimum bed thickness decreases. This is evident by the fact that the mass transfer coefficient is greatly affected by flow rate.

Actually, not only the electrolyte flow rate has an effect on the mass transfer coefficient. The mass transfer coefficient is affected by many factors rather than flow rate like diffusivity, temperature, and physical properties of electrolyte,

and that is supported by Wilson and Geankoplis (1966) expressions. Since each reference considered here has its own specific operating conditions, temperature, and the same physical properties, the flow rate of electrolyte shows up as the dominant among these factors.

Also, at low flow rates (u 1.0 cm.s^{-1}), a new emergence of controlling factor appears, which facilitates the penetration of the process (or maximize the optimum bed thickness) into the porous electrode. This factor is most likely to be the abrupt decrease in the electroactive component concentration over the electrode depth as shown in figs. 3and 4, and the corresponding increase in the polarizability of the electrode as concluded by Masliy & Poddubny (1997).

Figs. 2 and 3 show in general that increasing flow rate reduces optimum bed thickness, but it is also emphasizing in some way that every single case could be a special one for mass transfer prediction. This can be seen from the style of each curve in the figures of each reference and explains why that is different. The benefits of such study are beyond the scope of broad range of data to make it possible to examine, analyze and study the phenomenon of these factors and parameters.

Briefly, according to models (1 – 4) as the electrolyte flow rates increase the mass transfer coefficient and increase in the limiting current density and consequently decrease the optimum bed thickness. While model 5 by Newman et al. (1975, 1984 and 1986) indicates the opposite to the previous four models, which will be discussed in another section of this paper.

3.1.2 Electrolyte Concentration (Reactant)

The effect of concentration on optimum bed thickness can be seen by fig. 4 at various temperatures. The figure shows how the optimum bed thickness decreases as the electrolyte concentration increases at certain temperature and flow rate. This is also true for other temperatures, but further increase in temperature in fig.4 refers to its effect on optimum bed thickness, not on concentration. Najim's et al. (2006); shows that the temperature has no effect on the concentration, but it affects the physical properties of any solution as well as the electrolyte conductivity in this case.

As shown in fig. 4, the concentration has an observed effect on optimum bed thickness. This effect is calculated from the increasing in limiting current plateau as electrolyte concentration increases. This is shown by the following equation:

$$i_L = zFK_mC_o \qquad (14)$$

The increase in limiting current is due to increase in concentration leads to the observed decrease in optimum bed thickness, Doherty et al (1996).

3.1.3 Electrolyte Conductivity & Temperature

Fig. 5 shows the effect of electrolyte conductivity on optimum bed thickness based on Kreysa and Jüttner's data and model. While fig. 6 shows the effect of electrolyte conductivity on optimum bed thickness at various temperatures and concentrations based on Najim's et al (2006) data and Kreysa's (1978) model. These figures show the increase of the optimum bed thickness with increases in electrolyte conductivity. It is also clear that there are some factors which have an effect on the electrolyte conductivity. The figures show that increasing in concentration and temperature leads to increase in the solution conductivity. The reason is beyond the optimum bed thickness as increasing in electrolyte conductivity come from the fact that increasing in electrolyte conductivity means decreasing in electrolyte resistivity, which leads to a decrease in ohmic potential drop in solution, and that decrease leads to increases in electrode polarization which positively is reflected on optimum bed thickness.

It is important to say here that temperature has a considerable effect on electrolyte conductivity which is greater than that of concentration. These effects are shown in figs. 5 and 6. The increase in temperature has been by one magnitude if the concentration doubled, while it is twice if the temperature has increased to 30% of its initial value, this behavior is due to the increase of the solubility of the ions in the electrolyte and its kinetic energy when increasing the temperature. However, all these results are directed up to the evidence that increasing in electrolyte conductivity leads to increasing in optimum bed thickness, and this is also true for temperature which enhances the situation of models (1 – 4).

3.1.4 Specific surface Area & Void fraction

Fig. 7 shows the effect of the specific surface area on the optimum bed thickness. The data used in this plotting based on Nava's data and model. The results show that the increase in specific surface area of the porous electrode leads to decreases in the optimum bed thickness according to Nava's

results and model which are considered as a support for what is concluded by models (1 – 4). A little increase in the optimum bed thickness at the right side end of fig. 7 for a = 193 cm^{-1} have been seen. This has happened because of the increasing in void fraction (see the referred reference) which will be seen in fig. 7.This is also true at various flow rates, where fig. 7 shows the effect of specific surface area at more than one condition.

The reason behind that decrease in optimum bed thickness with increases in specific surface area belongs to the fact that porous electrode provides a large space (interfacial area) for the electrochemical reaction, and that enables to take a small volume. Therefore, any additional increase in this part leads to decrease in the optimum bed thickness. This also have been proved by several studies; where, for, e.g., Coeuret et al. (1976 & 1977) found out that the increase in size of particle (for the packing of spherical particles) leads to increase in bed effectiveness which consequently means decrease in the interfacial area.

Since the new types of packing (i.e. RVC, fiber, etc.) make possible to control simultaneously void fraction and specific surface area. Fig. 8 shows how the optimum bed thickness can be strongly affected at certain conditions if the electrode void fraction is made to change. This figure shows the increase in bed void fraction leads to increase in optimum bed thickness according to [2 and 15].

3.1.5 Overpotential Difference

The effect of overpotential on optimum bed thickness has been represented in models (1 to 4). Fig. 9 shows polarization curve for a simple electrochemical reaction displaying region where electrode reaction proceeds under mass transport control. Fig. 9 emphasizes that the effect of the overvoltage determined by the width of the limiting current plateau, or in other word, as the overpotential range increases the effect on optimum bed thickness takes a big effect. This effect is indicated regarding models which refer to the increase in overpotential range leads to increases in optimum bed thickness.From practical point of view, that's true since the increase in voltages which represent the driving force for any electrochemical reaction leads to increase in reaction areas and consequently reflects on the penetration depth of the reaction inside pores or which here called optimum bed thickness.

3.2 Models Results

3.2.1 Kreysa's (1978) and Doherty's et al. (1996), models (1 & 2).

Kreysa's and Doherty's models can be considered as the most appropriate candidates to represent the optimum bed thickness of a FTPE electrochemical reactor operates under mass transfer control. That's because the most effective parameters are represented in these two models and also the results show the most acceptable and reasonable results than others. In addition, models 1& 2 show a flexibility to interact with different packing type.

It is also important to mention the disadvantages in these two models and the most important one that is related to the overpotential difference (range) $\Delta\eta$. The way that has been suggested to represent this parameter by several studies based on the polarization curve when reaction proceeds under mass transfer region. This method could be associated with some mistakes and most likely with such theoretical study. These mistakes usually occur when it has to select a start and end point of the mass transfer region. It has been found that the average approximate error might occur for this case between $\mp$ (50 – 100) mV in a worst probability based upon experience, but this range of error can cause a noticeable change in optimum bed thickness appreciable to 6 – 13 % for $\Delta\eta$ equal to 400 mV and that percent is a candidate to increase as the overpotential range decreases (Sadeq et al. 2009).

The results of these two models (i.e., 1 & 2) are completely matched because they are already matched as mentioned before. The results of these models over the considered experimental data that have been used in the study show a good agreement for all data at high flow rates, while for low flow rates, the results are overestimate for Kreysa (1978) and short bed length (2 cm) for Najim et al (2006). That's probably because the limiting current plateau is so low due to the very low reactant concentration in Kreysa's data which makes the optimum bed thickness represented in these models high even up to or over its actual length. This especially occurs at low flow rates; while the results in short bed length (2 cm) of Najim et al. which overestimating the optimum bed thickness and also the actual bed length probably because of the low specific surface area and flow rates, but even that, the optimum bed thickness

has been found experimentally by Najim et al. between 2 and 3 cm, which are shown up in Sadeq et al. (2009).

The most unfavorable situation occurs for the profile $\eta(x)$ and $C(x)$ with the opposite character of behavior, that is, the minimum solution concentration corresponds to the most loaded point of the porous electrode and vice versa (Masliy et al 2007). This makes the attainment of the limiting diffusion current over the entire porous electrode surface difficult, but in this case the reason is the depletion of the solution in the depth of the porous electrode also causes an increase in the polarization resistance at these points and current redistribution towards the less loaded layers. Eventually, this leads to the efficient function of the entire porous electrode (maximum optimum bed achieved) and that which appears in [Newman and Matloz (1986), Kreysa (1978), and Najim et al. (2006)] at so low flow rates, but it is more costly because of the lower flow rate, high current overload and decrease in the current efficiency (Masliy et al. 2007). However, the average optimum bed thickness over the total results at six different flow rates of Kreysa (1978) about 2.37 cm, which is approximately the actual bed length (2.3 cm) for that case. In addition, a comparison of specific surface area a = 5.66 cm^{-1} of Najim et al. (2006) within that used for example by Kreysa (1978) a = 36 cm^{-1} or Newman (1986) a = 66 cm^{-1}, shows how it is small for such application to be justified by high interfacial area. From practical point of view and according to reasons mentioned above, it can be concluded that results reflect the whole bed are considered as an optimum more than its value.

2-Kreysa and Jüttner's (1993) & Masliy and Poddubny's (1997), Models (3 &4)

These two models are so close to that predicted by Kreysa (1978) and Doherty et al. (1996), the differences only by ignoring the void fraction ε as mentioned before. But this neglected parameter causes a dramatic change in the results compared with the previous models (1 & 2). These changes or effects of this parameter can be seen through figs. (10 – 13). Figs. (10 – 13) show the variation or difference between models 1 and 2, and models 3 and 4 are proportional to or justified by $(1 - \varepsilon)^{0.5}$. As the void fraction decreases the differences between the models curves increase and that would vindicate the variation of the shifting ratio among the referred figures.

Furthermore, these figs. emphasize the importance of that parameter and its effect on the optimum bed thickness. Fig. 13 shows how much close could be between models 1 and 2, and 3 and 4 if the void fraction is high, which reflects perhaps the reason beyond the neglecting of this parameter especially before the most recent studies concentrated to use new types of packing that provides simultaneously high specific surface area and void fraction.

One more thing, in spite of these two models sometimes overestimate the optimum bed thickness when the void fraction is small and even overestimate the actual bed length.

The surprising thing about these models is even that overestimating results, but it never overtakes the rules of model 7 (i.e. exceeding the side reaction value or hydrogen evolution start) that predicted by Nava et al. (2008), as shown in figs. 15 and 16. Everything else mentioned about these models is all that is mentioned in discussion about models 1 and 2.

3.2.3 Newman's et al. (1975, 1984 and 1986), Model 5.

The behavior of this model shows variant behavior compared to other models that have been accomplished by [Doherty et al. 1996, Kreysa 1978, Masliy et al. 1997 and Nava et al. 2008] rather than un-reasonable results in many parts. Even that, this variant does not represent the evident scientific mechanisms. But from another point of view, one can notice that the results obtained from the same data source of (Newman and Matloz 1986) or from data have the same conditions is quite reasonable values and that obviously seen in fig. 14 and that's most likely for low velocities and high specific surface area. However, fig. 14 also shows variant behavior in model 5 to that shown in model 7 and the other four models (i.e. the optimum bed thickness increases as the velocity). That could happen at typical conditions of so low flow rates. The poor representation of the parameters and the variant behavior does not give the possibility for considering this model to express the optimum bed thickness of a FTPE under wide range of conditions. However, from other point of view, the reason which makes **Newman [6, 19, and 20]** to consider that represent the penetration depth at first, perhaps because it is a simple model that might give a quick estimation with percent of error for a certain situation, and that's most likely with high specific surface areas

and low flow velocities [6, 20] as mentioned before.

3.2.4 Masliy's et al. (1997, 2007), Model 6

Unfortunately, there are no experimental data to meet this theoretical model which requires to be executed as a fair action in the present study, in order to make sure to show the method of solution and to cover all the models. A test of this model has been made from a theoretical data based on a simulation study in Sadeq et al. (2009).

5.2.5 Nava's et al. [26], Model 7

The result of this model which is completely graphical shows a good way to estimate the optimum bed thickness through the entire results. The behavior indicated in this model agreed with that of models 1–4 which are supported by figs. 4.5 and 4.9. The major idea of this model based on Coulombic efficiency calculations. As the Coulombic efficiency of the reaction is 100%, the bed is considered optimum at that efficiency. The Coulombic efficiency ψ can be defined as the percentage of the measured current supported by the main deposition reaction [17], i.e.

$$\psi = \frac{i_{main}}{i_{main} + i_{side}} \times 100\% \qquad (15)$$

Since model 7 is already adopted, then all the optimum bed thickness obtained from this model operates with 100% Coulombic efficiency according to eq. 15. One more thing, the results of optimum bed thickness obtained from model 7 is always greater than that for models 1– 4, that are evident between figs. 15 and 16. This reflects two facts, the first is that model 7 represents a range wider than mass transfer region, and the second is the validity of models 1 – 4 to represent the optimum bed thickness in the mass transfer region (especially model 1 and 2), and avoiding the side reaction.

4- CONCLUSIONS

The increase in electrolyte flow rate, mass transfer coefficient, concentration, limiting current density, and specific surface area reduces the optimum bed thickness. The increase in electrolyte conductivity, porosity, and overpotential range increases optimum bed thickness. The first four models (1 – 4) can be used with relatively high flow rates and specific surface area ($u \geq 0.1$ cm/s, $a \geq 12$ cm^{-1}). The best models among the first four that have been tested are models 1 and 2 predicted by Kreysa (1978) and Doherty et al. (1996) to represent the optimum bed thickness for reactor operating under mass transfer control. Models 3 and 4 predicted by Kreysa and Jüttner (1993) and Masliy and Poddubny (1997) are used to estimate the optimum bed thickness when bed porosity is high ($\varepsilon \geq 0.9$).Model 5 predicted by Newman et al. (1975, 1984 and 1986), can be used for low flow rates and high specific surface area (u< 0.09 cm/s, $a \geq 25$ cm^{-1}).The graphical model presented by Nava et al. (2008)can be a useful way to use in processes when high degrees of conversion are required per pass. The exact value of the optimum bed thickness cannot be deduced analytically, but model 1 gives a first approximation value which can be useful for a rough engineering design. The bed of a FTPE can be whatever size in diameter, but the thickness of the reactor is very important to take into account for this configuration.

NOMECULATURE

a	Specific surface area of electrode; (cm^{-1})
C	Electrolyte concentration; (mol/cm^3)
C_o	Inlet electrolyte concentration; (mol/cm^3)
d_p	Size diameter of spherical particle; (cm)
F	Faraday's constant (96,487); (C/g.equ.)
i_o	Exchange current density; (A/cm^2)
i	Current density; (A/cm^2)
i_L	Limiting current density; (A/cm^2)
K_m	Mass transfer coefficient; (cm/s).
k_m	Solid phase conductivity; (Ω cm)$^{-1}$
k_s	Effective electrolyte conductivity; (Ω. cm)$^{-1}$
L	Electrode length; (cm)
L_d	Thickness of porous electrode layer operating at the limiting diffusion current as in eq. 9; (cm).
L_{eff}	Effective operating thickness as in eq. 11; (cm).
L_{op}	Optimum bed length (cm).
P	Penetration depth as in eq. 10; (cm)
p	Penetration depth as in eq. 7; (cm)
R	Gas constant = 8.314 (J/mol. K)
T	Temperature (K)
u	Electrolyte flow rate (cm/s)
V_c	Applied potential at the cathode current feeder (*or* collector); (Volt)
z	Number of electrons involved in reaction

GREEK LETTERS

ε	Void fraction
η	Overpotential
υ	Group parameter defined in eq. 3.19
ϕ_m	Electrode potential
ϕ_s	Electrolyte potential
ψ	Coulombic efficiency defined in eq. 15

REFERENCES

Bennion, D. N., Newman, J., "Electrochemical removal of copper ions from very dilute solutions" *J. Appl. Electrochem.* **2**, 133, (1972).

Coeuret, F., Hutin, D., Gaunand, A., "Study of the effectiveness of fixed flow-through electrodes" *J. Appl. Electrochem*. **6**, 417 (1976).

Doherty, T., Sunderland, J.G., Roberts, E.P.L., Pickett, D.J., "An improved model of potential and current distribution within a flow-through porous electrode" *Electrochim. Acta.* **41** (4), 519 (1996).

El-Deab, M. S., Saleh, M. M., El-Anadouli, B., E., Ateya, B. G., "Electrochemical removal of lead ions from flowing electrolytes using packed bed electrodes" *J. Electrochem. Soc.* **146** (1), 208 (1999).

Gaunand, A Hutin, D. and Coeuret, F., "Potential distribution in flow-through porous electrodes under limiting current" *Electrochim. Acta.* **22,** 93 (1977).

Kreysa, G., "Kinetic behavior of packed bed and fluidized bed electrodes" *Electrochim. Acta.* **23**, 1351 (1978).

Kreysa, G., Reynvaan, C., "Optimal design of packed bed cells for high conversion" *J. Appl. Electrochem*. **12**, 241 (1982).

Kreysa. G., Jüttner, K., "Cylindrical three-dimensional electrodes under limiting current conditions" *J. Appl. Electrochem*. **23**, 707 (1993).

Lanza, M.R.V., Bertazzoli, R., "Removal of Zn(II) from chloride medium using a porous electrode: current penetration within the cathode" *J. Appl. Electrochem.* **30**, 61 (2000).

Masliy, A.I., Poddubny, N.P., "influence of solid phase conductivity on spatial localization of electrochemical processes in flow-through porous electrodes" *J. Appl. Electrochem*. **27** (9) 1036 (1997).

Masliy, A. I., Poddubny, N. P., Medvedev, A. Zh., Zherebilov, A. F., "Modeling of the dynamics of metal deposition inside a flow-through porous electrode with low initial conductivity" *J. Electroanalytical Chemistry.*

Matloz, M.J., Newman, J., "Experimental investigation of a porous carbon electrode for the removal of mercury from contaminated brine" *J .Electrochem. Soc*. **133** (9), 1850 (1986).

Najim, S. T., Kashmoula, T. B., Slaiman, Q. J. "Laboratory scale production of *p*-aminophenol using electrochemical reactor" Ph.D. thesis, *Nahrain University* (2006).

Nava, J.L., Oropeza, M.T., Ponce de León, C., González-García, J., Frías-Ferrer, A. J., "Determination of the effective thickness of a porous electrode in a flow-through reactor; effect of the specific surface area of stainless steel fibres, used as a porous cathode, during the deposition of Ag(I) ions" *Hydrometallurgy*. **91**, 98 (2008).

Newman, J., Tiedemann, W., "Porous-electrode theory with battery applications" *AICHE Journal*. **21** (1), 25 (1975).

Newman, J., Risch, T., "A theoretical comparison of flow-through and flow-by porous electrode at the limiting current" *J. Electrochem. Soc*. **131** (11), 2551 (1984).

Paulin, M., Hutin, D., Coeuret, F., "Theoretical and experimental study of flow-through porous elecrtrodes" *J. Electrochem. Soc*. **124** (2), 180 (1977).

Podlaha, E.J., Fenton, J.M., "Characterization of a flow-by RVC electrode reactor for the removal of heavy metals from dilute solutions". *J. Appl. Electrochem.* **25**, 299 (1995).

Ponce de León, C., Pletcher, D., "The removal of Pb(II) from aqueous solutions using a reticulated vitreous carbon cathode cell—the influence of the electrolyte medium". *Electrochim. Acta* **41** (4), 533 (1996).

Sabacky, B.J., Evans, J.W., "Eectrodeposition of metals in fluidized bed electrodes Part I. Mathematical model". J. *Electrochem. Soc.* **126**, 1176 (1979).

Sadeq A. A., Najim, S. T., Slaiman, Q. J. "Theoretical analysis of the optimum bed thickness of an electrochemical reactor" M.Sc. thesis, *Nahrain University* (2009).

Saleh, M.M., "On the effectiveness factor of flow-through porous electrodes" *J. Phys. Chem.*, **B 108**, 13419 (2004).

Soltan, E.A., Nosier, S.A., Salem, A.Y., Mansour, I.A.S., Sedahmed, G.H., "Mass transfer behaviour of a flow-by fixed bed electrochemical reactor under different hydrodynamic conditions". *Chem. Eng. J.* **91**, 33 (2003).

Sioda R. E., "Distribution of potential in a pore electrode under conditions of flow electrolysis" *Electrochim. Acta.* **16**, 1569 (1971).

Trainham, J. A. and Newman, J., "A flow-through porous electrode model: Application to metal-ion removal from dilute streams" *J. Electrochem. Soc.* **124** (10), 1528 (1977).

Wilson, E. J., Geankoplis, C. J., *Ind. Eng. Chem. Fund.* **5**, (1966).

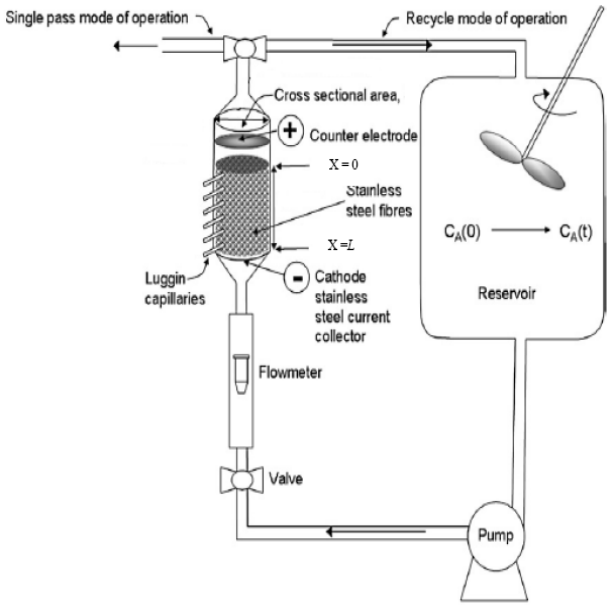

Fig. 1 Experimental flow circuit and flow-through packed bed electrochemical reactor; Nava (2008).

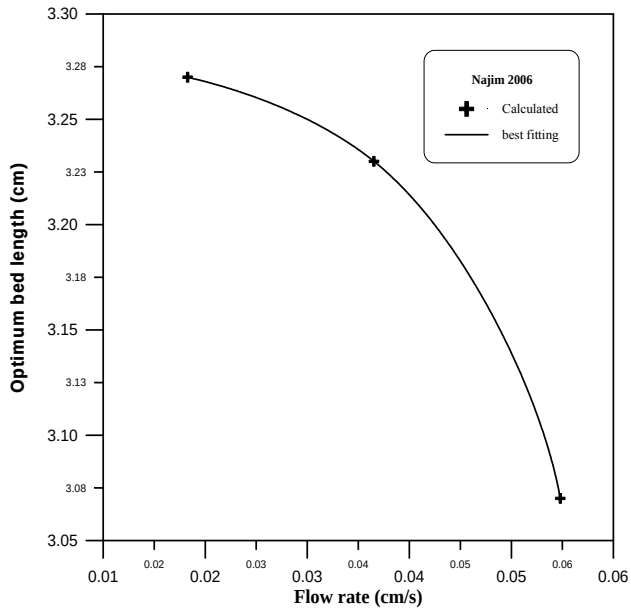

Fig. 2 Effect of flow rate on OBT, Najim et al. (2006) data based on models (1&2).

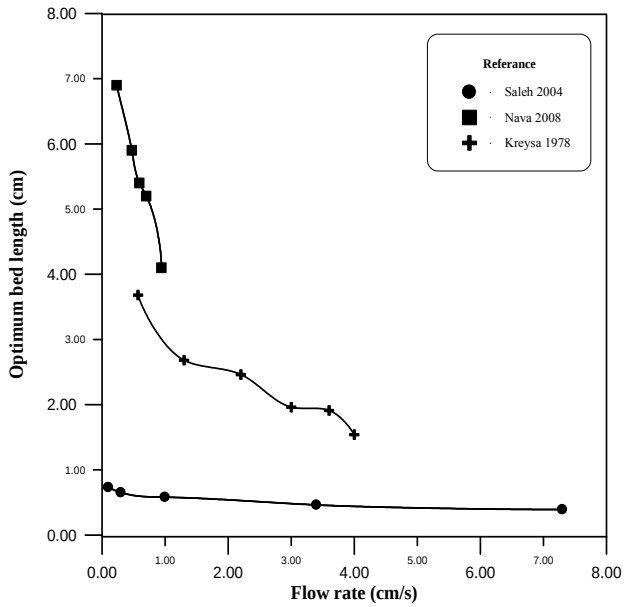

Fig. 3 Effect of flow rate on OBT based on models (1, 2, and 7).

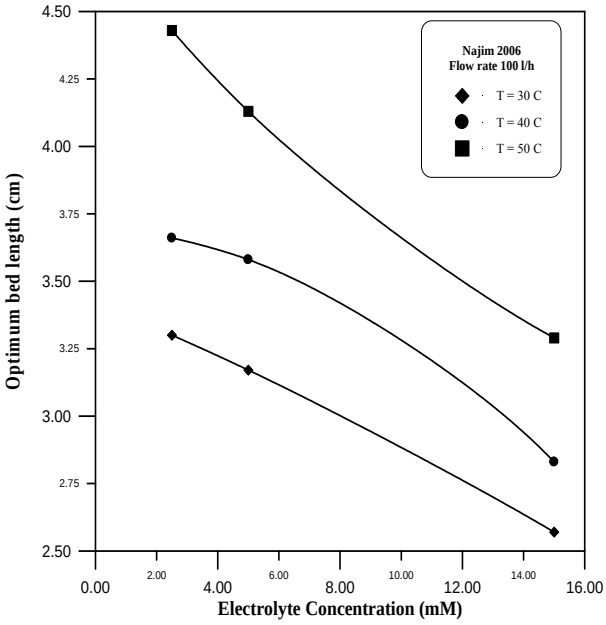

Fig. 4 Effect of electrolyte concentration on OBT at various temperatures [Najim et al. (2006) data].

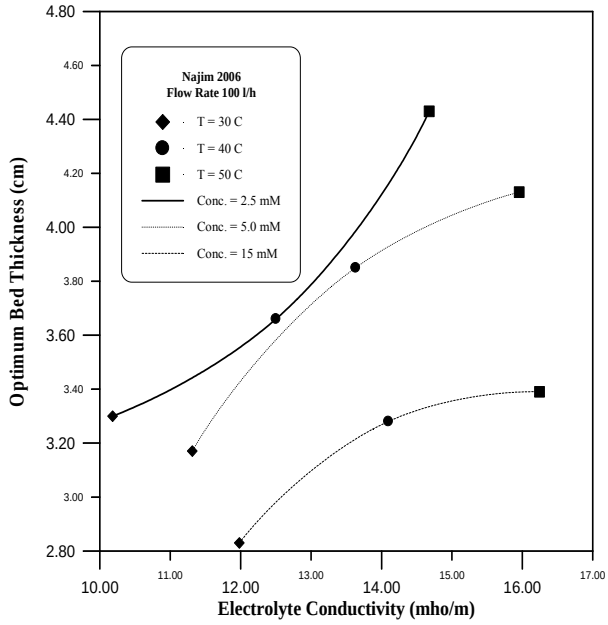

Fig. 6 Effect of electrolyte conductivity on OBT from Najim (2006) data.

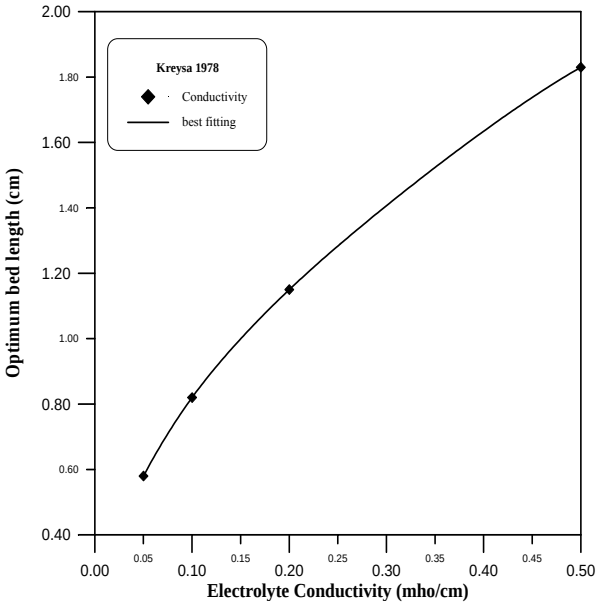

Fig. 5 Effect of electrolyte conductivity on OBT [Kreysa and Jüttner].

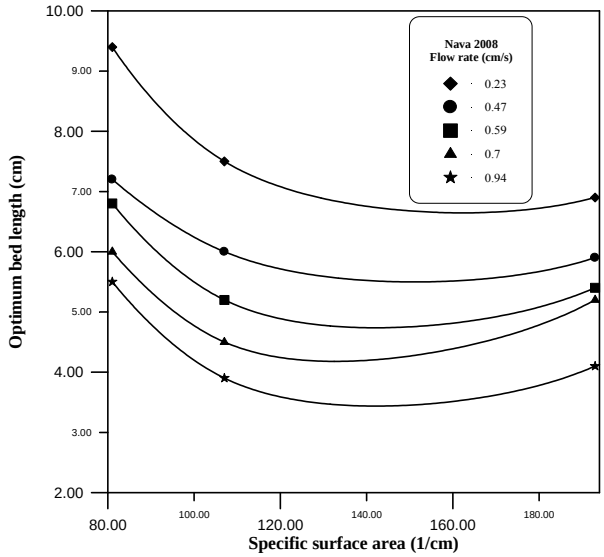

Fig. 7 Effect of specific surface area on OBT at various flow rates from Nava's (2008) data.

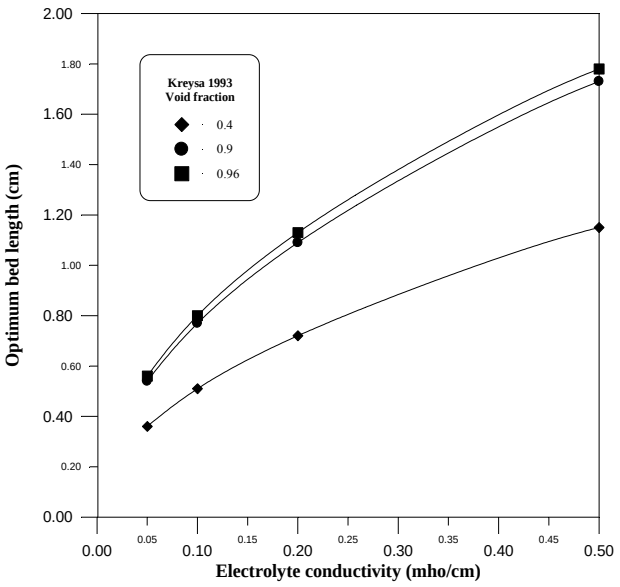

Fig. 8 Effect of void fraction on OBT at various conductivities from Najim's (2006) data.

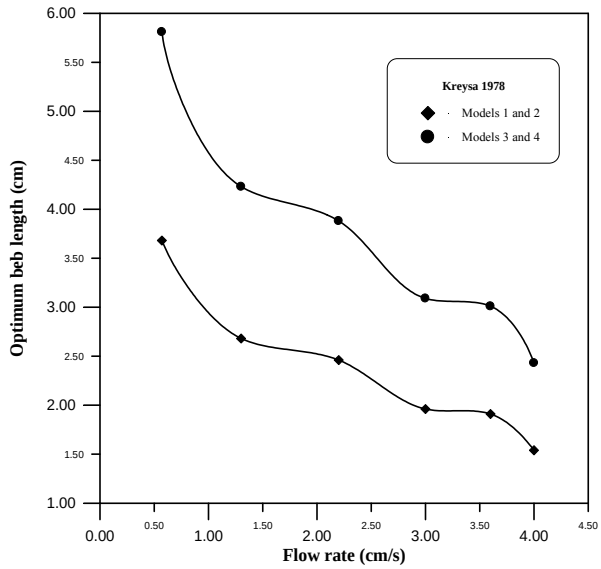

Fig. 10 Models comparison based on Kreysa's (1978) data.

a)

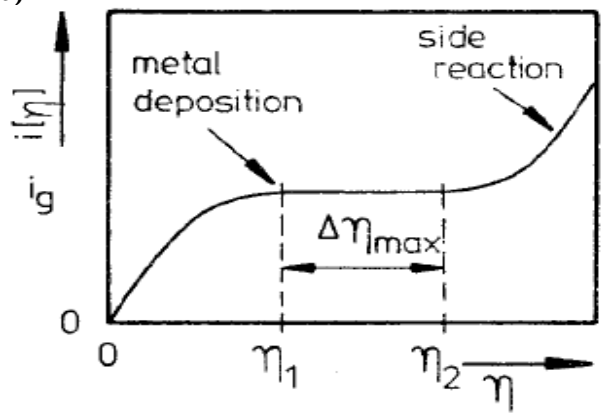

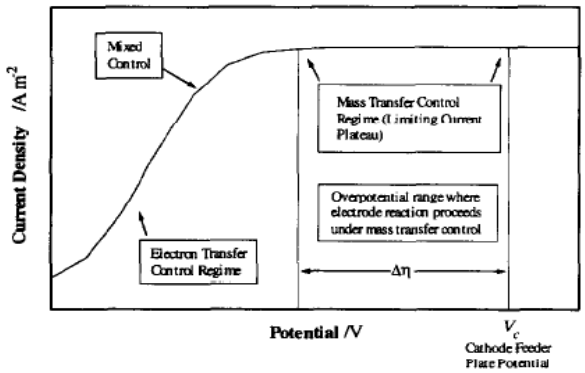

b)

Fig. 9 Polarization curve for a simple electrochemical reaction **a)** Kreysa and Reynvaan (1982), **b)** Doherty et al. (1996).

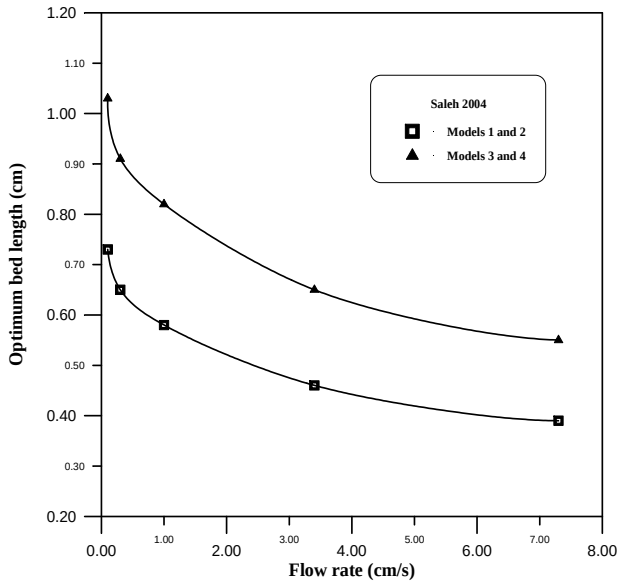

Fig. 11 Models comparison based on Saleh's (2004) data.

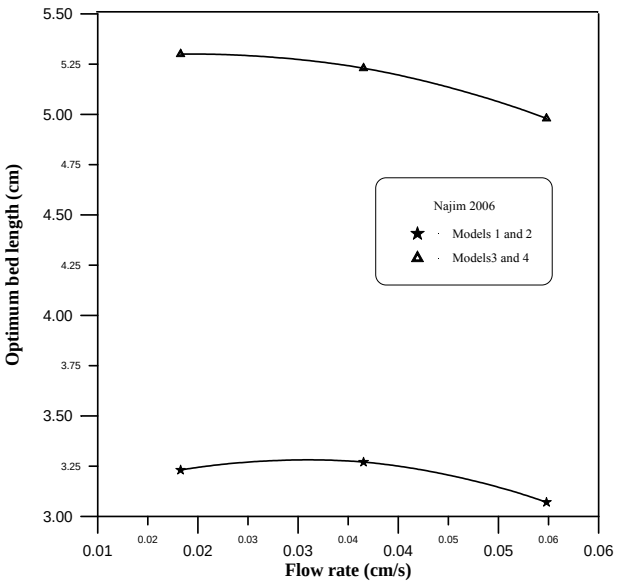

Fig. 12 Models comparison based on Najim's et al. (2006) data.

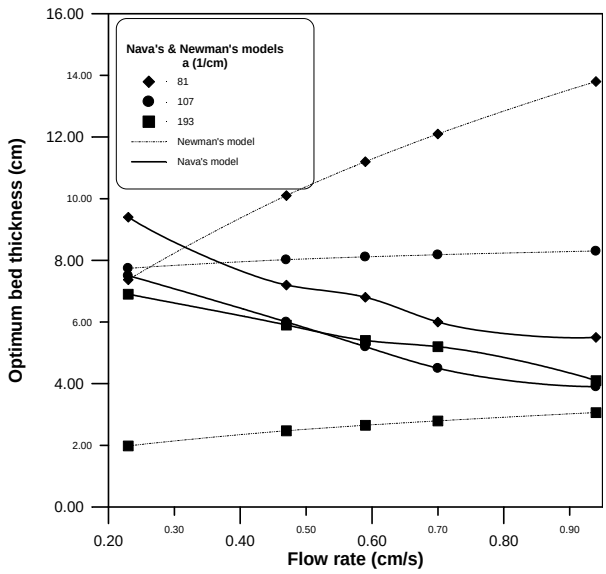

Fig. 14 Comparison between Newman's (1986) and Nava's (2008) models

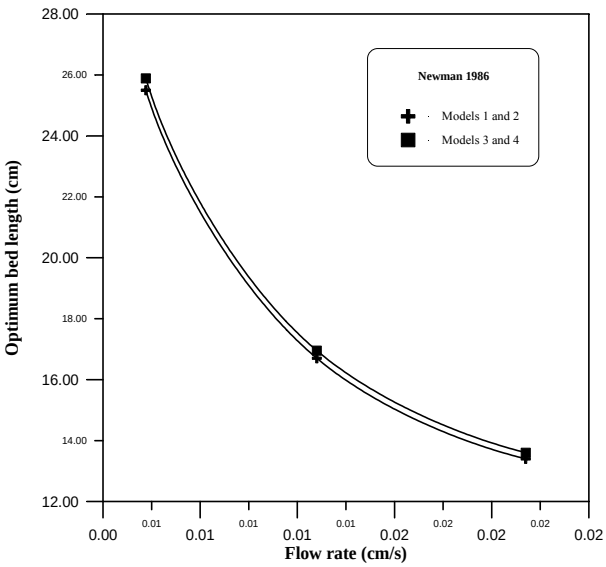

Fig. 13 Models comparison based on Newman's (1986) data.

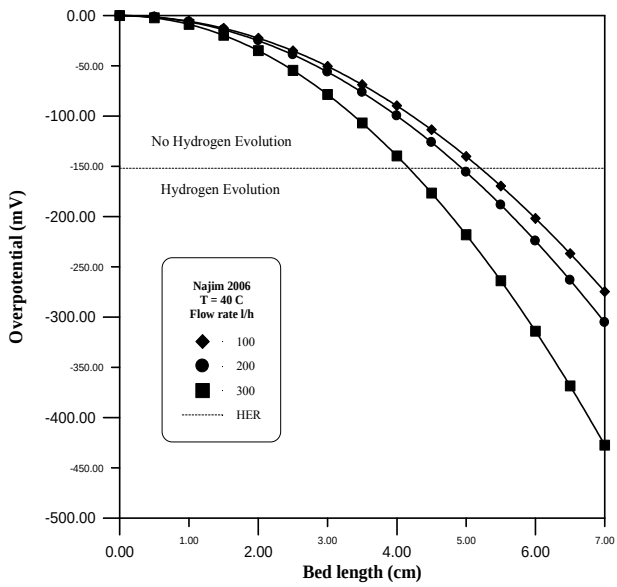

Fig. 15 Potential distribution for bed length L = 7 cm, $[Fe^{3+}]$ =15mM based on model 7; eq. 12.

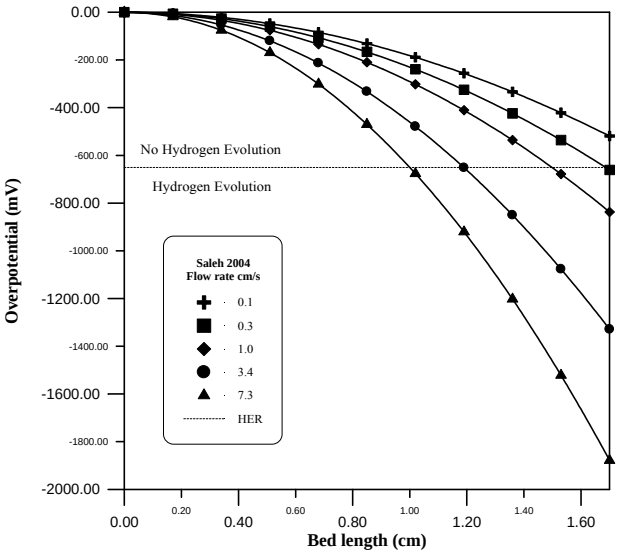

Fig. 16 Potential distribution for bed length L=1.7cm based on model (7) eq. 12.

Laminar Natural Convection in nonrectangular Enclosure with and without Fins

Miss.Sajida Lafta Ghashim Jassim
Department of Mechanical Engineering
College of Engineering
University of Baghdad

Abstract:

In the present work, steady, laminar natural convection in nonrectangular enclosures is analyzed numerically with and without fin. Vertical walls insulated while horizontal walls maintained isothermal at different temperature and the fin was placed on horizontal surface. The length of fin was equal (B/L=0.22, 0.44 and 0.66) and thickness of fin was constant. Various parameters are studied: Rayleigh number (from 10^4 to 10^7), Prandtl number (0.7), number of fin change from (1-3) and aspect ratio (H/L= 0.15 to 0.5). The problem is formulated in terms of the vorticity-stream function procedure. A numerical solution based on program in Fortran 90 with Tec plot program. The finite difference method is used. Streamlines and isotherms are presented for different values of parameters studied. A Nusselt number correlation is derived by using program (DGA v1.00) and mean Nusselt numbers on hot walls are also calculated at different cases. The results show the mean Nusselt numbers decreases with increasing aspect ratio (H/L).Also, predictions reveal a decrease in heat transfer in the presence of fins. The results of the calculations are compared with the previous works and it showed a good agreement.

Key words: Natural convection, fin, square enclosure, partitioned enclosure.

الخلاصة:

يتضمن البحث الحالي دراسة نظرية عددية لانتقال الحرارة بالحمل الحرللجريان المستقر داخل حيز مربع بوجود او عدم وجود الزعانف. الجدران العمودية للحيز معزولة بينما الجدران الافقية ذات درجات حرارة ثابتة لكن مختلفة.ارتفاع الزعانف الموضوعة داخل الحيز (B/L= 0.22,0.44, 0.66) وموضوعة على الجدران الافقية وذات سمك ثابت . الدراسة تغطي المدى لرقم رايلي من10^4 الى 10^7 ولعدد برانتل (Pr=0.7) ونسبة(H/L=0.15-0.5) واعداد مختلفة للزعانف تتراوح من(1- 3). الحل العددي تم باستخدام طريقة دالة الانسياب- الدوامية بأستخدام طريقة الفروق المحددة مع بناء برنامج حاسوبي بلغة(فورتران 90) مع برنامج Tec plot program.تم دراسة تاثير كل من رقم رايلي ، عدد الزعانف ، ونسبة (H/L) على شدة الدوامات الدوارة و انتقال الحرارة داخل الحيزبوجود او عدم وجود الزعانف . بالاضافة الى ذلك تم اشتقاق معادلة التصحيح لرقم نسلت باستخدام برنامج (DGA v1.00) و ايجاد معدل قيم رقم نسلت على طول الجدار المسخن. بينت النتائج ان متوسط نسلت يقل مع زيادة نسبة (H/L) وزيادة عدد الزعانف. وتم مقارنة النتائج العددية مع النتائج العددية المتوفرة وكانت نتائج المقارنة جيدة.

1- Introduction

Natural convection heat transfer inside irregular and complex shaped enclosures has a wide variety of technological applications involving double-wall thermal insulation, underground cable systems, solar-collectors, electric machinery, cooling system of micro-electronic devices, natural circulation in the atmosphere, the molten core of the Earth, etc.

Miomir Raos [2002], investigated numerically using FVM the laminar natural convection phenomena in two-dimensional rectangular enclosure with differentially heated sides and adiabatic horizontal walls, and the effect of rotation of the enclosure is presented in this study too. The study assumed Pr=0.7 and Rayleigh number from 10^3 to 10^6. The results showed complex flow patterns heat transfer rates, with different orientation of the enclosure. Angle of rotation about 65-75 maximize Nu number value for named conditions.

Dias and Milanez [2004] studied numerically a 3-D laminar natural convection in air filled enclosure using finite volume technique .The results were obtained for Ra no. ranges from (10^3 to 10^6) and aspect ratios ranging from (1 to 20).They found that the two dimensional approximation, frequently compared to experimental results, deviates from the three dimensional results as the Rayleigh number increases.

Ben Yedder and Bilgen [1997], studied numerically the effect of laminar natural convection in inclined enclosures bounded by a solid wall for the range $10^3<Ra<10^6$ and the inclination angle (from 30° to 180°) with Ar=1 and thermal conductivity ratio K_r was varied (from 1 to 10). Flow, temperature fields and heat transfer rates are examined for these ranges of the Rayleigh number and geometrical parameters of the problem. They found for K_r=10, which correspond to the case with employing a polynomial-base differential quadrature method. The results show that the presence of a vertical partition has a considerable effect on the circulation intensity, and therefore, the heat transfer high wall conductivity, the temperature gradient within the solid wall is very small and the temperature at the internal surface is almost the same as the imposed uniform temperature at its outer boundary. For increasing Ra number, the isotherms show a stratified flow within the enclosure with steep gradients near the vertical boundaries.

Syeda and Shohel [2006] studied numerically the effect of the buoyancy induced flow and heat transfer characteristics inside an inclined L-shaped enclosure. A control volume based Finite-Volume method is applied to discretize the governing equations with collocated variable arrangement. SIMPLE algorithm is used and the system of equations is solved by Stone's SIP solver with full multigrid acceleration. Results are presented in the form of the average Nusselt number for a range of inclination angle =0°–360°; Rayleigh number, Ra=1–10^5; and aspect ratio, A=0.1–0.5.

Shaw et al. [1987], studied natural convection in an enclosure fitted with a partial vertical adiabatic partition. Horizontal walls were adiabatic and vertical walls were maintained at different temperatures. The governing equations were solved with the aid of a cubic spline collocation method. Numerical simulations showed that the height and location of the partition have significant effects on the flow and heat transfer characteristic of the enclosure.

Kamil Kahveci [2007] presented numerical study of laminar natural convection in an enclosure divided by a partition with a finite thickness and conductivity. The enclosure is assumed to be heated using a uniform heat flux on a vertical wall, and cooled to a constant temperature on the opposite wall. The governing equations in the vorticity-stream function formulation are solved by characteristics across the enclosure. The average Nusselt number decreases with an increase of the distance between the hot wall and the partition. With a decrease in the thermal resistance of the partition, the

average Nusselt number shows an increasing trend and a peak point is detected. If the thermal resistance of the partition further declines, the average Nusselt number begins to decrease asymptotically to a constant value. The partition thickness has little effect on the average Nusselt number.

Nuri and Hakan [2003], studied natural convection heat transfer in partially divided square enclosures. A finite difference computer program based on control volume approach is developed for the solution. The study assumed Pr=0.7 and Rayleigh number from 10^3 to 10^6. Vertical side walls are kept at different constant temperature, while the horizontal walls are insulated. The effects of Ra number and number of partitions on heat transfer are investigated. They found that , the heat transfer rate increases with increasing Ra number, and at low Ra numbers the conduction is the dominant heat transfer mode, and at Ra=10^3 , the mean Nusselt number remains constant around unity for all numbers of partitions.

Nienchuan and Bejan [1983] experimentally and analytically studied the phenomenon of heat transfer by natural convection in a partially divided enclosure. The nonconducting partition was fitted to the floor of cavity. Heat transfer measurements and flow visualization studies were conducted in Rayleigh number range 10^9–10^{10} for aperture ratios (height of the internal opening above the partition: height of the enclosure) of 1, 1/4, 1/8, 1/16 and 0. It was found that, as the aperture ratio decreases from 1 to 0, the Nusselt number decreases by a factor of 15.

Moukalled and Darwish [2003] Numerical results are reported for natural-convection heat transfer in partially divided trapezoidal cavities representing industrial buildings. Two thermal boundary conditions are considered. In the first, the left short vertical wall is heated while the right long vertical wall is cooled (buoyancy-assisting mode along the upper inclined surface of the cavity). In the second, the right long vertical wall is heated while the left short vertical wall is cooled (buoyancy-opposing mode along the upper inclined surface of the cavity). The effects of Rayleigh number, Prandtl number, baffle height, and baffle location on the heat transfer are investigated. Results are displayed in terms of streamlines, isotherms, and local and average Nusselt number values. For both boundary conditions, predictions reveal a decrease in heat transfer in the presence of baffles, with its rate generally increasing with increasing baffle height and Pr. For a given baffle height, greater decrease in heat transfer is generally obtained with baffles located close to the short vertical wall.

Eric and Mohamed [2005] investigated natural convection heat transfer and fluid flow characteristics from a horizontal fluid layer with finned bottom surface numerically and experimentally. The effects of fin height and fin spacing have been investigated for a sufficiently wide range of Rayleigh number. Quantitative comparisons of heat transfer rates and finned surface effectiveness have been reported. The insertion of heat conducting fins has been found to induce an upward fluid motion along the fin walls. For a given value of fin spacing, the number of convection cells between two adjacent fins is function of the values of fin height and Rayleigh number. In comparison with a bare plate, the heat transfer rates for low values of fin height may be decreased by the insertion of fins. For high values of fin height, the finned surface effectiveness is greater than one for a wide range of fin spacing. For low values of Rayleigh number and high values of fin height, the finned surface effectiveness increases linearly with the decrease of fin spacing. Useful guidelines have been suggested to enhance the heat transfer rates from the finned surface.

There are several experimental and numerical studies on natural convection heat transfer in enclosures; however, studies about the nonrectangular enclosure partially divided are rare .In this study, natural convection of air with the Prandtl

number of (0.7) has been analyzed for different cases considered given below:
Case-1- without fin and change value of aspect ratio (H/L).
Case-2- with different numbers of fin.
Case-3- with different height of fin at lower wall.

2-Physical model

The problem studied in this paper is a two dimensional laminar flow and heat transfer in a nonrectangular enclosure with and without fins. The considered Rayleigh numbers was ranged from (10^4 to 10^7), The working fluid was air with (Pr=0.70) .Vertical walls insulated while horizontal walls and the fins were placed on horizontal surface are maintained isothermal at different temperature as shown in Fig.(1). The length of fins was taken equal (B/L=0.22, 0.44, and 0.66) and number of fin change from (1 - 3).

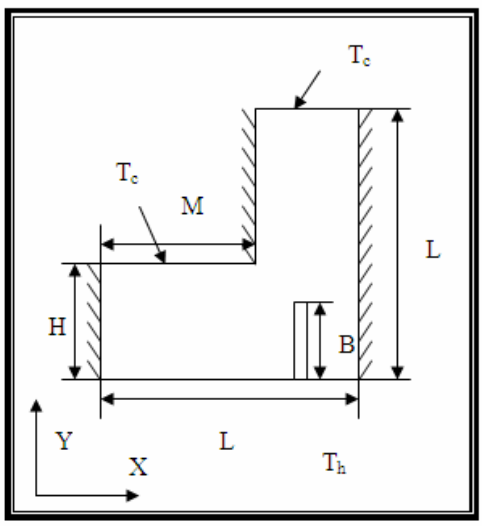

Fig. (1) Shematic of problem and the coordinate system

3- Mathematical model

The fluid is Newtonian and the flow is steady, laminar, two dimensions and incompressible. The non-dimensional governing equations for the conservation of mass, momentum and energy are [Eric and Mohamed 2005]:

Continuity:

$$\frac{\partial U}{\partial X}+\frac{\partial V}{\partial Y}=0 \qquad (1)$$

X- momentum:

$$\frac{\partial}{\partial X}(UU)+\frac{\partial}{\partial Y}(VU)=-\frac{\partial P}{\partial X}+\Pr\left[\frac{\partial^2 U}{\partial X^2}+\frac{\partial^2 U}{\partial Y^2}\right] \qquad (2)$$

Y- momentum:

$$\frac{\partial}{\partial X}(UV)+\frac{\partial}{\partial Y}(VV)=-\frac{\partial P}{\partial Y}+\Pr\left[\frac{\partial^2 V}{\partial X^2}+\frac{\partial^2 V}{\partial Y^2}\right]+Ra\Pr\theta \qquad (3)$$

Energy:

$$U\frac{\partial\theta}{\partial X}+V\frac{\partial\theta}{\partial Y}=\left[\frac{\partial^2\theta}{\partial X^2}+\frac{\partial^2\theta}{\partial Y^2}\right] \qquad (4)$$

With: $U=\frac{uL}{\alpha}$, $V=\frac{vL}{\alpha}$, $X=\frac{x}{L}$, $Y=\frac{y}{L}$,

$P=\frac{pL^2}{\rho\alpha^2}$, $\theta=\frac{T-T_c}{T_h-T_c}$,

$\Pr=\frac{\nu}{\alpha}$, $Ra=\frac{g\beta(T_h-T_c)L^3}{\nu^2}$, Ra=Gr*Pr

The governing equations can be written in dimensionless stream function–vorticity form as:

$$\frac{\partial}{\partial X}(U\omega)+\frac{\partial}{\partial Y}(V\omega)=\Pr\left[\frac{\partial^2\omega}{\partial X^2}+\frac{\partial^2\omega}{\partial Y^2}\right]+(Ra\Pr)\frac{\partial\theta}{\partial X} \qquad (5)$$

$$U\frac{\partial\theta}{\partial X}+V\frac{\partial\theta}{\partial Y}=\frac{\partial^2\theta}{\partial X^2}+\frac{\partial^2\theta}{\partial Y^2} \qquad (6)$$

The only non- zero component of the vorticity is:

$$\omega=\frac{\partial V}{\partial X}-\frac{\partial U}{\partial Y} \qquad (7)$$

From the definition of stream function which verify the continuity equation, vertical and horizontal components can be written as:

$$V=-\frac{\partial\psi}{\partial X} \qquad (8)$$

$$U=\frac{\partial\psi}{\partial Y} \qquad (9)$$

By substituting equation (8) and (9) into equation (7) to obtain the following stream equation:

$$-\omega = \frac{\partial^2 \psi}{\partial X^2} + \frac{\partial^2 \psi}{\partial Y^2} = \Delta^2 \psi \qquad (10)$$

For the solid region (in the fins), the energy equation for the heat transfer by conduction becomes [Kamil Kahveci 2007]:

$$\frac{\partial^2 \theta}{\partial X^2} + \frac{\partial^2 \theta}{\partial Y^2} = 0 \qquad (11)$$

The following equation was defined for the interface between the fin and fluid [Nogotov 1978]:

$$K_f \frac{\partial \theta}{\partial n} = K_{fin} \frac{\partial \theta}{\partial n} \qquad (12)$$

Where:
(K_f) and (K_{fin}) is the thermal conductivity of fluid and fin respectively, (n) represent the normal distance.

4- Boundary conditions

The boundary conditions for the problem can be written in dimensionless form as [Nuri and Ahmed 2003] :

1. The left wall (Insulated wall) (X=0):

$$U = 0, V = 0, \psi = 0, \frac{\partial \theta}{\partial n} = 0 \qquad (13)$$

2.The right wall (Insulated wall) (X=L):

$$U = 0, V = 0, \psi = 0, \frac{\partial \theta}{\partial n} = 0 \qquad (14)$$

3.The lower wall (hot wall) (Y=0) :

$$U = 0, V = 0, \psi = 0, \theta = 1 \qquad (15)$$

4.The upperr wall (cold wall) (Y=L):

$$U = 0, V = 0, \psi = 0, \theta = 0 \qquad (16)$$

5- For the all surface walls the vorticity on the rigid walls is calculated by using the Woods formulae (Woods 1954):

$$\omega_o = \frac{3}{\Delta n^2}(\psi_o - \psi_1) + \frac{1}{2}\omega_1 \qquad (17)$$

5- Numerical Solution

The numerical solution of this system may be obtained by solving its difference system with some available iteration procedure. Consider the second order conservative, monotonic finite difference scheme approximating system of equations (5), (6) (10) and (11). The scheme has been used for steady convective problems involving wide ranges of process parameters and has given good results. It employes the integrointerpolation method. A system of difference equations is obtained by integrating the original system (5), (6),(10)and (11) [Nogotov 1978].

Following is the procedure in [Nogotov 1978], the governing finite difference equations for (ω, θ, and ψ) can be written in the standard five point formula form. These finite difference equations which subject to appropriate boundary conditions are solved by an iterative method known as successive substitution. If (ω^s, θ^s, and ψ^s) denote functional values at the end of sth iteration, the value of (ω,θ, and ψ) at (s+1)th iteration level are calculated from the following expressions:

$$\theta_{i,j}^{s+1} = (1 - F_\theta)\theta_{i,j}^{s} + \frac{F_\theta}{A_\theta}(a_\theta \theta_{i+1,j}^{s} + b_\theta \theta_{i-1,j}^{s+1} + c_\theta \theta_{i,j+1}^{s} + d_\theta \theta_{i,j-1}^{s+1}) \qquad (18)$$

$$\omega_{i,j}^{s+1} = (1 - F_\omega)\omega_{i,j}^{s+1} + \frac{F_\omega}{A_\omega}\left[\begin{array}{l}(a_\omega \omega_{i+1,j}^{s} + b_\omega \omega_{i-1,j}^{s+1} + c_\omega \omega_{i,j+1}^{s} + d_\omega \theta_{i,j-1}^{s+1}) \\ + 0.5(Ra/\Pr)h\left(\theta_{i+1,j}^{s+1} - \theta_{i-1,j}^{s+1}\right)\end{array}\right] \qquad (19)$$

$$\psi_{i,j}^{s+1} = (1 - F_\psi)\psi_{i,j}^{s+1} + \frac{F_\psi}{4}(\psi_{i+1,j}^{s} + \psi_{i-1,j}^{s+1} + \psi_{i,j+1}^{s} + \psi_{i,j-1}^{s+1} + h^2 \omega_{i,j-1}^{s+1}) \qquad (20)$$

$$\theta_{i,j}^{s+1} = (1 - F_{\theta\theta})\theta_{i,j}^{s+1} + \frac{F_{\theta\theta}}{4}(\theta_{i+1,j}^{s} + \theta_{i-1,j}^{s+1} + \theta_{i,j+1}^{s} + \theta_{i,j-1}^{s+1}) \qquad (21)$$

Where (s) is the iteration number, and $F_\theta, F_\omega, F_\psi$ and $F_{\theta\theta}$ are the relaxation parameters which depend on the mesh size and fluid mechanical parameters.

For the interface region, the equation (12) is solved forward or backward according to the location of the

partition. The final form of equation (12) is:

$$\theta_{\text{int}} = (K_r\,\theta_{fin} + \theta_f)/(1+K_r) \qquad (22)$$

Where:

$$K_r = \frac{K_{fin}}{K_f} \qquad (23)$$

A converged solution was defined as one that meet the following criterion for all dependent variables.

$$\max\left|\frac{\phi^{n+1}-\phi^{n}}{\phi^{n+1}}\right| \le 10^{-6} \qquad (24)$$

6- Calculation of Mean Nusselt Number

The mean Nusselt number can be calculated from equation below:

$$Nu = \frac{hL}{k} \qquad (25)$$

The above equation can be written in dimensionless form as follows:

$$Nu = \int_0^1 \left.\frac{\partial\theta}{\partial Y}\right|_{Y=0} dX \qquad (26)$$

The integration can be evaluated by using numerical integration (Simpson's rule) to obtain an overall Nusselt number as below [Nogotov 1978]:

$$Nu = \frac{h}{3}\left[Nu_{L(1)} + 4\sum_{i=2}^{m-2} Nu_{L(i)} + 2\sum_{i=3}^{m-1} Nu_{L(i)} + Nu_{L(m)} \right] \qquad (27)$$

7- Correlations

A correlation equations had been written to show the aspect ratio, number of fins, and height of fin effects on the rate of heat transfer.

Several analyses where performed, by using program (DGA v1.00 and Excel) to find correlation of Nusselt number for different cases considered given below:

1- Effect of aspect ratio (H/L)

Nusselt number for any aspect ratio (H/L) can be written in the following form:-

$$Nu = cRa^{n1}\left(\frac{H}{L}\right)^{n2} \qquad (28)$$

The above equation is valid for:

$10^4 \le Ra \le 10^7$,$0.15 \le (H/L) \le 0.5$, with out fins.

The final form :

$$Nu = 0.231Ra^{0.273}\left(\frac{H}{L}\right)^{-0.267} \qquad (29)$$

2- Effect number of fins

Nusselt number correlasion can be written in the following form:-

$$Nu = cRa^{n1}D^{n2} \qquad (30)$$

D= number of fin from (1-3)

The above equation is valid for:

$10^4 \le Ra \le 10^7$

The final form :

$$Nu = 0.111Ra^{0.313}D^{-0.137} \qquad (31)$$

3-Effect of height of fin (B/L)

Nusselt number for any value of height of fin (B/L) can be written in the following form:-

$$Nu = cRa^{n1}\left(\frac{B}{L}\right)^{n2} \qquad (32)$$

The above equation is valid for :

$10^4 \le Ra \le 10^7$, $0.22 \le (B/L) \le 0.66$, number of fin=1.

The final form :

$$Nu = 0.115Ra^{0.325}\left(\frac{B}{L}\right)^{0.010} \qquad (33)$$

8- Results and Discussions

Numerical results for the laminar and natural convection in nonrectangular enclosures with and without fin is considered for various values of the Rayleigh number.

*** Effect of aspect ratio (H/L)**

Figs.(2),(3),(4) and (5) respectively, show effects of Ra number on the stream function and temperature contours for number of fins (0) ande for aspect ratio change from(H/L=0.15 to 0.5). For small Rayleigh numbers (Ra=10^4), the free convection currents are small and the values of stream function in enclosure

increases with the increasing Rayleigh number. When the Rayleigh number increases, the temperature gradient next to hot and cold wall increases. Also development of the plume effect can be seen as the Rayleigh number increases.

*** Effect number of fins**

In Fig.(6) the streamline and isotherm contours for different Rayleigh numbers are plotted for number of fin (1) and fin height (B/L= 0.22).The value of stream function (the strength of flow) in enclosure increases with the increasing Rayleigh number. At low Rayleigh numbers there is two circulating cells forms inside the enclosure; with further increase in Rayleigh numbers, the number of circulating cells formed in the enclosure becomes three or more. To analyze the effects of the fin on the temperature contours, It can be observed that the convection cells move outward away from the fin surface with the increase of Rayleigh numbers. Also, the temperature gradient at the cold wall above the fin tip increases with the increase of Rayleigh numbers.As the number of fins increases, the strength of flow decreases and the secondary cells rotating opposite to the direction of main cell can be seen Figs. (7) and (8).

***Effect of height of fin (B/L)**

To analyze the effects of the fin height on the flow and heat transfer characteristics, the computations are performed for different fin heights at different Rayleigh numbers. Figs.(6),(9) and (10) , it is seen that, the increase of the height of fin lowers the fluid flow in the enclosure and retards the heat transfer from the warm wall to the cold wall efficiently. As a result, the stream function values and the mean Nusselt number decrease with increasing fin heights. Temperature gradient at the fin tip increases with the increase of fin height, no significant differences can be seen on temperature contours for different fin heights.

***Nusselt numbers.**

Fig. (11) Shows the relation between the Nu numbers with Ra number for various aspect ratios (H/L). Results showed that the Nu number increases as aspect ratio decreases.

The variation of mean Nu number with Ra number at different number of fin is shown in Fig.(12). As seen the mean Nusselt number increases with increasing Rayleigh number. The decrease in heat transfer in the presence of fin can easily be depicted from the profiles presented in Figure. As the fluid moves up along the hot wall, its temperature increases and the temperature difference between the fluid and the hot wall decreases.This results in a decrease in Nu values as depicted. It is also seen that variation of mean Nu number decreases with increasing number of fins. As the number of fins increases, fin partially block the motion of fluid flow and as a result, the effect of convection decreases.

In Fig. (13), the variation of the mean Nu number with Ra number is shown for different height of fin. It is seen in this figure, the mean Nusselt number decreases with increasing heights of fin**.**

***Comparison of present work**

The numerical result of the present work is compared with available numerical result of [Syeda and Shohel 2006]. As displayed in Figs. (14) and (15), the present simulation shows good agreement with the numerical data.

The values of numerically computed Nu are compared with that of Nu calculated from correlation equation (31) for case study effect number of fins. Excellent agreement is observed as is evident from Fig. (16).

9- Conclusion

1- The flow structure is strongly affected by increasing the Rayleigh number.

2- The values of stream function (the strength of flow) in enclosure increases with the increasing Rayleigh number and decrease with increase aspect ratio (H/L).

3- Mean Nusselt numbers decreases with:

- Increasing aspect ratio (H/L)
- In the presence of fins
- For a given fin height, greater value.

10-Nomenclature

Symbol	Description	Unit
B	Height of the fin	m
H	Height of wall	m
g	Gravitational acceleration	m/sec^2
K_f	Thermal conductivity of fluid (air) $K_f = 0.024W/m.C)$	W/m.K
$K_{f\,in}$	Thermal conductivity of fin(copper) ($K_{fin} = 202$W/m/C)	W/m.K
Kr	Thermal conductivity ratio	
L	Enclosure total length	
Nu	Mean Nusselt number	
Pr	Prandtl number	
Ra	Rayleigh number	
T	Temperature	K
T_c	Cold wall temperature	K
T_h	Hot wall temperature	K
U	Dimensionless velocity component in x-direction	
V	Dimensionless velocity component in y-direction	
x	Horizontal axis	m
X	Dimensionless horizontal axis	
y	Vertical axis	m
Y	Dimensionless vertical axis	
υ	Kinematic viscosity	m^2/sec
θ	Dimensionless temperature	
ψ	Stream function	
ω	Vorticity	

11-References

Ben Yedder. R.,and Bilgen. E., “Laminar Natural Convection in Inclined Enclosures Bounded By A Solid Wall”, International Journal of Heat & Mass Transfer, Vol.32, pp.455-462 ,October (1997).

Dias. T. J., and Milanez. L.F., “Natural Convection in High Aspect Ratio Three-Dimensional Enclosures with Uniform Heat Flux on the Heated Wall”, Engenheria Termica Journal (Thermal Engineering), Brazil.Vol.3.No.2., pp.96-99 Dec (2004).

Eric Arquis , and Mohamed Rady , "Study of natural convection heat transfer in a finned horizontal fluid layer" ,International Journal of Thermal Sciences,Vol. 44 ,PP. 43–52, (2005) .

Kamil Kahveci ,"Natural Convection in a Partitioned Vertical Enclosure Heated With a Uniform Heat Flux", Journal of Heat Transfer ,Vol. 129, PP.717-726, June (2007).

Moukalled F., and M. Darwish ," Natural convection in a partitioned trapezoidal cavity heated from side ", Journal of Numerical heat transfer, Vol. 43.PP.543-563,(2003).

Miomir Raos,"Nusselt Number Dependence on Inclination of Paralelogramic Enclosure under Natural Convection Conditions", Faculty of Occupational Safety, University of Nis, Serbia, Yugoslavia, Vol.2, pp. 135-142 ,July (2002).

Nuri Yucel, and Ahmed Hakan Ozdem, “Natural Convection in Partially Divided Square Enclosures”, International Journal of Heat and Mass Transfer, Vol.40, pp.167-175, (2003).

Nienchuan N.L., and Bejan A.," Natural Convection in a Partially Divided Enclosure. International Journal of Heat Transfer 26,pp. 1867–1878,(1983).

Nogotov E.F, "Applications of Numerical heat transfer", Hemisphere publishing corp. Washington. (1978).

Syeda Humaria Tasnim, and Shohel Mahmud, “Laminar Free Convection Inside an Inclined L-Shaped Enclosure”, International Journal of Heat and Mass Transfer, Vol.33, pp.936-942, (2006).

Shaw H.J., Chen C.K., and Cleaver J.W.," Cubic spline numerical solution for two-dimensional natural convection in a partially divided enclosure", Journal of. Numerical. Heat Transfer12,pp. 439–455,(1987).

Woods L.C., " A note on the numerical solution of fourth order differential equations", Aero Quart 5, PP. 176–184, (1954).

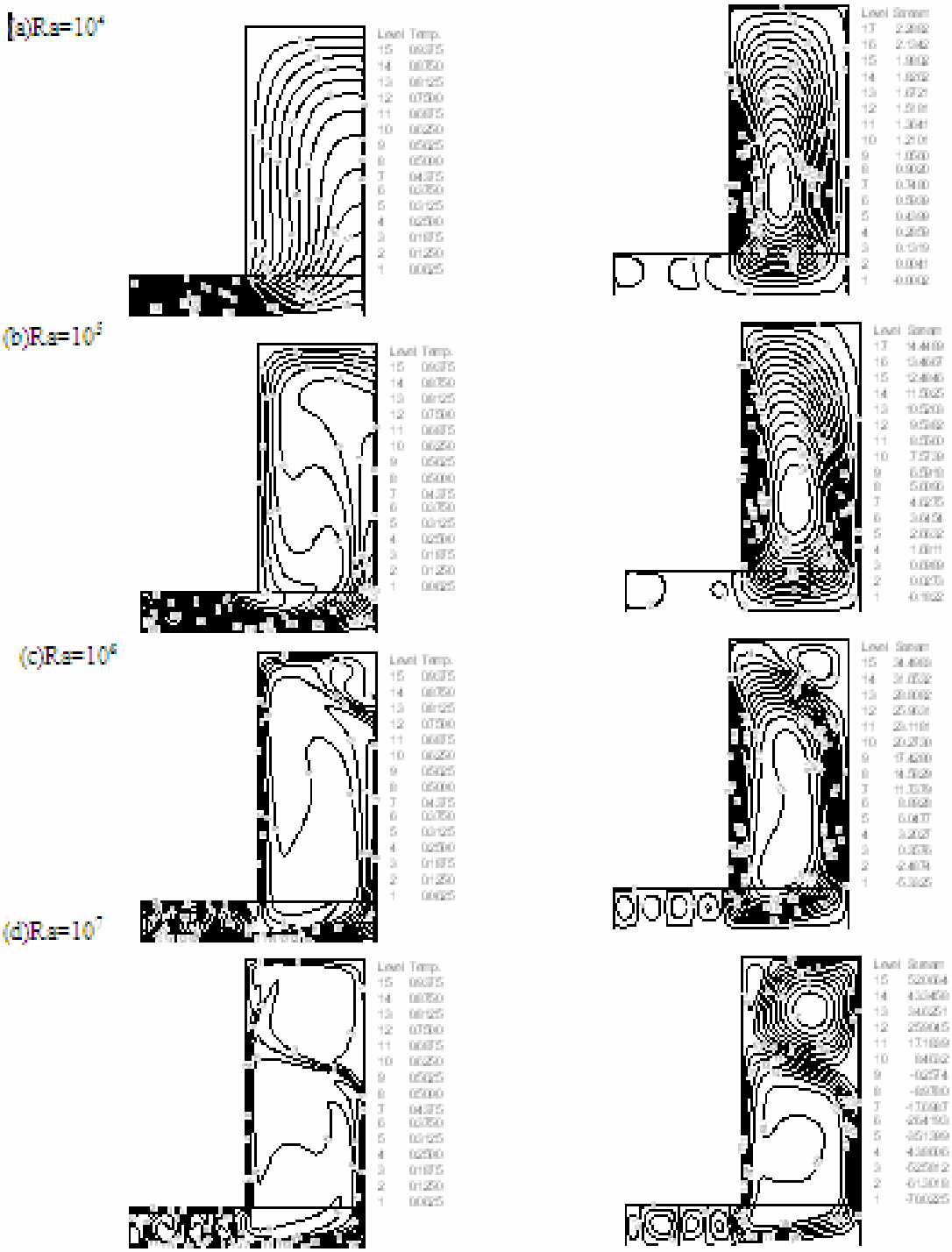

Fig. (2) Effects of Ra number on the temperature contours and stream function without fins and aspect ratio (H/L= 0.15).

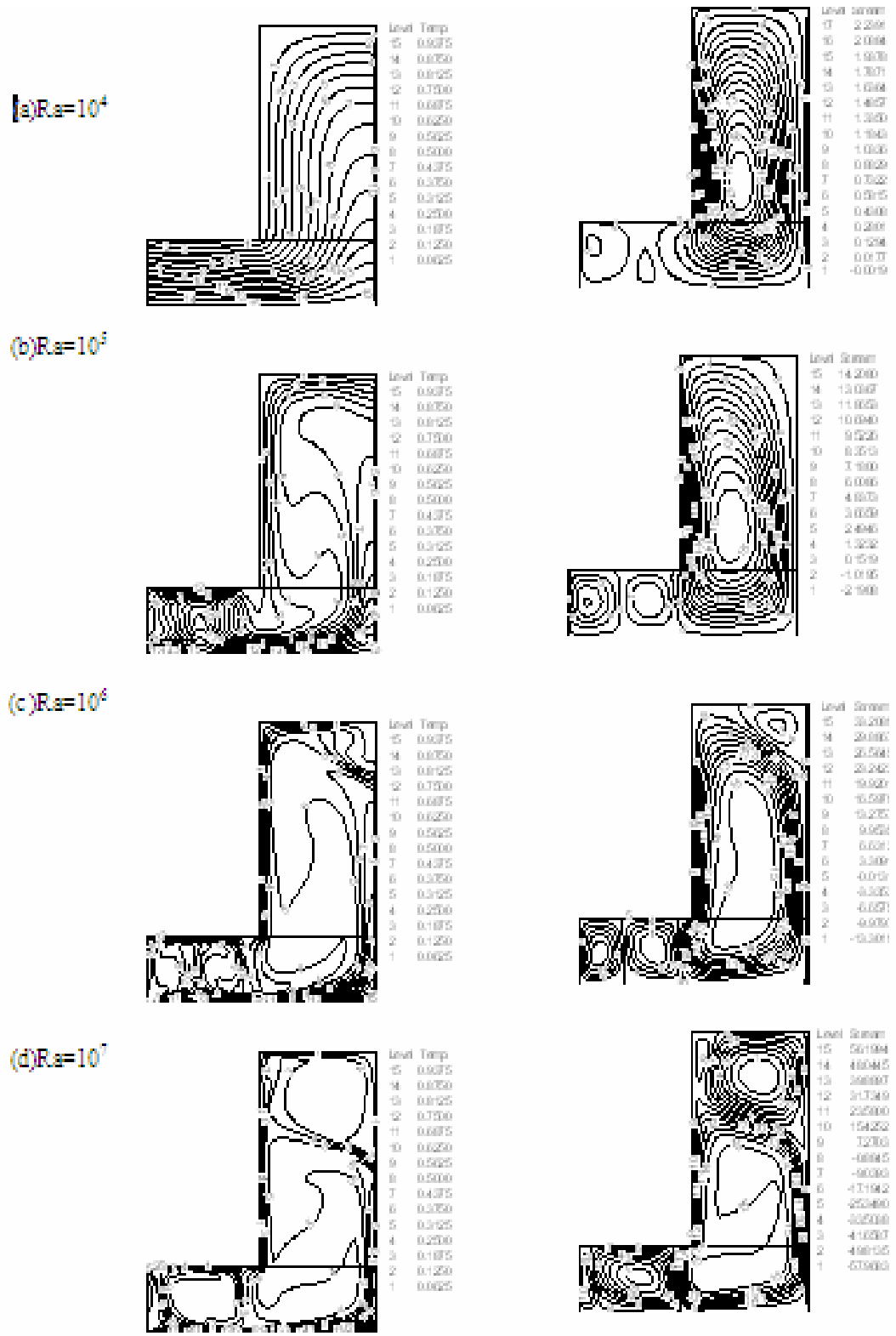

Fig. (3) Effects of Ra number on the temperature contours and stream function without fins and aspect ratio (H/L= 0.25).

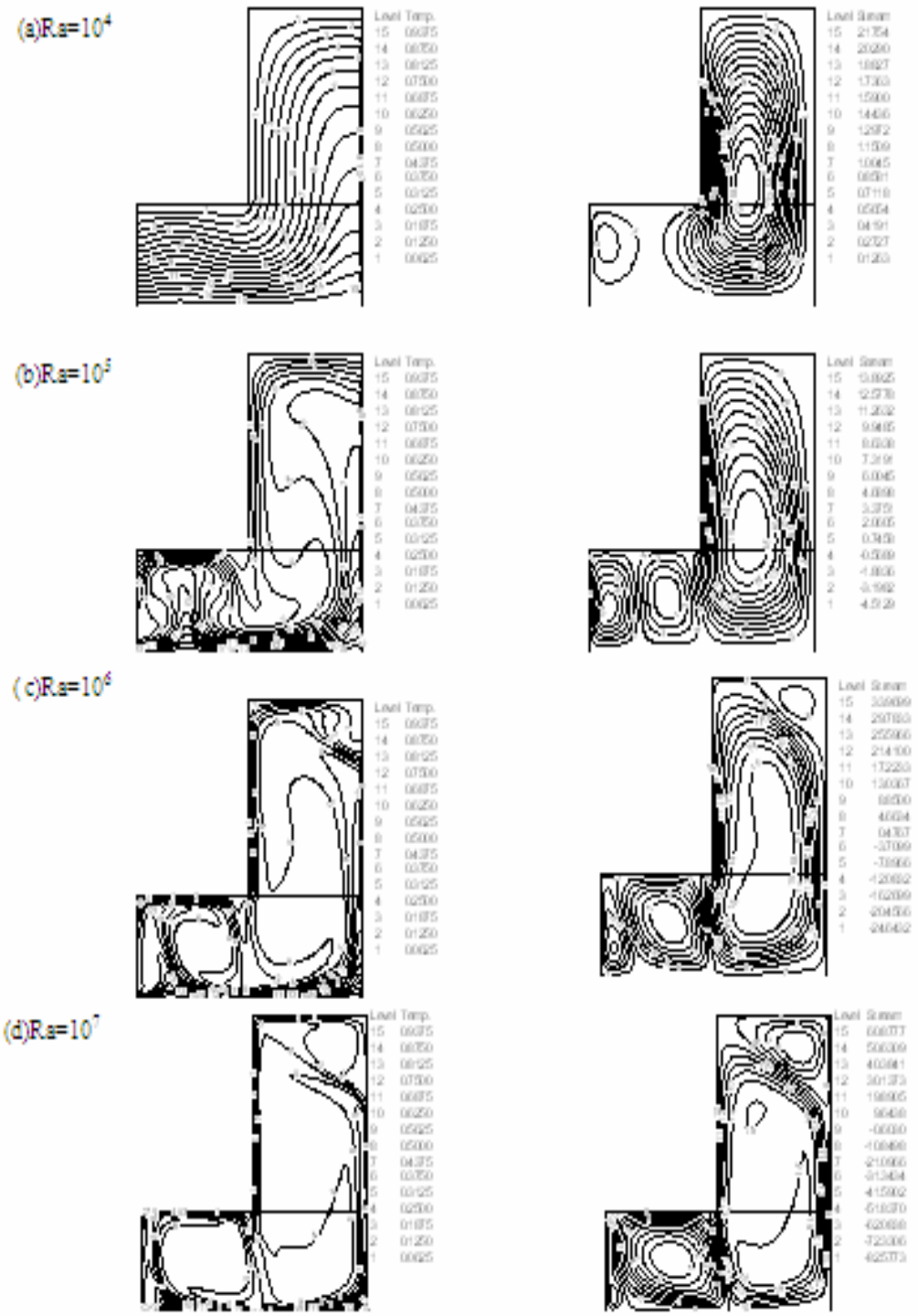

Fig. (4) Effects of Ra number on the temperature contours and stream function without fins and aspect ratio (H/L= 0.35).

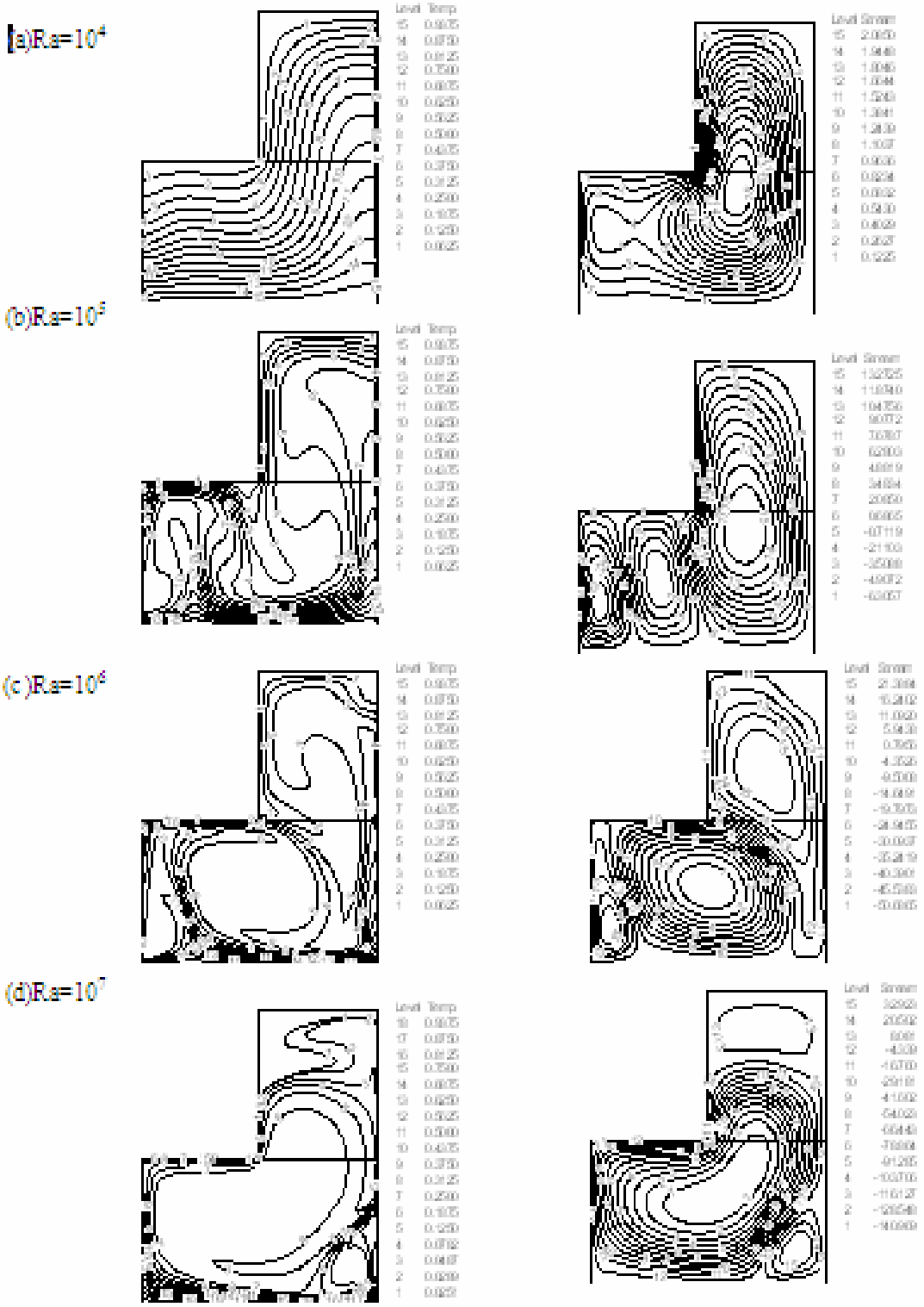

Fig. (5) Effects of Ra number on the temperature contours and stream function without fins and aspect ratio (H/L= 0.5).

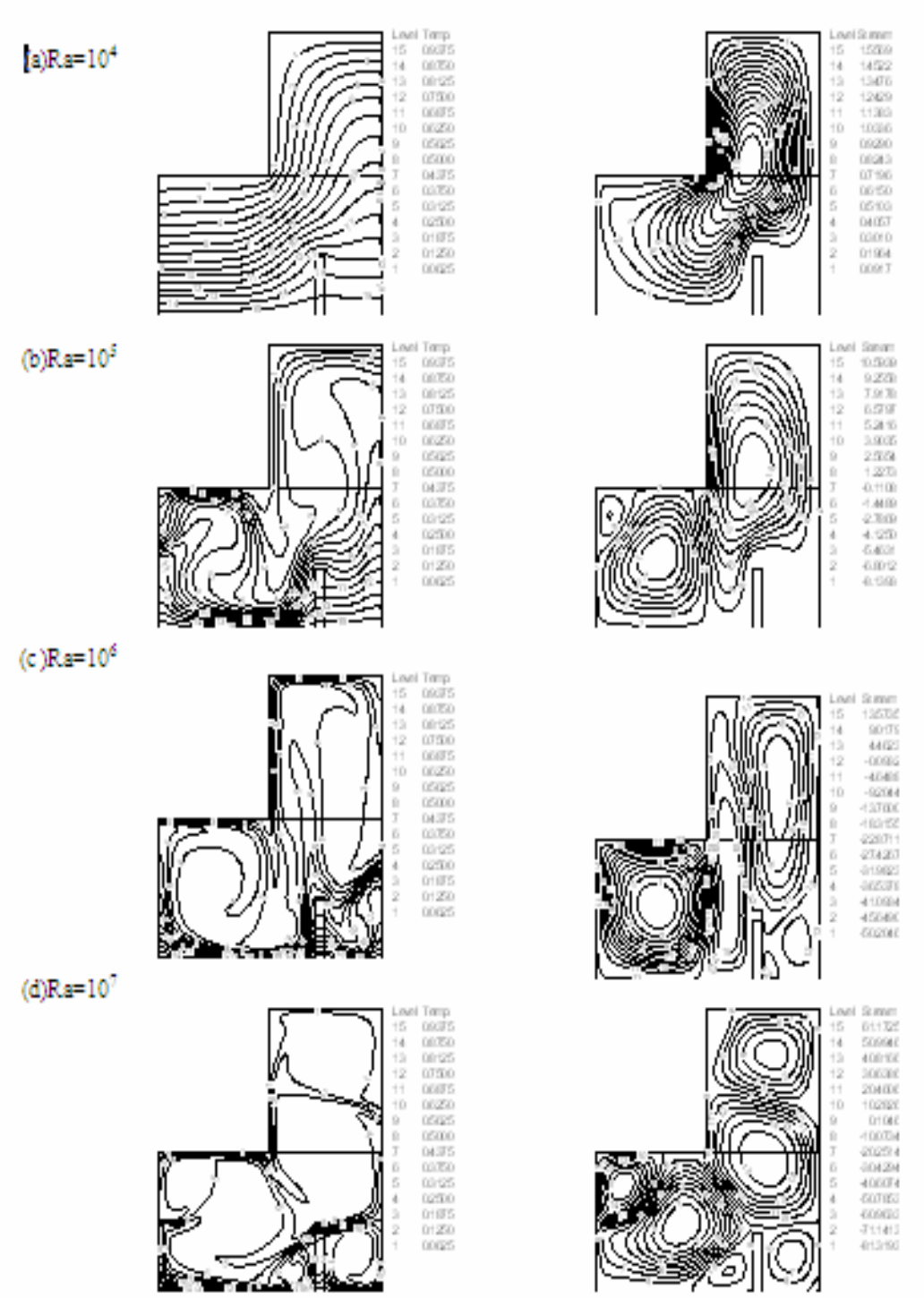

Fig. (6) Effects of Ra number on the temperature contours and stream function for fin at lower wall, height of fin (B/L=0.22) and aspect ratio (H/L= 0.5).

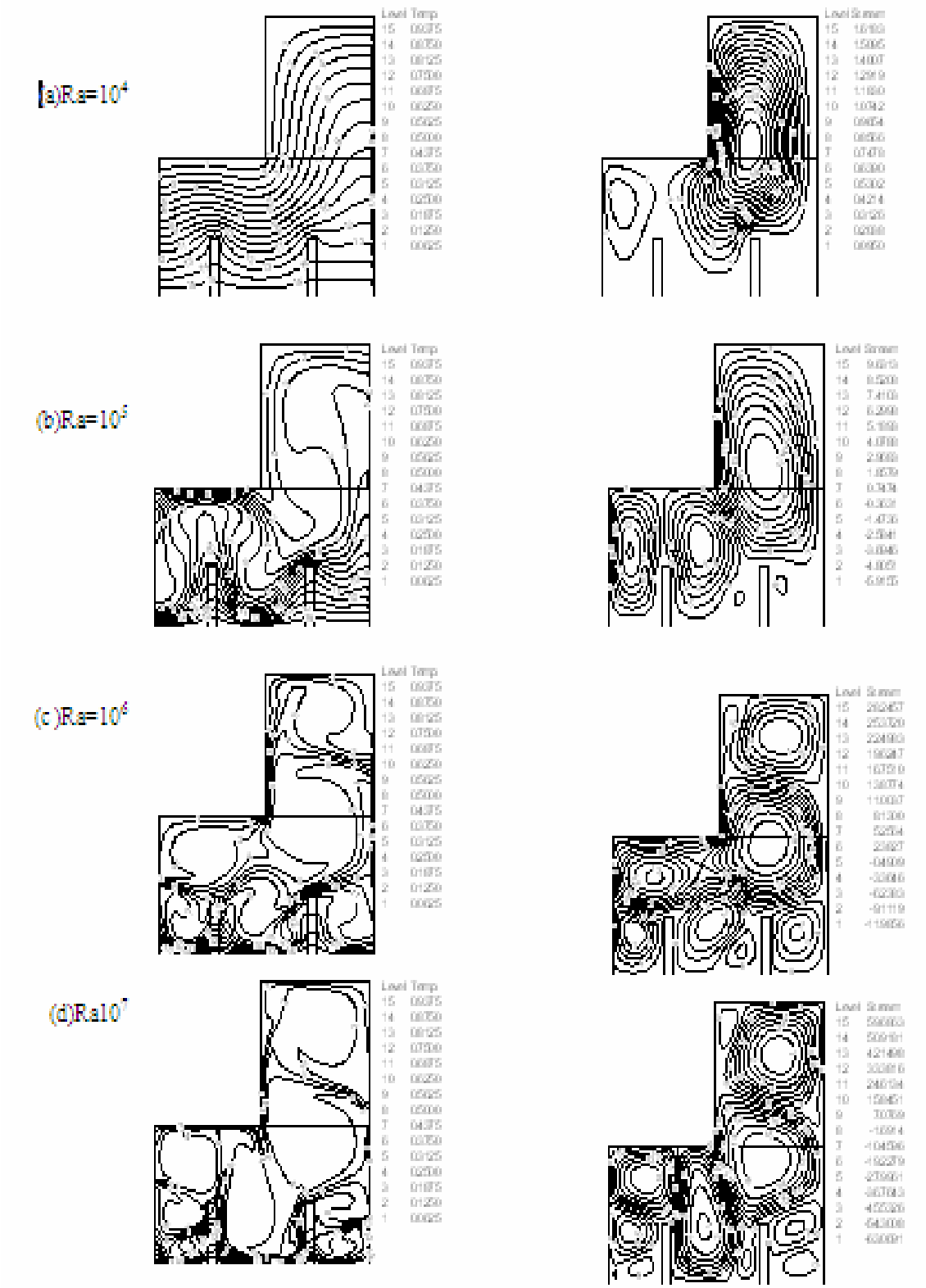

Fig. (7) Effects of Ra number on the temperature contours and stream function for number of fin (2), height of fin (B/L=0.22) and aspect ratio (H/L= 0.5).

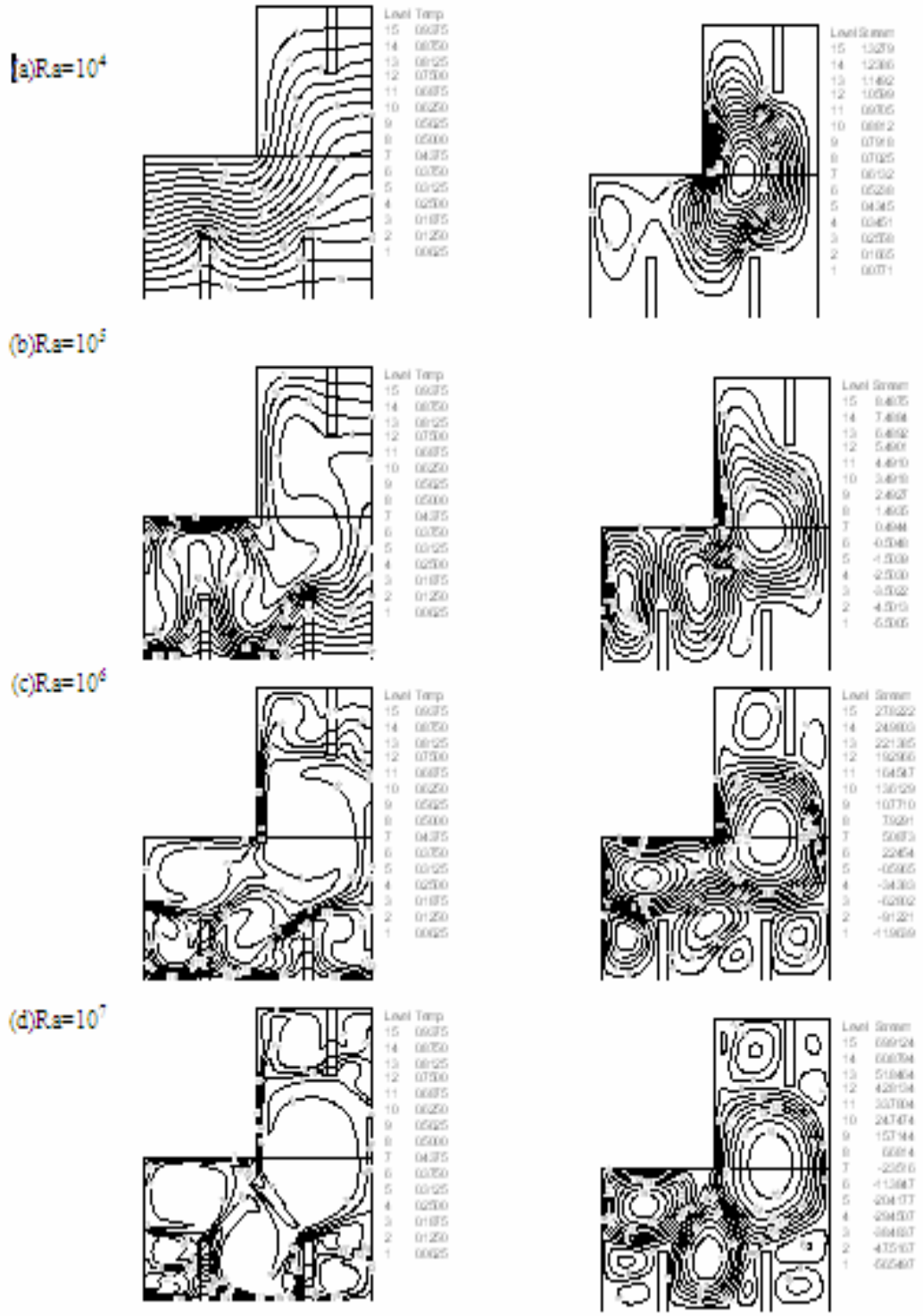

Fig. (8) Effects of R.a number on the temperature contours and stream function for number of fin (3),height of fin (B/L=0.22) and aspect ratio (H/L= 0.5).

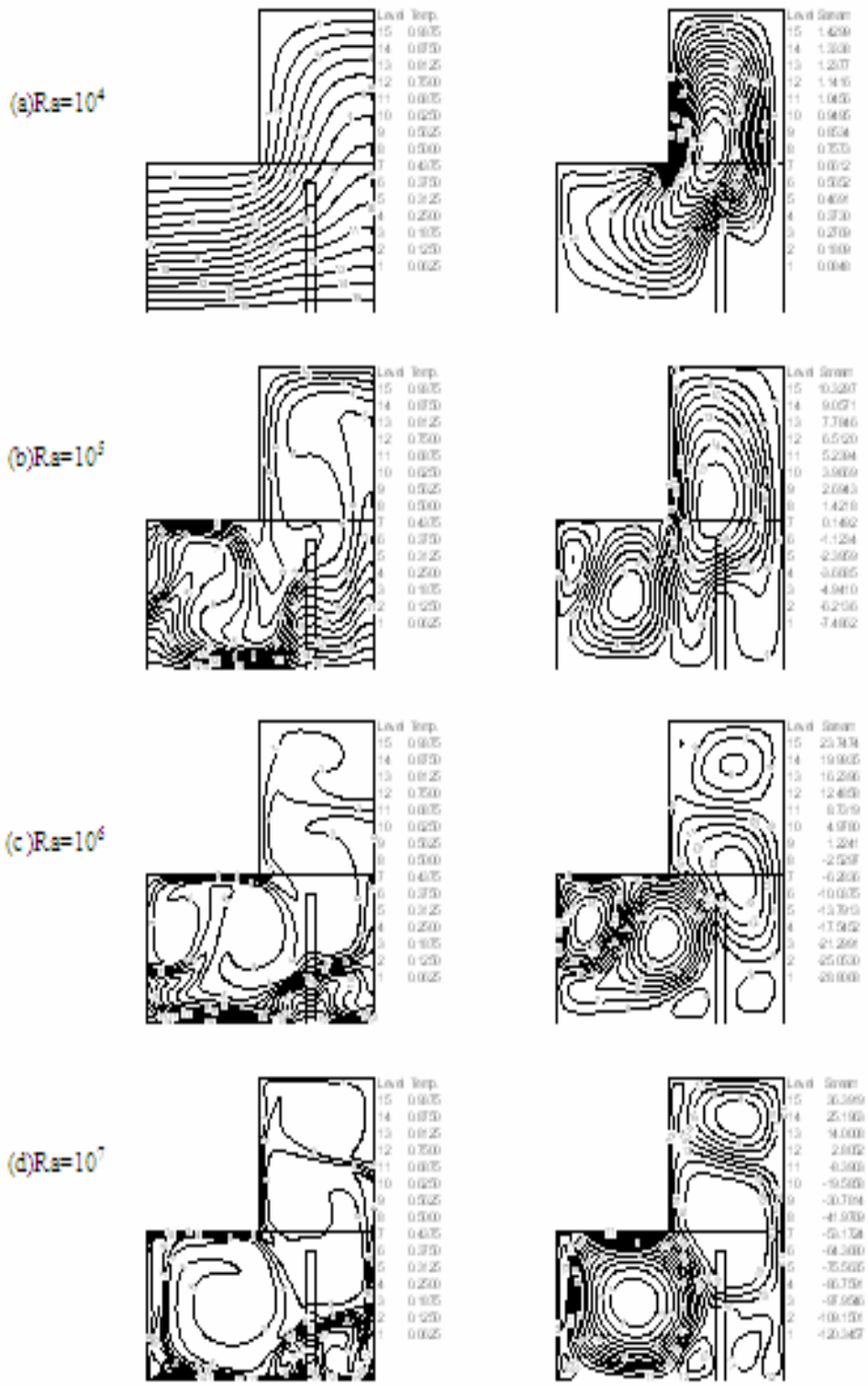

Fig. (9) Effects of Ra number on the temperature contours and stream function for fin at lower wall, height of fin (B/L=0.44) and aspect ratio (H/L= 0.5).

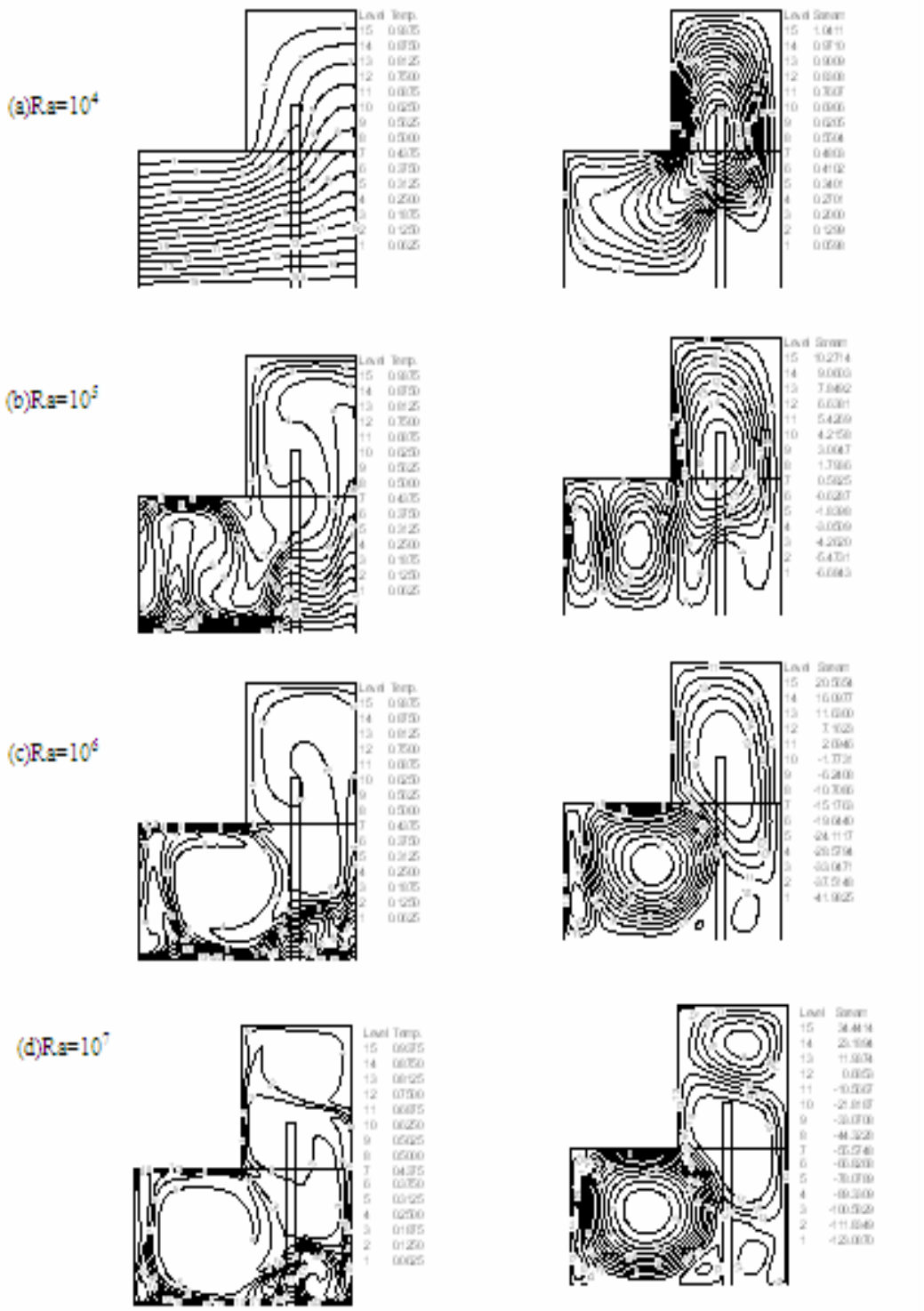

Fig. (10) Effects of Ra number on the temperature contours and stream function for fin at lower wall, height of fin(B/L=0.66) and aspect ratio (H/L= 0.5)

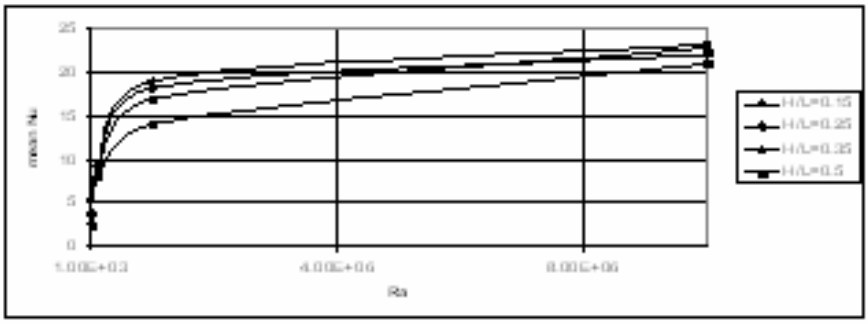

Fig.(11)Variations of mean Nusselt number with the Rayleigh number at different number of aspect ratio (H/L).

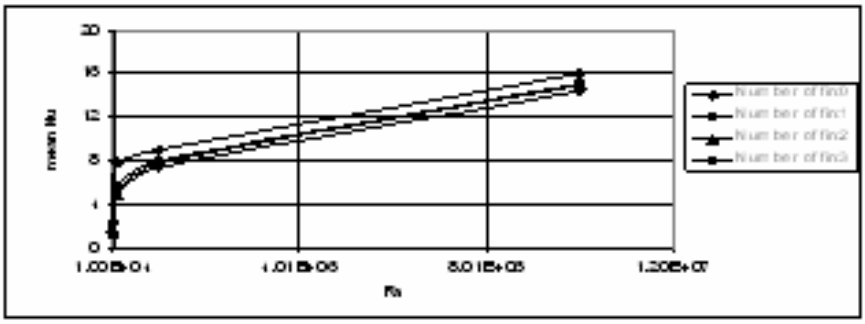

Fig.(12)Variations of mean Nusselt number with the Rayleigh number at different number of fins for (H/L = 0.50).

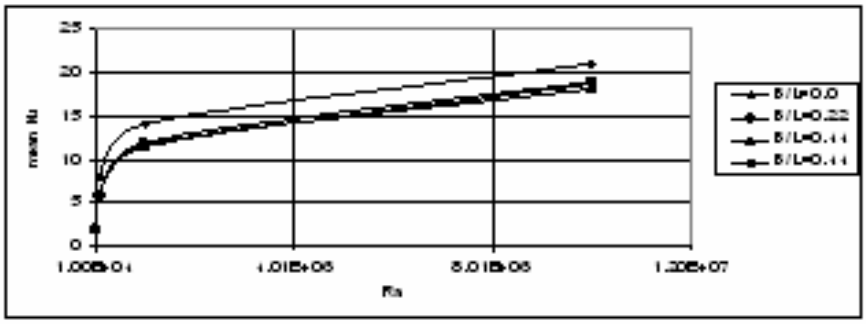

Fig.(13)Variations of mean Nusselt number with the Rayleigh number at different value height of fin (B/L).

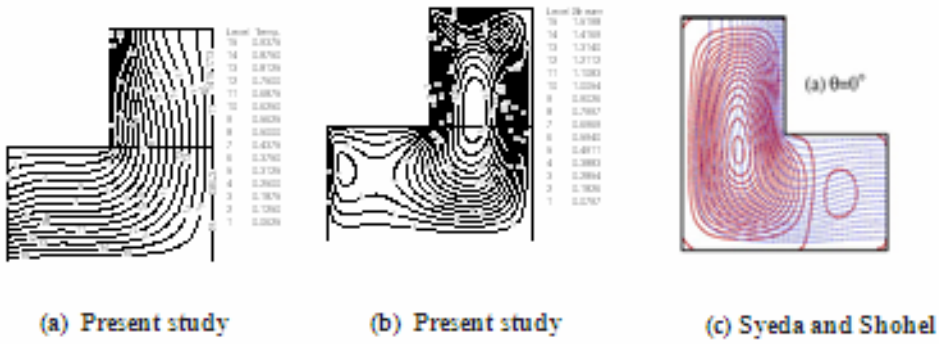

Fig. (14) Comparison between present Study and [Syeda and Shohel 2006] for Streamlines (solid lines) and isothermal lines (dashed lines) for $Ra=10^4$.

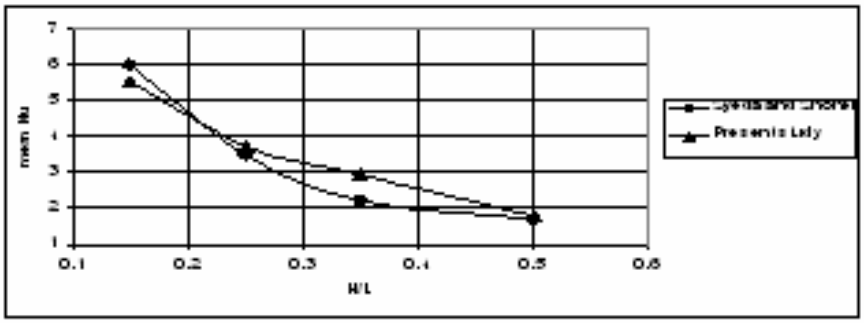

Fig. (15) Comparison between present Study and [Syeda and Shohel 2006] for mean Nusselt number with aspect ratio (H/L) at $Ra=10^4$.

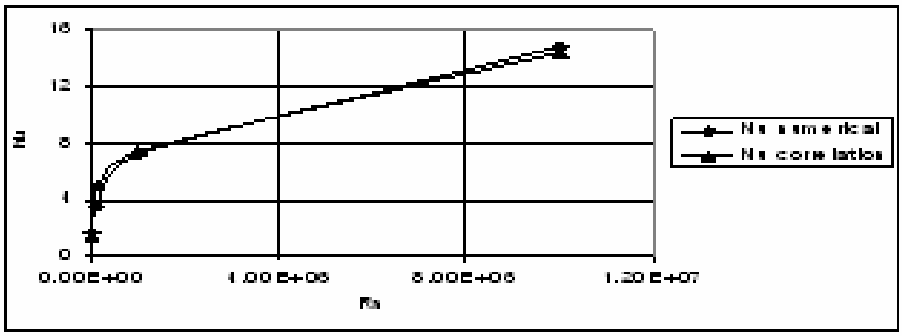

Fig. (16) Comparison of Nu computed numerically with Nu calculated from correlation Eq. (31) for case effect number of fins.

ADJUSTING OFF – CENTERING PROCESS FOR A BLOW MOLDED PLASTIC PRODUCT BY USE OF WINQSB SOFTWARE

Dr. Ahmed A. Al - Khafaji
Mechanical Engineering Department
University of Baghdad
aa.alkhafaji@yahoo.com

Mcs. Kawakib A. AL - Mendwi
Mechanical Engineering Department
University of Baghdad
Kawakib.Mendwi@yahoo.com

Dursaaf M. H. Al - saady
Quiet-angeL10@yahoo.com

ABSTRACT

In most manufacturing processes, and in spite of statistical control, several process capability indices refer to non conformance of the true mean (μ_c) from the target mean (μ_T), and the variation is also high. In this paper, data have been analyzed and studied for a blow molded plastic product (Zahi Bottle) (ZB).

WinQSB software was used to facilitate the statistical process control, and process capability analysis and some of capability indices. The relationship between different process capability indices and the true mean of the process were represented, and then with the standard deviation (σ), of achievement of process capability value that can reduce the standard deviation value and improve production out of theoretical control limitations and cost reduction.

The study exhibits that when adjusting the center to the target value by adjusting the mold to the machine, the capability index (C_p) enhanced by (14.56 %), capability index (C_{pk}) is enhanced by (14.48 %), capability index (C_{pm}) is enhanced by (12.5 %) and accuracy index (C_a) is enhanced by (14.49 %). The percentage of the specification band used up by the process (P) is reduced by (12.8 %) and the degree of variation increases.

ضبط عدم تمركز العملية لمنتج بلاستيكي مصنع بماكنة نفخ باستخدام برامجيات (WinQSB)

الملخص

في أغلب العمليات الانتاجية، وبالرغم من حالة الضبط الاحصائي فان مؤشرات المقدرة المختلفة تشير الى حالة عدم المطابقة للمتوسط الحقيقي عن المتوسط المستهدف، وكذلك مقدار التشتت يكون كبير. في هذا البحث تم دراسة وتحليل البيانات لمنتج بلاستيكي مصنع بطريقة النفخ (علبة زاهي).

استخدمت برامجيات (WinQSB) لتسهيل عملية الضبط الاحصائي وكذلك تحليل مقدرة العملية وبعض مؤشرات المقدرة. رسمت العلاقة بين مؤشرات المقدرة المختلفة مع متوسط العملية الفعلي ومن ثم مع مقدار التشتت لغرض الوصول الى مقدار مؤشر مقدرة الغاية منه تقليل قيمة التشتت وتحسين الانتاج خارج حدود الضبط النظري وتقليل الكلفة.

نتائج البحث بينت انه عند تعديل التمركز الى القيمة المستهدفة من خلال تضبيط القالب على الماكنة تحسن مؤشر المقدرة (C_p) بمقدار (% 14.56) و مؤشر المقدرة (C_{pk}) بمقدار (% 14.48) و مؤشر المقدرة (C_{pm}) بمقدار (% 12.5) ومؤشر الدقة (C_a) بمقدار (% 14.49) وقلت نسبة الاستفادة من حدود المواصفة (P) بمقدار (% 12.8) واصبحت حرية التشتت اعلى.

KEYWORDS: Process Capability, Process Capability Analysis, WinQSB Software, Process Capability Index, Control Charts, Mean Shift, Off – Center.

INTRODUCTION

In any manufacturing operation [**Groover, 10**], variability exists in the processes output, the operated parts may appear to be identical, but close inspection reveals dimensional differences from one part to the next. Manufacturing variations can be divided into two types: random and assignable. There are four factors [**Besterfield, 09**] that contribute to these variation (processes, materials, operators and miscellaneous). As long as these four factors fluctuated in a normal or expected manner, a stable pattern of many random or chance cause of variation develops. They are inevitable, very small in magnitude, and difficult to identify. Those causes of variation which are large in magnitude and therefore readily identified, are classified as assignable causes. As long as [**Arnold, Chapman, 07**] only chance variation exists, the process is said to be in statistically controlled. If there is an assignable cause of variation, the process is not in control and is unlikely to produce a good product. The objective of Statistical Process Control (SPC) is to detect the presence of assignable causes of variation. SPC has two objectives: first is to help select processes capable of producing the required quality with minimum defects. Second is to monitor process to be sure it continues to produce the required quality and no assignable cause of variation exists. The output of every process has a unique pattern that can be described by its shape, center, and spread. A histogram is [**Geng, 04**] a frequency distribution that graphically displays the measurements taken from a process and shows how those data points are distributed and centered over a measurement scale. Histograms give a picture of what the process is producing over a specified period of time, although not sequentially. A clear picture of the process variation for the specified time frame become evident and comparisons can be made against the expected process output vs. the actual production. Taguchi looked for [**Waters, 96**] both high quality and low costs. He gets this by defining target performance in key areas. When the process aims not just to be within specified quality limits – in which being just inside the limits is good enough – but to be near the target value (the center). The organization can then use statistical methods to find the most important factors that set product quality. Taguchi's advice is to aim for a target performance rather than get within some limits. But the random variations in all processes mean that it can't always hit the target. When the variations are too large it produce defect. Whenever a defective unit is produced, it is a sign that something has gone wrong with the process. The organization should find the cause of the defect and correct it before any more defects are made.

CONTROL CHART

A control chart [**Stapenhurst, 05**] was developed specifically to determine whether process outputs exhibit common cause variation only, or whether, and when, special cause variation is occurring. When samples are taken **[Schilling, Neubauer, 08]** periodically on a process, the average of the samples will tend to cluster about some overall average, or process level. The control chart consists of three parallel lines: two outside lines, called Upper Control Limit (UCL) and Lower Control Limit (LCL), and a Center Line (CL). The CL reflects the average of the data, while the control limits are calculated to have a high probability of the sample data being contained between them if the process is stable. If the process level shifts, however, points will plot outside the limits, indicating the need for corrective action on the process.

A control chart, in control for 20 or 30 samples have been collected on the chart [**Kulkarni, Bewoor, 09**], the UCL and LCL of the process may already be computed. Control limits define the boundaries of the normal behavior of the process. Their values depend only on the output data generated by the process in the immediate past. Control limits are therefore independent of specification limits. However, both sets of limits are used in the practice of SPC, although in different ways. The UCL and the LCL may be calculated from the mean and standard deviation for all samples (or σ) of the plotted data as follows:

$$UCL = \text{Grand Mean} + (3 \times \sigma) \quad (1)$$
$$LCL = \text{Grand Mean} - (3 \times \sigma) \quad (2)$$

The $\bar{x}$ - R chart, which it is one of the control charts for variables consists [**Stapenhurst, 05**] of two parts, the $\bar{x}$ chart and the R chart. The $\bar{x}$ chart is conventionally drawn above the R chart. The S (standard deviation) chart can be used in place of the R chart when sample sizes (n) rise above about 9 or if calculations are automated or particularly if the sample size varies from group to group. Whereas $\bar{x}$ is the mean of the sample and calculated us summation of the data and divided by the sample size, R is the range of the

data which is the deference between maximum and minimum value, and s is standard deviation of the sample. Two considerations [**Allen, 10**] for sample size selection First, the larger the sample size, the closer the control limits and more sensitive the chart will be to assignable causes. Second, n should ideally be large enough that the sample averages of the value follow a specific pattern. The pattern in question relates to the so-called "normal" distribution. In many situations, this pattern happens automatically if $n \geq 4$. The grand mean $\overline{\overline{X}}$ and $\overline{R}$ and σ calculated as follows:

$$\overline{\overline{X}} = \frac{\sum_{i=1}^{m} \overline{X}}{m} \quad (3)$$

$$\overline{R} = \frac{\sum_{i=1}^{m} R}{m} \quad (4)$$

$$\sigma = \frac{\overline{R}}{d_2} \quad (5)$$

Whereas, d_2 is a constant depends on the sample size n.

PROCESS CAPABILITY

Capability indices that [**Pearn, Kotz, 06**] qualify process potential and process performance are practical tools for successful quality improvement activities and quality program implementation. Apparently, the first Process Capability Index (PCI) to appear in the literature is the precision index C_p, defined as:

$$C_p = \frac{USL - LSL}{6 \times \sigma} \quad (6)$$

While the precision index C_p measures the magnitude of the process variation, the index *k*, to be defined below, describes the process capability in terms of departure of the process mean μ from the center (midpoint or Target) *T* and provides a quantified measure of the extent that a process is off-center. The index *k* is one of the original Japanese indices and is defined as:

$$k = \frac{|\mu - T|}{\frac{USL - LSL}{2}} = \frac{|\mu - T|}{d} \quad (7)$$

Where μ is the process mean, d = (USL – LSL) / 2 is the half specification width, and *T* is the midpoint between the upper and lower specification limits (*T* = (USL + LSL) / 2). This index measures the departure of process mean from the midpoint of specifications.

The complementary index $C_a = 1 - k$, referred to as the accuracy index, is defined to measure the degree of process centering relative to the manufacturing tolerance. The index is expressed as:

$$C_a = 1 - \frac{|\mu_c - T|}{d} \quad (8)$$

It measures the degrees of process centering, and alerts the user if the process mean deviates from the center *T* (which is often the target value). Whereas $C_a = 1$ when $\mu = T$, and $0 < C_a < 1$ when the process center is shifted, and $C_a = 0$ when $\mu = LSL$ or $\mu = USL$, and $C_a < 0$ when $\mu < LSL$ or $\mu > USL$.

The PCI in equation (6) has [**Montgomery, 05**] a useful practical interpretation (P) namely, is the percentage of the specification band used up by the process.

$$P = \left(\frac{1}{C_p}\right) \times 100 \quad (9)$$

Equation (6) assumes that the process has both upper and lower specification limits. For Upper Specification only (C_{pu}) and Lower Specification only (C_{pl}), one sided PCIs defined as follows:

$$C_{pu} = \frac{USL - \mu}{3\sigma} \quad (10)$$

$$C_{pl} = \frac{\mu - LSL}{3\sigma} \quad (11)$$

The process capability ratio C_p does not take into account where the process mean is located relative to the specifications. C_p simply measures the spread of the specifications relative to the six sigma spread in the process. It may be more accurately reflected by defining a new process capability ratio that takes process centering into account. This quantity is:

$$C_{pk} = \min(C_{pu}, C_{pl}) \quad (12)$$

If $C_{pk} = C_p$, the process is centered at the midpoint of the specifications, and when $C_{pk} < C_p$ the process is off – center. Thus, C_p measures potential capability in the process, whereas C_{pk} measures actual capability.

For any fixed value of μ in the interval from LSL to USL, C_{pk} depends on σ and becomes large as σ approaches zero. That large value of C_{pk} does not really tell us anything about the location of the mean in the interval from LSL to USL. One way to address this difficulty is to use a process capability ratio that is a better indicator of centering C_{pm} as follows:

$$C_{pm} = \frac{\text{USL - LSL}}{6 \times \tau} \qquad (13)$$

$$\tau = \sqrt{\sigma^2 + (\mu - \text{T})^2} \qquad (14)$$

When both C_{pk} and C_{pm} coincide with C_p when $\mu = T$ and decrease as μ moves away from T. However $C_{pk} < 0$ for $\mu > USL$ or $\mu < LSL$, Whereas C_{pm} approaches zero asymptotically as $|\mu - T| \to \infty$.

An important assumption [**Montgomery, 05**] underlying this discussion of process capability and the ratios C_p and C_{pk} is that their usual interpretation is based on a normal distribution of process output. If the underlying distribution is non normal, then the statements about expected process fallout attributed to a particular value of C_p or C_{pk} may be in error. However,

For large values [**Spiegel, Stephens, 08**] of samples $N\,(N \geq 30)$, the sampling distribution of means is approximately a normal distribution with mean $\mu_{\bar{x}}$ and standard deviation $\sigma_{\bar{x}}$ irrespective of the population (so long as the population mean and variance are finite and the population size is at least twice the sample size). This result for an infinite population is a special case of the central limit theorem of advanced probability theory, which shows that the accuracy of the approximation improves as N gets larger. This is sometimes indicated by saying that the sampling distribution is asymptotically normal.

It is a good approximation that **[Booker, Raines, Swift, 01]** if the number of components in the stack is greater than 5, then the final assembly characteristic will form a normal distribution regardless of the individual component distributions due to the "Central Limit Theorm".

OBJECTIVES OF AN ANALYSIS OF PROCESS CAPABILIT

The basic [**Grant, Leavenworth, 96**] statistical problem in process quality control is that of establishing a state of control over the manufacturing process, which is, eliminating special causes of variation and then maintaining that state of control through time. Once a state of control has been established, attention turns to the question, "Is the output meeting specifications, and if not, can the process be adjusted to a level where it will?" Actions that result in change or adjustment in a process, directed at eliminating common causes, are frequently the result of some form of capability study. The comparison of natural tolerance limits with the specification range may lead to any of the following possible courses of action: (1) No action: If the natural tolerance limits fall well within the specification limits, usually no action will be required. (2) Action to adjust centering: When the natural tolerance range is about the same as specification range, a relatively simple adjustment to the centering of the process may be all that is necessary to bring virtually all products within specifications. (3) Action to reduce variability: This is usually the most complex action. In those cases where several product streams merge into one line prior to inspection, action may involve the relatively uncomplicated task of bringing the several streams under control separately at some standard $\bar{X}$. In other cases, a complex analysis of the sources of variation may be required resulting in changes of methods, tooling materials, and/or equipment. (4) Actions to change specifications: This is a design decision but one that should not be ignored by quality control personnel. Simply because specifications are stipulated in writing does not necessarily mean they are inviolate. On the other hand, quality control and manufacturing personnel cannot callously ignore them without running the risk of causing real trouble.

USES OF PROCESS CAPABILITY INFORMATION

Process capability information [**Juran, Godfrey, 99**] serves multiple purposes: (1) Predicting the extent of variability that processes will exhibit. Such capability information, when provided to designers, provides important information in setting realistic specification limits. (2) Choosing, from among competing processes or equipment, that which is best to meet the specifications. (3)

Planning the interrelationship of sequential processes. One process may distort the precision achieved by a predecessor process. Quantifying the respective process capabilities often points the way to a solution. (4) Providing a quantified basis for establishing a schedule of periodic process control checks and readjustments. (5) Testing theories of causes of defects during quality improvement programs. (6) Serving as a basis of quality performance requirements for purchased product or equipment. In certifying suppliers, some organization use a capability index as one element of certification criteria. In these applications, the value of the capability index desired from suppliers can be a function of the type of commodity being purchased.

THE WINQSB SOFTWARE

The Quantitative Systems for Business (QSB) [**Ionica, Edelhauser, 08**] software package contains the most widely used problem-solving algorithms in Operations Research and Management Science (OR/MS). The WinQSB is the Windows version of the QSB software package. The computer product WinQSB is intended [**Ciobanica, 11**] to solve quantitative problems in management, and it was realized in the Georgia Institute of Technology, Atlanta, USA by Y. L. Chang and presented in 1997 in the paper WinQSB Decision Support Software. The WinQSB software [**Ionica, Edelhauser, 08**] is one of the most important events in decision making process. Operations Research and Management Science (OR/MS) software systems are used to construct examples, to understand the existing concepts, and to discover useful managerial concepts. On the other hand, new developments in decision making process often motivate developments of new solution algorithms and revision of the existing software systems. OR/MS software systems rely on a cooperation of OR/MS practitioners, designers of algorithms, and software developers.

THE PRACTICAL WORK

Blow molding is used to produce plastic refills for different kinds of detergents. Zahi Bottle (ZB) was chosen as a case study in this research; to study the capability of the process for the machine which manufactures this type of bottle as shown in **figure (1)**, **figure (2)** shows the bottle mold.

Table (1) shows the collected data for Zahi Bottle Neck (ZBN) which is the critical character for this product. Thirty Samples (m = 30) were measured and five sample size (n = 5) were taken every one hour for five days. The measurements were taken by Vernier caliper, which was calibrated before use, and all measurements were gauged by the same inspector. The tolerance of the ZBN was (28 ± 0.5 mm).

After that the data in table (1) was entered by WinQSB software version (2), which is the updated version of the program. **Figures (3), (4) and (5)** show the control charts for ($\overline{X}$ - chart), (R – chart) and (s – chart) which were used to control the process under study. All charts clarified that the process was under control for all points; the first condition for the study process capability was realized.

Figure (6) shows the histogram for the data under study which was analyzed and displayed by the WinQSB software program, the second condition for studying the process capability was realized too.

Figure (7) shows the window for the process capability analysis by WinQSB software for the data entered, by analyzing Process Capability Ratios (PCRs). The result appears that the process is incapable and the mean shifted – off.

RESULTS AND CONCLUSIONS

The histogram in **figure (6)** and $\overline{X}$ - chart in **figure (3)** represent high magnitude dispersion for means for the data value. PCRs (C_{pk}, C_{pm}) and the process accuracy (C_a) were calculated by **equations (2), (3)** and **(8).**

This indicates that, with manufacturing continuity under similar conditions in the long run, some parts of the products will lay out of tolerance limits, mainly adjusting centering is highly recommended in such situations.

Table (2) shows the hypothetical values of the mean and graduating slightly above and below the target mean until the tolerance limits ($\mu_{c\ \text{hypo}}$) which were calculated for assessment for process capability without shifting off. **Equations (12), (13) and (8)** PCIs and process accuracy index C_{pk}, C_{pm} and C_a were calculated. **Figure (8)** exhibits the relationship, drawn by excel software, between the different process capability ratios and $\mu_{c\ \text{hypo}}$. **Figure (9)** magnified the upper area of **figure (8)** to show the value of PCIs when $\mu_c = 28$, which were $C_{pk} = C_{pm} = 0.969$ and $C_a = 1$.

By the same way different values were assumed for of the standard division σ to calculate different PCRs, the results were shown in **table (3)**. **Figure (10)** exhibits the results for C_p, C_{pk}

and C_{pm} calculated by different values of the variation σ. **Figure (11)** magnify the middle area of **figure (10)** to show the value of σ, which was 0.15 when $C_{pk} = 0.969$.

Figures (8) and (9) were cumulative to give a wide area to (μ) and (σ) against PCRs, to help the quality control engineers and designers by knowing the real limits of tolerance in conformity with different process variability.

Table (4) calculated the original and estimated data for the studied characteristic, the Percentage of Enhancements (PE) and Percentage of Utilization (PU) from new values. The values of PE and PU were calculated as follows:

$$\text{PE} = \frac{\text{Original values}}{\text{Hypothetical values}} \times 100\,\% \qquad (15)$$

$$\text{PU} = |100 - \text{PE}| \times 100\,\% \qquad (16)$$

Decreasing the standard deviation amount by (0.02) and increasing the process capability to (1.11) leads to the decrease of the percentage of product defects.

Improving a process by re-centering it is easier than changing the sources of variation. In most of manufacturing processes, the shifting between true mean and the target mean is caused mostly by the machine or by the fixtures on the machine. Re setup for the machine, for mold, raw material temperature, amount of injected raw material and the time before opening the mold improves the mean value. The cooling operation of the mold from times to time is important to gain products with high quality.

REFERENCES

Allen, T. T., “Introduction to Engineering Statistics and Lean Sigma, Statistical Quality Control and Design of Experiments and Systems", Second Edition, London: Springer, 2010.

Arnold, T. J., Chapman, S. N., "Introduction to Materials Management", Fifth Edition, New Jersey: Prentice Hall, 2003.

Besterfield, Dale H., "Quality Control", Eighth Edition, New Jersey: Prentice – Hall INC., 2009.

Booker, J. D., Raines, M., Swift, K. G., "Designing Capable and Reliable Products", Oxford: Butterworth-Heinemann, 2001.

Ciobanica, M. L., "The Modeling of Graphs Through Computer Product WinQSB", The 7th International Scientific Conference e Learning and Software for Education, Bucharest, April 28 29, 2011.

Geng, H., "Manufacturing Engineering Handbook", New York: McGraw-Hall, 2004.

Grant, E. L., Leavenworth, R. S., "Statistical Quality Control", Seventh Edition, New York: McGraw-Hall, 1996.

Groover, M. P., "Fundamentals of Modern Manufacturing, Materials, Processes and Systems" Fourth Edition, New York: John Wiley Sons Inc, 2010.

Ionica, A., Edelhauser, E., "Decision Tree Technique a Useful Tool for the Quality Management of a Project", Annals of the University of Petroşani, Mechanical Engineering, 89-92, 10 (2008).

Juran, J. M., Godfrey, A. B., "Juran's Quality Handbook", Fifth Edition, New York: McGraw-Hall, 1999.

Kulkarni, V. A., Bewoor, A. K., "Quality Control", New Delhi: Wiley, 2009.

Montgomery, D. C., "Introduction to Statistical Quality Control", Fifth Edition, New York: John Wiley Sons Inc, 2005.

Pearn, W. L., Kotz, S., "Encyclopedia and Handbook of Process Capability Indices, a Comprehensive Exposition of Quality Control Measures", New Jersey: World Scientific, 2006.

Schilling, E. G., Neubauer, D. V., "Acceptance Sampling in Quality Control", Second Edition, Boca Roton: CRC Press Taylor & Francis Group, LLC, 2008.

Spiegel, M. R., Stephens, L. J., "Theory and Problems of Statistics", Fourth Edition, New York: Schaum’s Outline Series: McGraw-Hill, 2008.

Stapenhurst, T., "Mastering Statistical Process Control a Handbook for Performance Improvement Using Cases", Amsterdam: Elsevier, 2005.

Stapenhurst, T., "Mastering Statistical Process Control a Handbook for Performance Improvement Using Cases", Amsterdam: Elsevier, 2005.

Waters, D., "Operations Management, Producing Goods and Services", Harlow: Addison-Wesley Publishing Company, 1996.

ABBREVIATION

μ_c	True Mean (Non Conforming Mean)
CL	Center Line
LCL	Lower Control Limit
OR/MS	Operations Research and Management Science
PCI	Process Capability Index
PCRs	Process Capability Ratios
PE	Percentage of Enhancements
PU	Percentage of Utilization
QSB	Quantitative Systems for Business
SPC	Statistical Process Control
UCL	Upper Control Limit
ZB	Zahi Bottle

Figure (1) Zahi bottle refill product

Figure (2) Zahi bottle mold

Table (1) The collected data for ZBN

Date	Time	No.	X1	X2	X3	X4	X5	$\overline{X}$	R	s
1st day	9	**1**	27.7	27.9	28	28.1	28	27.94	0.4	0.151658
	10	**2**	28	28.1	28.2	28	27.9	28.04	0.3	0.114018
	11	**3**	28.1	27.9	27.8	28	28.4	28.04	0.6	0.230217
	12	**4**	28.3	28.1	28	27.9	28.2	28.1	0.4	0.158114
	1	**5**	28.3	28.4	28	28.2	28.1	28.2	0.4	0.158114
	2	**6**	28.1	28.2	28.4	28	28	28.14	0.4	0.167332
2nd day	9	**7**	27.7	28	27.9	28.1	27.9	27.92	0.4	0.148324
	10	**8**	28.2	27.7	27.9	28	28.1	27.98	0.5	0.192354
	11	**9**	28	28.4	28.3	27.9	28	28.12	0.5	0.216795
	12	**10**	28	28.1	28.3	28.1	27.9	28.08	0.4	0.148324
	1	**11**	28.4	28.1	28.4	28	28	28.18	0.4	0.204939
	2	**12**	28.1	28.2	28	28.3	27.8	28.08	0.5	0.192354
3rd day	9	**13**	27.9	28.1	28.1	27.8	27.9	27.96	0.3	0.134164
	10	**14**	27.6	27.8	28	28	27.9	27.86	0.4	0.167332
	11	**15**	28	28.2	28.3	28	28.4	28.18	0.4	0.178885
	12	**16**	28.1	28.2	28.2	28.4	27.9	28.16	0.5	0.181659
	1	**17**	28.3	28.2	28	28.4	28	28.18	0.4	0.178885
	2	**18**	28	28.4	28.1	27.9	28.2	28.12	0.5	0.192354
4th day	9	**19**	27.9	28	28.2	27.8	28	27.98	0.4	0.148324
	10	**20**	27.8	28	28.1	27.9	28	27.96	0.3	0.114018
	11	**21**	28.1	28.4	28	28.1	28.2	28.16	0.4	0.151658
	12	**22**	28	28	28.2	28.1	27.9	28.04	0.3	0.114018
	1	**23**	27.8	27.9	28	28.1	28	27.96	0.3	0.114018
	2	**24**	28.2	28.3	28.1	28	28.4	28.2	0.4	0.158114
5th day	9	**25**	28	27.9	27.6	27.8	27.9	27.84	0.4	0.151658
	10	**26**	28.1	28.2	27.8	28	27.9	28	0.4	0.158114
	11	**27**	28.3	28.4	28	28.1	28	28.16	0.4	0.181659
	12	**28**	27.9	28.2	27.9	28	28.1	28.02	0.3	0.130384
	1	**29**	28	28.3	28.1	28	28.1	28.1	0.3	0.122474
	2	**30**	28.4	28.2	28	28.3	28.1	28.2	0.4	0.158114

Remark (1): All dimensions in mm
Remark (2): All diagrams draw in excel

Figure (3) WinQSB ($\overline{X}$ - chart) for ZBN

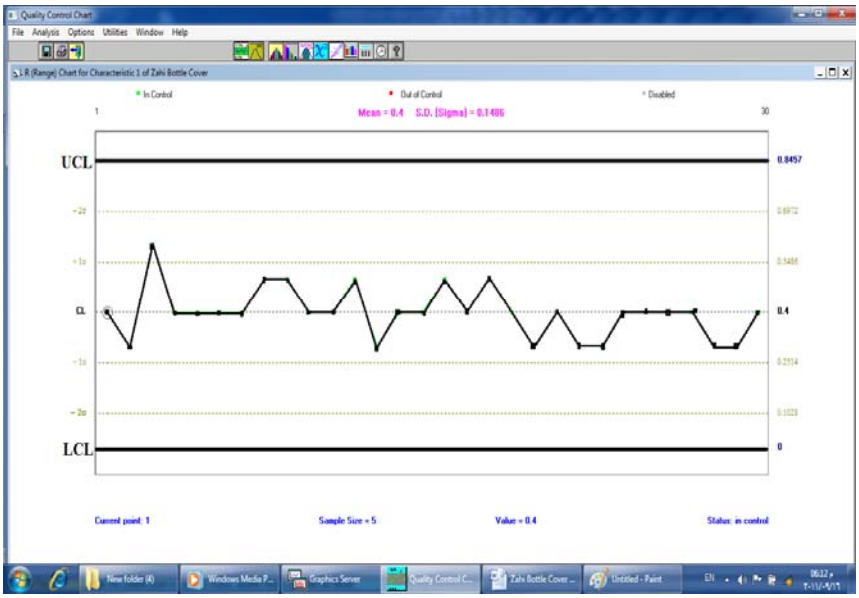

Figure (4) WinQSB (R- chart) for ZBN

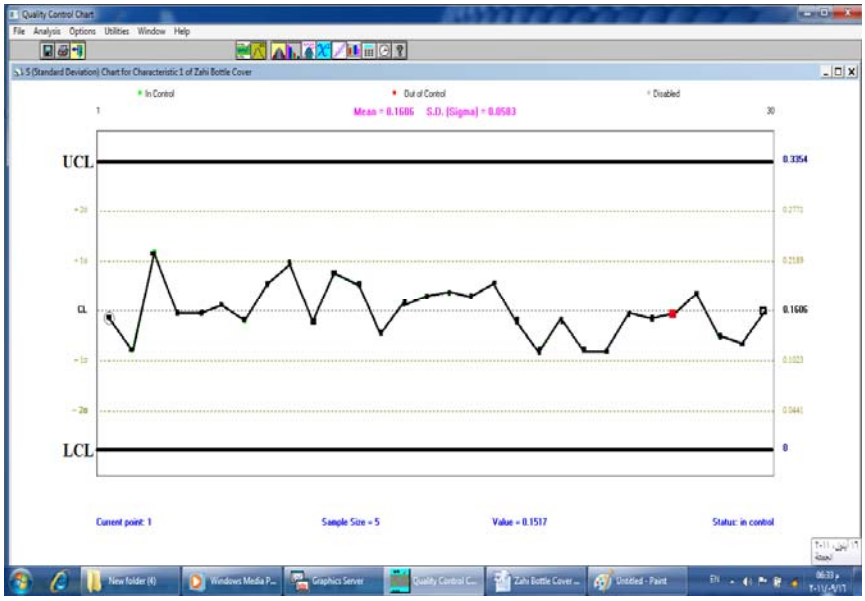

Figure (5) WinQSB (S - chart) for ZBN

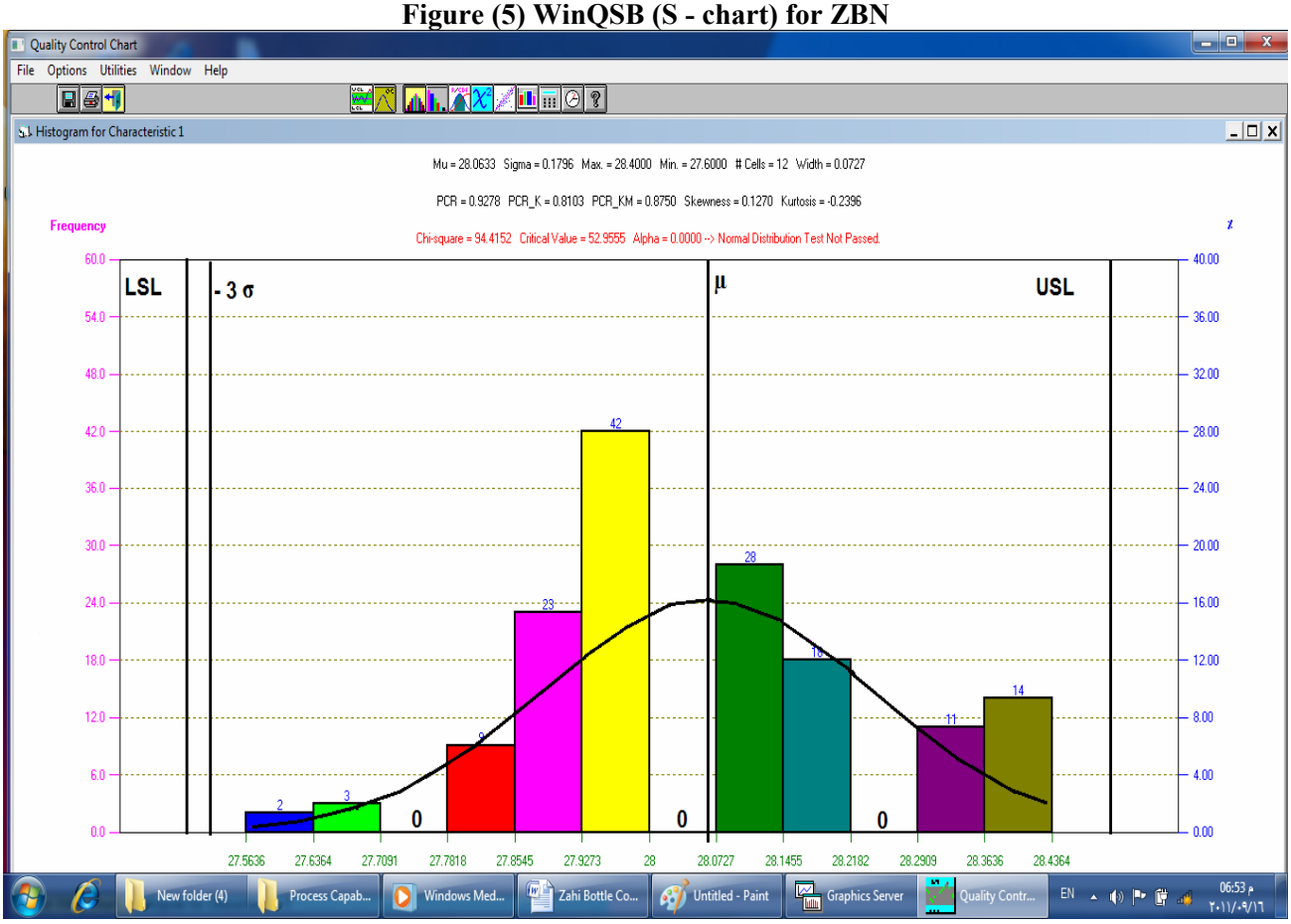

Figure (6) WinQSB Histogram for ZBN

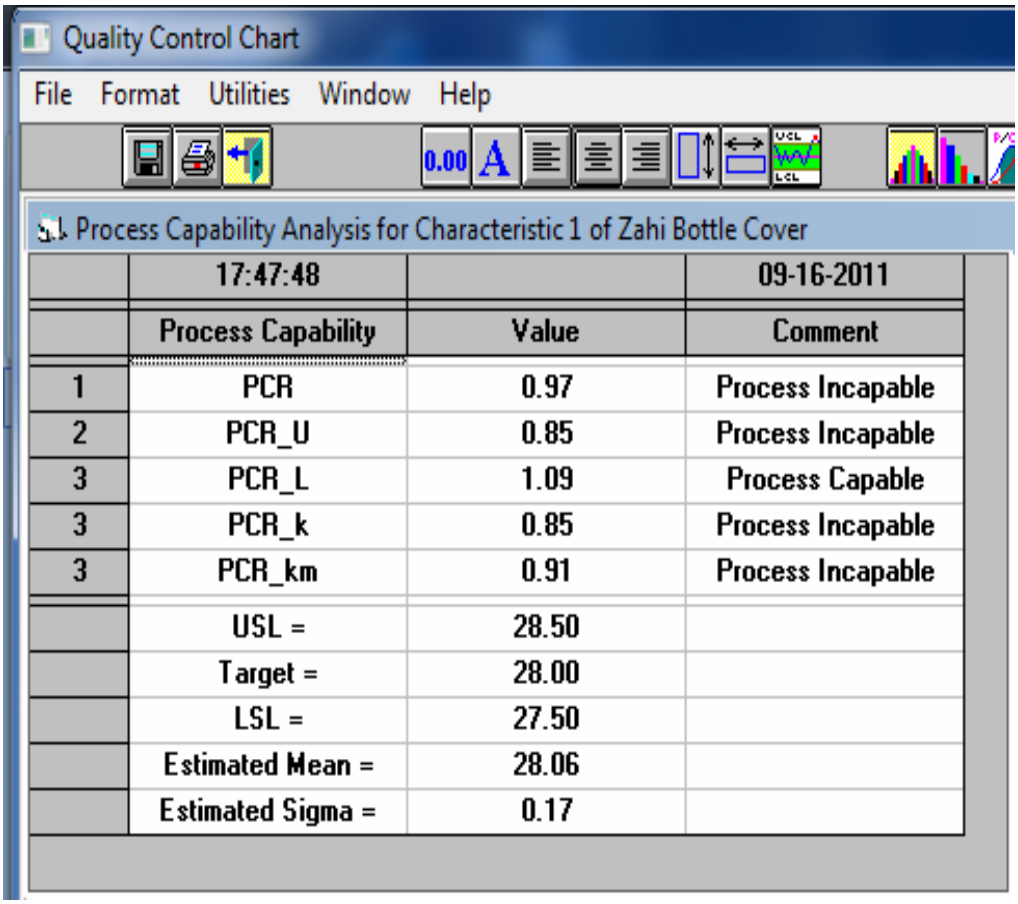

	17:47:48		09-16-2011
	Process Capability	Value	Comment
1	PCR	0.97	Process Incapable
2	PCR_U	0.85	Process Incapable
3	PCR_L	1.09	Process Capable
3	PCR_k	0.85	Process Incapable
3	PCR_km	0.91	Process Incapable
	USL =	28.50	
	Target =	28.00	
	LSL =	27.50	
	Estimated Mean =	28.06	
	Estimated Sigma =	0.17	

Figure (7) WinQSB for the PCRs

Table (2) The result for C_{pk}, C_{pm} and C_a calculated by hypothetical values of the calculated mean without shifting $\mu_{c\ \text{hypo}}$

μc	Cpk	Cpm	Ca
27.50	0.0000	0.3152	0
27.55	0.0969	0.3460	0.1
27.60	0.1938	0.3828	0.2
27.65	0.2907	0.4274	0.3
27.70	0.3877	0.4820	0.4
27.75	0.4846	0.5493	0.5
27.80	0.5815	0.6319	0.6
27.85	0.6784	0.7304	0.7
27.90	0.7753	0.8378	0.8
27.95	0.8722	0.9306	0.9
28.00	0.9692	0.9692	1
28.05	0.8722	0.9306	0.9
28.10	0.7753	0.8378	0.8
28.15	0.6784	0.7304	0.7
28.20	0.5815	0.6319	0.6
28.25	0.4846	0.5493	0.5
28.30	0.3877	0.4820	0.4
28.35	0.2907	0.4274	0.3
28.40	0.1938	0.3828	0.2
28.45	0.0969	0.3460	0.1
28.50	0.0000	0.3152	0

Table (3) The result for C_p, C_{pk} and C_{pm} calculated by hypothetical values of the variation σ

σ	Cp	Cpk	Cpm
0.01	16.6667	14.5567	2.6007
0.02	8.3333	7.2783	2.5106
0.03	5.5556	4.8522	2.3793
0.04	4.1667	3.6392	2.2258
0.05	3.3333	2.9113	2.0662
0.06	2.7778	2.4261	1.9109
0.07	2.3810	2.0795	1.7660
0.08	2.0833	1.8196	1.6338
0.09	1.8519	1.6174	1.5147
0.10	1.6667	1.4557	1.4082
0.11	1.5152	1.3233	1.3132
0.12	1.3889	1.2131	1.2285
0.13	1.2821	1.1197	1.1527
0.14	1.1905	1.0398	1.0847
0.15	1.1111	0.9704	1.0237
0.16	1.0417	0.9098	0.9686
0.17	0.9804	0.8563	0.9188
0.18	0.9259	0.8087	0.8735
0.19	0.8772	0.7661	0.8322
0.20	0.8333	0.7278	0.7945
0.21	0.7937	0.6932	0.7599
0.22	0.7576	0.6617	0.7280
0.23	0.7246	0.6329	0.6987
0.24	0.6944	0.6065	0.6715
0.25	0.6667	0.5823	0.6463
0.26	0.6410	0.5599	0.6228
0.27	0.6173	0.5391	0.6010
0.28	0.5952	0.5199	0.5806
0.29	0.5747	0.5020	0.5615
0.30	0.5556	0.4852	0.5436

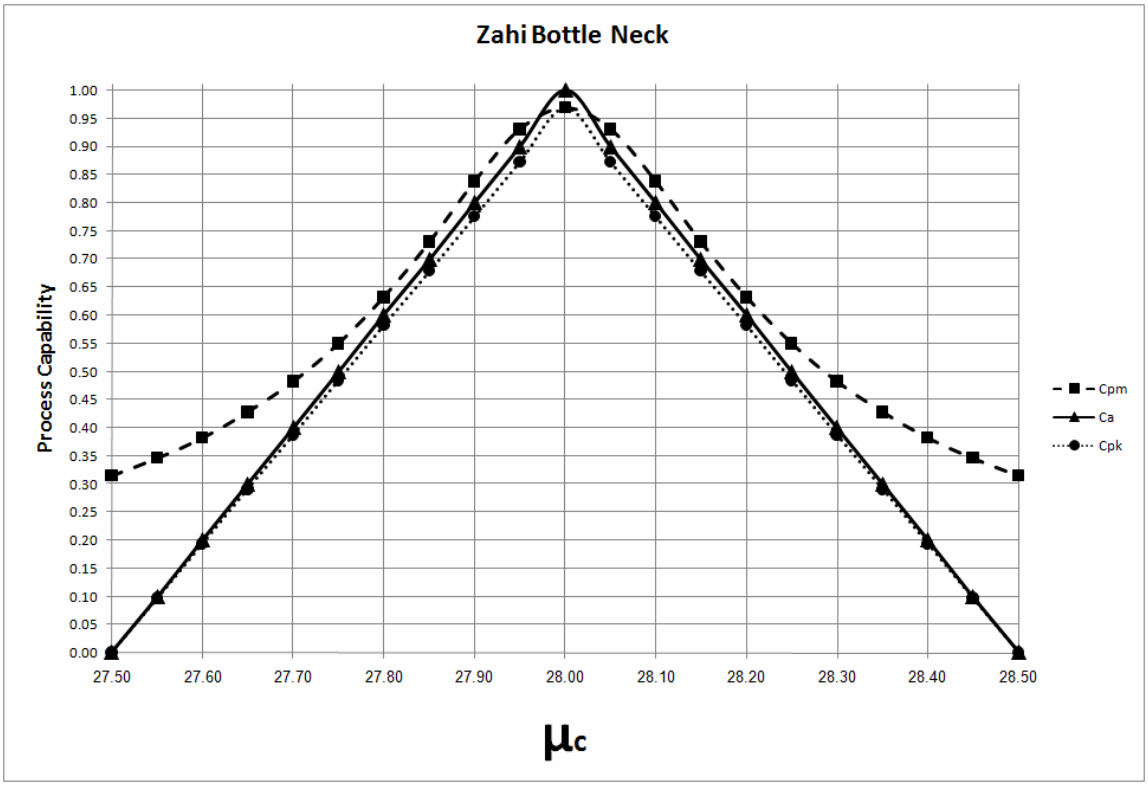

Figure (8) C_{pk}, C_{pm} **and** C_a **calculated by hypothetical value of the calculated mean without shifting** $\mu_{c\ \text{hypo}}$

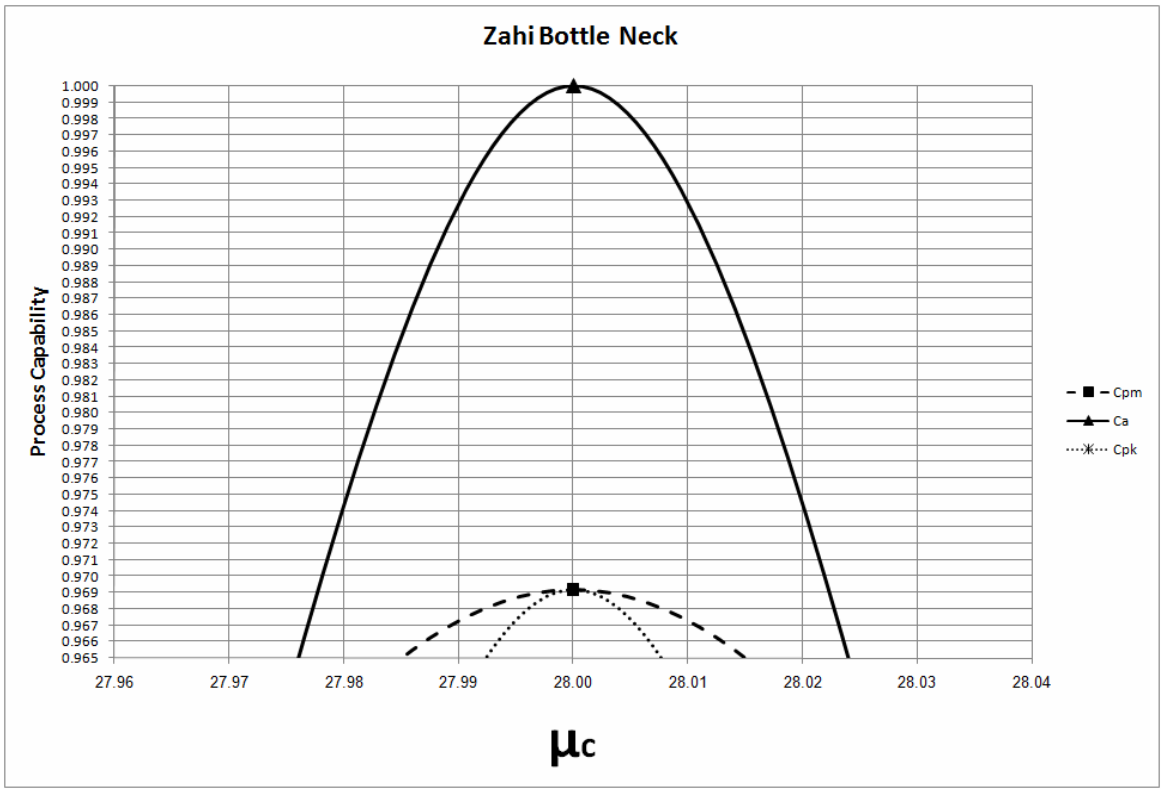

Figure (9) the upper area of figure (8) magnified to show the value of PCIs when $\mu_c = 28$

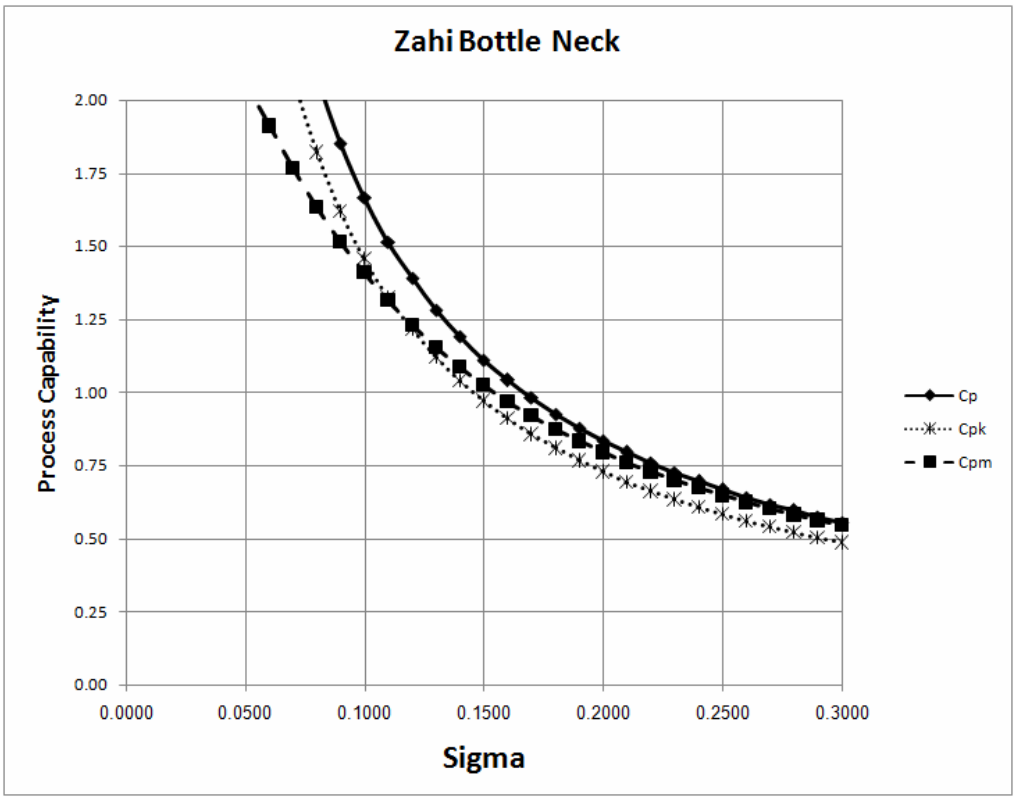

Figure (10) The result for C_p, C_{pk} and C_{pm} calculated by hypothetical values of the variation σ

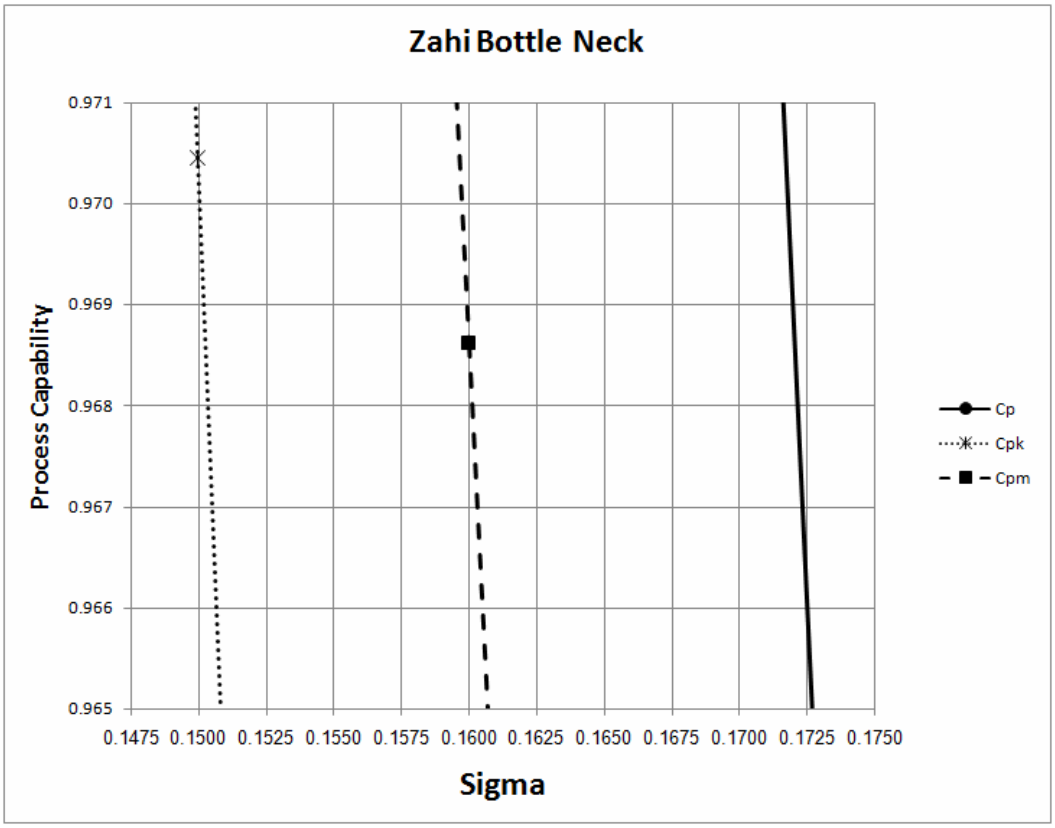

Figure (11) the middle area of figure (10) magnified to show the value of σ when $C_{pk} = 0.969$

Table (4) original and estimated data for the studied characteristic, the percentage of enhancements, percentage of utilization from new values.

Equation	Zahi Bottle Neck Original	Zahi Bottle Neck Hypothetical	Percentage of Enhancement	Percentage of Utilization
$\mu_C = \overline{\overline{X}}$	28.0633	28	99.77 %	0.23 %
$\overline{R} = \frac{\sum R}{N}$	0.40000	0.3489	87.22 %	12.78 %
$\sigma = \frac{\overline{R}}{d_2} = \frac{\overline{R}}{2.326}$	0.1720	0.15	87.20 %	12.8 %
$C_p = \frac{USL - LSL}{6 \times \sigma}$	0.9689	1.11	114.56 %	14.56 %
$P = (\frac{1}{C_p}) \times 100$	103.2 %	90 %	87.20 %	12.8 %
$C_{pk} = \min C_{pu}, C_{pl}$	0.8463	0.9689	114.48 %	14.48 %
$C_{pm} = \frac{USL - LSL}{6 \times \sqrt{\sigma^2 + (\mu_C - T)^2}}$	0.9093	1.023	112.5 %	12.5 %
$C_a = 1 - \frac{\lvert \mu_C - T \rvert}{d}$	0.8734	1	114.49 %	14.49 %